Hydrodynamics of viscous oil-water flow through horizontal and upward inclined pipelines

Dasari Anjali

Hydrodynamics of viscous oil-water flow through horizontal and upward inclined pipelines

THESIS

Submitted in Partial Fulfillment of the Requirements for the Degree of

Doctor of Philosophy
in
Engineering
by

Dasari Anjali

Under the supervision of

Dr. Tapas Kumar Mandal

DEPARTMENT OF CHEMICAL ENGINEERING
INDIAN INSTITUTE OF TECHNOLOGY GUWAHATI
GUWAHATI-781039, INDIA

September, 2014

Dedicated to my parents and

My dear Raja

INDIAN INSTITUTE OF TECHNOLOGY GUWAHATI
GUWAHATI - 781039, ASSAM, INDIA

DEPARTMENT OF CHEMICAL ENGINEERING

CERTIFICATE

This is to certify that the thesis entitled "***Hydrodynamics of viscous oil-water flow through horizontal and upward inclined pipelines***" submitted by **Dasari Anjali** in fulfillment of the requirement of the *Degree of Doctor of Philosophy in Engineering*, is a record of bonafide research work carried out by her, in the Department of Chemical Engineering, Indian Institute of Technology, Guwahati, under my guidance and supervision. In my opinion, the thesis has reached the standard fulfilling the requirements of the Ph. D. degree as prescribed in the regulations of this institute.

(Dr. Tapas Kumar Mandal)
Department of chemical Engineering
Indian institute of Technology Guwahati
Guwahati-781039, India

Acknowledgement

Words fail to express my sincere gratitude to my thesis supervisor Dr. Tapas Kumar Mandal for his constant encouragement, patience, insightful advice, guidance and sustained interest in successful completion of my dissertation. In addition, his philosophical guidance has built up a momentum inside me. I also thank almighty for making me to feel fortunate to work under his great stewardship.

I am grateful to Dr. Ashok Kumar Dashmahapatra for his valuable suggestions during the work and paper corrections.

I wish to acknowledge my respectful thanks to Dr. P.K. Saha, former HOD and Prof. V.S. Mohalkar present HOD of chemical engineering department for extending all the necessary facilities for carrying-out my research work. I am also grateful to all the professors in the department for their sincere cooperation.

I am thankful to Mrs. Guha Enterprises for their great help and sincere cooperation during fabrication of the experimental setup and its run.

I wish to thank all the non teaching staff of our department for the help received from them.

I would like to thank my co-researchers and friends Mr. Anand Babu Desamala, Mr. Seim Timung, Mr. Bharath Kumar, Mr. Rambhupal Naidu and Mr. Ravi Thej for their enormous help and support during research work.

I am thankful to my friends Mr. Rajesh Kumar Koduru, Mr. M.D. Wajeed, Mr. Ravikiran, Mr. Vikranth, Ms. Preethi, Ms. Praveena, Ms. Jayasree and Ms. Nagasree for their companion in this journey and have also for their indirect help that was rendered in the completion of my work.

I would also like to thank my family who have not only supported me in the completion of my Ph.D but also have stood by me throughout my life. They have patiently supported me at all instances in my research work.

I am indebted to my husband Raja whose constant encouragement, suggestion, patience and motivation, made me to achieve this endeavor in a peaceful and cheerful manner. He transformed all the odds into reality.

Date:

Place: (Dasari Anjali)

Abstract

The flow of two immiscible liquids through conduits is widely encountered in various fields such as the chemical and petroleum industries. Liquid-liquid two-phase flow has many applications in almost all fields of chemical engineering (such as solvent extraction, emulsification, bio diesel production, etc) and petroleum industry. In the petroleum industry oil is produced and transported along with water to minimize power consumption and pumping cost by reducing frictional pressure drop. Pressure drop is an important parameter in the design of an efficient transportation system, and is greatly affected by characteristics of transportation line and fluid properties. Since last 60 years, several attempts have been made in understanding the science behind the hydrodynamics of liquid-liquid flow through pipelines. Past literature shows that most of the available literature for oil-water flow through horizontal or vertical or incline pipes are with either less (0.936-9.87 m Pa s) or high (300-1300 m Pa s) viscous oil. The past works on oil-water system having the viscosity of intermediate range are very limited, especially in inclined pipeline. Hydrodynamics of intermediate viscous oil-water flow through pipelines is important due to the gradual exhaustion of lighter crude oil. Considering the aforementioned facts, the present study aims at the investigation of hydrodynamics of viscous oil-water (intermediate viscosity range) flow through 5° upward inclined pipeline. Prior to this, studies have been focused on the hydrodynamics of such flow through horizontal pipeline for the comparison and better understanding of the physics behind the flow phenomena.

In the present study experiments have been carried out in both horizontal and 5° upward inclined pipeline for a wide range of superficial velocities. Lubricating oil (μ_O= 107 mPa s and ρ_O = 889 Kg/m^3) and filtered tap water (μ_W = 1 mPa s and ρ_W = 1000 Kg/m^3) have been selected as test fluids. Visual observation and photographic technique has been used to identify the flow patterns in both the pipelines. Seven different flow patterns namely plug (P), slug (S), wavy stratified (SW), stratified mixed (SM), annular (A), dispersion of

oil in water ($D_{O/W}$) and dispersion of water in oil ($D_{W/O}$) flow patterns have been observed in horizontal and 5° upward inclined pipeline. Two separate flow pattern maps are constructed based on the information obtained from the experimental study,- one for horizontal and another for inclined pipeline. The flow pattern maps of both horizontal and inclined pipelines are compared to know the effect of inclination on flow patterns. Comparison shows that similar flow patterns are observed in both the cases,- only difference is in the range of superficial velocities. Plug and slug flow has been identified at lower superficial velocities in inclined pipeline. Inclination induces the instability on flow configuration. In inclined pipeline, stratified mixed flow pattern identified at lower superficial velocities and occupied a larger region than horizontal pipeline. The entire annular flow region has also been shifted to higher mixture velocities in inclined pipeline. This low inclination (5°) has no significant effect on dispersed flow patterns (either oil dispersed in water or water dispersed in oil). For better understanding the effect of oil viscosity on the flow pattern, present horizontal flow pattern map is compared with the existing experimental flow pattern map in the literature. It is observed that higher viscosity favors annular flow pattern. Dispersed flow patterns have also been observed at lower superficial velocities for high viscous oil.

Next an attempt has been made to predict the flow patterns and its transitions in horizontal and inclined pipeline. All the flow pattern transitions in horizontal and inclined pipeline have been predicted from the existing analytical models in the literature except wavy stratified to stratified mixed flow pattern transition boundary. This flow pattern transition boundary has been predicted from the new approach based on drop formation mechanism at the interface. The result (both inclined and horizontal flow) shows the poor prediction of flow pattern transition in some cases like transition of slug to annular, slug to wavy stratified, dispersion of oil in water at higher velocities, etc. Due to this reason, a simple accurate prediction technique has been tried to adopt in this work. Keeping these points in mind, Probabilistic Neural Network (PNN) technique has been adopted. A new network has been developed from the data collected from literature as well as present experimental work. The network has been used to predict the flow pattern maps of both horizontal and

inclined pipelines. The network has also been validated with various flow patterns available in the literature. Results obtained from both the techniques have also been compared and PNN is found to be a best predictive tool of flow patterns.

Extensive experimental studies have been carried out to measure the holdup and pressure drop in both horizontal and inclined pipelines. An attempt has been made to develop a correlation to predict pressure gradient in horizontal and inclined pipelines. For this purpose Lockhart-Martenelli correlation has been modified for horizontal liquid-liquid flow separately by correlating two-phase multiplier with Lockhart-Martenille parameter. The proposed correlation has been validated with present and literature data. The accuracy in prediction of pressure gradient by modified Lockhart-Martenille correlation is 22%, to improve the prediction accuracy another correlation has been developed based on dimensional analysis. Both the proposed correlation has shown accurate prediction than the existing correlation in the literature. The same approaches are extended to 5° upward inclined flow. The initiation has been taken for the development of a new correlation due to the poor prediction of available correlations. The pressure gradient data has also been predicted using phenomenological models. A model has been proposed to predict the pressure gradient of annular flow in both horizontal and inclined pipes by considering entrainment fraction. The predicted result shows improvement in prediction after incorporation of entrainment fraction. The measured holdup in both the pipelines have been predicted using existing correlations in the past literature. The predicted results are showing good agreement with the experimental results for annular and stratified wavy flow pattern.

PNN technique gives good prediction of the flow patterns for a closer viscosity ranges and pipe inclinations with which it is trained. PNN also cannot explain the physics behind the flow phenomena. Due to these limitations, Computational Fluid Dynamics (CFD) technique has been selected to predict the flow patterns obtained in the present study. In literature, CFD prediction of flow patterns in horizontal flow are reported while no such studies are available on inclined flow. So, a CFD simulation has been tried to predict the flow patterns indentified in 5° upward inclined pipeline. Volume of Fluid (VOF) method

has been employed to predict various flow patterns in inclined pipeline. Five flow patterns (plug flow, slug flow, wavy stratified flow, stratified mixed flow and annular flow) have been predicted using CFD simulation in upward inclined pipe line. The simulated results are validated with experimental results. It is evident from the present study that VOF method is capable of predicting all the five flow patterns except dispersed flow patterns.

List of Contents

Nomenclature

A	Cross sectional area of the pipe, (m^2)
A_O	Area of oil phase, (m^2)
$A_{oil\ wave}$	Cross sectional area of the oil wave, (m^2)
A_W	Area of water phase, (m^2)
C	Chislom constant (-)
C_d	Drag coefficient (-)
c_W	Water cut (-)
D	Diameter of pipe, (m)
E_O	Eotovs number (-)
f	Friction factor (-)
F_σ	Surface tension force, (Kg/m s^2)
F_d	Drag force acting on a wave crest,(Kg/m s^2)
F_g	Gravity force acting on wave, (m/s^2)
Fr	Froude number (-)
g	Acceleration due to gravity, (m/s^2)
G	Mass flow rate, (kg/s)
Ku	Kutadelaze number (-)
L	Length in deformed wave, (m)
$\dot{m}$	Mass velocity, (kg m^2/s)
Q	Volumetric flow rate, (m^3/s)
Q_O	Volumetric flow rate of oil, (m^3/s)
Q_W	Volumetric flow rate of water, (m^3/s)
Re	Reynolds number (-)
Re	Reynolds number (-)
S	Slip ratio (-)
S_i	Interface length, (m)
S_i	Interface length, (m)
S_O	Wall perimeter of oil phase, (m)
S_W	Wetted perimeter of water phase, (m)
U	Superficial velocity, (m/s)
U	Phase velocity, (m/s)
U_m	Mixture velocity, (m/s)
U_O	In-situ oil velocity, (m/s)
U_{OS}	Superficial oil velocity, (m/s)
U_{SO}	Superficial oil velocity, (m/s)
U_{SW}	Superficial water velocity, (m/s)
U_W	In-situ water velocity, (m/s)
U_{WS}	Superficial water velocity, (m/s)
v	*Volume of liquid, (m^3)*
v	Specific volume specific volume, (m^3/Kg)
We	Weber number (-)

x	Mass quality (-)
X	Martinelli parameter (-)

Greek Letters

ϕ_{fo}^2	Friedel two phase multiplier (-)
τ_i	Interfacial shear stress, (Kg/ms^2)
τ_o	Oil phase shear stress, (Kg/ms^2)
τ_w	Water phase shear stress, (Kg/ms^2)
$\frac{\Delta P}{L}$	Pressure gradient (Pa/m)
ϕ	Two phase multiplier (-)
ρ	Density, (Kg/m^3)
θ	Angle between the surface tension force and the horizontal, (°)
σ	Interfacial tension, (N/m)
λ	Wavelength, (m)
μ	Viscosity, (Pa s)
a	Wave amplitude, (m)
ε	Pipe roughness factor (-)
π	Dimensionless group (-)

Subscripts

bf	Bankoff
c	Continuous phase
ch	Chisholm
chaw	Chawla
d	Dispersed phase
g	Gas
g	Gas
h	Homogeneous
l	Liquid
M	Mixture
O	Oil phase
SO	Superficial oil
SW	Superficial water
tp	Two phase
W	Water phase

Abbreviations

A	Annular flow
ANN	Artificial neural network
B_O	Bubbly flow (oil)
B_W	Bubbly flow (water)
C	Churn flow
CFD	Computational fluid dynamics
$D_{O/W}$	Dispersion of oil in water
$D_{O/W\&W}$	Dispersion of oil in water and water
$D_{W/O}$	Dispersion of water in oil
P	Plug flow
PNN	Probabilistic neural network
R	Rivulet flow
S	Slug flow
SM	Stratified mixed
SS	Smooth stratified
ST	Stratified flow
SW	Wavy stratified
TL	Three layer flow

List of Figures

List of Tables

Chapter 1

Introduction

A major part of all chemical engineering process and operations is concerned with liquid-liquid two-phase flows like solvent extraction, emulsification, oil exploration, cross-country transportation of crude oil, reaction between liquid-liquid two immiscible phases (for example bio diesel production). One of the most economic ways to transport the viscous oil is water lubrication technique to reduce the power consumption and pumping cost. Knowledge of hydrodynamics of two immiscible liquids is important for the efficient design of extractor, reactor and transportation pipeline network, downstream separator, etc. During the flow of two immiscible fluids through pipelines, phases distribute themselves in different interfacial configurations known as flow patterns or flow regimes to minimize their total energy. The flow regime depends on the fluid properties, relative velocities, entrance geometry, pipe diameter, pipe inclination. Same as gas-liquid flows there are many different flow patterns in liquid-liquid flows due to the complex interaction between two phases. But phase inversion, three-layer are the unique appearance in liquid-liquid flow those are absent in gas-liquid system. These are due to difference in physical properties of the gas-liquid and liquid-liquid system. Especially interfacial tension, wetability properties, oil-water viscosity ratio vary widely and the rheological behavior sets this diversification in liquid-liquid two-phase flow.

In petroleum industry, two-phase oil-water flows are important in the production and transportation through sub-sea pipelines. Production of oil from off shore reservoirs also implies the simultaneous production of free water. Transportation of viscous oil through pipes over long distances increases power consumption and pumping cost due to huge pressure drop. The pressure drop depends on the geometry and orientation of the pipeline and flow phenomena occurring in the pipeline. So, prior knowledge about the hydrodynamics of such flow is essential for efficient design of a transportation line.

Growing interest in liquid-liquid flow through pipelines with oil having intermediate viscosity is a consequence of gradual exhaustion of lighter oil and increasing demand for moderate to high viscous oils. From the literature it is evident that there is a lack of adequate understanding of the flow mechanism in liquid-liquid two-phase flow than gas-liquid flows because less work has been carried out on liquid-liquid two-phase flow. Several attempts have been made from the past six decades to understand the hydrodynamics of liquid-liquid flow. Even though there are many publications in liquid-liquid flows but not more on highly viscous oil-water two-phase flow through horizontal and inclined pipes, especially oil having viscosity of intermediate range. The past works on oil-water system having the viscosity of intermediate range are also very limited in inclined pipeline. The present work is mainly confined to study flow patterns, pressure drop and holdup of inclined pipeline. The details of the objectives are mentioned in Chapter 2.

Considering aforementioned facts, the present study aims to carry out the detailed investigation on hydrodynamics of viscous oil-water (intermediate range) flow through 5° upward inclined pipeline. Prior to this, hydrodynamics of the same fluid pair in horizontal pipeline has been studied for better understanding and comparison of the flow phenomena. In the present study, first an attempt has been made to experimentally study the hydrodynamics (flow patterns, pressure drop and holdup) of liquid-liquid horizontal and inclined flows. Visualizations and photographic based techniques have been adopted for the identification of flow patterns in the present study. The flow patterns thus obtained in both the cases (horizontal and inclined) have been represented in the form of flow pattern map. The flow pattern maps of both horizontal and inclined pipelines have been compared to study the effect of pipe inclination on flow patterns. The flow pattern map of horizontal pipeline has been compared with the available data in literature to know the consequence of viscosity on flow patterns. The flow pattern transition boundaries in both the pipelines have been predicted by analytical models. A need was next felt to develop a unified model for the prediction of flow patterns in both horizontal and inclined flows, which would be a kind of nonlinear mapping of physical measurable parameters to flow patterns. It may not required a prior knowledge about the mechanism involved in the transitions. Accordingly, the artificial neural network (ANN) has been adopted for this purpose. The flow pattern maps of both the pipelines been predicted by developed network. The results of both the prediction techniques (analytical and ANN) have been compared to know the best predictive tool of flow phenomena.

Efforts have been made to measure the holdup and pressure drop of horizontal and inclined pipeline. A correlation based methodology has been adopted for prediction of pressure drop in both the cases. Two new correlations have been developed to predict pressure drop in liquid-liquid horizontal and inclined flow. First correlation has been developed by modifying the Lockhart-Martinelli correlation and the other one is from dimensionless analysis based on the Buckingham's Pi-theorem. The measured holdup in both the horizontal and inclined pipelines have been predicted using the available models in the literature. Next an attempt has been made to develop a model to predict pressure drop of annular flow in both horizontal and inclined pipes by considering entrainment fraction. Finally, CFD simulation technique has been applied to numerically simulate the five (plug, slug, wavy stratified, stratified mixed and annular) flow patterns identified in 5° upward inclined pipeline. The simulated results are validated with the experimental result.

The dissertation has been organized in eight different chapters. The first chapter (Chapter 1) i.e. the present chapter deals with introduction, importance and scope of the present work.

The second chapter (Chapter 2) depicts a thorough survey of the relevant past works on horizontal and inclined pipeline. The literature on vertical flow has also been discussed here for getting a comprehensive idea of the past work in the field of liquid-liquid two-phase flow. Then objectives of the present work are mentioned in the present chapter.

The third chapter (Chapter 3) depicts the details of the experimental setup and experimental procedure used in the present study. The different identification and measurement techniques used have also been discussed in this chapter.

The results in the present study have been discussed in chapters four to seven. The fourth chapter (Chapter 4) deals with experimental identification of flow patterns in both horizontal and 5° upward inclined pipeline. A comparison between horizontal and inclined flow pattern maps has been made to find out the effect of such low inclination on flow patterns.

The fifth chapter (Chapter 5) presents prediction of flow pattern maps by analytical and Probabilistic Neural Network (PNN) techniques. The results of both the techniques have been compared to find out the better predictive tool for flow patterns.

The sixth chapter (Chapter 6) gives the measurement of holdup and pressure drop in horizontal and inclined pipeline. The pressure gradient has been predicted using existing and newly developed correlations. An entrainment model has been developed to predict the pressure gradient of annular flow in both horizontal and inclined pipes by considering entrainment occurring at the interface. Holdup of both horizontal and inclined pipelines have also been predicted in this chapter.

The seventh chapter (Chapter 7) presents the numerical simulation of plug flow, slug flow, wavy stratified flow, stratified mixed and annular flow in 5° upward inclined pipeline using VOF technique. Simulated results have been validated with experimental results.

The salient conclusions drawn from the present study as well as the recommendations for future work have been given in the last chapter (Chapter 8) of the thesis.

Chapter 2

Literature review

2.1 Introduction

The increasing importance of liquid-liquid two-phase flow in petroleum and chemical industries is the driving force of the present study. Review of past literature shows that most of the work done in either low or high viscous oil-water flow. Limited works are available on oil-water flow having the viscosity of intermediate range. Similarly, a few studies on hydrodynamics of such oil-water flow through inclined pipeline are available in literature. Due to this reason, an attempt has been made to study the flow of such oil through horizontal and slightly inclined pipeline in the present work. A detailed review of literature on liquid-liquid flow has been presented here. During the survey of the literature, the main attention has been given to liquid-liquid horizontal and inclined pipe flow. The literature on vertical flow has also been discussed here for getting a comprehensive idea of the past work in the field of liquid-liquid two-phase flow. The review brings out the lacunae of the literatures and focuses on the need of the present study.

Research work on liquid-liquid two-phase flow has been started from the past six decades. Till date, a good number of experimental and theoretical works has been carried out in the field of multiphase flow. These studies describe and analyze the hydrodynamics of multiphase flow for various liquid pairs, conduit geometry and conduit orientations. For sake of simplicity, entire discussion have been divided into three major sections, - namely

past literatures in (1) horizontal, (2) inclined and (3) vertical pipelines. In every section, experimental outcomes have been highlighted first then theoretical works have been succeeded. A separate paragraph corresponding to every author has also provided in the following sections to highlight their individual's research which will help to extract the lacuna of the literature.

2.2 Two phase liquid-liquid horizontal flow

The study of liquid-liquid flows is not too long as gas-liquid flows. Interest in oil water flows arose in 1948 by the observation of the lubricating effect during the transportation of highly viscous oil with the injection of small amount of water by Clark (1948) a private communication.

After this work in 1949, **Clark and Shapiro** patented a process of pumping viscous petroleum by injection of water and demulsifying agent into a crude oil pipeline. They carried out experiments in 6-inch inner diameter three mile long pipeline with crude oil and water as test fluids. The viscosity of the oil used was 800-1000 cP. They used demulsifying agent (anionic surfactant) to diminish the emulsification of water into oil and additives to reduce the density difference between oil and water. They reported that injection of 7-24% water with respect to the total liquid reduced the pressure gradient by factors 7.8 to 10.5 and the optimum pressure reduction was occurred at 8-15% water injection. Finally they concluded that the added water has lubricating effect on crude oil during the flow.

After this study, many researchers performed experimental works on hydrodynamics of oil-water flow through pipes. They explored different techniques for identification of flow

patterns, like visual, imaging and probe techniques as well as different methodologies to measure two-phase pressure drop, holdup, entrainment fractions and other hydrodynamic parameters. All these are highlighted here through detailing of the following research works.

a) Experimental estimation of different hydrodynamic parameters:

Russell et a1. (1959) is the first who conducted experiments to study the flow characteristics of two-phase system in smooth transparent (Cellulose Acetate- Butyrate) horizontal pipeline of 0.0203 m internal diameter using white mineral oil (viscosity 18 cP) and water (viscosity 0.894 cP). They performed experiments over a range of input oil-water volume ranges from 0.1-10 at thirteen superficial velocities ranging from 0.116 ft/s to 3.55 ft/sec. They identified bubbly, stratified, and mixed flow patterns by visual observations. They measured the pressure drop in the pipeline with the help of manometer and they correlated the pressure drop with fanning's friction factor. Holdup of the two-phase flow is measured by quick closing valves technique. They reported that in the laminar region holdup is a function of liquid input ratio and viscosity and in turbulent region it is also depends on superficial water velocity.

Like Russell et a1. (1959) some of the authors identified flow patterns by visual observation. Similar works reported by various researchers are discussed as follows.

Charles et al. (1961) investigated equal density oil-water mixtures in 1-in ID pipeline. Oils of viscosity 6.29, 16.8 and 65 were used in their experiments. Flow patterns, pressure drop and holdup were studied for a range of superficial velocity of oil from 0.05 ft/s to 3 ft/s and water superficial velocity ranges from 1 to 3.5 ft/s. They observed flow patterns

various flow patterns such as water drops in oil, oil in water concentric (annular), oil slugs in water, oil drops in water, water drops in oil, water in oil concentric (inverted annular), oil slugs in water and oil bubbles in water by visual and photographic technique. They reported that characters of flow patterns and their relationship to oil-water flow rate are largely independent of viscosity of oils (6.29, 16.8 and 65) although the highest viscous oil showed dissimilar behavior at high oil-water input ratios. They reported that holdup ratio as greater than unity when the water was continuous medium and less than unity or equal to unity when oil phase was continuous. In their study they observed that addition of small amount of water in laminar region (Reynolds number not more than 1500) lowers the pressure drop to a minimum, after which addition of water increases the pressure drop of the system.

Charles and Redberger (1962) reported on the reduction of pressure gradients in oil (high viscous) pipelines with addition of less viscous liquid water. They found that maximum pressure reduction obtained was 12 and 31%. They observed that reduction factors were considerably lower than the experimental values this indicated the wave motion at the interface.

Guzhov et al. (1973) studied flow patterns in 0.039 m inner diameter steel pipe with viscosity ratio of 21.8 and density ratio of 0.898. They identified the flow patterns visually, those are namely stratified and mixed, dispersion of water in oil and oil in water. They also measured the pressure drop for all the flow patterns observed in their study.

Malinowsky (1975) performed experiments in a 38.4 mm Steel pipe with an oil with a viscosity of 4.6 cP, specific gravity of 0.850 and interfacial tension of 22.3 dynes/cm. The

mixture velocity varied from 0.6 m/s to 2 m/s. Dispersed oil in water and dispersed water in oil were the flow patterns observe d by them. Pressure gradients were also measured for different flow patterns.

Oglesby (1979) carried out experiments to study the flow patterns using mixture of SN-250 and Diesel oil No.2 in 0.038 m horizontal pipe and observed flow patterns from segregated to homogeneous with increase in mixture velocity. Oglesby also reported a slug-flow pattern near the point of inversion. There was a drastic change in pressure drop at inversion point and magnitude of pressure drop increases with increase in mixture velocity and oil viscosity.

Ooms et al. (1984) performed experiments to identify core annular flow in horizontal pipeline of 0.05 m and 0.020 m diameter pipelines with difference in density of 30Kg/m^3. They found that core annular flow is less advantageous for large pipe sizes.

Scott (1985) conducted some experiments with oil-water mixture in a large acrylic pipe of diameter 0.0508 m with viscosity ratio of 1.54 and 0.756 density ratio and identified slug, wavy and dispersed flows along withhold up studies.

Cox (1985) studied flow patterns and holdup in large diameter acrylic pipe with low viscous oil having the viscosity ratio of 1.54 and density ratio of 0.756. He noticed slug and dispersed flows in his experimental study. Cox also measured the holdup of various flow patterns to show the effect of holdup on flow pattern of the liquid-liquid flow system.

Oliemans et al. (1987) conducted experiments using 3000 mPa s fuel oil in 0.05m horizontal pipeline to find out the core annular flow. They also studied the wave amplitude

and length of waves at the interface. They found that wave length vary with water velocity and oil fraction. They proposed a correlation to predict pressure gradient of by incorporating turbulence of the surrounded water film.

Arirachakaran et al. (1989) investigated oil-water mixtures in 1 and 1.5 inch pipes to study flow pattern, pressure drop and holdup of oil-water flow through horizontal pipeline. Oils with viscosities of 4.7, 58, 84 and 115 cp were used in the 1.5-in pipe, while the 1-in tests were conducted using 237 cp and 2116 cp oils. They varied mixture velocities from 1.5 to 12 ft/s, while input water fractions ranged from 0.05 to 0.9. They observed stratified, stratified mixed flow, annular flow, intermittent flow and dispersion of oil in water and water in oil flow patterns.

Stapelberg and Mewes (1990) conducted experiments to study the pressure drop and flow pattern in 2.38 and 5.9 cm diameter acrylic and glass pipe with viscosity ratio of 30 and density ratio of 0.852, they observed stratified and mixed flow pattern, dispersed flow pattern (oil in water and water in oil) and wavy flow pattern.

Malhotra (1995) has conducted experiment with LVT 200-water mixture and reported three distinct flow patterns namely bubble, semi-segregated and semi-mixed flow. Bubble flow is observed for a mixture velocity in the range 0.4 - 0.6 m/s and an input oil percentage less than 10%. Semi-segregated flow is observed for an oil cut above 20% and mixture velocity in the range 0.4 to 0.8 m/s; above 0.8 m/s semi-mixed flow is observed. The volume occupied by the oil/water dispersion increases with an increase in mixture velocity. For velocities greater than 1.4 m/s almost homogenous mixture is obtained.

Extensive work on the variation of water percentage across a pipe cross section for two different oils (viscosity 2 cp and 100 cp) in horizontal pipes was also done.

For the high viscosity oil, not much mixing was observed at the interface. The viscous oil layer held up in the pipe occupying a much greater cross section than that calculated based on the input water cut. This results in a slow-moving oil phase and the compressed water phase at the bottom travels at a very high velocity. The in situ water layer velocity was three times the mixture velocity for certain water cuts. The increased water layer velocity leads to higher corrosion rates.

Andreini et al. (1997) conducted experiments in two small diameter horizontal pipes having the inner diameter of 0.3 and 0.6 cm by varying the pipe materials (borosilicate glass, steel, copper and PVC). The viscosity of oils used in their study are 562, 920 and1307 respectively. The observed flow patterns are plug flow, slug flow, water annular flow and dispersion of oil in water flow pattern. They also measured the pressure drop of all the flow patterns. They observed the variation in transitions of various flow patterns by changing the viscosity of the oil and pipe material as well.

Hapanpwicz et al. (1997) experimentally studied the effect of pipe diameter on flow pattern using three different pipes. They used 1.2, 1.6, 2.2 cm glass pipes for their study to identify flow patterns of moderately viscous oil with oil-water viscosity ratio of 40 and two different densities (0.915 and 1.2). They observed plug flow, stratified flow, dispersion of oil in water, dispersion of water in oil, dispersion of oil in water and water, dispersion of water in oil and water and dispersed annular flow pattern in their study.

Beretta et al. (1997b) conducted experiments in horizontal pipe of 3mm inner diameter with three different viscous oils to know the effect of viscosity on pressure drop. They noticed that a significant reduction in pressure loss because of favorable water "lubrication effect" in small diameter pipes in the "Y" section of the glass. They reported that an injection of small amount of water can produce a sensible reduction of pressure losses. From their experiments they concluded that high pressure loss reduction can be obtained at higher oil viscosity.

Bannwart et al. (2004) carried out experiments in 0.028m inner diameter horizontal and vertical pipeline using viscous crude oil of viscosity 488 mPa s and 925.5 Kg/m^3 density to identify various flow patterns. With the aid of special inlet device, many different flow patterns were identified by visual observation. However in their study continuous oil flow patterns are not observed due to high viscosity of the oil used in the experiments. In horizontal flow the basic flow patterns include stratified, bubbles, dispersed bubbles, intermittent and annular flow patterns were identified. They reported that core annular flow will tend to occur in a pipe when the fluids have very dissimilar viscosities but relatively close densities. This is often satisfied by heavy oils, crude or refined, since their viscosity is greater than 100cP.

Al-Yaari and Abu-Sharkh (2011) performed experiments in 0.025m inner diameter acrylic horizontal pipeline with oil (viscosity 0.00157 Pa s) and water to investigate flow patterns. They observed stratified flow patterns, three layer and dispersed flow patterns by visual observation. They have predicted the flow patterns using CFD analysis which is discussed in the respective section.

Latter on visual techniques was supplemented with imagining techniques due to the limitations of visual observation techniques. The visual observation methodology fails at higher flow rates and also at the transition of the one flow pattern to another one. Practically researchers adopted both the methods for identification of flow patterns and their transitions. Following section is the summery of such research works.

Fujii et al. (1994) conducted experiments to study flow patterns pressure drop and void fraction of silicon oil (55cp) and water flow through horizontal pipeline of 0.025m inner diameter acrylic pipe. They observed flow patterns by visual and high speed video techniques. The flow patterns identified are as follows slug flow, bubbly flow, annular flow, inverted slug flow, inverted bubbly flow and inverted annular flow. They measured holdup by quick closing valves technique.

Trallero et al. (1997) carried out experiments to study the oil-water flow pattern transitions and pressure drop in horizontal pipe in a transparent test section of 0.05m inner diameter and 15.54 m long acrylic pipeline with oil-water having viscosity ratio of 29.6 and density ratio 0.85. Flow patterns were identified by photographic and low speed video techniques. They measured the pressure drop by three differential pressure transducers in addition to this a validyne gauge pressure transducer has been used. They identified six different flow patterns and classified them into two groups such as segregate flow and dispersed flow and also predicted flow pattern transitions using two fluid model and a balance between gravity and turbulent fluctuations normal to the axial flow direction. Stratified flow has been predicted by the viscous Kelvin-Helmholtz analysis while inviscid KH theory predicted the stratified mixed flow pattern.

Beretta et al. (1997a) performed experiments to identify the flow regimes in small diameter tubes (3mm) horizontal pipeline. They used demineralized water and three oils having different viscosities were used in their study to observed flow patterns in 'Y' section of the glass. The flow regimes were observed by photographic technique such as dispersed flow, slug flow, bubbly flow, plug flow and annular flow in their experimental study. They also proposed a correlation to predict the transition boundaries of the flow patterns which is given in the respective section.

Simmons and Azzopardi (2001) performed experiments to identify flow regimes and to measure drop size and velocity distribution in a large diameter (0.063m) PVC pipe. They used lower viscous oil (1.12mPa s) and water as their test fluids and identified stratified mixed, dispersion of water in oil and water and dispersion of water in oil flow patterns in their experimental study. They compared their experimental results to the flow pattern map proposed by Trallero et al. (1997).

Raj et al. (2005) performed experiments in 0.025m inner diameter perspex horizontal pipe using kerosene and water as test fluids to study glow patterns and hold up. They used a mixer arrangement at the inlet section to study the flow patterns. For this they conducted experiments for different combinations of velocities of two fluids ranging from 0.03 m/s to 1.6 m/s. both photographic and visual observation techniques have been used for the identification of flow patterns. They identified smooth stratified, wavy stratified, three layer stratified and dispersed flow patterns in their study. They experimentally measured the holdup of the oil-water system. They modified existing correlation to predict holdup that is discussed in the next section.

Chakrabarti et al. (2005) investigated the pressure drop and flow pattern characteristics during the simultaneous flow of kerosene-water mixture through a 0.025m PMMA pipe. A 24PCB Honeywell differential pressure transducer is use to measure the pressure drop in the pipeline. Flow regimes were identified by visual and photographic technique. The regimes encountered in the experimental range studied were smooth stratified, stratified wavy, three layer flow, plug flow, and oil dispersed in water, and water flow patterns.

Wegmann and Rohr (2006) performed experiments in two small diameter pipes (0.0056 and 0.007 m) glass pipe with water and paraffin oil as test fluids. They varied the rage of viscosity from 4.3 mPa s to 5.2 mPa s. They identified flow patterns by visual and Photographic techniques. They observed stratified flow, intermittent flow, annular dispersed flow and dispersed flows in their study. Resultant flow pattern map has been compared with other flow pattern maps in the literature. They compared their results with the bigger diameter pipes than their study they reported few differences. Stratified flows occur in a much smaller region than the larger pipes. This is due to the interaction of interfacial tension forces and gravitational forces. Dispersed flows were observed at higher mixture velocities than bigger pipes. The specific surface area is related to the degree of turbulence, which is quantified by Reynolds number. Higher the Reynolds number higher the turbulence, so in smaller pipes high velocities are required to create turbulence. Here they mentioned three most important properties (density ratio, viscosity ratio and interfacial tension) and their effects on the flow patterns.

Rodriguez and Oleimans (2006) carried out experiments in a large diameter (0.0828 m) steel horizontal pipe and inclined pipe to identify flow patterns, measure pressure gradient and hold up using oil of viscosity 7.5 mPa s and water as experimental fluids. The

characterization of flow patterns and its transition boundaries was achieved via visual observation of recorded movies and by analysis of its deviation for homogeneous behavior. Holdup of each fraction was measured by gamma rey densitometers. They observed stratified, stratified mixed and dispersion of oil in water and dispersion of water in oil flow patterns in their experimental study. Pressure gradient and holdup of the system were predicted using two fluid model for stratified flows and homogeneous model for dispersed flows.

Mandal et al. (2007) conducted experiments to find out the effect of conduit diameter on flow regimes of two phase liquid-liquid flow and also the mixer geometry. They selected 0.025m and 0.012m inner diameter PMMA horizontal pipe for their experimental study. They carried out experiments using kerosene (ρ =787 Kg/m^3; μ =1.2 mPa s) and water as fluids. The flow patterns were identified by visual and photographic techniques in both the pipes. They observed smooth stratified, plug, wavy stratified, oil dispersed in water, white emulsion, and three layer flow pattern in 0.025m pipeline. They did not identified slug, churn, rivulet flow patterns in 0.025m pipeline. Wavy stratified and there layer flow pattern were absent in 0.012m pipeline. They reported that changes in the flow patterns may be due to increase effect of contact angle in the narrow pipe. The design of the mixer section also appears to influence the downstream distribution of the two liquids and the flow pattern map may change remarkably merely by changing the way of introducing the two fluids in the test rig.

Al-Wahaibi and Angeli (2007a) studied the characteristics of waves at the interface oil-water stratified flow and at the onset of entrainment both experimentally and theoretically. The experimental studies on the onset of entrainment were carried out in a 38 mm ID

stainless steel pipe with 'Y' junction as inlet. Oil and water were used as test fluids with viscosity ratio of 5.5 and density ratio of 828. High speed video recording was used to identify the onset of entrainment occurring from oil-water stratified flow. They observed stratified, dual continuous and dispersed flow patterns in their study. They also conducted theoretical study which is given in the respective section.

Al-wahaibi et al. (2007b) investigated conditions and mechanism of drop formation at the interface of oil-water stratified flow that leads to the onset of drop entrainment and transitions to dual continuous flow pattern both in experimentally and theoretically. Experiments were conducted in 0.014m acrylic pipe to capture the drop formation of oil (5.5 mPa s and 828Kg/m^3) and water stratified flow in horizontal pipe. Stratified, dual continuous, slug, bubbly and annular flow patterns were identified by high speed video imaging technique.

Yiping et al. (2008) experimentally studied segregate flow pattern in 26.1 mm diameter stainless steel pipe with diesel oil (viscosity 3.47 mPa s and density 838 Kg/m^3) and water. Insitu phase fractions are measured by conductance probes. They observed stratified smooth, stratified mixed, three layer, dispersion of water in oil and oil and dispersion of oil in water and water flow pattern by videography technique. They developed a model to predict pressure drop the details are given in the particular section.

Sotgia et al. (2008) carried out experimental study of water continuous oil-water flow in horizontal pipes using mineral oil and tap water of viscosity ratio about 900 and density ratio 0.9. A set of seven different pipes of perspex and plexi glass were used with diameters ranging from 21 mm to 40 mm. Identification of flow patterns and its transition

boundaries is performed by visual observations and also by photographic and video techniques. They investigated wavy stratified, annular, transition and dispersed flow patterns in both the pipes, but slug flow was absent in 40 mm Pyrex pipe. Experimental results were compared to a model devised by Brauner (1991) and Arney et al. (1993) for pressure drop of annular flow.

Grassi et al. (2008) experimentally studied the pressure drop and flow pattern of oil-water in horizontal and slightly inclined pipes. They used oil-water system with viscosity ratio of 800 and density ratio of 886. The test pipe consists of six transparent poly carbonate tubes of 21mm inner diameter pipes. Flow patterns were identified by visual and photographic technique. They predicted pressure drop of annular flow by the two fluid model proposed by Brauner (1991) and dispersed flows using homogeneous flow model.

Poesio (2008) conducted experiments to study oil-water slug flow in high viscous oil (viscosity 1200 mPa s) - water (viscosity 1 mPa s) 0.021m inner diameter glass pipe. Flow regimes were determined by visual and photographic technique. A differential pressure transducer is used to measure the pressure drop in the test section. He noticed dispersed, slug, core annular and stratified flow in their study. Measure pressure drop of slug flow has been predicted using existing models in the literature. Slug frequency has been measured and predicted using the original relation proposed by Greskovich and Shrier (1972).

Al-wahaibi and Angeli (2009b) carried out experiments to study the transition from stratified to dual continuous oil-water as well as the dispersed phase fractions in the layers of dual continuous patterns. The studies were carried out in a 38 mm ID horizontal stainless steel test section using two different inlet geometries a T- and a-Y junction in

acrylic section. Transition to dual continuous flow pattern was identified using high speed video camera. Entrainment fraction was measured using impedance probe technique. They reported that onset of entrainment was found to occur at lower superficial velocities as the superficial oil velocity increased, while there is no significant difference between the two inlet geometries. The entrained fraction of water in the oil layer was increased with increase in water velocity. The entrainment fractions were higher when in T-inlet and the difference increased with increasing oil and water velocities.

Poesio et al. (2009) performed experiments to study the effect of air injection on pressure drop of liquid-liquid annular flow in horizontal pipeline. They conducted experiments in two different test sections one is 21mm ID glass test section with tap water, air and oil with viscosity of 1200 mPa s and a density of 886 Kg/m^3 is used. Oil (U_{SO}= 0.03-0.7 m/s) and water (U_{SW}= 0.1-2.6 m/s) superficial velocities are varied by keeping air velocity constant at U_{SA}= 0.29 m/s. the other set up is glass pipe with 28 and 40 mm ID horizontal pipeline with oil viscosity of 900mPa s. oil water and air superficial velocities are in the ranges U_{SO}= 0.46-1.08 m/s, U_{SW}= 0.04-0.67 m/s and U_{SA}= 0.06-4m/s. They also proposed a model for the pressure drop prediction the details are presented in that particular section. **Rodriguez et al. (2009)** conducted experiments to measure the pressure drop of core annular flow in horizontal and vertical pipeline of 28mm ID 2.5 m length glass tube with tap water and crude oil of 500mPa s and 925kg/m^3 and 77mm ID 274m length steel pipeline conveying an ultra-viscous crude oil (36,950 mPa s and 972.1 5kg/m^3). Core annular flow pattern was identified by high speed camera. They predicted pressure gradient using existing correlations.

Balakhrisna et al. (2010) experimentally studied the effect of sudden expansion and contraction on flow pattern using lubricating oil (0.2 Pa s), kerosene (0.0012 Pa s) and water as experimental fluids in horizontal test section. The flow patterns for different combinations of oil and water are observed visually and photographically with high speed camera. Honey well differential pressure transducers have been used to measure the pressure difference. They used two acrylic test rigs, both consists of acrylic resin tubes of diameter 0.0254 and 0.012, in first test section larger pipe is followed by smaller one and in the other one is reverse. They identified various flow patterns like thick core flow, thin core flow, plug, distorted plug and oil dispersed flow in lube oil-water system. In kerosene-water system stratified smooth, stratified wavy, plug flow, three layer flow, kerosene dispersed flow, water dispersed flow patterns were identified. They reported that interfacial distributions are more pronounced fro lube oil-water system than kerosene-water system. Thick core configuration can be established by sudden expansion in the horizontal flow path. On the other hand thickness of the core is reduced by the contraction of the flow path.

Chakrabarti et al. (2011) carried out oil-water two phase flow experiments in 0.025m ID Perspex pipe to investigate various flow patterns using kerosene and water. They observed flow regimes by visual and photographic technique. They also predicted the flow patterns identified, which is reported in that particular section.

Yusuf et al. (2011) studied effect of oil viscosity on flow structure and pressure gradient of oil-water flow through 25.4 mm acrylic pipeline has been investigated experimentally. They conducted experiments with oil of viscosity 12 cP and tap water as experimental fluids in a Y junction. High speed camera and visual observations were used to identify the flow patterns and its transitions during the flow. The pressure drop in the test section was

measured by digital differential manometer. They reported that at lower oil velocities the water velocity required to initiate the transition from stratified to non stratified increased as the oil viscosity increased. They observed large variation in pressure gradient with increase in oil viscosity. They proposed a simple correlation to predict pressure gradient of oil dispersed in water flow pattern which is given in the respective section.

Al-wahaibi et al. (2012) investigated the effect of oil and water velocities, pipe diameter and oil viscosity on the transition from stratified to non-stratified patterns experimentally. The investigations were carried out in acrylic test section with 25.4 and 19 mm ID with water and two oil viscosities (6.4 and 12 cP) as test fluids. A high speed video camera is used to study the flow structure and its transition. They reported that the transition was found to occur at lower water superficial velocities as the superficial oil velocity increased. Bubbly flow was found when the Eotovs number is greater than one while it disappeared when the number is less than one. They found that pipe diameter has significant effect on the transition between stratified and non stratified flow. At certain oil velocity, water superficial velocity required to form bubbly flow increases as the pipe diameter increased. This is due to the decreased contribution of interfacial effect with pipe diameter. On the contrary water superficial velocity required to initiate transition to dual continuous flow decreased as the pipe diameter increased. The maximum wave amplitude in the stratified region and up to the transition to non stratified region was measured and correlated with the mixture velocity.

Even after getting good result with imaging techniques some of the researchers used probe techniques for the better accuracy in measurement of hydrodynamics parameter of liquid-liquid two-phase flow. They used either intrusive probes like conductivity and capacitance

probe or nonintrusive probes like optical probes, γ-ray, X-ray etc. techniques. The outcomes of those works are discussed below.

Valle and Kvandal (1995) studied pressure drop and dispersion characteristics of oil-water flow through glass pipe of diameter 3.75 cm and the viscosity and density ratios were 2.55 and 0.792 respectively. They measured the pressure drop, hold up and also studied about the conductivity and sampling probe techniques. Flow patterns found are stratified, stratified and mixed, dispersed flow (oil in water and water in oil) and wavy flow pattern.

Angeli (1996) experimentally studied flow patterns and pressure drop in 0.0243 m inner diameter stainless steel horizontal pipe with low viscous oil (1.6 mPa s) and water as test fluids. She identified stratified wavy/drops and there layer flow by visual and impedance probe technique.

Nadler and Mewes (1997) conducted experiments of two immiscible liquids in a horizontal pipe with an inner diameter of 59 mm and a total length of 48m Perspex horizontal pipeline to know the effect of emulsification and phase inversion on pressure drop for different flow regimes. Viscosities of the liquids are varied by changing the temperature of liquid phases in the rage of 18° to 30°. In the present study the range of viscosities used are from 35 to 28 respectively. They identified stratified flow, stratified mixed flow, unstable water in oil emulsions, unstable oil in water emulsions and dispersion flow patterns. They identified phase inversion and emulsion by changes in the conductance of the oil-water mixture. They reported that phase inversion takes place within the dispersion layers and hence only in a restricted part of the cross-sectional area of the pipe.

by contrast “emulsion” takes place within the whole pipe cross sectional area and results only one continuous liquid phase flowing in the pipeline, while the second phase completely dispersed in the first phase.

Vedapuri et al. (1997) studied hold up and flow pattern for oil water mixture in plexi-glass pipe of diameters 10, 12 cm with oil of 2 cP viscosity and standard ASTM salt water. The flow patterns observed are stratified and mixed, dispersed flow (water in oil and oil in water). They also carried out isokinetic probe technique.

Hamad et al. (1997) studied liquid-liquid flow using kerosene and water with the help of tow optical probe system for the measurement in liquid-liquid flow. They applied signal analysis technique for bubbly flow of kerosene-water flow to measure volume fraction.

Kurban (1997) conducted experiment in 2.43 and 2.4 cm steel and acrylic test section using low viscous oil having viscosity of 1.6 cp to study the flow patterns and pressured drop of liquid-liquid two phase flow through horizontal pipe. He used conductivity and impedence probe technique to identify flow patterns and pressure drop of the oil-water system. He observed stratified flow, stratified mixed flow and dispersion of oil in water flow pattern using the above mentioned technique.

Valle and Utvik (1997) conducted experiments in a steel pipe of inner diameter 0.0762 m to study the pressure drop and flow pattern using conductivity probe. They used low viscous oil-water system with viscosity ratio of 1 and 0.741 density ratio. They observed stratified flow, dispersion of oil in water and dispersion of water in oil flow patterns. They also studied the pressure drop of all the flow patterns using conductivity probe.

Angeli and Hewitt (1998) experimentally studied the effect of pipe material on pressure drop of low viscous oil-water two-phase flow through horizontal pipeline. They conducted experiments in 1-inch nominal bore horizontal test section made from stainless steel and acrylic pipe material with oil having viscosity of 1.6mPa s viscosity and 801 Kg/m^3 density. Pressure drop was measured with Validyne DP45 variable reluctance differential pressure transducer with variable diaphragm. Pressure gradients were measured in both pipes for mixture velocities ranging from 0.3 to 3.9 m/s for input water volume fraction ranging from 0 to 100%. They reported that material of the tube wall strongly influence the pressure gradient during the two phase liquid-liquid flow. The pressure gradients measured in the acrylic tube were lower than those measured in steel pipe. However the difference were often much greater than what would be expected from the difference in tube roughness. They observed significant drag reduction in both the pipes for oil continuous flows.

Soleimani (1999) performed experiments using less viscous oil with viscosity ratio of 1.6 and density ratio of 0.803 in a 0.0243m inner diameter stainless steel pipe to study the flow patterns, pressure drop and holdup using high frequency impedance probe and gamma densitometer. They observed stratified mixed and dispersion of water in oil and oil in water flow pattern. They identified flow patterns using impedance probe technique.

Angeli and Hewitt (2000) carried out experiments to study the flow structure occurring during the concurrent flow of oil (1.6mPa s viscosity and 801 Kg/m^3 density) and water in two 1-in nominal bore horizontal test sections of stainless steel and acrylic resin respectively. They used two flow determination techniques namely high speed video recording technique and determination of local phase fractions with high frequency

impendence probe and the continuous phase in the dispersed flows was recognized with a conductivity needle probe. They conducted experiments for mixture velocities varying from 0.2 to 3.9m/s and input water volume fractions from 6% to 86%. They mainly aimed at the influence of the pipe wall material on flow behavior. They observed stratified wavy flow pattern, three layer flow pattern, stratified mixed flow pattern, stratified wavy with drops flow pattern, fully dispersed or mixed flow patterns were identified in both the pipes. They reported that they observed narrow stratified wavy region in the steel tube and the mixed region started at lower velocities than in acrylic pipe. They identified a wide range of oil continuous flow patterns such as stratified mixed, three layer flow patterns in acrylic pipe this is may be due to the different wettability characteristics of the pipe material used in their study.

Lovick et al. (2000) studied flow pattern, pressure drop and hold up of oil-water system with viscosity ratio of 5.25 and density ratio of 0.828 in 0.038 m inner diameter stainless steel horizontal pipeline. They used conductivity probe technique to study the hydrodynamics of the oil-water system. They observed stratified flow, stratified mixed flow pattern, dispersion of oil in water and dispersion of water in oil flow patterns.

Fairuzov et al. (2000) conducted to study the flow pattern and volume fraction in a large diameter (36.35 cm) steel horizontal pipeline using low viscous oil-water system (viscosity ratio 5.07 and density ratio 0.853). They identified stratified flow, dispersion of oil in water and water flow patterns in their study. In their study they used multi-point sampling probe technique to measure volume fraction of oil-water flowing through the pipe.

Angeli et al. (2002) experimentally studied the flow pattern, pressure drop and phase distribution in a stainless steel pipe of 0.038m inner diameter horizontal pipeline. They used 5.25 mPa s viscous oil and water as test fluids. They used video and probe (impedance and conductivity) techniques to identify flow patterns. They observed stratified wavy, dispersion of oil in water, dispersion of water in oil and oil in water and dispersion of water in oil flow pattern in their study.

Liu et al. (2004) investigated flow patterns and their transitions of oil-water systems in a 40 mm inner diameter pipe. In a similar way to Angeli and Hewitt (2000) they used both a stainless steel and a plexi-glass pipe. Additionally, they developed semi theoretical transition criteria to predict the transition lines.

Lovick and Angeli (2004) studied the dual continuous flow pattern (both phases retain their continuity at the top and bottom of the pipe while there is inter dispersion), which occurs during the pipe flow of two immiscible liquid phases was studied in detail, and pressure gradient, insitu volume fraction and phase distribution were also examined. The experimental work was performed in a 0.038m diameter stainless steel test section using water and oil (6 mPas viscosity and 828 Kg/ m^3) as test fluids. The dual continuous flow pattern was identified by impedance and conductivity probe technique. Pressure drop was recorded using a differential pressure transducer (Validyne DP103). The average insitu phase volume fractions were measured using quick closing valves technique. They observed stratified wavy, dual continuous flow, dispersion of oil in water and dispersion of water in oil flow patterns in their study. They reported that dual continuous flow appeared at intermediate mixture velocities for a range of input oil fractions between the stratified

and dispersed patterns. The standard two fluid model was unable to predict pressure gradient and holdup of the dual continuous flow.

Chakrabarti et al. (2006) conducted experiments to study the transition from oil continuous to water continuous flow pattern in 0.0254 inner diameter PMMA horizontal pipe. In their study they developed a flow pattern indicator to identify phase inversion during liquid-liquid two phase flow. They used optical probe for this purpose. Experiments were performed using kerosene and oil as test fluids. At lower velocities they used photography technique and at higher velocities optical probe technique has been used. The probe works based on the difference in optical properties of the two liquids. Recoded signals during the oil-water flow through the pipeline has been analyzed using statistical analysis of the random signals namely by the probability density function (PDF), and the wavelet multi resolution technique have been used to detect phase inversion of the flow patterns. The indicator denotes the distribution to invert from an oil in water dispersion to water in oil dispersion when the PDF shifts to V/V_{max} =0.5 and the skewness changes sign. The PDF spread is also maximum under these conditions. The study has also revealed the presence of inverted plug flow and inverted dispersed flow when the oil is the predominant liquid in the conduit. The ambivalent range as predicted in the present study is in close agreement to the results reported in literature.

Jana et al. (2007) developed a non-intrusive optical probe for the identification of flow patterns during the liquid-liquid two-phase flow through a conduit. It is based on the difference in optical properties of the respective phases and works on the basis of the proportion of light attenuated and scattered by the two phase mixture. Experiments were conducted in two different test rigs (horizontal and vertical) of same diameter (0.025m

perspex pipe using kerosene and water as test fluids. They observed separated, mixed and dispersed flow patterns using this optical probe technique. They analyzed the signals by PDF analysis.

Chakrabarti et al. (2007) investigated stratification during the simultaneous flow of two immiscible liquids through horizontal conduit. For the identification of various flow patterns an indigenous developed unique optical probe has been used. Experiments were performed in 0.025m PMMA horizontal pipeline using kerosene and water as test fluids. Flow phenomena was identified by photographic and also probe techniques. The probe signals for different patterns have been quantified by means of the moments of the probability density function and wavelet multi resolution analysis. The flow pattern map constructed form the objective indicator consist of smooth stratified, stratified wavy, three layer and dispersion of oil in water flow patterns. They reported that closer agreement with the flow pattern map available in the literature reveals the effectiveness of the objective flow pattern indicator for liquid-liquid horizontal flows.

Demori et al. (2009) proposed a sensor system for the oil fraction estimation in a two phase oil-water flow. The estimation is based on the capacitance measurement between the electrodes flush-mounted on the external surface of nonconductive section of the pipe. The system has been realized and experimentally tested and reported good results.

De et al. (2010a) performed experiments to investigate phase inversion in a small diameter (0.012m) horizontal pipeline using kerosene and water as test fluids. The flow phenomenon has been identified using optical probe, pressure drop measurements and isokinetic sampling probe technique. They conducted experiments for mixture velocities

ranging from 1 m/s to 2.5 m/s. they reported that the transition from oil-in-water to water-in-oil occurs via emulsified homogeneous mixture at high velocities.

De et al. (2010b) conducted experiments in 0.012m inner diameter perspex pipe with low viscous oil (viscosity 1.2 mPa s) and water in horizontal pipeline. They used visual observation, optical probe and isokinetic sampling probe techniques to identify flow patterns. The probe signals have been analyzed by probability density function and fast Fourier transformation methods. They identified a new flow pattern named rivulet flow pattern in their experimental study. They predicted pressure drop and hold up of rivulet flow by drift flux model and two fluid model. They stated that this type of flow pattern has not been reported in the literature in larger pipes.

Kumara et al. (2010a) used single beam gamma densitometer for measuring water holdup in oil-water flow through horizontal pipeline. They performed experiments in 56 mm diameter stainless steel pipe using Exxsol D60 oil (viscosity 1.64 mPa s, density 790 Kg/m^3) and water as test fluids. They measured water hold up, and frictional pressure drop data are measured.

Xu et. (2010) carried out experimental investigation on the pattern transition and hold up behavior of oil-water flow through 20 mm diameter acrylic pipe using diesel (3 mPa s viscosity and $830Kg/m^3$ density) and tap water. Flow patterns and their transition boundaries were achieved via visual observation, video technique and also by conductance probe. They identified stratified, stratified mixed and dispersion flow patterns. They predicted the transition boundaries and hold up of the flow patterns using various two fluid model and homogeneous flow model for dispersed flows.

Mandal et al. (2010) investigated slug flow in acrylic vertical, horizontal and in an undulated pipeline of liquid-liquid flow. For this the experiments have been performed in narrow (0.012 m ID) vertical and horizontal pipes and an undulated pipe of 0.025m ID. Kerosene and water have been selected as test fluids and optical probe technique and visual observation have been used to identify flow patterns. They compared the flow pattern maps of their study with other literature flow pattern maps.

El-sebakhy (2010) used a new technique named neuro-fuzzy inference system learning scheme to predict flow pattern and liquid holdup. He implemented this technique using different real world industry database. He carried out comparison studies with most popular existing approaches in identifying flow regimes and liquid holdup, which showed that neuro-fuzzy is flexible, reliable and outperforms the existing techniques.

Wang et al. (2011) experimentally studied flow patterns, pressure drop and hold up of oil-water flow through a steel pipe of 50m length in 0.025 m inner diameter pipe. They used high viscous crude oil with viscosity 628 mPa s and water collected from an oil field are used as test fluids. Flow patterns were identified by visual and sampling probe technique. Pressure drop has been measured by differential pressure transducer and insitu water volume fraction has been measured by quick closing valves technique. They premixed the two fluids before entering the test section. They compared experimental results with those of literature data available to for model oil (same viscosity as crude oil) to show the difference between the two oil flow characteristics. They observed various flow patterns like emulsion of water in oil dispersion, emulsion of water in oil partial segregated flow, emulsion of water in oil and water stratified flow, water and emulsion of water in oil semi

annular flow and water and emulsion of water in oil annular flow patterns. The insitu hold up and pressure gradient data has been compared with model oil data.

Al-Wahaibi and Angeli (2011) investigated the interfacial wave characteristics in oil-water stratified flow at the transition to dual continuous flow. Experimental investigations were carried out in a stainless steel test section of 38 mm ID pipe with water and oil (density 828Kg/m^3 and viscosity of 5.5mPa s) as test fluids. Wave characteristics were observed by high speed video camera and a parallel wire conductance probe. They conducted experiments 2m and 6m apart from the inlet section. They reported that no drops formed when there were no interfacial waves. The amplitude of waves increased as the superficial velocities increased. At the onset of entrainment the relative velocity between the oil and water are the main factors determining the wave amplitude and length.

Strazza et al. (2011) conducted an analysis of high viscosity oil-water flow through horizontal and slightly inclined pipeline. The test pipe consists of six transparent Plexiglas tubes with 21mm I.D. and six glass tubes with 22 mm I.D. The fluids used are high viscous oil with viscosity of 900 mPa s and tap water. A capacitance probe is used to collect the holdup data and differential pressure transducer (GE Druck STX 2100) for pressure drop measurement. They identified oil in water dispersion, core-annular flow and oil in water dispersion, core annular flow in both the test sections.

Yaari et al. (2012) experimentally studied the effect of drag reduction polymer on water hold up in 2.54 cm Plexiglas pipe of oil-water flow. Oil with viscosity 1.57 cP and tap water were used as test fluids for the measurement of holdup. They used conductivity probe for water holdup measurement. They reported that water holdup for the case of oil-

water with drag reduction polymer is larger than that for the case of without drag reduction polymer.

Morgon et al. (2012) carried out experiments in stainless steel pipe of 0.0254 m inner diameter with kerosene and glycerol solutions. They used a non intrusive optical visualization technique namely laser induced florescence technique to identify the flow patterns and also for estimating the distribution and the droplet size in two phase flow. They observed eight flow patterns in their study.

Xu et al. (2012) used a novel conductance sensor to measure the water holdup in oil-water stratified flow. The array consists of 24 needle like electrodes. The relation between water holdup and level of the oil-water interface. They conducted experiments in cylindrical metal pipe with inner diameter 125 mm and length 300 mm. A stainless steel pipe of outlet diameter 40 mm was installed coaxially with the cylindrical metal pipe.

Morgan et al. (2013) conducted experiments to study the flow characteristics of liquid-liquid flow through 1-inch stainless steel circular pipeline. They used Exxsol D80 oil and homogeneously mixed solution of glycerol and water. They used high speed planar laser induced fluorescence (PLIF), Partcial Image Velocimetry (PIV) and Particle Tracking Velocimetry (PTV). They observed eight different flow patterns in their experiments by using above mentioned techniques. They also measured phase distribution, phase fraction, interface level, drop size and velocity profiles and they compared their measurements with square cross section results and simple laminar models.

b) Theoretical studies on prediction of hydrodynamic parameters:

Apart from the experimental studies conducted by various authors, some of the researchers theoretically studied to find out the physics behind a hydrodynamic phenomena and to predict the hydrodynamic parameters. For this they approached empirically or fully theoretically or combination of both. Complex analysis like ANN, CFD, etc. also are used for these purpose. The details of such works are mentioned here. Whole discussion has been classified in two categories,- (1) first one is related to flow patterns and their transition, (2) second one is prediction of holdup and pressure drop.

(1) Flow patterns and their transition

Brauner and Maron (1992) proposed models to predict flow pattern transition boundaries in liquid-liquid system based on mechanistic models. They incorporated all the geometric and physical properties of fluids. The correlation to predict stratified flow pattern to others (annular or intermittent) has been derived based on stability analysis of the flow pattern. They also given criteria for annular/slug transition in their work. The transition boundary between stratified-dispersed transition criteria is the drops of lighter phase agglomerate at the upper cross-section due to buoyancy and tens to stick together. However the drops may contain their shape so that surface tension forces overcome those due to buoyancy, the balance yields the critical diameter. They also mentioned the transition criteria for dispersed flows in terms of maximum dispersed phase diameter.

The study by **Brauner and Moalem Maron, (1993)** attempted to propose a form of interfacial shear, which incorporates an explicit functional dependence on the interface slope due to interfacial waviness. The implementation of the proposed model as a closure law in the stability analysis of stratified flows was found to reveal the crucial role of the dynamic term in

determining the stability characteristics. They had shown that the inclusion of the newly proposed dynamic term of interfacial shear can predict the stratified-smooth/stratified-wavy transitional boundary (Brauner and Moalem Maron, 1992) satisfactorily for a wide range of two-fluid systems.

Beretta et al. (1997a) predicted the transition boundaries of intermittent and annular flow. Dispersed/intermittent transition is characterized by an in-situ holdup of ε = 0.2-0.3, where ε is the ratio of oil superficial velocity to the total superficial velocity (oil and water):

$$\varepsilon = \frac{U_{OS}}{U_{OS} + U_{WS}} \tag{2.1}$$

The transition between intermittent and annular flow for laminar-laminar regime is predicted using the following equation:

$$U_{OS} = \frac{2 + k + \sqrt{(2+k)^2 - 4}}{2} U_{WS} \tag{2.2}$$

Where $k = \mu_w / \mu_O$

They reported that the theoretical and experimental transition boundaries are matched fairly well.

Brauner et al. (1998) developed a tool for predicting stratified flow with curved interfaces. They used two fluid model for modeling stratified flow with curved interfaces. The solutions of two fluid model are used to construct 'flow monograms' which provide a relation between a specified interface curvature and the in-situ holdup under given

operating conditions. Interface curvature is obtained by invoking the principle of minimal total system energy. The combination of 'interface monogram' and 'flow monogram' yields an 'operational monogram' which gives the complete solution, it includes the interface shape, in-situ holdup and pressure drop. For laminar-laminar, turbulent or mixed flow regimes in two phase flow. They verified experimental data obtained by Valle and Kvandal (1995) for stratified flow.

Brauner (2001) suggested a unified approach for predicting the transition to dispersed flow pattern transition boundary. It is based on the revised models for predicting the maximal drop size in turbulent filed which account for holdup of the dispersed phase. The transition to dispersed flow pattern takes place when the continuous phase turbulence is sufficiently intense to break the dispersed phase into droplets smaller than the critical size. Thus the transition criterion is

$$d_{\max} \le d_{crit} \tag{2.3}$$

Here $d_{\max} = Max\left\{\left(\frac{d_{\max}}{D}\right)_0 \left(\frac{d_{\max}}{D}\right)_\varepsilon\right\}$

(2.4)

$$\left(\frac{d_{\max}}{D}\right)_0 = 1.88\left[\frac{\rho_c\left(1-\varepsilon_d\right)}{\rho_m}\right]^{-0.4} We_c^{-0.6}\,\mathrm{Re}_c^{-0.08} \tag{2.5}$$

$$\left(\frac{d_{\max}}{D}\right)_\varepsilon = 2.22C_H^{3/5}\left(\frac{\rho_c U_c^2 D}{\sigma}\right)^{-0.6}\left[\frac{\rho_m}{\rho_c(1-\varepsilon_d)}f\right]^{-0.4}\left(\frac{\varepsilon_d}{1-\varepsilon_d}\right)^{0.6} \tag{2.6}$$

$$\frac{d_{crit}}{D} = Min\left(\frac{d_{c\sigma}}{D}, \frac{d_{cb}}{D}\right) \tag{2.7}$$

$$\frac{d_{c\sigma}}{D} = \frac{0.224}{\left(\cos\beta'\right)^{1/2} EO_D^{1/2}} \tag{2.8}$$

$$\frac{d_{cb}}{D} = \frac{3}{8} f \frac{\rho_c}{\Delta\rho g} Fr_c \tag{2.9}$$

Here'd' is dispersed phase and 'c' is continuous phase. Brauner (2001) predicted the flow pattern boundaries of various authors and found good agreement with experimental results.

Brauner and Ullmann (2002) proposed a criterion to predict critical conditions for phase inversion by combining criterion of minimum of the system free energy. The evaluation of the dispersed free energy requires the availability of models for predicting the characteristic drop size in dense dispersion and its variation with holdup. This study combines the models suggested by Brauner (2001). The model suggested here gives criterion for the critical holdup corresponding to phase inversion. They predicted the experimental data available for phase inversion in the literature.

Sharma et al. (2011) developed a model to predict flow behaviors including flow patterns, pressure gradient and holdup in horizontal and slightly inclined pipes. The model is based on the principle that a system stabilizes to its minimized total energy. They assumed smooth interface, smooth pipe, negligible surface energy between wall and fluids,

homogeneous dispersion and steady state flow. Unlike existing oil-water flow models the current model does not force to confirm to a particular flow pattern and captures the gradual changes in flow configuration. They reported that this model provides extensive information about flow like flow pattern, droplet size, pressure gradient and holdup. They validated against data from experimental studies of Atmaca (2007), Alkaya (2000), Trallero (1995) and Abduvayt et al. (2006) and predicted results matched well with the experimental results.

Chakrabarti et al. (2011) applied artificial neural network technique to predict flow pattern in liquid-liquid two phase flow. They used Levenbarg-Megahed learning algorithm for training the ANN. They predicted their experimental flow patterns with minimum error of 4%.

Al-Yaari and Abu-Sharkh (2011) predicted the flow patterns using CFD analysis which is discussed in the respective section. They simulated stratified flow pattern identified in their experimental study using Fluent 6.2 software package. They used volume of fluid (VOF) multiphase model with RNG-k-ε model has been used for the simulations. They reported good agreement with the experimental results.

Ooms et al. (2012) made a numerical study (taking into account inertial, viscous, and pressure forces) on concentric core-annular flow through a horizontal pipeline, special attention being paid to vertical force on the core. They reported that shape of the wave is based on the experimental results published earlier. Due to the eccentricity the centre line of the core is shifted in the upward vertical direction with respect to the centre line of the tube. The vertical force on the core is found to be dependent on Reynolds number, which

means that at large values of the Reynolds number an upward buoyancy force on the core due to a density difference between core and annulus can be counter balanced. So a stationary core-annular flow is possible.

Kaushik et al. (2012) performed a computational fluid dynamic simulation to investigate core annular flow through sudden contraction and expansion. They used lubricating oil-water as test fluids in their study. They used k-ε model to simulate the flow conditions (laminar oil and turbulent water). They performed simulations using VOF technique to include the effect of surface tension and wall adhesion. They used PRESTO discretization scheme for continuity while momentum, turbulent kinetic energy and dispersion rate equation are discretized by first order upwind method. They used PISO algorithm for pressure velocity coupling. They reported that validation of model with experimental results of Balakrishna et al. (2010) indicates a good agreement for both the cases.

Hadziabdic and Oliemans (2007) predicted the oil-water superficial velocities of stratified and dual continuous flow patterns. They used flow pattern dependent two fluid model for stratified flow and Homogeneous model for dual continuous flow. They also conducted parametric study of stratified flow pattern to calculate oil and water wall shear stresses that satisfy the two fluid model equations when the pressure drop and water holdup are imposed. They also have taken into account of interfacial waves and drop entrainment. They proposed a two dispersion model to calculate the entrainment drops. They calculated oil and water velocities by taking an extra term in the momentum equations. They predicted the entrainment flow rates of Valle and Kvandal (1995) which are in good agreement.

(2) Prediction of holdup and pressure drop

Russell and Charles (1959) presented a general mathematical analysis for two immiscible liquids flowing in a two layers between parallel plate and concentrically in a circular pipe. They derived equations relating the volumetric flow rates and viscosities of liquids. They proposed equations for the minimum pressure gradient as a function of volumetric flow rate as follows

For layers flowing between wide horizontal parallel plates:

$$Q_A = \frac{bg_c}{12\mu_A}\left(\frac{\Delta P}{\Delta L}\right)\left[\frac{M_1\mu_A + M_2\mu_B}{M_3\mu_A + M_4\mu_B}\right] \tag{2.10}$$

$$Q_B = \frac{bg_c}{12\mu_B}\left(\frac{\Delta P}{\Delta L}\right)\left[\frac{N_1\mu_A + N_2\mu_B}{N_3\mu_A + N_4\mu_B}\right] \tag{2.11}$$

For concentric flow in horizontal circular pipe:

$$Q_A = \frac{\pi\eta^4 g_c}{8}\left(\frac{\Delta P}{\Delta L}\right)\left[\frac{1}{\mu_A} + \frac{2}{\mu_B}\left(\frac{r_o^2}{r_i^2}\right)\right] \tag{2.12}$$

$$Q_B = \frac{\pi\eta^4 g_c}{8\mu_B}\left(\frac{\Delta P}{\Delta L}\right)\left[r_o^2 - r_i^2\right]^2 \tag{2.13}$$

Where Q_A and Q_B are the volumetric flow rates of liquid A and B, μ_A and μ_B are the viscosities of fluids. These equations lead to theoretical prediction that reductions in power

requirement. They reported that maximum reduction obtained in the pipe system with concentric flow is considerably greater than in the parallel system.

Charles (1963) presented a theoretical analysis of concentric flow of cylindrical capsules in laminar or turbulent annuli. This study was followed by several experimental studies on the transportation of single cylindrical or spherical capsules in a steam of water.

Ooms et al. (1984) developed a theoretical model to predict pressure drop of core annular flow. According to this model the movement of the rippled oil core with respect to the pipe wall induces pressure variation in the water film. The proposed model correctly predicted the effect of pipe size on pressure drop of liquid-liquid flows.

Oliemans et al. (1987) proposed a correlation to predict pressure gradient of by incorporating turbulence of the surrounded water film.

Arirachakaran et al. (1989) proposed correlations to predict pressure drop of stratified flow and homogeneous flow patterns. They also proposed a correlation to predict phase inversion point of oil-water dispersed flows.

Brauner (1991) presented a simple predictive model for predicting pressure drop and in situ hold-up associated with the annular flow of two immiscible liquids in horizontal pipelines. She correlated pressure drop as a function of Martinelli parameter and fluid flow rate ratio for a wide range of flow rates covering all possible flow situations. Wall shear friction factor is also considered in this model.

Bannwart (1998) proposed a kinetic wave theory to measure the wave speed and volumetric fraction of the core. Kinematic wave theory is also used to calculate the slip

ratio and volume fraction of the core. They reported that the measured core volume fraction using wave theory is in good agreement with direct holdup measurement.

Arney et al. (1993) presented holdup and pressure drop data of a horizontal core annular flow. Waxy crude oil (μ = 27 P) was used as the core fluid. The experiment was done through a glass pipe of 15.9 mm to observe the flow pattern. The following empirical formula was used to predict the holdup,

$$H_W = \beta\,[1+0.35\,(1-\beta)] \qquad (2.14)$$

Where H_W is the in situ water holdup and β is the input water fraction. In their study Reynolds number and friction factor were modified based on simple concentric cylindrical CAF (core annular flow) model.

Bannwart (2001) presented a view on hydrodynamic aspects of core annular flow, including occurrence conditions, volume fraction and pressure drop. They gave criteria for annular flow existence by considering stability of a viscous liquid flowing at the core, surrounded by turbulent annular flow is as follows

$$\mu_1 > \mu_2 + 0.005\rho_2 J_2 D$$

for $\dfrac{\rho_2 J_2 D}{\mu_2} > 2000$ and

$\varepsilon > 0.5$ Here ρ_2 is the density of annulus fluid and J_2 its superficial velocity.

They also proposed an expression for volume fraction prediction of annular flow. The correlation suggested for pressure gradient prediction in core annular flow in horizontal pipe is as follows

$$\Gamma = kQ^{2-n}\left[1-\left(1-\frac{\rho_1}{\rho_2}\right)\varepsilon\right]^{1-n}\left[1-\left(1-\frac{\mu_1}{\mu_2}\right)\varepsilon\right]^{-n} \quad (2.15)$$

Where Q is the mixture flow rate and ε is hold up calculated from

$$\varepsilon = \frac{1-C_2}{1+(s_{i,o}-1)C_2}$$

where $C_2 = Q_2/Q$

They predicted pressure gradient data from various sources and shown very good agreement.

Hapanowicz and Troniewski (2002) presented the determination of characteristic parameters in two-phase liquid-liquid flow. They calculated physical properties of droplet flow of water. They described flow viscosity as a function of Reynolds number and Froude number of both the fluids and holdup. They calculated pressure drop of the drop let flow using the following equation

$$\left(\frac{\Delta P_{c-c}}{\Delta L}\right)_{(KW)} = \lambda_z \frac{w_{c-c}^2 \rho_{c-c}}{2d_o} \quad (2.16)$$

Here "c-c" is liquid-liquid mixture. They also estimated viscosity change of liquid-liquid mixture in droplet flow of water.

Raj et al. (2005) predicted holdup using existing correlations. They modified Taitel and Duckler (1976) holdup prediction model for gas-liquid flows with smooth interface by incorporating Brauner et al. (1996) of curved interface model to predict liquid holdup of liquid-liquid flow.

Chakrabarthi et al. (2005) developed a model to predict the pressure drop by total energy minimization concept. They considered smooth interface between the phases. They validated their model by predicting the literature data.

Hapanowicz (2008) studied the slip phenomena between the phases that occur in unstable oil-water flows in pipes. He emphasized on the relation between slip and real water fraction in a flowing mixture and physical properties of whole two-phase system. He proposed a new model for calculating the phase fractions in liquid-liquid flow.

Yiping et al. (2008) developed a model to predict pressure drop and in-situ phase fraction of segregate flow by considering curved interface, pipe roughness and liquid wettability with pipe material. They validated the proposed model by predicting the experimental results.

Walvekar et al. (2009) numerically simulated the three-dimensional flow of two immiscible liquids in horizontal pipe. The transient simulations of two phase dispersed flow in a pipe of 0.025 m diameter have been carried out using commercial CFD package of Fluent 6.2 in conjunction with Eulerian-Eulerian model. They have used oil and water as fluids in their work. They used k-ε model to account the turbulence in continuous phase. They predicted pressure drop and phase holdup. They reported that predicted results of phase distribution were in good agreement at higher mixture velocities while discrepancy was observed at lower mixture velocities.

Rodriduez et al. (2009) proposed a model to predict frictional pressure gradient by incorporating slip ratio. They gave expression for mixture velocity as a function of slip ratio. They used the same expression in perfect core annular flow model to get the pressure

drop. They observed good agreement with the experimental results of their own and other literature data.

Poesio et al. (2009) predicted their experimental data using Lockhart-Martinelli equivalent liquid (LMEL) model and observed poor accuracy. They proposed a new model (LM2FM) which incorporates a tow fluid model for the computation of pressure drop for liquid-liquid flow which is then used in Lockhart-Martinelli model for the computation of overall pressure drop. They reported that proposed model predicted both the pressure drops with less error in prediction.

Yusuf et al. (2011) proposed a simple correlation to predict pressure gradient of oil dispersed in water flow pattern which is as follows

$$\frac{dp}{dx} = 435.1U_m^2 \tag{2.17}$$

where U_m is mixture velocity. They validated this correlation with experimental results and got good agreement. They experimentally found the phase inversion point at water cut of 0.25-0.3 which is close to the value predicted by Brauner and Ullmann (2002).

Al-Wahaibi (2012) developed a simple pressure drop correlation for horizontal oil-water separated flow (stratified and dual continuous). He proposed the correlation to predict pressure gradient by modifying the friction factor correlation associated with the liquid-liquid flow. The proposed correlation is as follows

$$\frac{dp}{dx} = 2.4\left(\frac{f_{cor}\rho_m U_m^2}{2D}\right)^{0.8} \tag{2.18}$$

where *(dp/dx)* is pressure gradient, f_{cor} is the two-phase friction factor, ρ_m is density of mixture, U_m is mixture velocity and D is diameter.

while the correlated friction factor is given as

$$\frac{1}{\sqrt{f_{cor}}} = -2\log\left(\frac{\varepsilon/D}{0.25} - \frac{4.518}{\mathrm{Re}_m}\log\left(\frac{6.9}{\mathrm{Re}_m} + \left(\frac{\varepsilon/D}{0.25}\right)^{1.11}\right)\right) \tag{2.19}$$

He validated the accuracy of the proposed model with various literature data collected for separated flows.

Zhang et al. (2012) developed a model to predict holdup and pressure drop of horizontal, inclined and vertical oil-water stratified flow. They proposed a new approach for modeling the interfacial shear stress based on turbulence mixing length concept. The proposed expression for the interfacial shear is as follows

$$\tau_i = \sqrt{\frac{f_W\Theta_W + f_O(1-\Theta_W)}{2}}\sqrt{\rho_m\left[\Theta_W\tau_W + (1-\Theta_W)\tau_O\right]}\times(U_O - U_W) \tag{2.20}$$

Where Θ_W is water wall wetted wall fraction defined as:

$$\Theta_W = \frac{S_W}{S_W + S_O} \tag{2.21}$$

They validated their model with experimental literature data with high viscosity.

Al-Wahaibi and Angeli (2007a) A criterion for the transition between stratified stable and unstable liquid-liquid flow was derived theoretically based on KH instability and finite wave length. They reported that critical wave lengths to initiate instability decreases as the viscosity ratio increases. For the low viscosity oils the critical amplitude to initiate instability acquire maximum value at almost zero slip velocity, while for higher viscosity oils the maximum values was reached for water velocities higher than that of oil velocity.

Al-Wahaibi and Angeli (2007b) developed a model to find out the critical amplitude and wave length required for the drop formation. They validated this model with the experimental results.

Al-Wahaibi and Angeli (2009a) developed a two dimensional model to predict entrained fraction in the upper and lower layers of dual continuous oil-water flow. This model is based on the balance between rate of drop entrainment and rate of drop deposition. They have calculated the volume of wave entrainment by the correlation given by Al-Wahaibi et al. (2007b). They suggested a correlation for calculating the entrainment fraction of one phase into the other. They compared their model against few available experimental data. They observed reasonable agreement between the predicted and experimental results of various researchers.

2.3 Two phase liquid-liquid inclined flow

There are limited number of studies were carried out in inclined pipe lines to know the effect of inclination on hydrodynamics. As discussed in the horizontal section here also the

research this field has been categorized into two categories like experimental and theoretical work. Experimental measurement techniques are discussed as follows.

a) **Experimental estimation of different hydrodynamic parameters:**

Soot and Knudsen (1972) conducted experiments in a brass pipe of 0.0189 m inner diameter 90° downward incline pipeline with three different oils having the viscosity ratio of 0.98,8.6 and 180 to study the flow pattern, pressure drop and holdup. They observed dispersion of oil in water flow pattern.

Mukhopadhyay (1977) carried out experiments to study the effect of pipe inclination on pressure drop and holdup of oil and water flow (viscosity ratio of 5-6 and density ratio of 0.85) through a Lexan pipe of 3.81 m ID with inclinations varying from ±30° to ±90°.

Mukherjee et al. (1981) studied the effect of inclination on flow pattern, pressure drop and holdup for inclinations ranging from ±30° to ±90° from horizontal in 1.5 inch diameter pipe. Diesel fuel and water with viscosity ratio 5-6 and density ratio 0.852 were used as test fluids. They reported that the water phase being denser, buoyancy causes slippage of oil past the water layer in upward flow and reverse in down ward flow. It was found that minimum slippage occurred at -30° the smallest inclination angle studied. They observed dispersion of oil in water and water in oil flow pattern in their experimental study. Based on their studies they recommended that further studies need to be carried for an inclination angle between+30° and -30°as maximum slippage might be observed in that range.

Hill and Oolman (1981) experimentally studied the effect of pipe inclination, pipe material and pipe diameter on flow pattern, pressure drop and holdup of low viscous oil

(viscosity of 1.6 mPa s) and water as test fluids for the inclinations ranging from +30 to +90. They conducted experiments in 15.2, 21.6, 11.4 cm ID steel and acrylic pipe and observed bubbly and stratified flow. They also measured the pressure drop and holdup in their experimental study.

Cox (1985) conducted experiments in downward inclined pipe of -15° and -30° Plexi glass pipe of 0.0508 m ID pipeline using low viscous oil-water system (viscosity ratio 1.54 and density ratio of 0.756) to study the flow regimes and holdup. They reported stratified, dispersion of oil in water and dispersion of oil in water and water flow patterns along with their holdup.

Scott (1985) studied the flow of a mixture of water and mineral oil (Soltrol 130) in upward inclined pipes. The experimental system used allowed for a variation in inclination from horizontal to 30 degrees and flow rates from 0 to 1400 barrels per day of the combined liquid. The physical phenomena studied were flow regime occurrence and holdup, as function of flow rate and pipe inclination. They observed rolling wavy countercurrent, rolling wavy concurrent, bubble flow stratified and bubble flow massive were the flow patterns. The change in flow regime transition lines when proceeding 15° to 30° shows the rolling wavy regimes increasing in size. As inclination was increased the effect of gravity tended to act upon the fluid more parallel to the pipe, but against flow, thus increasing the rolling motion of the phases (i.e., generating more of a fluid fall back effect). Scott also studied the holdup as a function of the flow pattern. He reported that in bubbly flow the holdup ratio was close to unity. In inclined flow as the superficial velocity was increased the holdup ratio merged to a constant value slightly greater than one, indicative of single fluid flow.

Vigneaux et al. (1988) have conducted experiments on kerosene-water mixture for inclinations between 5° and 65° from vertical in 10 cm and 20 cm ID pipes and for mixture velocities range 0.1 to 0.5 m/s. They observed dispersion of oil in water flow pattern. Their studies are concentrated on the effect of inclination and mixture velocity on the slip velocity between the oil and water and on water volume fraction radial gradient. As the oil cut is increased the oil content at the bottom of the pipe increases and the slip velocity reduces. In inclined pipes the gradient of the water volume fraction is very large in the center part of the pipe. The upper part of the pipe section is almost occupied only by oil and the lower section by water, the transition between the two occurring over a relatively thin zone.

Ding et al. (1994) conducted experiments to investigate liquid holdup behavior in two-phase vertical and inclined pipes. They used large diameter transparent pipe with inclinations ranging +30, +45, +60 and +90. They characterized flow regimes by visual and qualitative flow regime transition criteria. They predicted holdup by various existing correlations to check the applicability of such correlations in oil-water systems. They reported that modified drift flux model was found to be the most useful water holdup prediction model in vertical and deviated oil-water flow systems.

Experimental and theoretical studied on oil-water flow were carried out by **Flores (1997)** in vertical and inclined pipes to characterize flow patterns and develop a model to predict flow pattern transitions, holdup and pressure drop. Studies were carried out in a transparent test section (2 inch, 51 long) using mineral oil (viscosity 20 cP, density 845 kg/m^3) and water for inclination angles of 90°, 75°,60°, and 45° from horizontal. Fig.2.1 is the schematic representation of flow patterns observed in inclined oil-water flows. In water

dominant flow patterns significant slippage was observed with a decrease in inclination increasing the slip. In his study at low to moderate superficial oil and water velocities, dispersed oil in water countercurrent flow pattern is observed. This flow pattern is characterized by oil droplets flowing at the top and a localized countercurrent flow within the water layer at the bottom .a typical this flow pattern is characterized by increased values for water hold up with difference between insitu water holdup and input water cut as high as 39%.

Kurban (1997) conducted experiments in a stainless steel pipe of 0.0779 m ID with 1° upward inclination to study the flow patterns suing oil-water system with viscosity ratio of 45 and density ratio of 0.865. They identified stratified, stratified mixed, dispersion of oil in water and water and dispersion of water in oil and water flow patterns in their experimental study though visual observation.

Hassan and Kabir (1999) presented an experimental study and a semi theoretical analysis of two phase flow of oil-water flow through vertical or deviated systems. Their study focused on the water-dominated flow regimes. They used Plexiglas pipes with two different diameters (6.24 and 12.7 cm). Experiments were conducted with lower viscous oil-water system with viscosity ratio of 1.6 and density ratio of 0.801. They identified bubbly and slug flow patterns in their experimental study. They reported that pipe deviation causes the lighter to move preferentially closer to the upper wall, thereby making the cross-sectional droplets distribution different from the one observed in the vertical system.

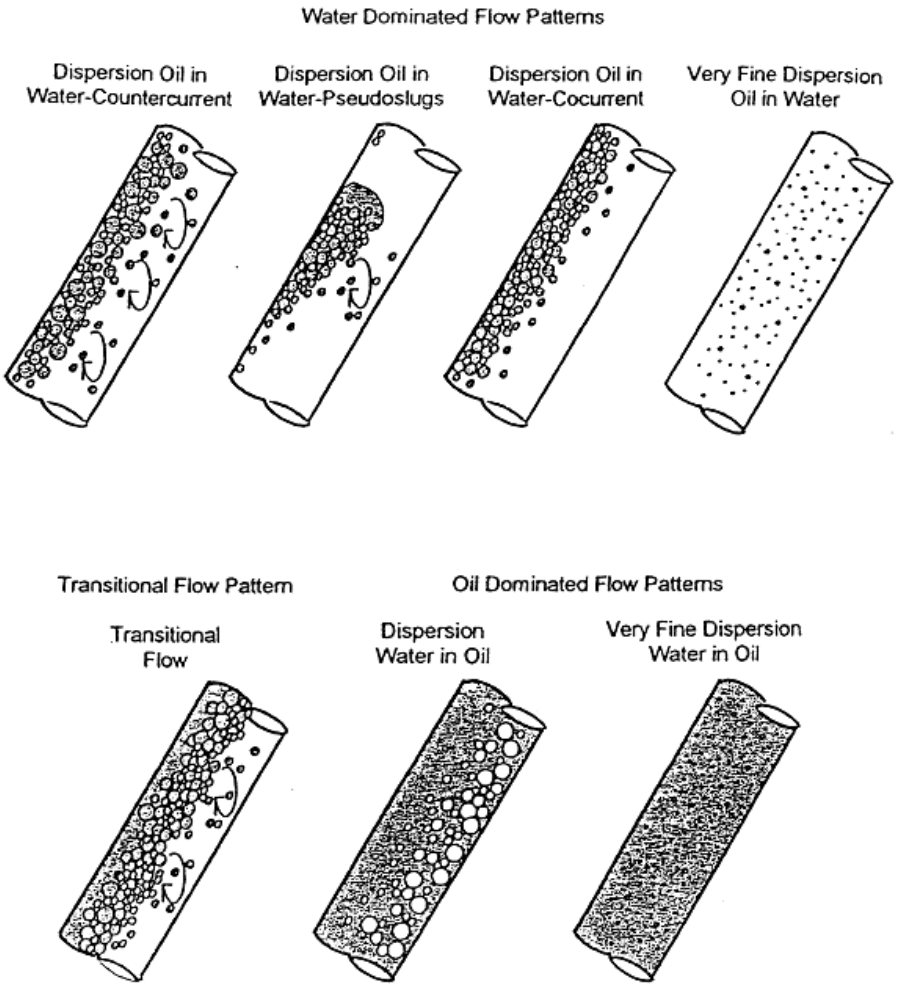

Fig. 2.1 Schematic representation of oil-water flow patterns (Flores (1997))

Alkaya (2000) performed experiments to study the effect of pipe inclination on flow pattern, pressure drop and holdup of oil-water system through acrylic pipe of 0.0508m inner diameter pipe. She used oil with viscosity 12.9 mPa s and water as test fluids with various inclinations ±0.5, ±1, ±2 and ±5. She observed stratified and stratified mixed flow patterns in their study and pressure gradient and holdup were also measured.

Gat (2002) conducted experiments in 0.0144m inner diameter glass pipe to study the effect of inclination on flow pattern and holdup in oil-water flow through inclined pipes. Gat

used oil-water system with viscosity ratio of 9.7 and density ratio 0.835 in the range of inclinations 0-±30. Gat reported stratified, stratified wavy, bubbly and slug flow pattern and observe various changes in their transitions with inclination.

Lum et al. (2004) studied two phase liquid flows at 5 degree upward inclined pipeline for mixture velocities between 0.7 and 2.5 m/s and input water fractions between 10% 50 90%. The investigations were performed in a 38 mm ID stainless steel test section with water and oil (viscosity 5.5 mPa s and density 828) as test fluids. They identified stratified wavy, dual continuous, dispersion of oil in water and dispersion of water in oil flow patterns by visual observation. The differential pressure gradient was measured by a Validyne DP103 pressure transducer. The average in-situ composition of the flow was mainly measured using quick closing valves technique. They have compared the flow patterns observe with the flow pattern map of Alkaya (2000) with same pipe inclination to know the effect of viscosity on flow pattern. They modified two fluid model by incorporating entrainment factor to predict pressure gradient of dual continuous flow. The proposed model predicted experimental results with over prediction.

Kumara et al. (2010a) performed experiments in a 15m long stainless steel pipe section with internal diameter 56 mm using Exxsol D60 oil (density 790 Kg/m^3 and viscosity 1.64 mPa s) and water (density 996 Kg/m^3 and viscosity 1mPa S) are used as test fluids. The pipe inclination is changed from 5° upward to 5°downward. The measurements are made for two different mixture velocities, 0.50 and 1.00 m/s at water cut 0.50. The cross-sectional distribution of phase fractions in oil-water flow is measured using a traversable single-beam gamma densitometer. The different flow regimes are determined based on visual observations. The particle image velocimetry (PIV) is utilized in order to obtain

non-invasive instantaneous velocity measurements of the flow field. They reported stratified flow with some mixing at the interface is at mixture velocity 0.5 m/s for all pipe inclinations. A good agreement between the water volume fraction measurements and visual observations are observed. The interface was found to become wavier as the degree of inclination increased from the horizontal. The oil–water interface is noticeably wavier and more irregular at +5°. Some interfacial waves with smaller amplitudes are observed in the downwardly inclined pipes. The oil phase tends to move faster than the water phase as the pipe inclination increases upwardly. On the other hand, the water phase is faster in downwardly inclined flows. The degree of mixing between the phases largely depends on the pipe inclination.

Due to the limitation of visual observation technique few authors adopted imaging technique for the hydrodynamic study. Combination of both the techniques is used for the better understanding of low phenomena. Such works are given here as follows.

Zavareh et al. (1988) carried out experiments in a large diameter (18.41 cm) Plexiglas pipe with oil-water viscosity ratio of 2.46 and density ratio of 0.783 in an inclined pipe of 5 and 15 degrees from vertical to study the flow regimes and its transitions. They characterized flow regimes by visual observations and video grapy technique. They identified a new flow pattern named counter current bubble flow over a wide range of flow conditions. They observed variation in flow pattern transitions with angle of inclination. They predicted the experimental flow pattern transition boundaries with the theoretical transition boundaries.

Vedapuri (1999) performed experiments in 10.16 cm ID flexible hose pipe to study the flow pattern, pressure drop and holdup. Studies were carried out at six different inclinations ±2°, ±5° and ±15° inclined pipeline with oil viscosity 2cP and water as test fluids. He identified flow patterns by visual and VHS video camera. The pressure drop between the static and dynamic heads was measured by a manometer. A detailed study of the oil-water distribution across the cross section from the top to bottom of the pipe was carried out for input water percentage of 20, 40, 60 and 80% for all the inclinations mentioned above. Semi segregate and semi dispersed flow patterns were identified in his experimental study. He also studied the ratio of the thickness of the liquid layer from the bottom of the pipe to the diameter of the pipeline as function of water percentage. He reported that in down ward inclined pipes gravity driven buoyancy effect causes the water layer to stratify. The water layer travels faster. This could result higher corrosion rates due to increase in mass transfer. In downward inclined pipes the ratio of insitu holdup to input holdup was less than unity. But in upward inclined pipes it is greater than unity as result of the accumulation of water. At lower water cuts the slip was relatively high and at higher water cuts the values approximately unity.

Ullmann et al. (2003a) studied the effect of inclination on the characteristics of laminar countercurrent liquid-liquid flow are investigated both experimentally and theoretically. The solvent system used is a mixture of ethyl acetate, water and ethanol. The this solvent system forms two phases with a density ratio of 0.95, viscosity ratio (μ_W/ μ_O) of 1.7 where subscript ‘w’ denotes the heavy (water-rich) phase and ‘o’ denotes the light (organic-rich) phase. The corresponding Eotvos number of the system is 20 hence, the system is gravity dominated. The range of inclinations varied from 0° and 90° to horizontal. The flow

patterns and the location of the interface are identified and recorded using a commercial camera (Panasonic NV-RX11EN/EU). They identified heavy phase dominated and light phase dominated flow patterns in their study. The characteristics of counter current stratified flow pattern are analyzed using laminar two-phased flow between parallel inclined plates (TP) and two fluid model (TF) for pipe geometry. These models are applied to the case of plane interface. The holdup values predicted by TP model are in good agreement with experimental data on the other hand the predictions by TF model are less favorable.

Oddie et al. (2003) carried out steady state transient experiments of oil-water flow through a large diameter (15 cm), inclinable pipe using kerosene and tap water as test fluids. The pipe inclination was varied from 0° (vertical) to 92° and the flow rate of each phase varied over wide ranges. Holdup is measured by nuclear densitometer as well as ten electrical probs. they observed dispersed, mixed and segregate flows were observed by video recordings. They reported the effect of pipe inclination and phase flow rates on holdup. Steady state holdups from nuclear measurement were in a reasonably close agreement with the in-situ measurements.

Rodriguez and Oliemans (2006) performed experiments in Oil-water two-phase flow experiments were conducted in a 15 m long, 8.28 cm diameter, inclinable steel pipe using mineral oil (density of 830 kg/m3 and viscosity of 7.5 mPa s) and brine (density of 1060 kg/m3 and viscosity of 0.8 mPa s). Steady-state data on flow patterns, two-phase pressure gradient and holdup were obtained over the entire range of flow rates for pipe inclinations of -5°, -2°, -1.5°,0°,1°,2° and 5°. The characterization of flow patterns and identification of their boundaries was achieved via observation of recorded movies and by analysis of the

relative deviation from the homogeneous behavior. Pressure gradient was measured by differential, gauge and absolute pressure meters and insitu volumetric fraction of the phases (holdup) is measured by gamma-ray densitometry (density meter Berthold LB 444). They observed seven different flow patterns for horizontal, upward and downward inclined flow are reasonably well described by the Trallero's flow pattern map. For downward inclined flow a stable wavy structure was observed. For upward inclined flow regions with high water recirculation were detected. The stratified smooth flow pattern disappears with inclination and is replaced by a stratified wavy flow pattern. The measured pressure gradient and holdup have been predicted by two fluid model for stratified flows and homogenous flow model for dispersed flows.

Grassi et al. (2008) experimentally studied the flow patterns and pressure drop in upward (+10°, +15°) and down ward (-10°) inclined pipes to know the effect of inclination. The experiments were carried out in transparent polycarbonate 21mm inner diameter pipe. They used high viscous oil (viscosity 0.799 Pa s) and water as test fluids. They identified stratified flow, core annular, plug or slug flow, stratified flow and dispersion of oil in water, core annular flow and oil in water dispersion and stratified flow by visual observation and photography technique. The measured pressure gradient has been predicted by the model proposed by Brauner (2002).they reported that they did not observed any significant difference among the inclined systems. In their study large core annular flow, oil in water dispersion regions was identified and few stratified wavy and none of the smooth stratified flow pattern was noticed due to low Eotvos number system.

Xu et al. (2010) conducted experiments in downward and upward vertical pipeline to study the phase inversion, holdup and frictional pressure drop of white oil (44 mPa s

viscosity and 860Kg/m^3 density) and water as test fluids in perspex pipe of 50 mm diameter. They used high speed camera for flow pattern characterization. The holdup was obtained experimentally by the quick closing valves technique. The points of phase inversion are always close to an input oil fraction of 0.8 for upward flow and of 0.75 for down- ward flow, respectively. Several theoretical models have been used to predict phase inversion point. Measured frictional pressure gradient have been predicted using the correlations available in literature.

Castro et al. (2012) studied the effect of geothermal and kinetic interfacial wave properties on stratified wavy flow pattern through incline pipeline of various inclinations. The experimental work was conducted in a glass test line of 12 m and 0.026 m ID oil (density and viscosity of 828 kg/m3 and 0.3 Pa s at 20°C, respectively) and water as the working fluids at several inclinations from horizontal (-20°, -10°,0°,10°,20°). They measured the in-situ phase volume fractions by quick closing valves technique. Pressure drop was measured by differential pressure transducer (Validyne DP15). High speed video camera has been used to record the flow patterns during the study. They reported that the collected wave amplitudes, wave length and wave characteristics are dependent on holdup, pipe inclination and the relative velocities of the phases. They proposed a Froude number that includes all the above mentioned parameters. High wavelength/amplitude ratios were observed at low Froude numbers and upward flow. They developed homemade image analysis software to extract and analyze the data. The average wave shape in stratified liquid-liquid flow is for the first time presented and it is a function of a proposed two-phase Froude number.

As discusses earlier in the horizontal section various probes techniques (impedance, conductance, γ-ray etc) have been adopted for the hydrodynamic parameter study. In inclined pipeline few researchers studied these methodologies. Some of their outcomes have been given here in detail.

Angeli et al. (2002) carried out experiments in horizontal and 5° upward inclined pipeline to study the effect of inclination on flow pattern, pressure drop and phase distribution by impedance conductivity probe technique. Experiments were conducted in 0.038 m ID stainless steel pipe with oil-water viscosity ratio 5.25 and density ratio 0.828 as test fluids. They observed stratified, dispersion of oil in water, dispersion of water in oil and dispersion of water in oil and water flow patterns. They measured the pressure gradient using differential pressure transducer and phase distribution by conductivity probe technique.

Zong et al. (2010) experimentally investigated the inclined oil-water two-phase flow characteristics in 125mm inner diameter transparent Plexiglas pipe by using the vertical multi electrode array (VMEA) conductance probe and mini conductance probes. Experiments were carried out with oil and water as test fluids in upward inclined pipe of 15° and 45° from vertical. They observed four different flow patterns namely dispersion of oil in water-pseudo slugs (DO/WPS), dispersion of oil-in water-counter current (DO/WCT), transition flow (TF) and dispersion of water in oil flow pattern. They used non linear analysis method to effectively distinguish the flow patens long with VMEA probe technique. They compared their experimental flow pattern map with the flow pattern map given by Flores et al. (1999) and identified various differences due to different diameter used in their study. Recurrence quantification analysis and attractor geometry

morphological description methods were used to analyze the signal time series measure from VEMA and reported good flow pattern classification results.

Kumara et al. (2010b) presented the application of single-beam gamma densitometer to investigate oil-water flow in horizontal and inclinable stainless steel pipe using Exxsol D60 oil (density 790 Kg/m^3 and viscosity 1.64 mPa s) and water (density 996 Kg/m^3 and viscosity 1mPa s) are used as test fluids. The experiments were performed in 0.056 m ID steel pipe with inclinations ranging from +5° to -5° at three different velocities, 0.25, 0.5 and 1 m/s and the inlet water cut is varied from 0 to 1. In this study frictional pressure drop is estimated based on water holdup. The measured water holdup and slip ratios are strongly dependent on pipe inclination. They reported that in general higher water holdup values are observed for upward inclined pipes and lower values for downward inclined pipes than horizontal. The measurement shows that water holdup values are very sensitive to pipe inclination at lower mixture velocities. For all the pipe inclinations at mixture velocity 0.25 and 0.5m/s, the slip ratio decreases as water cut increases. As the mixture velocity increases the slip ratio approaches to one, due to increased level of mixing. They reported good consensus of measured holdup and slip ratio with the previous investigations.

Strazza et al. (2011) conducted an analysis of high viscosity oil-water flow through slightly inclined pipeline. The test pipe consists of six transparent Plexiglas tubes with 21mm I.D. and six glass tubes with 22 mm I.D. The fluids used are high viscous oil with viscosity of 900 mPa s and tap water. A capacitance probe is used to collect the holdup data and differential pressure transducer (GE Druck STX 2100) for pressure drop measurement. They identified oil in water dispersion, core-annular flow and oil in water dispersion, core annular flow in both the test sections. They predicted the annular flow

transition boundary by the CAF model proposed by Brauner (2004). They predicted pressure drop of core annular flow by theoretical models proposed by Arney et al. (1993), Bannwart (1999) and Brauner (1991). All the models had shown a good agreement with the experimental results. Holdup data have been predicted with the correlation proposed by Arney et al. (1993) and two fluid model developed by Brauner (2004) and found good agreement.

Ullmann et al. (2003b) presented maps of multi holdup regions in co-current and countercurrent stratified flows. These maps clearly demonstrated the symmetrical relationship between upward and downward co-current inclined flows. They validated the feasibility of obtaining multiple holdups experimentally. Experiments were conducted in 14.4 mm ID perspex pipe with mineral oil (Marcol 52) and water as test fluids. The corresponding Eotvos number of the system is 10, which is smaller hence capillary and wall wetting effects may play a role. A simple procedure, which is based on the analytical solution of laminar flow between two-plates, is established for identifying the regions where multiple holdups are suspected in co-current flows. This procedure avoids the tedious search required by other models for identifying these regions. They reported that the commonly used two fluid model failed in indicating the multi holdup regions due to problematic modeling of the interfacial and wall shear stress in inclined flows. This is probably the reason that the possibility of obtaining multi-valued holdup in downward flows has not been discussed so far in the literature.

b) Theoretical studies on prediction of hydrodynamic parameters:

Unlike horizontal flow there are very less number of theoretical studies have been carried out in inclined pipeline. The proposed correlations to predict holdup and pressure drop are presented here.

Hassan and Kabir (1999) proposed a correlation to predict oil holdup during oil-water flow in vertical/deviated systems for all the flow patterns. They verified the correlation form their experimental result and also from the published data.

Gada and Sharma (2012) used a novel dual grid level set method based on 2D numerical simulation for developing smooth stratified and stratified wavy flow pattern in horizontal and inclined pipes at certain critical value of inlet velocity, inlet interface height, inclination angle, reduced surface tension and reduce gravity.

2.4 Two phase liquid-liquid vertical flow

Even though the present work is directed towards study of hydrodynamics in horizontal and inclined pipeline, the work done in the vertical pipeline is discussed here to get a comprehensive idea on hydrodynamics. The past studies on liquid-liquid two phase flow through vertical pipeline have been given in Table 2.1. Only brief literature is mentioned in this table.

Table 2.1 List of literature for vertical oil-water flows

Authors	Pipe ID and material	μ_o/μ_w	ρ_o/ρ_w	σ N/m	Work done
Govier et al. (1961)	0.0264m Cellulose Acetate Butyrate	0.936 20.1 150	0.78 0.854 0.88	35.3 50.2 49.8	Holdup, pressure drop
Brown and Govier (1961)	0.0264m Cellulose Acetate Butyrate	21.5	0.85	50.34	Pressure drop, bubble velocity, bubble distribution
Vigneaux et al. (1988)	0.02 m		0.741	-	Phase distribution
Zavareh et al. (1988)	0.1184 m Acrylic	2.46	0.783	-	Bubbly flow, pressure drop and holdup
Hasan and Kabir (1990)	0.0635, 0.127 Plexiglas	1.544	0.756		Holdup
Flores (1997)	0.0508 Acrylic	20	0.858	33.5	Flow pattern (DO/W, VFD O/W, O/W CF), holdup and pressure drop
Hassan and Kabir (1999)	0.0635, 0.127 Plexiglas	1.544	0.756		Flow pattern (bubbly flow, pseudo slug flow and churn flow) drift velocity of the lighter oil phase.
Hamad et al. (2000)	0.078 m Perspex	1.6	0.803	17	Drop velocity, size distribution
Simmons and Azzopardi (2001)	0.063 m PVC	1.125	0.684	10	Drop size distribution
Bannwart et al. (2004)	0.0284 m glass	500	0.925	29	Flow pattern (B,DB,I,A)
Jana et al. (2006)	0.025 m Perspex	1.2	0.787	45	Flow pattern (B, DB, CT, CA) parallel wire conductivity probe
Rodriguez and Bannwart (2006)	0.0284 m Glass	500	0.93	29	Core annular flow (wave amplitude, interfacial waves), holdup
Ghosh et al. (2010)	0.012 m Glass	20	0.96	-	Flow patterns (B,S,A), pressure drop and CFD simulation
Du et al. (2012)	0.02 m	12	0.856		Flow pattern (VFD O/W, Do/w, DW/O, TF) and holdup

2.5 Lacunae in the past literature

The above literature shows that most of the available work on oil-water flow through horizontal or incline pipes are either with high (300-1300 m Pa s) or less (1.2-9.87 m Pa s) viscous oil. Number of experimental works on inclined pipeline with high viscous oil are very less. The past works on oil-water system having the viscosity of intermediate range are also very limited in inclined pipeline. Due to these facts an interest was felt to carry out the detailed investigation on hydrodynamics of viscous oil-water (intermediate range) flow through 5° upward inclined pipeline to fulfill the lacuna of the literature. There are some works in literature at 5º inclination with different viscosity ratios. These viscosity ratios are either higher or lower than the viscosity ratio used in the present work. Those literature results can easily be compared with the present work to find out the effect of viscosity since inclination is same. Due to this reason, a 5 º inclination has been selected in the present work. Prior to this, aims have been focused on the hydrodynamics of such flow through horizontal pipeline for the comparison and better understanding of the physics behind the flow phenomena. The objectives of the present work are given in Section 2.6.

2.6 Objective of the present study

Considering the vast field of liquid-liquid two-phase flows and the lacunae in the past literature the present study aims at

- ⇨ Experimental study and comparison of hydrodynamics (flow pattern, pressure drop, and holdup) of viscous-oil water flow through horizontal and inclined pipelines.

- Prediction of flow patterns by analytical models and Probabilistic Neural Network (PNN) technique.
- Models for the investigation of holdup and pressure drop (existing and modified models).
- Prediction of flow patterns by computational fluid dynamic (CFD) analysis.

Chapter 3

Experimental facility and procedure

3.1 Introduction

The experiments reported were performed in both horizontal and 5° upward inclined pipe. A schematic representation of experimental setup is shown in Fig. 3.1 and corresponding photograph in Fig. 3.2. The experimental setup has been designed and fabricated to investigate hydrodynamic aspects of simultaneous flow of viscous oil and water through the pipes. The test facility and the measurement techniques of the various parameters have been described in this chapter. The test facility comprises of the fluid handling systems (storage tanks, pumps, and rotameters) and two different test rigs (horizontal and inclined) as shown in Fig 3.1. The main goal of the experimental work is to generate a comprehensive set of oil-water flow data, which would cover the entire range of flow rates. The detailed description of each test rig and experimental procedure is as follows.

3.2 Fluid handling systems

The test fluids used are lubricating oil (SAE 40 grade) and filtered tap water. The lubricating oil is produced from Pawan enterprisers, Guwahati. The physical properties, namely density, viscosity and interfacial tension of the fluids are listed in Table 3.1. These have been checked from time to time for accuracy of estimation. Interfacial tension has been measured by K-9 tensiometer (make: KARUSS , Gemany; model: K9) following ring

method. Viscosity has been measured by a Rheometer (make: M/S Thermo Electron, Germay; Model: Rheo stress RS1).

Table.3.1. Physical properties of water and lubricating oil (at 298K and atmospheric pressure)

Fluid	Density (Kg/m^3)	Viscosity (mPa s)
Water	1000	1
Lubricating oil	889	107
Interfacial tension	24×10^{-3}N/m	

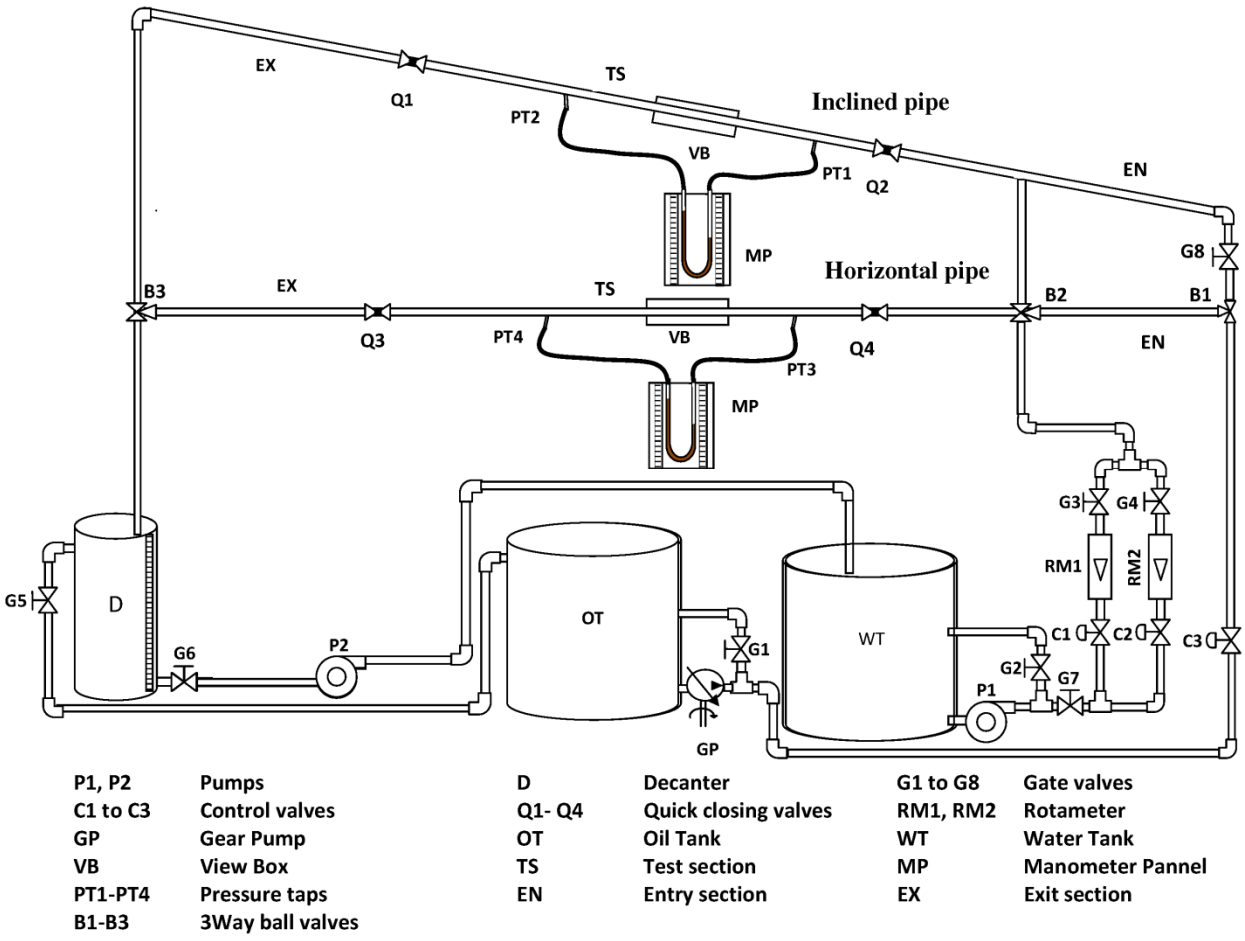

Fig. 3.1 Schematic of experimental setup

Fig. 3.2 Photograph of experimental setup

3.2.1 Water supply system

Water stored in PVC tank (WT in Fig. 3.1) of capacity 0.5 m^3 is circulated through the test section by a centrifugal pump (P1in Fig. 3.1) of 5 hp. The simultaneous adjustment of the bypass valve (G2) and the online control valves (C1 and C2) regulate the flow of water. The flow rate of flowing water is measured by a pair of rotameters RM1 and RM2 connected in parallel. They have been calibrated prior to start of experiment.

3.2.2 Lubricating oil supply system

A gear pump (GP in Fig 3.1) is used to circulate the lubricating oil from its the storage tank (OT in Fig. 3.1) to the entry section of the setup. The simultaneous adjustment of the

bypass valve (G1) and the online control valve (C3) gives the controlled flow rate of lubricating oil to the entry section of the test rigs. Oil flow rate has been calibrated by volumetric technique. Moreover, this measured oil flow rate (measured by volumetric technique) has further been calibrated with mass flow meter after purchasing the Micro Motion Corolis mass flow meter (Make: Emerson Process Management, Sensor Model: R100S128NQBZEZZZZ, Transmitter Model:1700R11ABFEZZZ), which is shown in Appendix, Fig. A4.1 (page 263). The calibration plot (Fig. A4.1) shows a goo correlation coefficient ($R^2 = 0.99$).

3.2.3 Rotameters

The water flow rate is measured with two rotameters. The rotameters for water range from 0 to 1.67 x $10^{-4}m^3/s$ with a least count of 3.34 x 10-6 m^3/s (for RM1) and 1.667×10^{-5}-9.17×10^{-4} m^3/s. with a least count of 1.67 x 10-5m3/s (for RM2). The rotameters with two different ranges are installed to enable measurement of flow rate over a wider range. The rotameters are calibrated by the standard method of noting the flow rates of the liquids collected in a measuring cylinder over a measured interval of time. The flow rates are measured for a sufficiently long time to stabilize the flow and getting a better average flow rate. The reading shows a repeatability of each reading with an average error of ±1% for both the rotameters (RM1 and RM2).

3.3 Experimental setup

The experimental setup is designed and fabricated to investigate hydrodynamics of simultaneous flow of oil and water through a horizontal and 5° upward inclined pipe. The test facility is described here which consist of two test rigs (horizontal and inclined). Each test rig has an entry section, test section and an exit section with a common separator in order in the direction of flow. All the test sections are made of Perspex for visualization and photographic studies. A schematic representation of experimental setup is given in Fig. 3.1.

3.3.1 Entry section

Entry section consists of two parts, T-junction and straight developing section.

3.3.2 T-junction

The schematic representation of T-junction and details of dimensions are depleted in Fig. 3.3. It comprises of two concentric tubes of diameter 0.018 m. The two fluids are introduced through the two tubes. Water is passed through the pipe A (in Fig. 3.3) while lubricating oil is introduced through pipe B as shown in the figure. The directions of flow of both the fluids are indicated by arrows in the figure. A reducer connects the mixer to the test rig of diameter 0.0254 m.

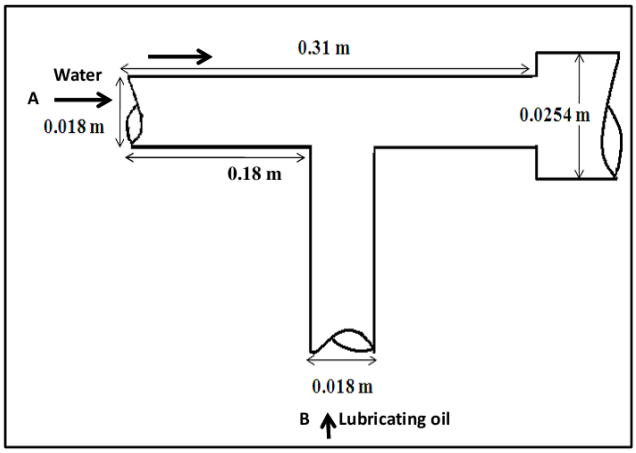

Fig. 3.3 Schematic of T-junction

3.3.3. Straight developing section

The outlet of the T-junction enters to the straight developing section. The section is of length 3 m and diameter 0.0254 m. A length to diameter ratio of 120 has been maintained to ensure fully developed flow before the test section. Care has been taken for maintaining the horizontal level of the section.

3.3.4 Test section

An experimental setup consisting of a horizontal and a 5° upward inclined pipeline has been fabricated and installed to fulfill the present objectives decided in Section 2.6 (Chapter 2). The description of the test sections is given below.

Horizontal test section

The test section (TS1in Fig. 3.1) is 0.0254 m in diameter and 1 m in length. The perfectly horizontal alignment has been ensured and checked from time to time. The set up has been constructed of Perspex to enable visual observation of the flow phenomena occurring

inside the tube. A view box (VB1) has also been installed at a distance of 3.62 m from the T-junction to minimize the lens effect during photography. The rectangular box filled with water has been installed to eliminate the effects of reflection and refraction by the circular cross section of the pipe. This box has a length of 24cm, width of 11cm and height of 11cm.

Test section is the main portion to concentrate on the flow; in this section two quick closing (B1 and B2 in Fig.3.1) valves are connected at the two ends of the test section. These two quick closing valve arrangements have been made for arresting the flow suddenly in the test section to measure the holdup in the test section. Tapings are made in the bottom part of the test section for collecting the holdup inside the test section. Two pressure taps PT1 and PT2 have been provided at a distance of 0.8 m to measure the pressure difference in the test section as shown in Fig.3.1. A U tube manometer (MP) has been connected to the two pressure taps, carbon tetrachloride is used as manometer fluid.

Inclined test section

Finally experiments have been carried out in a 5° upward inclined test rig of 0.0254 m diameter and 7.2 m length. The lengths of the different sections are same as horizontal test rig. The distance of T-junction and view box (VB) the entry section are same as it is in horizontal test section.

3.3.5 Exit section

Exit section of length 3 m and 0.0254 m diameter. The main purpose for this exit section is to reduce the effects of flow disturbance, in the test section.

3.3.6. Decanter

A separator is attached at the end of exit pipe for the separation of oil and water. The phases are separated by gravity. The water and oil are recycled back to their respective storage tank.

3.4 Valves

Two valves (C1-C2 in Fig. 3.1) before rotameter and one valve (C3) connected to Gear pump (GP in FiG.3.1) to control the flow and bypass valves (G1-G5), of the pumps, are globe valves. Rests of the valves are gate valves. In other they are 'full open or full close' valves. C1, C2 and C3 are 0.025 m brass valves. Two 1.27cm quick closing valves (Q1 and Q2), used in the test section are made of stainless steel. Two three way ball valves (B1 and B2) are used to pump fluids into horizontal or inclined pipeline.

3.5 Instrumentation Scheme

The scheme consists of photography technique. Specifications of the camera have been mentioned in Section 3.5.1. Apart from the visual observations, photographic technique has been adopted for the better appraisal of the flow phenomena.

3.5.1 Photography

A digital camera (SONY DSC- HX100V, Sony Electronics Inc. NJ, image device-7.77 mm (1/2.3 type), CMOS sensor with enhanced image processing, lens with focal length of 4.8-144 mm, and more precisely 27 - 890 mm when converted to a 35 mm still camera) with

30Xoptical zoom is used in still and video mode with proper lighting arrangement to visualize the nature of the two-phase flow.

3.6 Experimental procedure

Experiments have been carried out to estimate the flow patterns, the in situ fraction of the two phases inside the pipe and the pressure differential in two test sections (horizontal and 5° upward inclined). Operating the control valves (C1-C3) in proper way, water and lubricating oil can be send to the desired test section by the pump P1 and GP respectively. The pre-calibrated rotameters RM1-RM2 are used to measure the water flow rate. Oil flow rate is measured by volumetric method where volumetric flow rate of oil which is obtained by subtracting volumetric flow rate of water (obtained from pre calibrated rotameter) from total volumetric flow rate of oil-water mixture. Mixture volumetric flow rate (total volumetric flow rate) is measured from total liquid height of the mixture present in the calibrated decanter at the exit and time required to reach a particular liquid level. A detail uncertainty analysis in measurement of volumetric flow rate is presented in the Appendix, which shows a very less error, in the order of 10^{-4}. The two-phase mixture is introduced at the entry section and flows through the test passage. After flowing through the test section the oil-water mixture entered into the decanter (D) where gravity separation of both phases took place. From the separator, lubricating oil and water were recycled back to their respective storage tank after separation. Photographs of the different flow patterns have been taken by a digital SONY camera (DSC- HX100V). Specifications of this camera have been mentioned in section 3.5.1.

To cover the entire flow pattern (plug to dispersed) the experiment has been performed in a wide range of superficial velocities of both phases. During experiments keeping oil flow rate at a constant value water flow rate has been increased gradually up to the maxima. After completion of a set of experiment, oil flow rate has been set at next higher value then water flow rate has been changed in same manner. The experiments have been repeated thrice to check its reproducibility and a good reproducibility has been observed with an average deviation of 0.5%.

The different ranges of the flow rate are given below.

a) **Horizontal test section**

   Water and oil superficial velocity ranges from 0.1 m/s to 1.1 m/s and from 0.015 m/s to 1.25 m/s respectively.

b) **Incline test section (5°upward)**

   Water and oil superficial velocity ranges from 0.068 m/s to 1.23 m/s and from 0.052 m/s to 1.28 m/s respectively.

3.6.1 Estimation of flow patterns

The most common way to identify the different flow patterns is to observe the flow in a transparent channel or through a transparent window on the pipe wall. As an extension to visual observation, photographic or video techniques have also been widely used; for very rapid phenomena, high speed photography or video is necessary. The experiments have been carried out in a wide range of superficial velocities for both fluids to get all probable flow patterns. During the experiment water has been pumped first into the test section and then oil. After reaching the steady state observations have been noted and a snap shot of

the phenomena has been taken with a camera (Model no: DSC-HX100V, Make: Sony) at the test section. Flow pattern has been identified from this photograph. The same experiment has been repeated thrice at the same flow conditions to check the reproducibility of flow pattern and more than 99% reproducibility has been observed. Then a new set of experiment has been started to get the results at next water flow rate. For this, water superficial velocity has been kept constant, whereas the oil superficial velocity has been increased to the next higher value. After completion of one set of experiment, oil and water have been separated from the mixture present in the decanter (where the gravity separation taking place due to density difference of the fluids). Separated oil and water have been recycled into the respective storage tanks.

3.6.2 Holdup measurement

Holdup at different flow rates has been measured by quick closing valve (QCV) technique in both horizontal and inclined test rigs. The two quick closing valves (Q3- Q4) for horizontal setup and Q1- Q2 for inclined setup in Fig. 3.1 are placed at the two ends of the test section, 1 m apart, with a 500 ml trapped mixture volume between them. Once the system reaches steady state at particular flow rate of two fluids, the flowing mixture has been arrested by closing these two valves in the test section instantaneously. The arrested mixture has been collected in a measuring flask. During this operation two pressure taps (PT1-PT2) placed diametrically opposite at a distance of 0.8 m from each, are used for drainage of the liquid mixture from horizontal setup. To collect the residing fluids from the test section completely, compressed air is passed through PT1 and mixture has been

collected through PT2. On the other hand the taps (PT3-PT4) are used to drain out the phase mixture from the inclined setup. The collected mixture is allowed to settle for some time, and the volume of both the fluids is recorded. By knowing the volume of both the fluids, the holdup is calculated as,

$$H_W = \frac{V_W}{V_W + V_O} \tag{3.1}$$

Where V_W is Volume of water i.e. heavier phase,

V_O is Volume of oil i.e. lighter phase.

3.6.3 Estimation of pressure drop

The pressure drop has been measured over the entire range of phase velocities in both horizontal and inclined test rigs. For the pressure drop measurement, one carbon tetrachloride manometer has been used as shown in Fig.3.1. Two pressure taps (PT1 and PT2 for horizontal and PT3 and PT4 for inclined) have been provided at a distance of 0.8 m to measure the pressure difference in the test section. Before the measurement, the densities of the two fluids have been measured. Pressure drop data have been noted from the manometer at the steady state of a particular flow rate and the experiments have been repeated thrice at this operating condition to check the reproducibility of the data (pressure drop and oil flow rate). Small variations in the measurement (±0.5%) have been observed and an average value has been reported for the analysis. The detail of error analysis for the measurement of pressure drop has been given in appendix, which is very less (0.058).

Chapter 4

Identification of flow patterns

4.1 Introduction

Oil having viscosity of intermediate range are becoming important due to the gradual exhaustion of lighter crude oil (Lovick and Angeli (2004), Ghosh et al. (2010)). Survey of past literature in Chapter 2 shows that less amount of studies have been done on the hydrodynamics of such viscous oil-water two-phase flow. Resent industrial trend has also triggered the demand for a comprehensive understanding of the hydrodynamics of two-phase viscous oil-water flow through pipes in order to advance their design and process control. In the present work, an interest was felt to study the hydrodynamics of oil-water flow (oil having viscosity of intermediate range) through upward inclined (5°) pipe. Flow behavior of such viscous oil has also been explored in horizontal pipeline for better understanding of flow characteristics and comparison. This chapter deals with the identification of flow patterns of viscous oil-water flow through horizontal and inclined pipeline.

Experiments have been performed in a wide range of superficial velocities of both the phases to investigate the hydrodynamics of viscous oil-water flow through horizontal and inclined pipelines. Visual and photographic techniques have been used for identification of flow patterns. A flow pattern map has been developed for both the systems. Horizontal and inclined flow pattern maps have been compared to study the effect of inclination on flow patterns.

The maps have also been predicted with the help of probabilistic neural network (PNN) with a good accuracy which is given in next chapter. Pressure drop and holdup of this flow pattern have been measured and predicted with modified correlation as given in Chapter 6.

4.2 Flow patterns in horizontal pipeline flow

Flow patterns of viscous oil-water flow through horizontal pipeline have been identified from visual and photographic observations. The different flow patterns observed during the experiments are plug flow, slug flow, wavy stratified flow, stratified mixed flow, dispersion of oil in water and dispersion of water in oil. Images of the observed flow patterns are shown in Fig. 4.1a-4.1g as they appeared during the experiments with increasing the mixture velocity. At lower phase flow rates, oil plugs are appearing periodically into continuous water phase. There is a liquid bridge between two consecutive plugs. This pattern is termed as plug flow (P, Fig. 4.1a). With increasing the oil superficial velocity the size of the plug increases where as length of liquid bridge decreases and this large plug is termed as an oil slug. The liquid bridge is also termed as liquid slug. This type of flow pattern is called as slug flow (S). Photograph for slug flow have been given in Fig. 4.1b. In the figure yellow colored bullet shape indicates the presence of oil slug and the colorless continuous liquid is the water. In literature both plug and slug flows are considered as intermittent flow pattern including churn flow which is not observed in the experimental range. Now keeping water superficial velocity constant and continuous increasing the oil superficial velocity, the length of liquid bridge is decreased and it is finally disappeared. As a result two continuous streams are appeared in the form of stratification. It has been observed that the interface between two phases is wavy.

Amplitude of wave increases with increasing the phase superficial velocities. This type of flow is known as wavy stratified flow pattern (SW), snapshot is given in Fig. 4.1c. The flow pattern shown in Fig. 4.1d where stratification of the phases persists but oil droplets appeared at the oil-water interface with gradually increasing the phase velocity of oil. This is termed as the three layer (TL) flow pattern or stratified mixed flow (SM) pattern in literature. With increase in oil velocity number of droplets at the interface are increased. Onset of dispersion has been observed on further increasing the water superficial velocity. It is examined that at moderate superficial velocities of both the phases, oil core is enveloped by water. This pattern is termed as core annular flow (A) in the past research studies. Photograph of the flow pattern identified during the experiment is shown in Fig. 4.1e. At higher water superficial velocities oil drops distributed uniformly in the continuous water phase. This phenomenon is designated as oil dispersed in water ($D_{O/W}$), picture of the same is given in Fig. 4.1f. At higher superficial velocity of oil it is observed that some amount of water is dispersed into the continuous oil phase, which was termed as inverted dispersion or dispersion of water in oil ($D_{W/O}$) as shown in Fig. 4.1g.

4.2.1 Horizontal flow pattern map

The flow patterns observed during aforementioned experiments have been shown in graphical form in Fig. 4.2 which is known as flow pattern map. Water superficial velocity has been plotted along Y-axis and oil superficial velocity along X-axis in the figure. Different symbols and abbreviations have been used for various flow patterns in the flow pattern map. The significance of symbols has been mentioned in figure caption and

abbreviations of the corresponding flow patterns in the section of description of observed flow patterns.

Fig. 4.2 shows that plug flow has been observed at lower oil and water velocities. The present data shows that, Plug flow pattern starts at U_{SO} = 0.038m/s and U_{SW} = 0.2 m/s and extends up to U_{SO} = 0.031m/s and U_{SW} = 0.4 m/s in the map. Slug flow has been observed at lower oil and water velocities. The present data shows that, the slug flow regime begins at oil velocity of U_{SO} = 0.015m/s and at water velocity of U_{SW} = 0.1 m/s. It continues up to U_{SO} = 0.035m/s at the same water velocity. The flow pattern exists up to the velocity range of U_{SO} = 0.015 - 0.327 m/s and U_{SW} = 0.6 m/s. Further increment in the phase velocity, the flow pattern appeared is totally gravity dominant and the flow configuration is separated flow with wavy interface (viz., wavy stratified flow).

The existing range of wavy stratified flow regime is U_{SO} = 0.09-0.286m/s and U_{SW} = 0.1-0.362 m/s. The map shows that the stratified mixed flow region occupied a wide range of superficial velocities of both the phases (U_{SO} = 0.273-0.65m/s and U_{SW} = 0.1-0.4 m/s). It is sandwiched between stratified wavy and inverted dispersion in the flow pattern map. Annular flow pattern papered at moderately high superficial velocities of both oil and water (U_{SO} = 0.22-0.52 m/s and U_{SW} = 0.4-0.67m/s). Various dispersions have appeared at two extreme sides of the map. Dispersion of oil in water appears in an oil velocity range of U_{SO} = 0.08-0.505 m/s and water velocity range of U_{SW} = 0.433-1.06 m/s at the upper portion of the map. Whereas dispersion of water in oil is noticed at extreme right of the map in a velocity range of oil and water U_{SO} = 0.6-1.22m/s and U_{SW} = 0.133-1.1 m/s respectively.

Fig. 4.1a Plug flow (U_{SO}=0.082m/s; U_{SW}=0.433 m/s).

Fig. 4.1b Slug flow (U_{SO}=0.04m/s; U_{SW}=0.165 m/s).

Fig. 4.1c Wavy stratified flow (U_{SO}=0.103m/s; U_{SW}=0.267m/s).

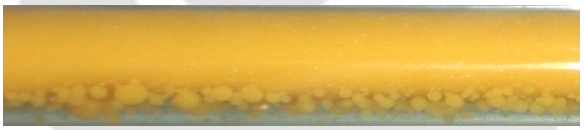

Fig. 4.1d Stratified mixed flow (U_{SO}=0.4m/s; U_{SW}=0.55 m/s)

Fig. 4.1e Annular flow (U_{SO}=0.45m/s; U_{SW}=0.43 m/s).

Fig. 4.1f Dispersion of oil in water (U_{SO}=0.188m/s; U_{SW}=0.8 m/s).

Fig. 4.1g Dispersion of water in oil (U_{SO}=1.1m/s; U_{SW}=0.4m/s).

Fig. 4.1 Photographs of different flow patterns in horizontal pipeline.

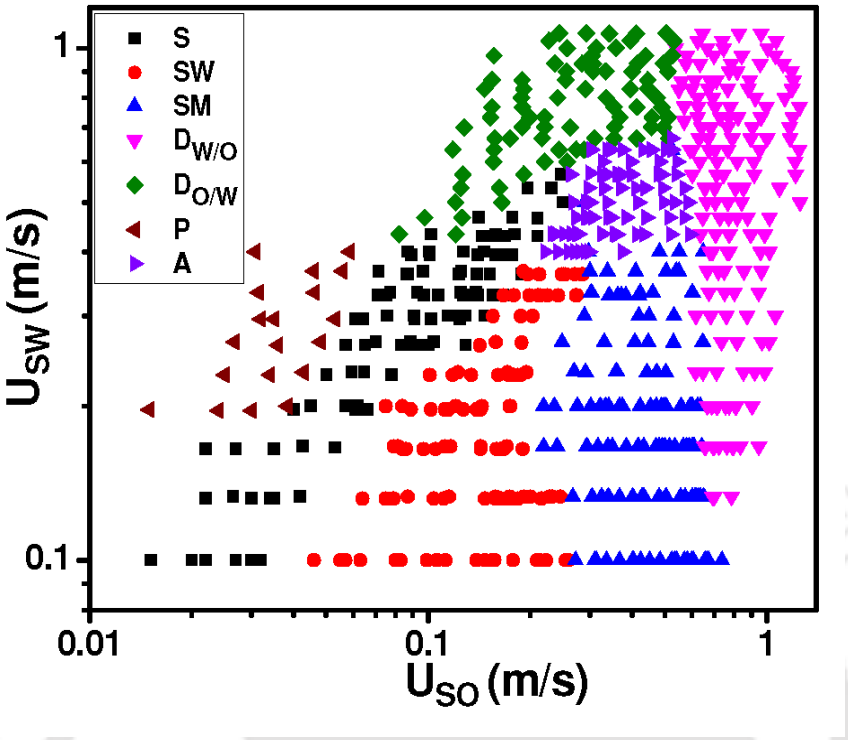

Fig. 4.2 Experimental flow pattern map horizontal pipeline

4.3 Flow patterns in inclined pipeline flow

Experiments have been conducted in 5° upward inclined pipeline and observed the same flow patterns as reported in the horizontal pipeline (Section 4.2) with variation in transition boundaries. The images of the flow patterns observed in 5° upward inclined pipeline have been given in Fig. 4.3. The description of flow patterns is same as described in horizontal flow pattern section (Section 4.2), again the same is not discussed here to avoid repetition.

4.3.1 Inclined flow pattern map

All the flow patterns observed in 5° upward inclined pipeline have been represented in flow pattern map as shown in Fig. 4.4. Plug flow pattern has been identified at lower phase flow rates of oil and water (U_{SO}= 0.0045-0.12 m/s and U_{SW}=0.067-0.567 m/s). The slug has been resulted from flow oil velocities U_{SO}= 0.008-0.30 m/s and water velocities U_{SW}=0.067-0.567 m/s. In the present study wavy stratified flow has been identified in the range of superficial velocity of oil (U_{SO}= 0.023-0.226 m/s) and water superficial velocity of (U_{SW}=0.067-0.204 m/s). At these velocities gravitational forces are dominated and minimum instability at interface rises due to low velocity. With further increase in the oil velocity the wavy interface is broken into droplets along with stratification of the phases. The map shows that stratified mixed flow pattern has been occupied in a wide range of superficial velocities of both water and oil phase (U_{SW}=0.067-0.44m/s to U_{SO}= 0.15-0.63 m/s). In this study this flow pattern is surrounded by slug, wavy stratified, annular and dispersion of water in oil flow patterns. At moderately higher velocities of oil and water phase a small water layer has been observed on above of oil layer and an annular flow pattern appears. The range of annular flow pattern in this study is varying from U_{SW} = 0.37-0.8 m/s to U_{SO} = 0.35-0.7 m/s. Two dispersions have been noticed on the two extreme sides of the present flow pattern map. Dispersion of oil in water flow pattern has been investigated at

Fig. 4.3a Plug flow (U_{SO}=0.042m/s; U_{SW}=0.169 m/s)

Fig. 4.3b Slug flow (U_{SO}=0.046m/s; U_{SW}=0.169 m/s)

Fig. 4.3c Wavy stratified flow (U_{SO}=0.055m/s; U_{SW}=0.169m/s)

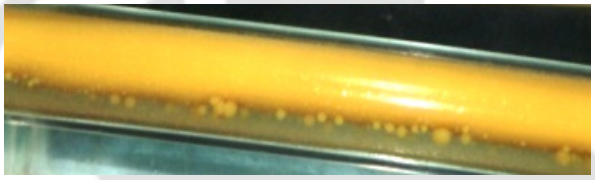

Fig. 4.3d Stratified mixed (U_{SO}=0.258m/s; U_{SW}=0.135 m/s)

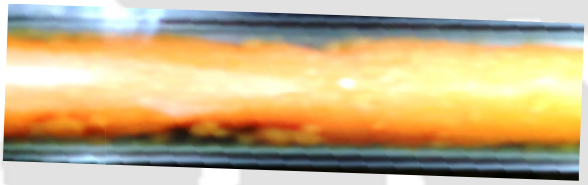

Fig. 4.3e Annular flow (U_{SO}= 0.71 m/s; U_{SW}= 0.48 m/s)

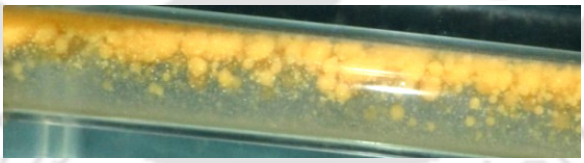

Fig. 4.3f Dispersion of oil in water (U_{SO}=0.6m/s; U_{SW}=0.65 m/s)

Fig. 4.3g Dispersion of water in oil (U_{SO}=0.82m/s; U_{SW}=0.24 m/s)

Fig. 4.3 Photographs of different flow patterns in 5° upward inclined pipeline

U_{SW} = 0.61-1.22 m/s and U_{SO} = 0.134-0.57 m/s. At lower water velocities plug flow was observed but with increase in the water velocity it is transformed to dispersion of oil in water flow pattern. At higher oil superficial velocities dispersion of oil in water flow pattern is inverted to dispersion of water in oil flow pattern. It is observed in the range of U_{SW} = 0.067-1.22 m/s to U_{SO}= 0.615-1.38m/s in the present flow pattern map.

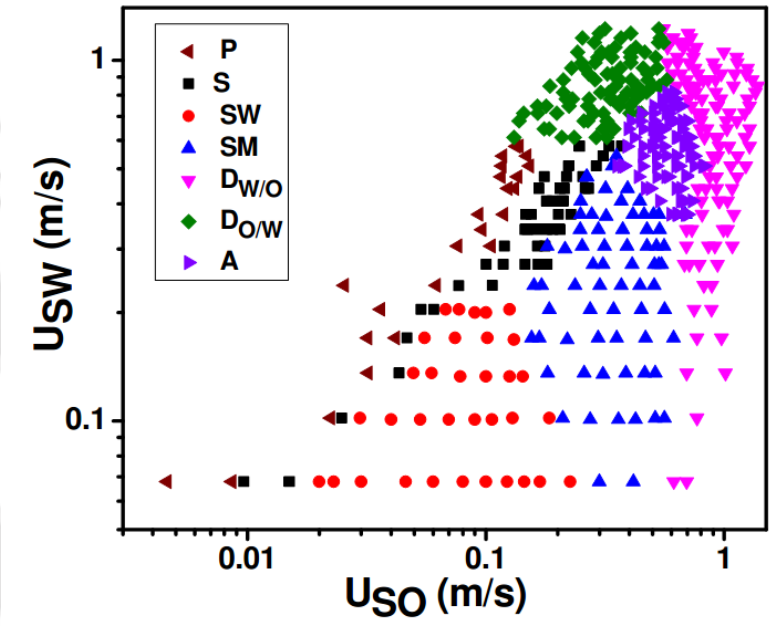

Fig. 4.4 Experimental flow pattern map inclined pipeline

4.4 Comparison between horizontal and inclined flow pattern map

The flow pattern map of inclined flow has been compared with the horizontal flow pattern map to know the effect of inclination on flow patterns. The parity plot of the same has been given in Fig. 4.5. Experimental flow pattern transition boundaries of horizontal pipe

have been drawn on inclined flow pattern map. In this figure scattered points are flow patterns acquired in 5° upward inclined pipeline and solid lines are horizontal flow patterns transition boundaries (section 4.2.1).

The Fig. 4.5 shows that the inclination enhances the slugging because it starts at lower water velocity ($U_{SW} \approx 0.07$ m/s) than the horizontal flow ($U_{SW} \approx 0.2$ m/s). Accordingly the transition line has been shifted and shown by line 1 in Fig. 4.5. A significant deviation has been observed in the transition boundary between slug and wavy stratified flow patterns as mentioned in the Fig. 4.5. The area of wavy stratified flow reduced in inclined flow pattern map (upward blue triangle) as compared to horizontal flow pattern map (transition boundary marked by line 2). It indicates that the inclination induces the interfacial instability in two-phase flow. At higher phase flow rate ($U_{SW} \geq 0.2$ m/s and $U_{SO} \geq 0.08$m/s), flow remains wavy stratified in horizontal flow while it becomes either slug or stratified mixed in inclined flow. As a consequence, earlier onset of stratified mixed in inclined map (compared to transition boundary given by line 3 for horizontal map) has been observed. Most interesting thing is that transition boundary between stratified mixed flow (SM) to water dispersed in oil ($D_{W/O}$) is almost same in horizontal (line 4) and inclined pipeline (diamonds). The transition boundary of dispersion of oil in water ($D_{O/W}$) flow pattern has been deviated at lower flow rates and no significant difference is observed at higher flow rates as shown by line 5 in Fig. 4.5. It indicates that the gravity is less important at higher velocity. The transition boundary between dispersion of oil in water and water in oil is not effected by pipe inclination as shown in Fig. 4.5 line 7. Inclination destabilizes interface and it shifts annular flow towards higher flow rate. The major difference observed with horizontal flow pattern map is that the annular flow pattern has

been shifted to higher flow rates in the present study which is shown by transition boundary 6 in Fig. 4.5.

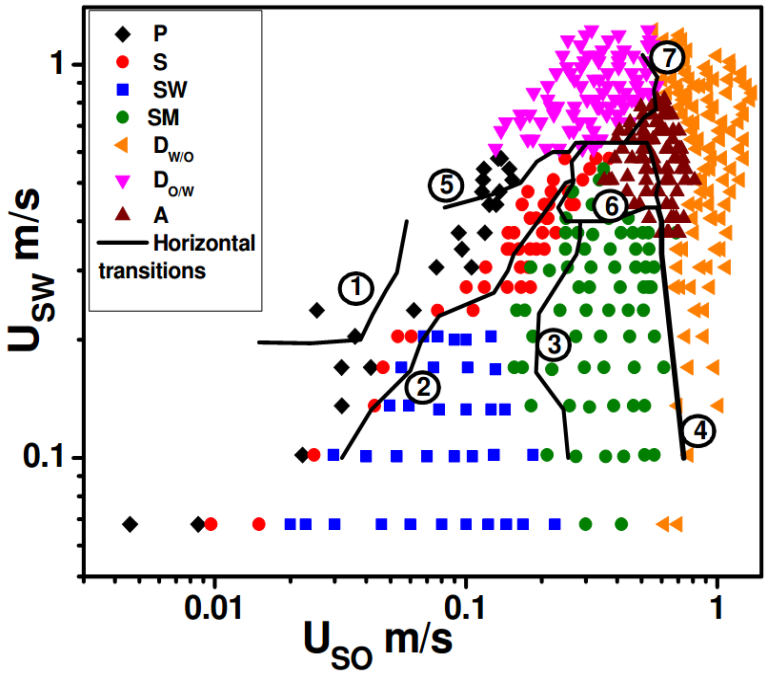

Fig. 4.5 Parity plot of inclined and horizontal flow pattern map (♦- Plug flow, ●- Slug flow, ■-Wavy stratified flow, ●- Stratified mixed flow, ▲ – Annular flow, ▼- Dispersion of oil in water flow ($D_{O/W}$), ◄- Dispersion of water in oil flow ($D_{W/O}$), '——'-transition boundaries of horizontal pipe .

4.5 Effect of viscosity on Flow patterns

For better understanding the effect of oil viscosity on the flow pattern, present horizontal flow pattern map is compared with the existing experimental flow pattern map from literature. The assessment of literature shows that flow patterns identified by various

authors vary due to change in fluid properties. In the present study, the experimental flow pattern map has been compared with the maps given by Raj et al. (2005) (viscosity ratio of 1.2 and density ratio of 0.786) in Fig. 4.6 and significant differences have been identified between the flow pattern maps. These maps have been selected because they have same diameter of the pipe with variation in viscosity of oil used in preset study. In the figure, the scattered data points show the present experimental results whereas solid lines and broken lines represent flow pattern transition boundaries obtained from the above references as discussed below.

A comparison between Raj et al. (2005) and present horizontal flow pattern map is shown in Fig. 4.6. The major difference in both the studies is that Raj et al. (2005) have not identified annular flow pattern, which was noticed in this study. At lower phase flow rates of both the fluids they have observed smooth stratified flow pattern, but in the present study plug flow has been identified. Raj et al. (2005) reported both the dispersions at higher superficial velocities than present experimental study. Transition boundary of stratified wavy to stratified mixed flow pattern of Raj et al. (2005) has not matched with this experimental transition boundary of stratified wavy to stratified mixed flow pattern. Order of flow patterns appeared in the experimental study has also diverged than Raj et al. (2005) this is due to difference in the viscosity of the test fluids used.

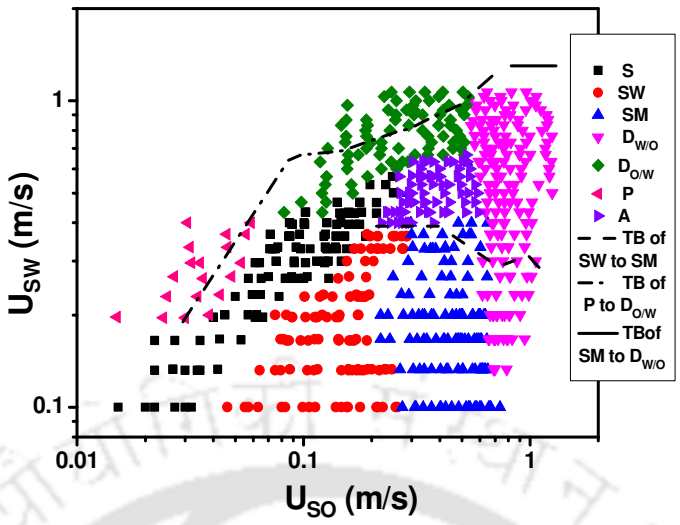

Fig. 4.6 Comparison with Raj et al. (2005) transition boundaries

Higher viscosity of the present fluid is main reason behind it because viscous force induces the stability of an annular flow. Annular flow is observed at moderate fluid velocities. Inertia force of primary fluid is quite high at these velocities which try to break the continuous oil stream of annular flow and viscous force opposes it. So higher viscosity fluids favor the annular flow (Joseph et al. (1984)) as observed in the present work. Viscosity also enhances the plug and slug flow at lower mixture velocity (Beretta et al. (1997)). So plug flow instead of stratified flow has been identified in the present work as mentioned above. On the other hand, interfacial drag force of stratified flow tries to break the oil stream into small droplets at interface. Here the surface force is playing a tricky role to stabilize the interface. It tries to prevent rupturing of the interface. Finally, drag force overcomes the surface force at certain velocity and it forms stratified flow (Al-Wahaibi and Angeli, 2009b). Therefore, stratified mixed flow appears at lower velocity as discussed above.

4.6 Conclusions

Plug flow, slug flow, wavy stratified flow, stratified mixed flow, annular flow, dispersion of water in oil and dispersion of oil in water flow patterns have been identified in both horizontal and incline pipeline. The flow pattern maps of horizontal and incline pipelines are compared to know the effect of inclination of flow patterns. The plug and slug flow has been identified at lower velocities in inclined pipeline than horizontal pipe. Velocity rage of this flow pattern is larger in inclined flow than the horizontal one. The annular flow region in inclined pipeline is shifted to the higher mixture velocities than that of horizontal pipeline. In inclined pipeline stratified mixed flow pattern observed at lower mixture velocities than horizontal pipeline. Low inclination has no significant effect on transition boundaries of dispersed flow patterns. Horizontal flow pattern map has been compared with literature data to know the effect of viscosity on flow pattern. Higher viscosity favors annular flow pattern, which is identified in the present study and it is not reported in Raj et al. (2005). Viscosity also onset earlier transitions of dispersed flows as observed in this study.

Chapter 5

Prediction of flow pattern maps

5.1 Introduction

To complement the experimental works, some of the researchers have theoretically predicted flow patterns by various correlations, analytical model and artificial intelligence like artificial neural network (ANN) as given Chapter 2. Literature survey shows that most of the available models to predict the flow pattern transitions are developed for horizontal flows and extended for vertical and inclined pipelines and there is no combined model to predict flow transitions of horizontal, inclined and vertical flow. An attempt has been made here to develop a combined model which predicts the transition boundaries of all the inclination for various fluid properties. In the present study experimental transitions observed in both horizontal and inclined pipeline (Chapter 4) are predicted by both analytical and ANN technique.

An artificial neural network (ANN) is a computational tool, extensively used in various fields of science and technology, especially for pattern recognition. It is an information processing tool, which processes input data to develop a best possible correlation. Based on this correlation it can predict the patterns of the input data. The information processing is carried out in its various inbuilt nodes which are very closer to the human brain. The details of this tool have been given in the respective section. It has been successfully applied by several researchers to predict the flow pattern map of air-water and water-

kerosene two phase flow. All the data are based on the single fluid pair during the training of the network.

The flow pattern maps obtained in both horizontal and inclined pipeline has been predicted by analytical models and Probabilistic neural network (PNN). The details of the prediction are discussed in the next sections. Probabilistic neural network (PNN) is a special type of artificial neural network (ANN). The input parameters of the network were superficial velocities of both the fluids, diameter of the conduit, angle of pipe inclination, viscosity ratio, density ratio and interfacial tension of the two liquids. The detailed methodology and prediction technique is discussed in the respective sections. The developed PNN has been validated with various fluid properties. The predicted flow pattern transition boundaries using both the techniques are compared to find the superior the method for prediction.

5.2 Prediction of flow pattern transition boundaries

Among the various techniques available for the prediction of flow pattern transition boundaries analytical and ANN technique has been adopted here for the prediction of flow pattern transition boundaries in both pipelines. The particulars of prediction are given in the individual sections.

5.2.1 Prediction of flow pattern map by Analytical models

All the flow patterns transitions identified during the experimental study (Chapter 4) of viscous oil-water flow through horizontal and 5° upward incline pipeline have been predicted using analytical models available in literature. The details of the models have

been discussed below. A comparison between the predicted and experimental transition boundaries of horizontal and inclined pipeline has also been made in this section.

5.2.1.1 Transition boundary of dispersion of oil in water

The experimental transition boundary between separated flow patterns and dispersion of oil in water flow pattern has been predicted using the model applied by Brauner (2001) for liquid-liquid flow though horizontal and +5° inclined pipeline. Dispersion of oil in water flow pattern has been observed when the turbulence in the continuous water phase is high enough to disperse the oil phase as small and stable droplets. The criterion for oil in water dispersed flow pattern is that maximum drop size (d_{max}) (it resist the stress due to dynamic pressure formed due to eddies is less than the critical diameter (d_{crit}) of droplet. The condition for the transition is given by,

$$d_{\max} < d_{crit} \tag{5.1}$$

Where,

$$d_{\max} = \max\left\{\left(d_{\max}\right)_o \left(d_{\max}\right)_\varepsilon\right\} \tag{5.2}$$

$$\left(\frac{d_{\max}}{D}\right)_o = 1.88 We_c^{-0.6} \mathrm{Re}_c^{0.08} \tag{5.3}$$

$$We_c = \frac{\rho_m D U_m^2}{\sigma} \tag{5.4}$$

$$\mathrm{Re}_c = \frac{D U_m}{\nu_w} \tag{5.5}$$

$$\left(d_{\max}\right)_{\varepsilon} = 7.61 C_H We_c^{-0.6} \mathrm{Re}_c^{0.08} \left(\frac{\varepsilon_d}{1-\varepsilon_d}\right)^{0.6} \left[1+\frac{\rho_d}{\rho_c}\frac{\varepsilon_d}{1-\varepsilon_d}\right]^{-0.4} \quad (5.6)$$

and dimensionless critical drop diameter d_{crit} is calculated from the following equation suggested by Barnea (1987)

$$\frac{d_{crit}}{D} = \min\left(\frac{d_{c\sigma}}{D}, \frac{d_{cb}}{D}\right) \quad (5.7)$$

$$\frac{d_{c\sigma}}{D} = \frac{0.224}{\left(\cos\beta'\right)^{1/2} Eo_D^{1/2}} \quad (5.8)$$

Where $Eo_D = \frac{\Delta\rho g D^2}{8\sigma}$ (5.9)

$$\frac{d_{cb}}{D} = \frac{3}{8} f \frac{\rho_c}{\Delta\rho g} Fr_c \quad (5.10)$$

$$Fr_c = \frac{U_c^2}{Dg\cos\beta} \quad (5.11)$$

For dispersion of oil in water the following parameters are considered, $U_c = U_m$, $U_{cs} = U_{ws}$, $U_{ds} = U_{os}$, $\rho_c = \rho_w$ and $\mu_c = \mu_w$ and $C_H = 1$. The predicted transition boundary (line 1) is superimposed on experimental maps as shown in Fig. 5.1 and Fig. 5.2. The predicted transition boundaries of both the pipeline have been deviated from the experimental results. Which shows large deviation in horizontal and small variation in inclined pipeline but it is observed that in both the pipelines the experimental transitions started at lower velocity.

5.2.1.2 Transition of dispersion of water in oil

Similarly, the transition boundary of dispersion of water in oil has been predicted (line 2) and compared with experimental results in Fig. 5.1 and Fig. 5.2. Dispersion of water in oil flow pattern occurs when the oil superficial velocity is high enough to create turbulence in continuous oil medium to diffuse the water phase as dispersed droplets. The transition boundary of water in oil dispersion has been predicted using Eq. (5.1) by considering oil as continuous phase and water as dispersed phase. The predicted transition boundary (boundary 2 in Fig.5.1) in horizontal pipeline shows good agreement with the experimental results. In inclined pipeline the transition boundary (boundary 2 in Fig.5.2) has shown good accuracy in prediction at lower superficial velocities and slightly deviated at higher water superficial velocities.

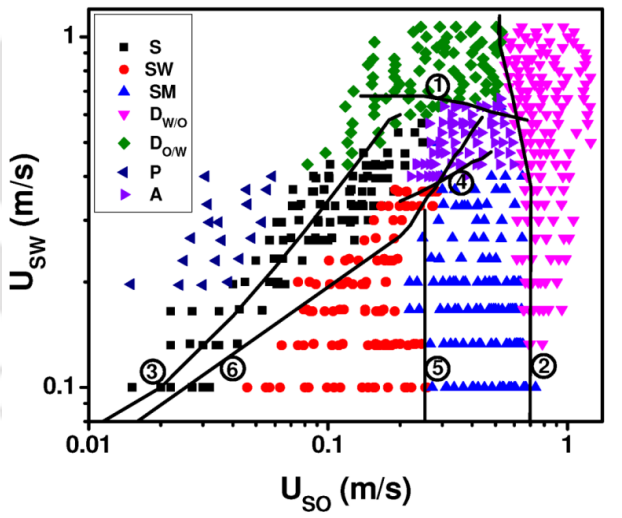

Fig. 5.1 Parity plot of Experimental and analytical transition boundaries in horizontal pipe (◄- Plug flow, ■ - Slug flow, ●-Wavy stratified flow, ▲- Stratified mixed flow, ►– Annular flow, ♦- Dispersion of oil in water flow ($D_{O/W}$), ▼- Dispersion of water in oil flow ($D_{W/O}$), '——' - analytical transition boundaries)

5.2.1.3 Transition from plug to slug

During the experiment (horizontal and inclined flow), plug and slug transition has been identified at lower oil and water superficial velocities where turbulence in the phases does not break the bubbles. Barena et al. (1985) proposed mathematical model to predict plug to slug transition boundary in gas-liquid two phase flow. The same equation is used here to predict plug to slug transition boundary in liquid-liquid two phase flow though inclined pipe by considering oil phase as gas by assuming α = 0.25.

$$U_{ws} = \frac{1-\alpha}{\alpha} U_{os} - 1.53(1-\alpha)\frac{g(\rho_L - \rho_o)\sigma^{1/4}}{\rho_L^2}\sin\beta \qquad (5.12)$$

The predicted transition boundary between plug and slug is depleted in Fig. 5.1 and Fig. 5.2 as boundary 3. In horizontal pipeline the prediction has shown very poor agreement with experimental results. The experimental transition boundary has been identified at higher mixture velocities. But in the inclined pipeline the predicted transition boundary (boundary 3 in Fig. 5.2) has been matched well with the experimental transition. The experimental transition of plug to slug flow has been identified at lower mixture velocities in inclined pipeline than horizontal (section 4.4).

5.2.1.4 Transition from slug to annular

To predict slug to annular flow pattern transition boundary the expression given by Weisman et al. (1981) has been used for both the pipelines and represented as boundary 4 in Fig. 5.1 and Fig. 5.2. The recommend expression for liquid-liquid flow as follows,

$$Fr_o Ku_o = 25\left(\frac{U_{os}}{U_{ws}}\right)^{5/8} \qquad (5.13)$$

Where $Fr_o = \dfrac{U_{os}^2}{gD}$ (5.14)

and $Ku_o = \dfrac{U_{os}\rho_o}{\left[g\left(\rho_w - \rho_o\right)\sigma\right]^{1/4}}$ (5.15)

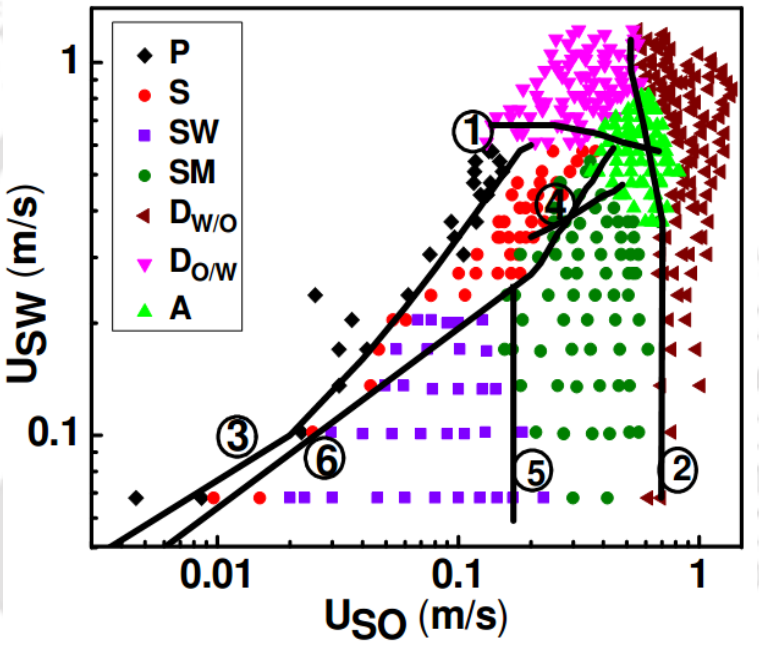

Fig. 5.2 Parity plot of Experimental and analytical transition boundaries in inclined pipe (♦- Plug flow, ●- Slug flow, ■-Wavy stratified flow, ●- Stratified mixed flow, ▲ – Annular flow, ▼- Dispersion of oil in water flow ($D_{O/W}$), ◄- Dispersion of water in oil flow ($D_{W/O}$), '——' - analytical transition boundaries)

Transition boundary of slug to annular flow (boundary 4 in Fig.4.1 and Fig.4.2) has been deviated much more from the experimental results in both the pipelines. It is unable to give the trend also. A delay in the onset of transition has been noticed in the experimental work. Viscosity of oil has a great role on the stability of annular flow but the expression

does not account the effect of viscosity. So further development is necessary to predict the annular flow.

5.2.1.5 Transition from wavy stratified flow to stratified mixed flow

As there is no direct expression for predicting stratified wavy to stratified mixed flow pattern transition boundary in horizontal and inclined pipes. An attempt has been made to predict wavy stratified to stratified mixed flow pattern transition boundary by using Al-Wahaibi (2007b) drop formation model for liquid-liquid flow. The wave should be unstable at the onset condition of drop formation at interface and the drag force acting on the wave should exceed the resisting force of surface tension. The forces acting on the deformed wave are shown in Fig 4.3. A force balance has been performed on the two dimensional sine wave for an inclined flow at the onset of entrainment. The drag (F_d) and surface tension (F_σ) forces are assumed to act on the full wave. The drag force has been calculated from drag coefficient. When the wave starts to deform, surface tension force on the wave tries to pull it back to its original form as the drag force tries to deform the wave. Therefore the drag force must be greater than surface tension force to form a drop, which is given as

$$F_d \cos\beta \geq F_\sigma \cos(\theta+\beta) \tag{5.16}$$

Here $$F_d = c_d A_{oilwave} \rho_o \frac{\left(U_w - U_o\right)^2}{2} \tag{5.17}$$

The drag coefficient c_d is given as

$$c_d = 4.9\times10^{-8} \times \mathrm{Re}_o^{0.77} \times \mathrm{Re}_w^{0.86} \times \frac{\mu_o}{\mu_w} \tag{5.18}$$

$$\mathrm{Re}_i = \frac{U_i D_i \rho_i}{\mu_i} \tag{5.19}$$

Here *i* represent the respective phase. *U* is the in situ phase velocity and *D* is the inner diameter. Surface tension force acting on the wave is sum of the forces acting along the length of the wave at the interface. The detailed procedure of the model has been given in Al-Wahaibi et al. (2007b). The net surface tension force is calculated from,

$$F_\sigma = \sigma(2S_i)\left(\frac{\lambda/2}{L}\right) \tag{5.20}$$

and $L = \sqrt{a^2 + (\lambda/2)^2}$ (5.21)

The criteria for oil drop formation is as follows

$$c_d A_{oilwave} \rho_o \frac{(U_w - U_o)^2}{2} \cos\beta \geq \sigma(2S_i)\left(\frac{\lambda/2}{L}\right)\cos(\theta+\beta) \tag{5.22}$$

$$S_i = \mathrm{D} \times \sqrt{\left(1 - (2\frac{\mathrm{h_w}}{\mathrm{D}} - 1\right)} \tag{5.23}$$

Here *Si* is the interfacial wave length, and h_w is the height of water at the interface which is calculated from the expressions given in Taitel and Dukler (1976). Wave length is taken as one pipe diameter as suggested by Al-Wahaibi et al. (2007b). Wave amplitude is calculated from the equation given by Al-Wahaibi et al (2009a). Experimental oil and water superficial velocities at which first drop of oil formed at the interface, has been used to calculate amplitude.

$$c_d A_{oilwave} \rho_o \frac{(U_w - U_o)^2}{2} \cos\beta = \sigma(2S_i)\left(\frac{\lambda/2}{L}\right)\cos(\theta+\beta) \tag{5.24}$$

The predicted transition boundary of stratified wavy flow pattern to stratified mixed flow pattern has been shown in Fig. 4.1 and Fig. 5.2 (boundary 5). In horizontal pipeline the transition boundary shows good agreement with experimental results. The predicted transition boundary of inclined pipeline (boundary 5 Fig. 4.2) has been deviated slightly at lower mixture velocities and in line with experimental results at higher velocities.

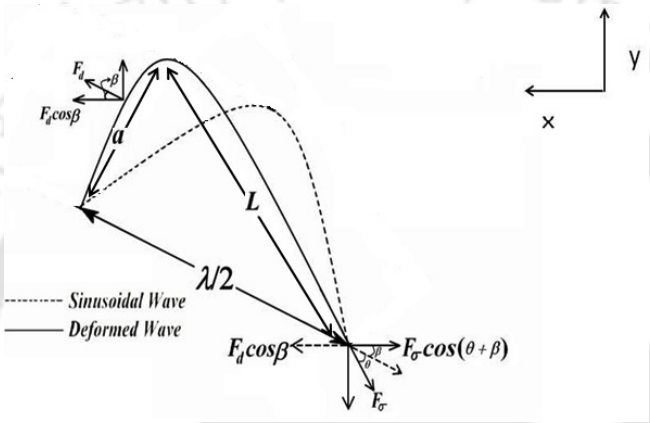

Fig. 5.3 Force balance on a deformed wave at the oil-water interface

5.2.1.6 Transition from slug to stratified flow

Expression suggested by Weisman et al. (1981) has been used for predicting transition from slug to stratified flow region of liquid-liquid two phase flow through horizontal and inclined pipe. The predicted transition boundaries of both the flows have been given as boundary 6 in Fig. 5.1 and Fig. 5.2 respectively. The expression for transition from slug to stratified flow in upward inclined liquid-liquid flow is as follows

$$\frac{U_{os}}{\sqrt{gD}} = 0.45\left(\frac{U_{os}+U_{ws}}{\sqrt{gD}}\right)\left(1-0.65\cos\theta\right) \tag{5.25}$$

The predicted transition boundary between slug to stratified flow of horizontal pipeline (Fig. 5.1) is deviated from the experimental transition. The transition has been observed at lower mixture velocities in the experiment. The predicted transition boundary of inclined pipeline (Fig. 5.2) has shown good agreement with experimental work at lower and higher flow rates. It is slightly departed from experimental transition boundary at moderately higher superficial velocities of water.

From above discussion it is noted that prediction accuracy of new approach for transition of SW to SM is good for both cases (horizontal and inclined flow). The predicted transition boundary between plug to slug flow pattern is good agreement with experimental transition in inclined pipeline and it shows mismatching in horizontal flow. Similarly slug to annular transition boundary has shown very poor prediction in both the cases. Transition boundary for slug to wavy stratified flow is in good agreement at lower flow rates and slightly deviates at higher flow rates in inclined flow. It shows large variation in horizontal flow. The predicted transition boundary of dispersion of oil in water has been departed from experimental boundary at higher velocities in both the cases. The above discussion states that analytical models have shown poor prediction for some flow patterns transitions. So PNN technique has been adopted to predict the flow patterns which is discussed in the next section.

5.2.2 Prediction of flow pattern maps by PNN technique

Based on the predicted results from the previous section (Section 5.2.1) an attempt has been made to develop a simple model which predicts all the flow pattern transitions for

various inclinations. For this purpose Artificial Neural Network (ANN) technique has been adopted.

5.2.2.1 Basic theory of PNN

Artificial neural network, an artificial intelligence technique which is implemented to predict flow patterns of viscous oil-water flow through different pipe inclinations. Neural networks have vast applications in science and technology such as pattern recognition, identification, classification, control systems, image processing, clustering of data, forecasting (Basheer and Hajmeer (2000)) prediction and identification of flow patterns (Sharma et al., (2006), Julia et al., (2011), Chakrabarti et al., (2011)). For many complex and non linear problems ANN has been found to be an alternative tool to solve the problem (Panagou (2007)). Feed forward back propagation (FFBP), generalized regression neural networks (GRNN), radial basis network (RBN), probabilistic neural network (PNN) and support vector machine (SVM) these are some types of artificial neural networks generally. The selection of a neural network has also been a tricky task. Appropriate selection of ANN involves the ANN topology, which depends on classification of the problem. PNN, a special type of artificial neural network (ANN) is selected for the current study for its accuracy in prediction, swiftness and ease in operation.

PNN is a feed forward neural network based on Bayes-Parzen classification theory which was first introduced by Spect (1990). The PNN approach combines both Bayes theorem of conditional probability and Parzen's method for estimating the probability density functions of the random variables (Hajmeer and Bhasheer (2002)). The detailed description of Bayes-Parzen theory has been given in Hajmeer and Basheer (2002). Classification can be estimated from Bayes' strategy if the probability density $f_k(x)$ of a sample is known. In

most of the case it is unknown and a Gaussian distribution is assumed to get the classification. High scale of misclassification is observed if there is a large difference between assumed distribution and true distribution of the sample. This misclassification can be minimized by introducing the concept of multivariate probability density function (PDF) estimator, $g(x)$, which is given by the following equation for the case of all equal smoothing parameters and a bell-shaped Gaussian function.

$$g_k(x) = \frac{1}{(2\pi)^{\frac{p}{2}} n\sigma^p} \sum_{i=1}^{n} \exp\left(-\frac{\|x - x_i\|^2}{2\sigma^2} \right) \tag{5.26}$$

Where 'x' is the vector of scattered variables and 'x_i' is the i^{th} training vector. σ is the smoothing parameters (also called bandwidth or kernel width) representing standard deviation around the mean of 'p' random variables $x_1, x_2, \ldots, x_p$, and 'n' is the total number of training data in the sample. Schematic representation of a simple PNN architecture has been given in Fig. 5.4 which consists of four layers namely input layer, pattern layer, summation layer and output layer. When an input is presented, input layer does not carry out any computational or arithmetic operations rather it simply pass the inputs to pattern layer. Number of nodes in the pattern layer is same as that of number of input data points. Pattern layer computes Euclidean distances from the input vector to the training input vectors and produces a vector which is close to a training input vector. The summation layer sums these contributions for each class of inputs 'C_k' to produce an arithmetic mean of its output vector of probabilities and from the maximum of these probabilities summation layer picks a complete transfer function. The output layer classifies any random variable by comparing the output of summation layer for each class and then following the Bayes' classification theorem as,

$$C_k(x) = \arg\max\left\{g_k(x)\right\} \tag{5.27}$$

PNN working procedure includes three basic steps, development of the network, training and testing of the network, and prediction of the patterns. Accuracy of PNN totally depends on training of the network and it requires huge number of training data. Therefore, collection of data is an important step prior to the construction of a PNN.

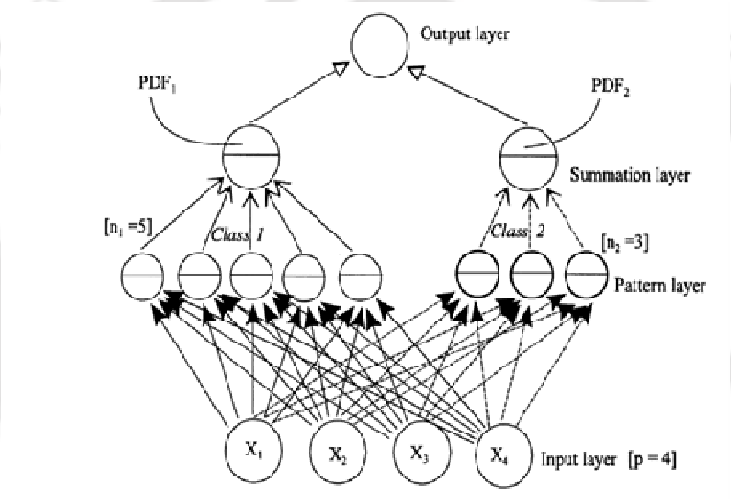

Fig. 5.4 A simple probabilistic neural network (PNN) Hajmeer and Basheer (2002)

5.2.2.2 Collection of data and flow pattern classification

About 2837 data points has been collected from seven literatures (Charles et al., (1961), Beretta et al., (1997a), Grassi et al., (2008), Sotgia et al., (2008)) and present work to construct the network which is shown in Table 5.1. It covers the diameter range from 0.3 cm to 8.29 cm, viscosity ratio ranging from 1.2 to 900 and inclination ranging 0°-90°. Table 5.1 is also showing the number of data of individual past work used for training and testing. 70% of 2837 data points have been used in training from different flow patterns

(for S: 314, SW: 234, SM: 244, A: 427, $D_{O/W}$: 429, $D_{W/O}$: 282). Remaining 30% (for S: 133, SW: 102, SM: 104, A:160, $D_{O/W}$:230, $D_{W/O}$: 116) are used for testing. This screening has been done manually in the present work. It is satisfying the basic requirement of an artificial neural network, which states that maximum 80% can be used in training and minimum 20% data should be used in testing (Hajmeer and Bhasheer (2002)). It has been noticed that terminology used by various authors for the same interfacial configurations are different from each other which created lots of perplexity. So for simplicity, few flow patterns with similar nature have been grouped together and a single nomenclature is chosen for this group which is explained in Fig. 5.5. For example, plug flow and slug flow have been considered here as slug flow (Fig. 4.1b). Similarly, smooth stratified and stratified wavy flow patterns are taken as stratified flow (Fig. 4.1c). Three layer flow and stratified mixed flow patterns have been considered as stratified mixed flow pattern (Fig. 4.1d). All kind of annular flow like core annular (Grassi et al. (2008), Sotagia et al., (2008)), wavy annular (Sotagia et al. (2008), Bannwart et al. (2004)) and dispersed annular (Bannwart et al. (2004), Grassi et al. (2008)), etc. have been consider as annular flow (A) (Fig. 4.1e). "Dispersion of oil in water and water" flow pattern, dispersion of oil in water and other oil dispersed flow (like oil in water homogeneous dispersion (Rodriguez and Oliemans (2006)), oil bubbles in water (Charles et al. (1961), etc) has been combined together and is considered as dispersion of oil in water flow pattern ($D_{O/W}$) (Fig. 4.1f). Similarly "dispersion of water in oil and water" flow pattern, dispersion of water in oil and other water dispersed flow (like water in oil homogeneous dispersion (Rodriguez and Oliemans (2006)), water bubbles in oil (Charles et al. (1961)), etc. has been taken as dispersion of water in oil flow pattern ($D_{W/O}$, Fig. 4.1g) to avoid the ambiguity coming

from various terminologies. Schematics of few flow patterns based on oil dispersion, water dispersion and annular flow have been shown in Fig. 4.6d,e, and f respectively. During the training of PNN flow patterns have been represented by numerical values and symbols which are given in Table 5.2.

Table 5.1: Source of data used in PNN

Sl. No	Angle of inclination from horizontal (°)	Pipe I.D (m)&material	Viscosity ratio	Density ratio	Interfacial Tension (N/m)	Reference	Total No. of data points	No. of points used in training	No. of points used in testing
1	0	0.0264 Cellulose acetate butyrate	65	1	0.03	Charles et al.(1961)	416	292	124
2	0	0.003 Glass	51.33 71.17	0.877, 0.874	0.036	Beretta et al. (1997a)	117	82	35
3	+1,+2 ,+5	0.0828 Steel	9.434	0.776.	0.0204	Rodriguez and Oliemans. (2006)	116	83	33
4	90	0.012 Acrylic	1.2	0.787	0.0315	Mandal et al.(2010)	153	108	45
5	0	0.0284 Glass	500	0.925	0.029	Bannwart et al. (2004)	346	243	103
6	0,+10,+15	0.021 Poly carbonate	800	0.889	0.05	Grassi et al. (2008)	405	284	121
7	0	0.026 Plexiglas and 0.004 Pyrex	900	0.9	0.02	Sotagia et al.(2008)	439	308	131
8	0	0.0254 Perspex	107	0.889	0.021	Present work horizontal	449	315	134
9	+5	0.0254 Perspex	107	0.889	0.021	Present work inclined	396	277	119
			Total				2837	1992	845

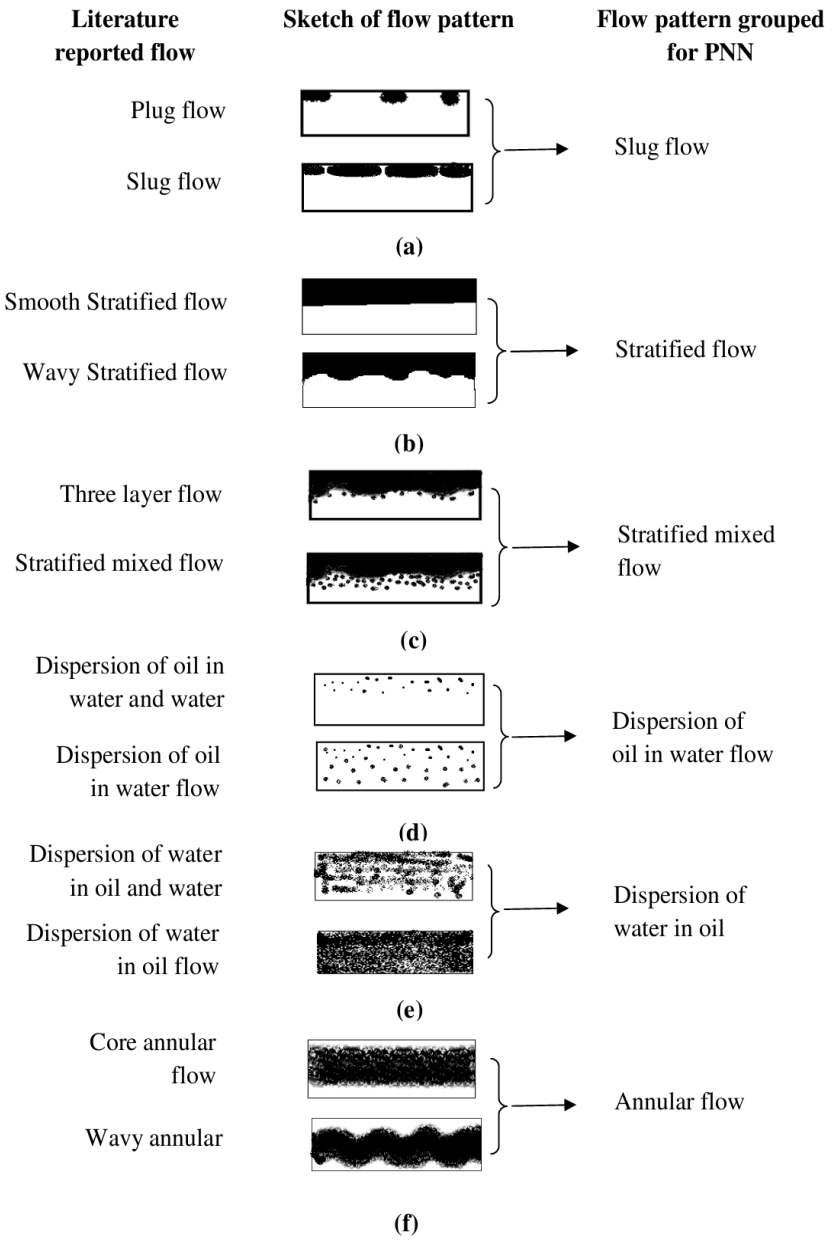

Fig. 5.5 Grouping of flow patterns

Table 5.2 Numerical values and symbols of different flow patterns used in PNN

Flow pattern	Numerical value	Symbol
Slug flow (S)	1	■
Stratified flow (SW)	2	●
Stratified mixed flow (SM)	3	▲
Dispersion of oil in water ($D_{O/W}$)	4	♦
Dispersion of water in oil ($D_{W/O}$)	5	▼
Annular flow (A)	6	◄

5.2.2.3 Design, training, and testing

A PNN has been designed, trained, tested and applied for prediction using inbuilt function in Matlab R2008a using the data listed in Table 5.1. If "P" is input vectors (here these are superficial velocities of both the liquids, conduit diameter, angle of inclination and physical properties of fluids such as density, viscosity and interfacial tension) and "T_C" is the target indices of corresponding input vector (here it is flow patterns), then target indices is converted into vector "T" by using "ind2vec(Tc)" function before forming a PNN. A new probabilistic neural network (PNN) has been created by using function "newpnn". It is used for initializing the weights of matrices to small random numbers and to set neurons. The function, "newpnn" consists of input vectors (superficial velocities of both the phases, physical properties of the fluids, pipe diameters and inclination), target vectors (corresponding flow patterns) and spread constant value as input parameters. In

this step, the selection of an optimum value of spread constant or smoothing parameter (σ) is very important as the shape of Gaussian function is totally influenced by this constant which is very important to develop a good PNN. Spread constant corresponds to standard deviation of a Gaussian distribution. Less the standard deviation leads to higher accuracy in the prediction. So, a combination of lower spread constant value and higher regression coefficient value is an optimum selection for a PNN. Various algorithm and techniques have been reported, to estimate the optimum spread constant such as genetic algorithm (Mao et al., (2000)) and trial and error method (Hajmeer and Bhaseer (2002) and Sharma et al., (2006)). This value is selected by trial and error method in the present work as it involves simple operation processes. The function "sim" simulates the probabilistic neural network which is required for testing the developed network on the design input vector. Finally output vectors are converted to indices to get the predicted class or pattern. In the testing process output obtained has been compared with the target values, it undergoes regression analysis which gives regression coefficient "R" (R=1 for perfect training). With higher regression coefficient and proper spread value, network has been prepared and tested with known data to get the accuracy in prediction. For a set of two input parameters' value (input and target vectors) one value of spread constant has been assumed in the function of "newpnn" during training. Flow patterns along with an optimum regression coefficient have been obtained as an output of the network by running "sim" function. An optimum spread value has been selected based on highest average % accuracy obtained in the prediction during tanning. The optimum value of spread constant has been used in testing steps to check accuracy of the trained PNN. If it gives good accuracy in testing also, then this spread constant has been used to predict the unknown data.

Spread constant in the present network has been selected from two graphs shown in Fig. 5.6a and Fig. 5.6b. Fig. 5.6a shows the variation of regression constant with spread values for a set of 1992 training data points. Similarly, Fig. 5.6b shows variation of average percentage accuracy in the prediction with different spread values for the same set of data. Comparing these two figures (Fig. 5.6a and 5.6b.), it can be concluded that a good training of the PNN has been achieved at a spread value of 0.02 with regression coefficient of 0.991 (Fig. 5.6a), which gives maximum average % correct prediction (Fig. 5.6b).

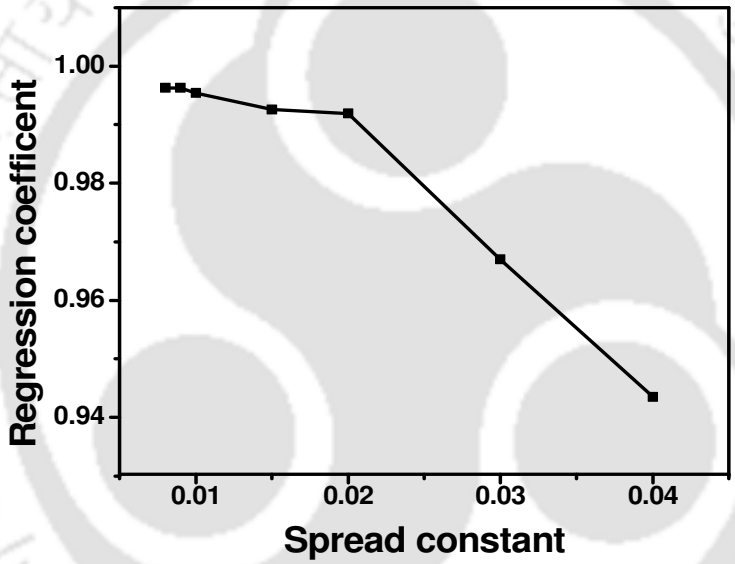

Fig. 5.6a. Variation of regression coefficient with spread constant

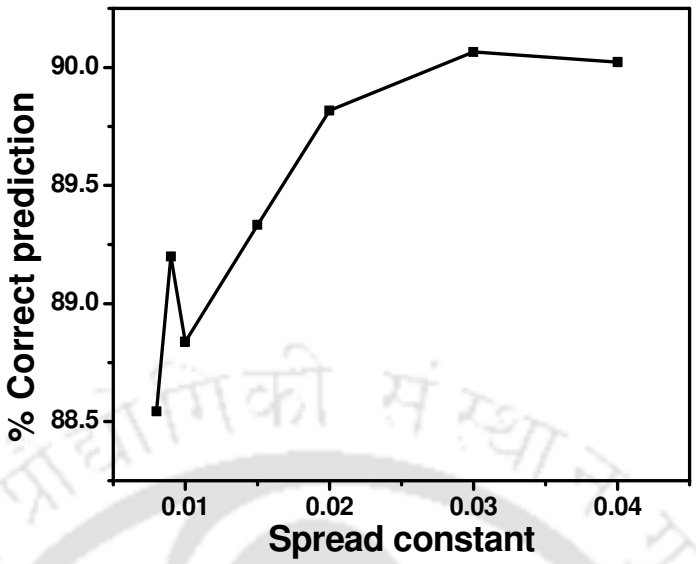

Fig. 5.6b. Variation of average % accuracy with spread constant

5.2.2.4 Prediction of horizontal flow pattern map by PNN

The completely trained PNN is tested for all flow regimes with different sets of data which was not used during the training as discussed in section 5.2.2.3. This well trained and tested PNN has been used to predict the experimental flow pattern map of oil-water flow through horizontal pipe pipeline as given in Chapter 4. The predicted flow pattern maps have been shown in Fig. 5.7 and experimental transition boundaries of different flow pattern have been drawn on the predicted map for comparison. The experimental transition boundaries have been drawn based on the outer most data series for a particular flow pattern. In the figure (Fig. 5.7) scattered data points are the flow patterns predicted by PNN and solid lines are experimental transition boundaries of various flow patterns observed in the present study. The points in the circle show the mismatching points of the flow patterns predicted by PNN. From the Fig. 5.7, it is clear that the mismatching points are very less in

the predicted flow regime map of horizontal flow. The accuracy in predicting different flow patterns

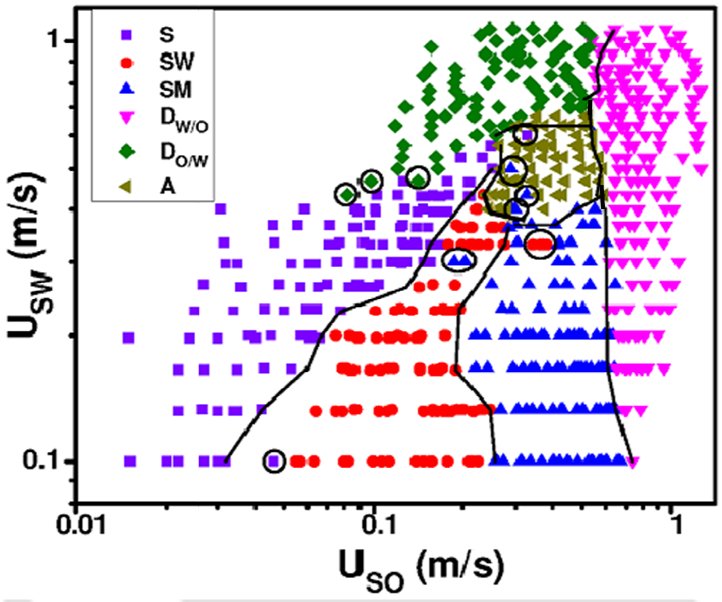

Fig. 5.7 Horizontal flow pattern map predicted by PNN

In horizontal flow using PNN has been shown in Fig. 5.8. The accuracy of prediction strongly depends on the number of data points used in the PNN training. Available data point for $D_{W/O}$ is much more compared to the stratified flow. As a result, $D_{W/O}$ achieves 99.8% accurate prediction compared to 91.5% accuracy of the stratified flow. Fig. 5.8 demonstrates that PNN has successfully predicted all the six flow patterns with an average error of 5% only.

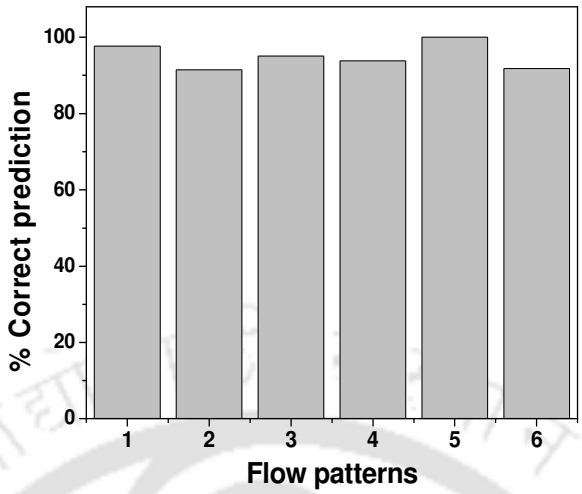

Fig. 5.8 Percentage correct predictions of flow patterns in horizontal flow (1-slug flow, 2-stratified flow, 3-stratified mixed flow, 4-dispersion of oil in water, 5-dispersion of water in oil, 6-Annular flow)

5.2.2.5 Prediction of inclined flow pattern map by PNN

Inclined experimental flow pattern map (Chapter 4) has also been predicted by the trained PNN and the predicted flow pattern map is shown in Fig. 5.9. In the figure various symbols are the predicted data by PNN and solid lines are experimental transition boundaries of inclined flow. The circled data are wrong prediction by PNN. The figure shows very less number of mismatching points in the predicted flow pattern map of inclined flow. The accuracy in prediction of different flow patterns of inclined pipeline using PNN has been shown in Fig. 5.10. Slug flow pattern has got more accurate prediction (98.5%) than the other flow patterns. Minimum (75%) accuracy in prediction has been observed for stratified flow this is due to less number of data available during the training process. Fig. 5.10 reveals that PNN has been predicted all the seven flow patterns with an average error of 10% only.

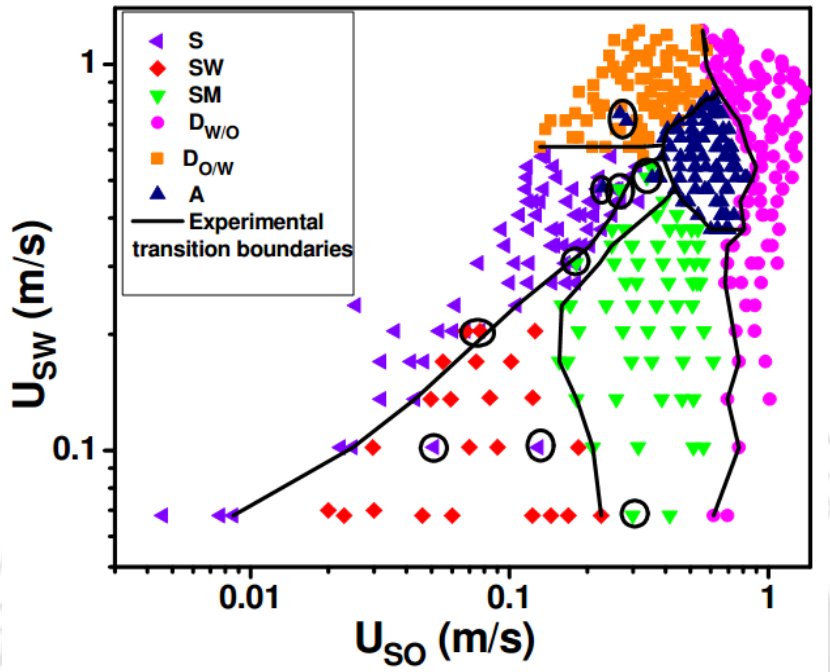

Fig. 5.9 Inclined flow pattern map predicted by PNN

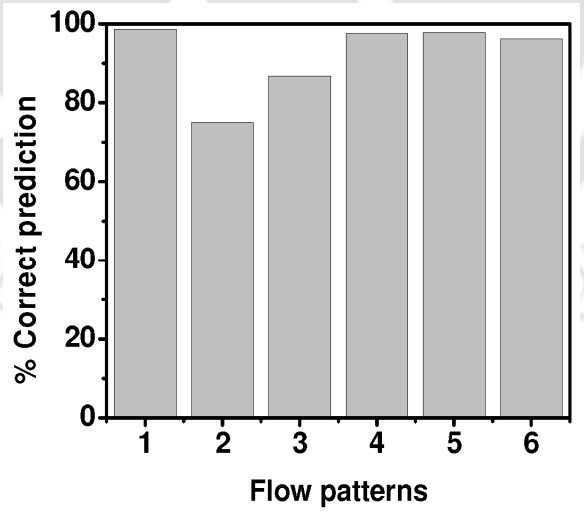

Fig. 5.10 Percentage correct predictions of flow patterns in inclined flow (1-slug flow, 2-stratified flow, 3-stratified mixed flow, 4-dispersion of oil in water, 5-dispersion of water in oil, 6-Annular flow)

5.3 Validation of PNN

The trained PNN successfully predicted both horizontal and inclined flow pattern maps. A well trained PNN can also predict a wide range of flow pattern data irrespective of system properties. So it can be used as a predictive tool for flow pattern maps. Different flow patterns from the literature work have been predicted demonstrating the pattern recognition capability of PNN as a predictive tool and its robustness. For this purpose, six flow pattern maps namely, - (1) Charles et al. (1961), (2) Rodriguez and Oliemans (2006) at 5º upward inclined, (3) Sotagia et al. (2008), (4) Rodriguez and Oliemans (2006) at 0º (horizontal), and (5) Fujji et al. (1994) and (6) Raj et al. (2005) have been selected for the prediction, dividing into two sections: 5.3.1 data which are used in training and 5.3.2 data which are not used in training. Data of first three have been used during the training process and predicted map of these are shown in Fig. 5.11a, b and c. Predicted maps of remaining three (data not used during PNN training) are presented in Fig. 5.12a, b and c. Last three data sets are completely independent of the trained PNN. These maps (all the six references) have been selected to test the suitability of the developed PNN for a wide range of system properties. In all the figures, scattered data points are obtained from PNN prediction and the solid lines are their respective experimental transition boundaries. The mismatching points are marked by circles. The nomenclature of the flow patterns are kept same as they appear in the original maps to avoid confusion. Predictions of flow pattern map for above two cases are discussed below.

5.3.1 Prediction of flow pattern data used in training

Fig. 5.11a represents the PNN predicted flow pattern map of Charles et al. (1961) with the viscosity ratio of 65, which is almost half of the viscosity ratio used in the present study. The X-axis and Y-axis represents water and oil superficial velocity (ft/s) respectively. The trained PNN successfully predicts oil slug flow which is considered as slug flow during flow pattern classification in the present work and is represented by blue square symbol in Fig. 5.11a. PNN also predicts oil bubble in water and oil drops in water (black triangles) as oil dispersed in water with good agreements. The predicted data have been segregated (oil dispersed in water as per our classification) according to their classification (oil drops in water and oil bubbles in water) and plotted in the figure to maintain similarity with the Charles et al. (1961)'s proposed flow pattern map. Few predicted data points are mismatching with the original map as marked by circles. Water dispersed in oil flow patterns have been predicted in a similar way and represented by inverted green triangles in the figure with a little deviation as marked in the figure. PNN is not trained for water slugs (due to lack of good number of literature data), and it predicts this region as a combination of oil slugs and annular flow pattern in the flow pattern map of Charles et al. (1961). The pink diamonds shown in Fig. 5.11a represent the annular flow pattern predicted by PNN and resulted good accuracy in prediction. Two major differences have been observed between the present work (horizontal flow pattern map) and the work by Charles et al. (1961):- (a) water slugs have not observed (b) observed stratified flow (wavy stratified and stratified mixed flow), which is not reported by Charles et al (1961). Important point to note that, the developed PNN successfully predicts the effect of system properties on flow pattern maps.

Prediction of a flow pattern map for 5^o upward inclined ($+5^o$) pipe line (Rodriguez and Oliemans (2006)) of a fluid pair having viscosity ratio of 9.4 and pipe diameter of 0.083 m has been presented in Fig. 511b for showing the wide applicability of a well-trained PNN. X-axis and Y-axis of the plot represents oil and water superficial velocities in m/s respectively as commonly done in literature. The PNN successfully predicts all the flow patterns, except few data points in the dispersion of oil in water and water, and oil in water homogeneous dispersion region (Rodriguez and Oliemans (2006)) as shown in Fig. 5.11b. Their flow pattern map consists of only stratified mixed flow and both the dispersion (oil dispersion in water and water dispersion in oil), which is according to present flow pattern classification. The difference in flow pattern map (as compared to the present inclined flow pattern map) is due to lower viscosity ratio (one tenth of the present work), higher pipe diameter (more than three times the present work) and upward inclination ($+5^o$), which destabilize the interface. Good prediction of flow pattern proves that all these effects have been successfully accounted for by our trained PNN.

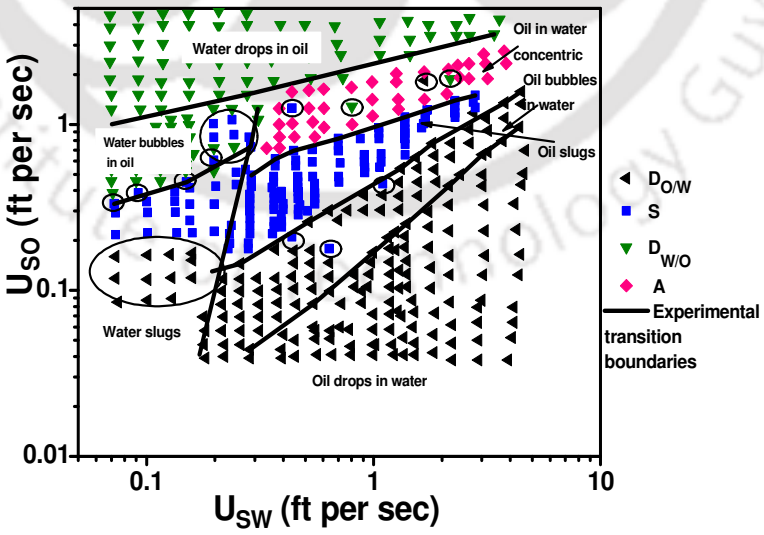

Fig. 5.11a Predicted flow pattern map of Charles et al. (1961) using PNN

Till now, the trained PNN have been tested against the fluids having lower viscosity as compared to present experimental fluid's viscosity. To demonstrate the applicability of trained PNN with higher viscosity ration, another flow pattern map has been selected proposed by Sotagia et al. (2008) for a fluid pair having viscosity ratio of 900, which is almost 9 times higher than the viscosity used in the present experimental study (Chapter 3) value. The predicted map (Fig. 5.11c) shows that PNN predicts well for all the flow patterns. The mismatching is found in their transition flow region, which is considered as oil dispersion in water in the present work.

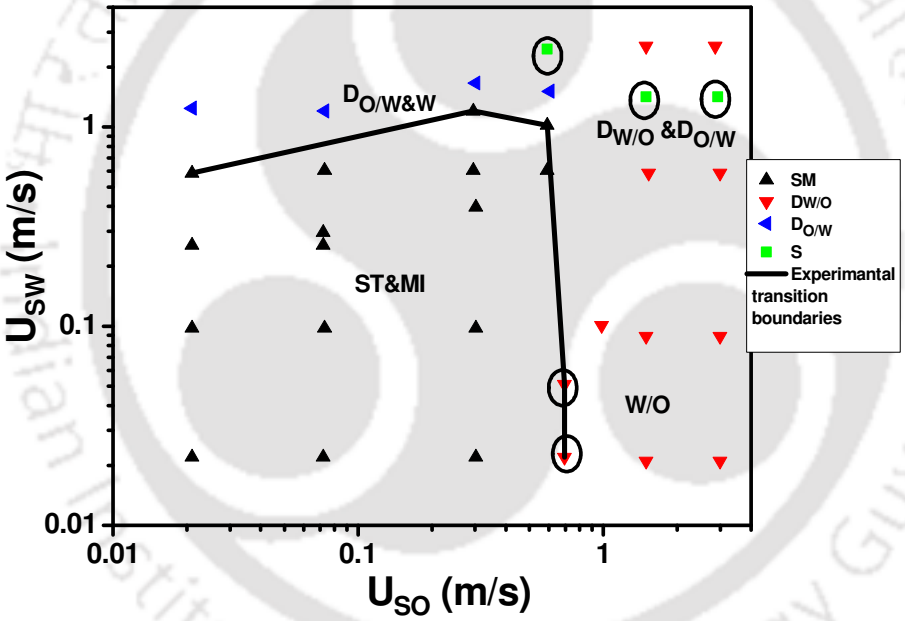

Fig. 5.11b Predicted flow pattern map (+5°) of Rodriguez and Oliemans (2006) using PNN

A relatively small deviation is observed in slug flow region with few mismatching points in annular flow region. Here, wavy annular and core annular flow have been considered as annular flow (See Fig. 5.5). Sotagia et al. (2008) observed core annular flow in a wide

range of superficial velocity of both the fluids because higher viscosity favors such kind of flow.

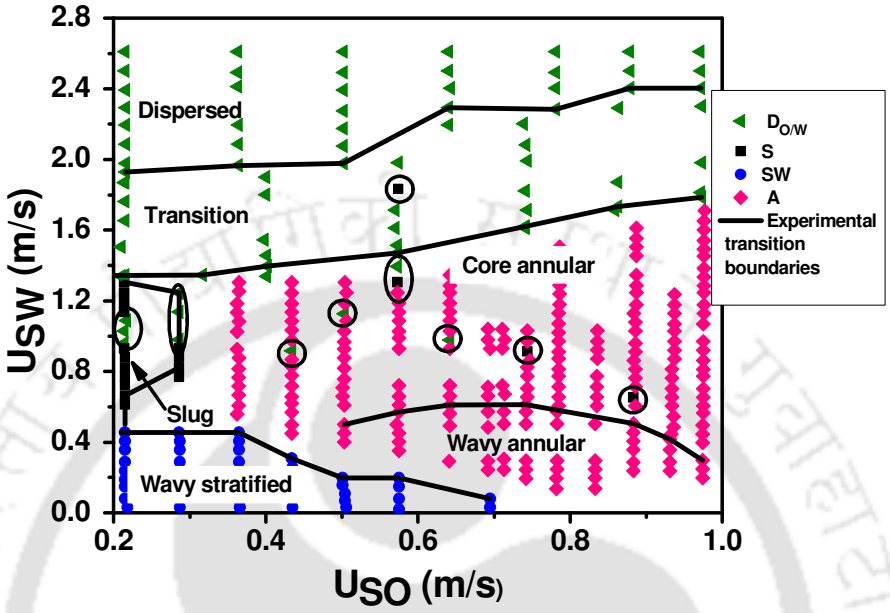

Fig. 5.11c Predicted flow pattern map of Sotgia et al. (2008) using PNN

5.3.2 Prediction of flow pattern data not used in training

Successful predictions of flow pattern maps have been observed by the trained PNN for the cases, where data have been incorporated during PNN development. Now, repotted the prediction of flow pattern maps for the cases, where data have not been incorporated during PNN development. It will also help to check its robustness in prediction. For this, predicted three flow pattern maps (horizontal) from literature with various fluid properties; they are flow pattern map of Rodriguez and Oliemans (2006), Fujji et al. (1994) and Raj et al. (2005) presented in Fig.5.12a, b and c respectively. Fig.5.12a shows good agreement with Rodriguez and Oliemans (2006)'s map, except few mismatching points. Their "oil in water homogeneous dispersion" and "dispersion of oil in water and water" are considered

as oil dispersed in water in the PNN. Similarly, "water in oil homogeneous dispersion" and "dispersion of water in oil and oil in water" are considered as water dispersed in oil flow**.** They observed smooth stratified flow in horizontal pipe which was absent in their 5^{o} upward flow pattern map (see Section 5.3.1). This difference is due to the absence of instability at the interface caused by the slope of the pipe line as discussed earlier. This difference is successfully accounted for by the developed PNN. In the present work (Chapter 4), a wavy flow pattern (long wave and short wave) is identified instead of smooth stratified flow in Rodriguez and Oliemans (2006) work. This is due to a long wave leads a smooth interface in larger diameter pipe. On the other hand, higher viscosity and smaller diameter enhance to the onset of waviness at the interface as observed in the present work.

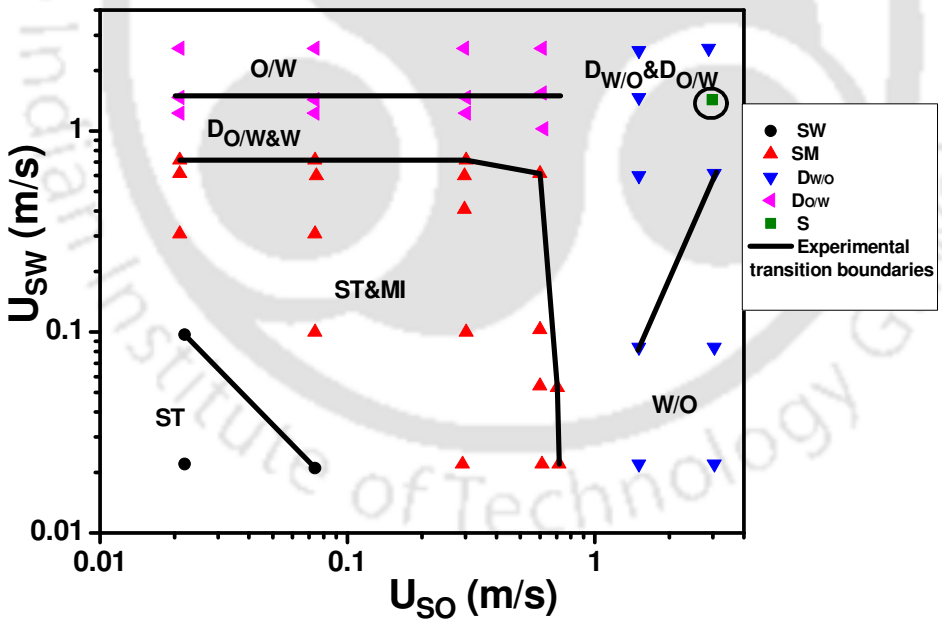

Fig. 5.12a Predicted flow pattern map (0º) of Rodriguez and Oliemans (2006) using PNN

Similarly, the trained PNN gives good prediction for the flow pattern map reported by Fujji et al. (1994) as shown in Fig. 5.12b. They used moderately viscous oil with viscosity ratio of 61.5 and density ratio of 0.98 in 0.025 m diameter horizontal pipe line. The trained PNN has predicted bubbly flow reported by Fujji et al. (1994) as dispersion of water in oil flow pattern. Similarly, inverted slug and inverted bubbly flow have been predicted as dispersion of oil in water flow pattern. Slug flow has been predicted with good accuracy with few mismatching points marked by circles in Fig. Fig. 5.12b. Present PNN has predicted inverted annular (Fujji, et al., (1994)) as annular flow pattern with good accuracy. Annular flow pattern reported by Fujji, et al. (1994) has been predicted with poor accuracy by present PNN. This is because they reported a different kind of annular flow (water in core and oil in annulus) in their work, and these types of data are not used in development of PNN. However, PNN gives good prediction for their inverted annular flow (as annular flow) which is commonly reported as annular flow in literature. They did not observe stratified flow patterns in their experimental study. The developed PNN successfully predicted flow pattern map of Fujji et al. (1994) with a wide range of fluid properties.

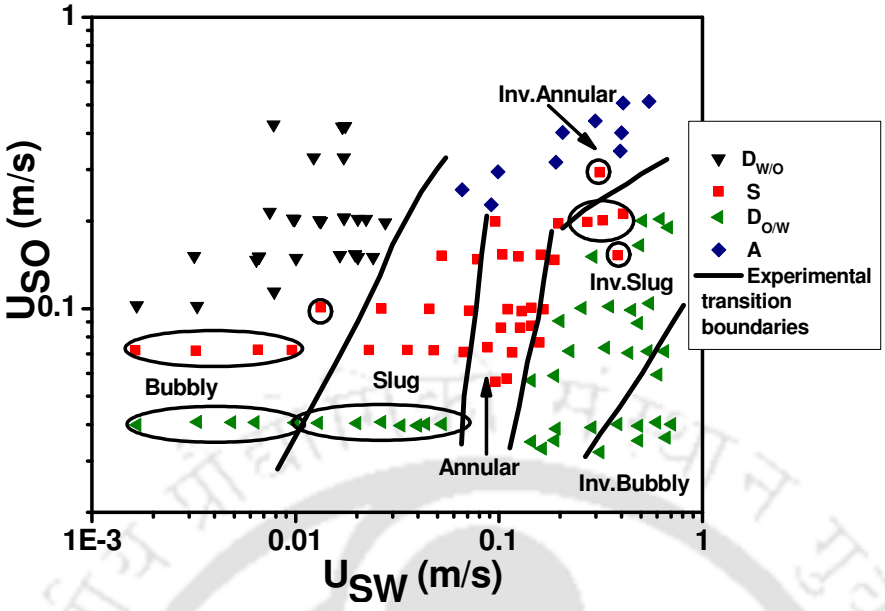

Fig. 5.12b Predicted flow pattern map of Fujji et al. (1994) using PNN

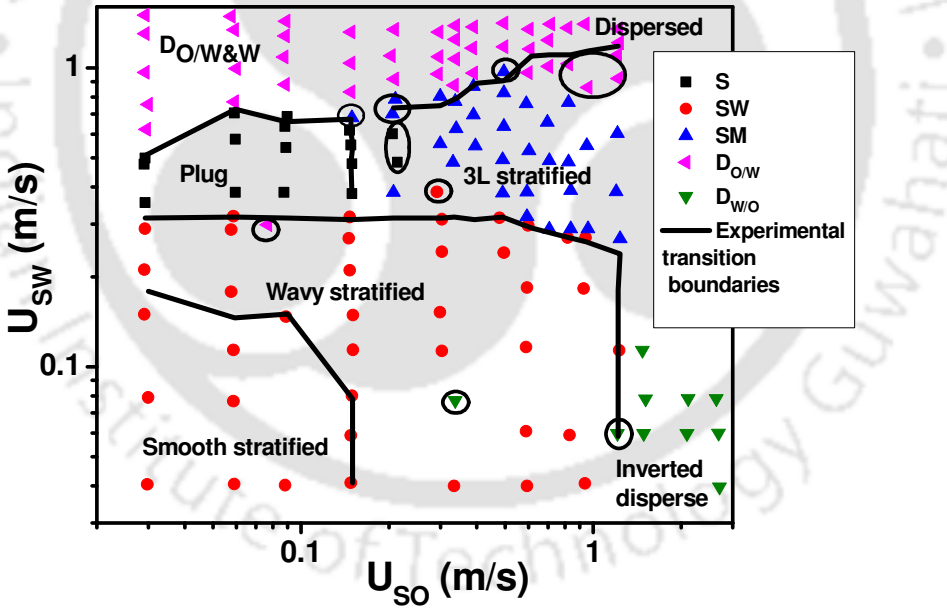

Fig. 5.12c Predicted flow pattern map of Raj et al. (2005) using PNN

Trained PNN has also predicted the flow pattern map of low viscous oil-water system reported by Raj et al. (2005) with viscosity ratio of 1.2 and density ratio of 0.787 in 0.025

m diameter pipe line. Developed PNN shows good prediction for the flow pattern map of Raj et al. (2005) as shown in Fig.5.12c with very less mismatching points.

During the PNN prediction we have observed that the prediction accuracy is highly influenced by the viscosity of the fluids. Therefore, to enhance the prediction accuracy for all the cases, the closer value of viscosity data should be used in development of PNN. It is also true for the pipe inclination.

5.4 Comparison between analytical and PNN predicted transition boundaries

The prediction accuracy of flow pattern transition boundaries has been obtained by comparing the transition boundaries of analytical and PNN with experimental flow pattern maps of horizontal and inclined pipeline. The parity plots for horizontal and inclined flows of various flow patterns transitions have been shown in Fig.5.13 and 5.14 respectively, in both the figures scattered data points are flow patterns identified in the experiments. Solid and broken lines are predicted transitions from analytical models and asterisk lines are the flow pattern transitions obtained from the PNN. From the figures it is evident that PNN gives better prediction than analytical models in both the pipelines. So PNN can be used as predictive tool for better prediction of flow patterns, if sufficient data has been for a system. The prediction accuracy of PNN strongly depends on viscosity and pipe inclination, the accuracy can be increased by using the closer values of viscosity and inclination during the training process.

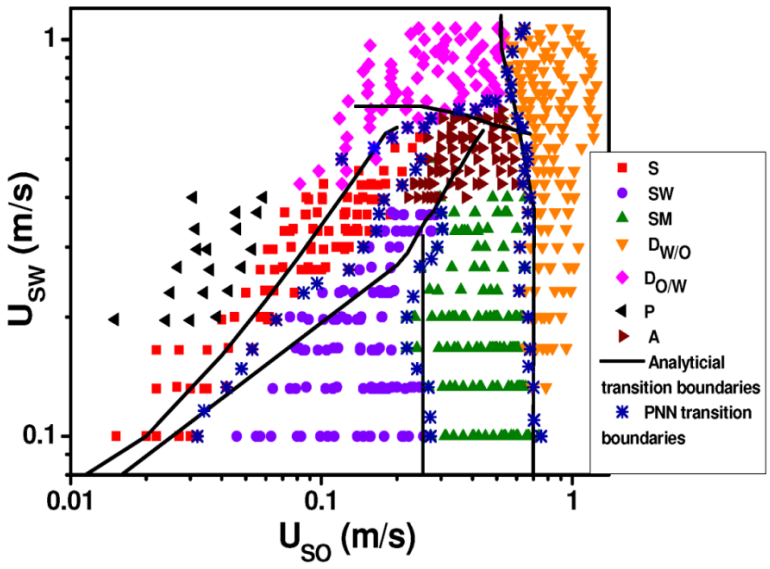

Fig. 5.13 Horizontal flow pattern map comparison with transition boundaries analytical and PNN

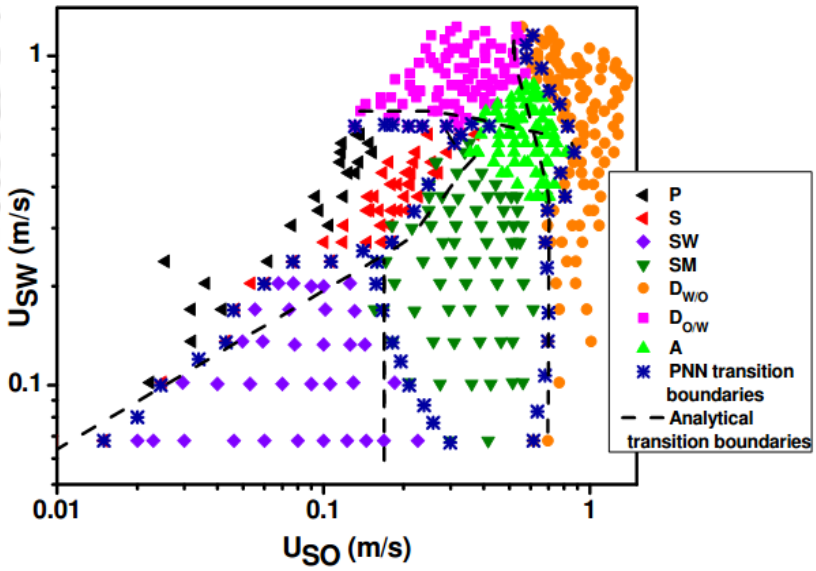

Fig. 5.14 Inclined flow pattern map comparison with transition boundaries analytical and PNN

5.5 Conclusions

The flow pattern transitions of horizontal and inclined pipelines have been predicted by analytical models. Analytical model gives the good prediction for transition boundary of dispersion of water in oil and wavy stratified to stratified mixed flow pattern in both the cases. Slug to annular, plug to slug, slug to wavy stratified and dispersion of oil in water flow pattern transition boundaries predicted by analytical models have shown poor accuracy. Due to this reason, another simple predictive technique (Probabilistic Neural Network) has also been adopted to predict flow patterns. Horizontal and inclined flow pattern maps have been predicted with good accuracy by developed PNN. PNN predicts all the flow patterns in horizontal pipeline within error of 5% and 10% in the inclined pipeline. The PNN has been validated with six other flow pattern maps available in literature to show its applicability as a predictive tool for wide range of fluid properties. The comparison between analytical and PNN prediction shows that PNN is giving better prediction than the analytical models. The accuracy in PNN prediction of flow patterns may be enhanced by using the closer viscosity ratios and inclinations during the training process of PNN.

Chapter 6

Hold up and pressure drop characteristics

6.1 Introduction

In petroleum industry, lubrication technique is used to reduce the frictional pressure loss during crude oil transportation through pipe network. Pressure drop is an important parameter in the design of an efficient transportation system, and is greatly affected by flow patterns, hold-up and fluid properties. Since last 60 years, several attempts have been made in understanding the science behind the pressure drop characteristics of liquid-liquid flow; and in most of the cases, theories based on gas-liquid flows have been followed.

It is very important to know the amount of water present in the transportation pipelines. The presence of water leads to corrosive environment and the free water leads to hydrate formation results the blockage of pipelines. At lower water cuts corrosion is not observed but at higher water cut significant corrosion rates are observed. So holdup plays a major role in designing a multiphase flow facility.

In the present chapter holdup and pressure drop characteristics in horizontal and inclined pipeline have been discussed. Experimental pressure drop data of horizontal flow has been predicted using the existing correlations (largely used for gas-liquid flow) to show the applicability of those correlations in the liquid-liquid two-phase flow. In addition to this, Lockhart-Martinelli correlation (Lockhart and Martinelli (1949)) has been modified to predict the experimental data of horizontal and 5° upward inclined flow. A correlation has

also been proposed based on dimensionless analysis for both the pipelines. A model has been developed to predict pressure drop of annular flow in both the systems (horizontal and inclined) by considering entrainment factor. The measured holdup in both the flows has been predicted using existing correlations in the literature.

6.2 Experimental holdup and pressure drop

The estimation of the in-situ volume fraction occupied by either of the phases in the both the conduit has been carried out. The quick closing valve technique as discussed in the 3rd chapter has been adopted for this purpose. The experimental results of holdup in horizontal and inclined pipelines are depicted below.

The in situ volume fractions for the entire flow range are plotted against the superficial velocity of one phase keeping other phase velocity as parameter. In the present system the data has been plotted as oil holdup (H_O) verses superficial oil velocity (U_{SO}) with water superficial velocity as parameter in Fig. 6.1 and Fig. 6.2 for horizontal and inclined pipeline respectively for all the flow regimes. From the figures it observed that oil holdup increases with increase in oil superficial velocity and decreases with water velocity. The increasing trend is same for all the flow regimes for both the pipelines.

Experiments conducted in horizontal and inclined pipeline with a constant diameter throughout the length. Therefore, manometer measures the frictional pressure drop only for horizontal pipeline and total pressure drop for inclined pipeline. Measured pressure gradients in both the systems (horizontal and inclined) are plotted as a function of input water cut ($C_W = (U_{SW}/U_{SW} + U_{SO})$) at constant water superficial velocity, as shown in Fig.

6.3 and Fig. 6.4 respectively. Input water cut is varied by varying water superficial velocity at constant oil superficial velocity. In both the figure different symbols represents various oil superficial velocity. Pressure gradient has been increased with increase in water cut as well as oil superficial velocity in both the cases. Mixture density **(ρ_m)** and velocity (Um) are increasing with increasing water cut while friction decreases at this condition. As a whole, pressure drop increases with water velocity.

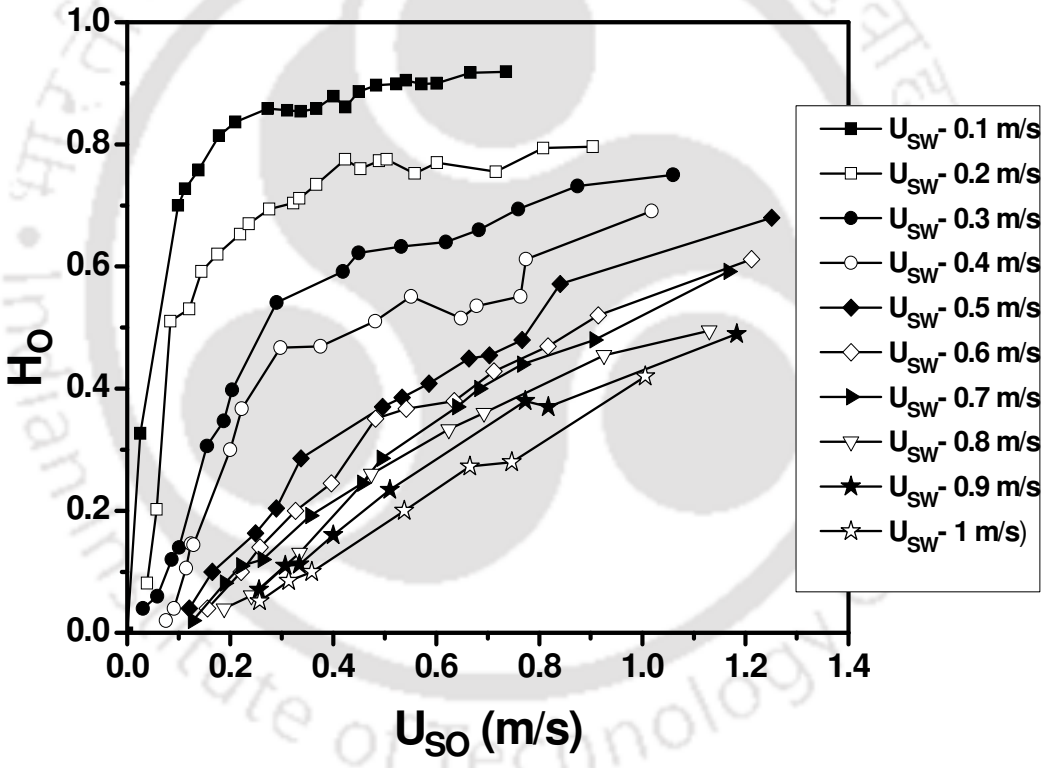

Fig. 6.1 Variation of oil holdup with superficial velocity of oil in horizontal flow

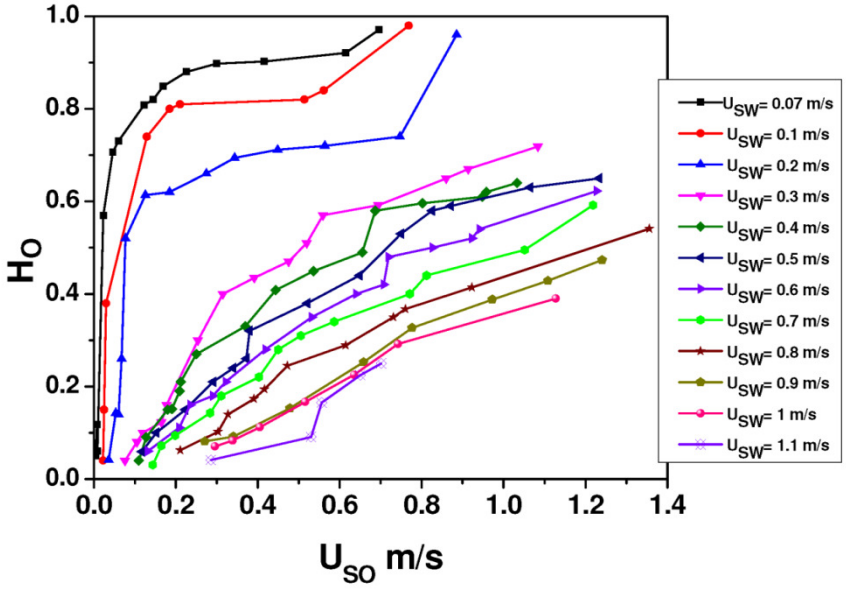

Fig. 6.2 Variation of oil holdup with superficial velocity of oil in inclined flow

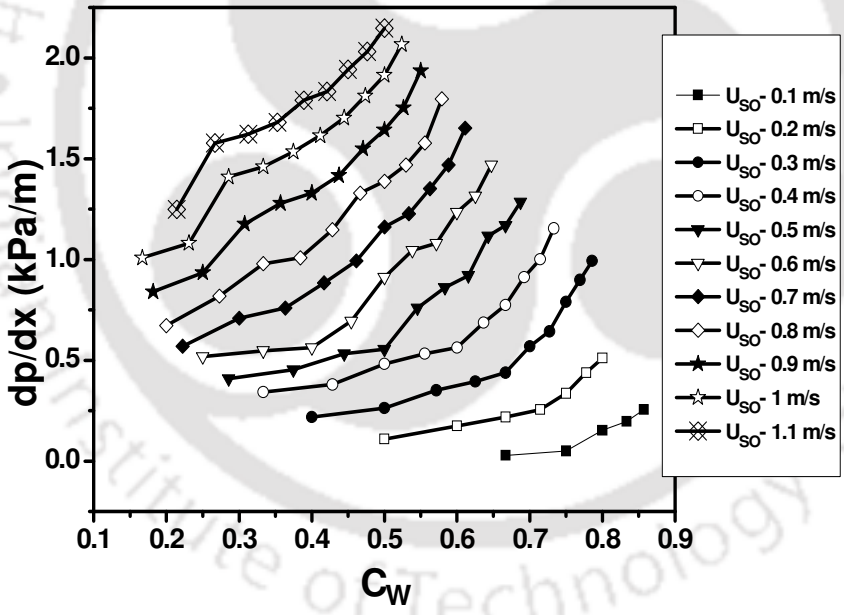

Fig. 6.3 Variation of experimental pressure gradient with water cut

$(C_W = (U_{SW}/U_{SW} + U_{SO}))$ in horizontal flow

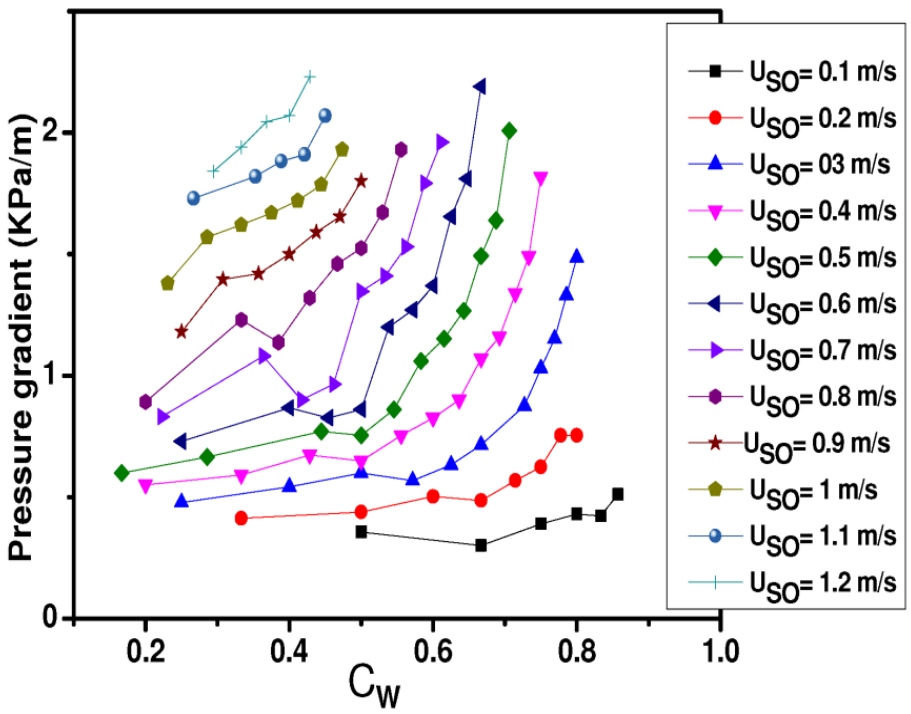

Fig. 6.4 Variation of experimental pressure gradient with water cut

$(C_W = (U_{SW}/U_{SW} + U_{SO}))$ in inclined flow

Fig. 6.4 shows a certain decrease in pressure drop in the range of water cut from 0.3 to 0.6 at oil superficial velocities between 0.6-0.8. The pressure drop again rises after these oil velocities, which shows the presence of annular flow in this region where the pressure drop decreases even with increase in superficial velocity. Decrease in pressured drop is very small in case of horizontal flow and it is observed in the range of oil superficial velocity 0.4-0.6 m/s (Fig. 6.3). This may be because of annular flow is less stable in horizontal pipeline.

6.3 Correlations for pressure drop prediction

An attempt has been made to predict the pressure drop of horizontal and inclined flow in this section based on correlations. The details of the prediction have been discussed in the following sections.

6.3.1 Prediction of pressure gradient in horizontal flow

Even though there are numerous experimental and theoretical studies, there is no general model for the reliable prediction of pressure drop in liquid-liquid two-phase flow. The reason behind this is the complex nature of multiphase flow like deformation of the interfaces, interaction and non-equilibrium effect among phases. To avoid these difficulties, simple correlations are used for the prediction of multiphase flow pressure drop. There are several empirical correlations to predict pressure gradient of gas-liquid two-phase flow. The following correlations have been selected to predict pressure drop in horizontal pipe from the literature which are applicable for pipe flow without phase change: Lockhart and Martinelli correlation (Lockhart and Martinelli (1949)), Chisholm correlation (Chisholm (1967)), Chisholm correlation (Chisholm (1973)), Chawla correlation (Chawla (1967)), Friedel correlation (Friedel (1980)), Muller-Steinhagen and Heck correlation (Muller Steinhagen and Heck (1986)), Cicchitti correlation (Cicchitti (1960)) and Bankoff correlation (Bankoff (1960)). The detailed of these correlations are discussed and predicted results are presented below.

a. Lockhart and Martinelli correlation (1949): The pioneering work in the area of gas-liquid two phase fluid has been done by Lockhart and Martinelli (Lockhart and Martinelli

(1949). They have formulated a graphical correlation, which is a combination of empirical analysis and resource-sensitive reasoning. Lockhart and Martinelli proposed a model for the calculation of two-phase pressure drop in gas-liquid flow using a simple concept that two-phase pressure drop is equal to a single phase pressure drop of either phase (gas or liquid) multiplied by a factor known as two-phase multiplier. The factor was defined as,

$$\phi_l^2 = \frac{\left(\frac{dp}{dx}\right)_{tp}}{\left(\frac{dp}{dx}\right)_l} \tag{6.1}$$

and $$\phi_g^2 = \frac{\left(\frac{dp}{dx}\right)_{tp}}{\left(\frac{dp}{dx}\right)_g} \tag{6.2}$$

$\left(\frac{dp}{dx}\right)$ is pressure gradient calculated using standard formula of as,-

$$\left(\frac{dp}{dx}\right) = \left(\frac{2 f \rho U^2}{D}\right) \tag{6.3}$$

$$f = \frac{16}{\text{Re}} \qquad \text{for Re} < 2100 \tag{6.4}$$

$$f = \frac{0.079}{\text{Re}^{0.25}} \qquad \text{for Re} > 2100 \tag{6.5}$$

$$\text{Re} = \frac{DU\rho}{\mu} \tag{6.6}$$

To find (ϕ_g) or (ϕ_l) they defined the following parameter known as "Martinelli parameter".

$$X^2 = \frac{\phi_g^2}{\phi_l^2} = \frac{\left(\frac{dp}{dx}\right)_l}{\left(\frac{dp}{dx}\right)_g} \tag{6.7}$$

The Martinelli parameter X was calculated easily by calculating single phase pressure drop whereas (ϕ_g^2) or (ϕ_l^2) was calculated from measured two-phase pressure drop and single phase pressure drop of either phase. They proposed a graphical relationship of X with ϕ_g^2 and ϕ_l^2 respectively. These graphical relationships are function of flow pattern (either laminar or turbulent). Four probable combinations of flow patterns are possible: (1) gas and liquid both in laminar (*l*-*l*), (2) gas in laminar and liquid in turbulent (*l*-*t*), (3) gas in turbulent and liquid in laminar (*t*-*l*), (4) gas and liquid both in turbulent (*t*-*t*). Based on these combinations they suggested four graphical correlations, which are widely used to calculate pressure drop of gas-liquid flow.

Present experimental data belongs to laminar (oil)-turbulent (water) region. Using the graphical correlations (which is valid for laminar turbulent flow), experimental value of pressure drop for viscous oil water flow has been predicted and a comparison with experimental data. The percentage deviation obtained from the prediction has been given in Table 6.1. The percentage error in the prediction is very high (~ 1400%), which may be attributed to the lower density and lower to higher viscosity ratio compared to gas-liquid system. Therefore, the Lockhart and Martinelli correlation needs to be modified to apply in liquid-liquid two phase flow.

b. Chisholm correlation (Chisholm (1967, 1973)): Chisholm (1967) attempted to develop a suitable mathematical expression for two-phase multiplier which was very

important parameter in Lockhart-Martinelli graphical correlations. He proposed the following empirical correlations for two-phase multipliers.

$$\phi_l^2 = 1 + \frac{C}{X} + \frac{1}{X^2} \tag{6.8}$$

$$\phi_g^2 = 1 + CX + X^2 \tag{6.9}$$

Where, the value of C depends on regimes of gas and liquid flow (laminar or turbulent). For example, C=5for laminar-laminar, C=20 for turbulent-turbulent, C=10 for laminar-turbulent flow and C=12 for turbulent-laminar flow. These values of C give a very close result to the Lockhart-Martinelli (Lockhart and Martinelli (1949)) plot for two-phase multipliers and it is widely adopted in place of Lockhart-Martinelli (Lockhart and Martinelli (1949)) plot. The value of C has been selected as 10 since present experimental data belong to laminar-turbulent flow regime. Table 6.1 shows a large mismatching (average error 1164%) with the experimental results, because this correlation is almost similar to the Lockhart-Martinelli (1949) graphical correlation and applicable for gas-liquid flow. It implies that a new correlation of two- phase multiplier is required for liquid-liquid flow. The modified forms of Chisholm correlation have also been proposed by Saisoron and Wongwises (2008) and Sun and Mishima (2009) for air water flow through circular micro and mini channel with appreciable accuracy.

Chisholm (1973) derived another correlation from the graphical correlation proposed by Baroczy (1965). Baroczy (1965) proposed two set of curves to calculate pressure gradient of two-phase flow with phase change and without phase change. One set of curves correlates two-phase multiplier and physical properties index $\left\{\left[\left(\mu_f/\mu_g\right)^{0.2}\left(\vartheta_f/\vartheta_g\right)\right]\right\}$ with

quality (x) at a mass velocity of 1356 kg/m^{2}s. Another set of curves represents the correction factor as a function of same physical properties index at different mass velocities with quality which is used to get a correction factor of two-phase multiplier. He developed the correlation from a large data bank of water-water vapor, air-water and mercury-nitrogen systems and it is widely used for the system like pipe line flow without phase change. Based on these graphical correlations, Chisholm (1973) gave the mathematical expression of two-phase multiplier as

$$\phi_{ch}^2 = 1 + \left(Y^2 - 1\right)\left[Bx^{2-n/2} + x^{2-n}\right] \tag{6.10}$$

Here $Y^2 = \Delta P_G / \Delta P_L$ and value of Y depends on B and mass flux:

If $0 < Y < 9.5$, $B = \dfrac{55}{G^{0.5}}$ for $G \geq 1900$ Kg/m^2 s, (6.11)

$B = \dfrac{2400}{G}$ for $500 < G < 1900$Kg/m^2 s, (6.12)

and $B = 4.8$ for $G < 500$Kg/m^2 s (6.13)

If $9.5 < Y < 28$,

$B = \dfrac{520}{YG^{0.5}}$ for $G \leq 1900$ Kg/m^2 s, (6.14)

and $B = \dfrac{21}{Y}$ for $G > 600$Kg/m^2 s (6.15)

If $Y > 28$,

$B = \dfrac{15000}{Y^2 G^{0.5}}$ (6.16)

And he calculated two-phase pressure drop from the following equation

$$\left(\frac{dp}{dx}\right)_{tp} = \phi_{ch}^2 \left(\frac{dp}{dx}\right)_l \tag{6.17}$$

This correlation has been used for the prediction of experimental pressure gradient values and a comparison between predicted and experimental result is shown in Table 6.1. It shows a large deviation (~3000%). It is clear that this correlation cannot be used for liquid-liquid two-phase flow.

c. Chawla correlation (1967): Slip between two phases is an important parameter in multiphase flow. It contributes a major role in the variation of void fraction in pipeline of the input volume fraction of the phases. It has a great role on two-phase multiplier which governs the two-phase pressure drop in Lockhart and Martinelli (1949) and Chisholm (1967, 1973) correlations. This parameter (viz., slip between the phases) was not considered in the correlations proposed by Lockhart and Martinelli (1949) and Chisholm (1967, 1973). Chawla (1965) incorporated slip parameter terms in the form of slip ratio (S) into the correlation of two-phase multiplier and his proposed correlation is as follows,

$$\left(\frac{dp}{dx}\right)_{friction} = \left(\frac{dp}{dx}\right)_g \phi_{Chaw} \tag{6.18}$$

$$\phi_{Chaw} = x^{1.75}\left[1 + S\left(\frac{1-x}{x}\frac{\rho_g}{\rho_l}\right)\right] \tag{6.19}$$

Here pressure gradient of gas phase calculated from Eq. (6.3)

$$S = \frac{1}{9.1\left(\frac{1-x}{x}\left(\mathrm{Re}_g\, Fr_H\right)^{-0.167}\left(\frac{\rho_l}{\rho_g}\right)^{-0.9}\left(\frac{\mu_l}{\mu_g}\right)^{-0.5}\right)} \tag{6.20}$$

Where, $Fr_H = \frac{G^2}{gD\rho_h^2}$ (6.21)

and $\rho_h = \left(\frac{x}{\rho_g} + \frac{1-x}{\rho_l}\right)^{-1}$ (6.22)

The correlation is valid for high gas phase quality like annular flow. Here this correlation used to predict present experimental data and the deviation is shown in Table 6.1. A significant improvement has been observed as compared to Lockhart and Martinelli (1949) and Chisholm (1967, 1973) correlations. Chawla (1965) has been observed with an average error of 750%.

d. Friedel correlation (1980): Friedel (1980) proposed a correlation for two-phase multiplier which is one of the most accurate correlations in two-phase flows with viscosity ration less than 1000. The proposed correlation is as follows:

$$\left(\frac{dp}{dx}\right)_{tp} = \left(\frac{dp}{dx}\right)_l \phi_{fo}^2 \quad (6.23)$$

and it is given by

$$\phi_{f0}^2 = E + \frac{3.24FH}{F_{rH}^{0.045} W_{eL}^{0.035}} \quad (6.24)$$

Where F_{rH}, E, F, H are expressed as follows

$$F_{rH} = \frac{G^2}{gD\rho_h^2} \quad (6.25)$$

$$E = (1-x)^2 + \frac{x^2 \rho_l f_g}{\rho_g f_l} \quad (6.26)$$

$$F = x^{0.78}\left(1-x\right)^{0.224} \tag{6.27}$$

$$H = \left(\frac{\rho_l}{\rho_g}\right)^{0.91}\left(\frac{\mu_g}{\mu_l}\right)^{0.91}\left(1-\frac{\mu_g}{\mu_l}\right)^{0.7} \tag{6.28}$$

$$W_{eL} = \frac{G^2 D}{\sigma \rho_h} \tag{6.29}$$

Homogeneous density ρ_h is calculated from Eq. (6.22). It is noted that two-phase multiplier is expressed in terms of physical properties of the fluids, Martinelli parameter and quality. It is a more logistic correlation and would be expected to give better prediction than the others. Here ρ_l and ρ_g are replaced by ρ_{water} and ρ_{oil} respectively for adopting the expression to oil-water system. Using this modified correlation, experimental pressure gradient has been predicted. A drastic improvement is observed in the prediction with an average error of 300%, nevertheless a better prediction than Chisholm correlation (1967) (average error 1164%). This improvement in the accuracy in the prediction may be due to the inclusion of individual viscosity, density and mixture density of the system in the correlations.

e. Muller Steinhagan–Heck correlation (1986): Muller Steinhagan-Heck (1986) checked the reliability of fourteen different correlations and found that Bandel (1973) correlation gives a close agreement with the experimental results. Although the correlation is quite complex in nature, it has potential practical applications. In an attempt to develop a simplified expression for the calculation of two-phase frictional pressure drop, Muller Steinhagan–Heck (1986) suggested the following expression:

$$\left(\frac{dp}{dx}\right)_{f,tp} = F\left(1-\dot{x}\right)^{1/3} + B\dot{x}^3 \tag{6.30}$$

$$F = A + 2(B - A)\dot{x} \tag{6.31}$$

$$\dot{x} = \frac{\dot{m}_g}{\dot{m}_g + \dot{m}_l} \tag{6.32}$$

A and B are the frictional pressure gradients of liquid $\left[\left(\frac{dp}{dx}\right)_l\right]$ and gas $\left[\left(\frac{dp}{dx}\right)_g\right]$ respectively and are calculated from Eq. (6.3)

Here calculated pressure drop of oil-water flow through horizontal pipeline and compared with the experimental results are shown in Table 6.1. The results show the significant improvement in the prediction with an average error of ±60%.

f. Cicchitti correlation (1960): Cicchitti (1960) proposed a correlation for two-phase pressure gradient instead of two-phase multiplier, developed principally for steam-water system. But it has been proven to work reasonably well for other systems too (Quben 2005) hence, this correlation is used to predict experimental data on oil-water system. The correlation is as follows:

$$\left(\frac{dp}{dz}\right)_{friction} = \frac{0.092}{D^{1.2}} G^{1.8} \left[\mu_L - x(\mu_L - \mu_G)\right]^{0.2} \left[v_L + x(v_G - v_L)\right] \tag{6.33}$$

The results of the prediction are presented in Table 6.1. It shows an average error of 60%, comparable to the Muller Steinhagan–Heck (1986) correlation.

The predicted results using the above mentioned correlations are shown in Table 6.1, along with the characteristics of the correlations and % error in prediction. The error given in

Table 6.1 is the average of absolute percentage error and is calculated using the following expression.

$$AAPE = \left[\frac{1}{n} \sum_{k=1}^{n} \left| \frac{\left(\frac{dp}{dx}\right)_{Pred} - \left(\frac{dp}{dx}\right)_{Exp}}{\left(\frac{dp}{dx}\right)_{Exp}} \times 100 \right| \right] \tag{6.34}$$

The above discussion reveals that no existing correlation is suitable for liquid-liquid two-phase flow, even after introducing the liquid properties in correlations. All correlations except Muller Steinhagan–Heck (1986) and Cicchitti (1960) has given large deviation in prediction. The deviation in Muller Steinhagan–Heck (1986) and Cicchitti (1960) correlations is less (60% only), as compared to others, which shows a drastic improvement in prediction. This is due to the basic difference in formulation of the correlations. Muller Steinhagan–Heck (1986) and Cicchitti (1960) proposed correlation for total frictional pressure gradient directly $((dp/dx)_{friction,tp})$, whereas, others have formulated the correlation for two-phase multiplier (ϕ_l^2 or ϕ_g^2), and total two-phase frictional pressure drop is calculated as ϕ_l^2 or ϕ_g^2 times of a single phase flow (either phases). However, error of 60% is also not a good agreement with present experimental results**.** This lack of predictability of existing correlations motivates to formulate new correlations for liquid-liquid two-phase flow. Here two approaches have been followed for this development - (1) Lockhart and Martinelli (1949) approach by introducing modified graphical correlation for two-phase multiplier and (2) dimensional analysis.

6.3.2 Development of correlation in horizontal flow

6.3.2.1 Lockhart and Martinelli approach

Data collection: Regression analysis is required for the application of above mentioned methodologies. A large number of data is needed for such analysis and to incorporate a wide range of fluid and conduit properties in the correlation. Combining the present experimental data and different literature data as shown in Table 6.2 a data bank of 701 data points have been prepared for liquid-liquid flow. 584 data points out of 701 have been used in developing the correlation as shown in Table 6.2. Remaining 117 data points are used for validation. The developed correlation is also validated with 48 data points (those are used in correlation development) taking from Trallero et al. (1995) and Rodriguez and Oliemans (2006) work (21 and 27 data points respectively). The prepared data bank contains pressure drop values with various physical properties and geometric properties of the system (Table 6.2). The table shows that the density ratios of the various fluids are varying in the range of 0.787-1. Densities of most of the crude oils are in this range. Data has also been collected for low viscous (viscosity ratio = 1.2) and high viscous (viscosity ratio = 800) fluids. Pipe diameter, roughness of pipe wall and wall wetting properties of the pipe material has a strong influence on the pressure drop. Organic pipes (like cellulose acetate butyrate, Polymethyl methacrylate, etc.) are smoother than the metallic pipes (steel). As a result, frictional pressure is more in metallic pipes than organic pipe. To encounter all the effects in correlation, organic and metallic pipe material have been considered with different diameters (Table 6.2).

Martinelli parameter (X) as shown in Eq. (6.7) and two-phase multiplier in terms of ϕ_W^2 has been evaluated using the data bank (Table 2) according to the Eq. (6.2). A multiple regression analysis has been done to correlate Martinelli parameter (X) and two-phase multiplier as shown in Fig.6.5. The range of Martinelli parameter (X) in the present work and in original Lockhart and Martinelli plots are 0.1-20 and 0.01- 100 respectively. On the other hand, the present experimental data belongs to laminar oil-turbulent water region (laminar-turbulent), Where oil ((Re_O)) and water (Re_W) Reynolds numbers varies from 3.15- 259.94 and 2500- 26 667 respectively. The Reynolds numbers are calculated based on superficial velocity of each fluid.

Table 6.1 Correlations used for prediction

Correlation	Flow conditions	Geometry	Flow pattern	Fluid Pairs	Features	%Error
Lockhart and Martinelli (1949)	Gas-liquid flow without phase change	Not specified	All flow regimes	Air-water	Graphical correlation of two-phase multiplier	1398
Chisholm (1967)	Gas-liquid flow without phase change	Not specified	All flow regimes	Air-water	Mathematical expression of two-phase multiplier	1164
Chisholm (1973)	Gas-liquid flow with and without phase change	Circular horizontal and vertical pipes	Turbulent flow of mixture	Air-water, Steam-water, Mercury-nitrogen	Two-phase multiplier for pipeline flow with and without phase change	3078
Chawla (1965)	Gas-liquid flow with and without phase change	Circular horizontal pipes	All flow patterns including annular flow	Air-water, Steam-water	Correlation of two-phase multiplier with slip ratio	750
Friedel (1980)	Gas-liquid flow with and without	Circular horizontal pipes and	All flow patterns	Air-water, Steam-water	Two-phase multiplier as a function of fluid	300

	phase change having $\mu_l/\mu_g<1000$	vertical pipes			properties	
Muller Steinhagan–Heck (1986)	Gas-liquid flow with and without phase change having $Re_l > 100$	Not specified	Annular, stratified, transition	Air-water, Steam-water, Air-oil, Nitrogen-Nitrogen,	Correlation for frictional pressure gradient	60
Cicchitti (1960)	Gas-liquid flow with phase change	Circular pipes	Not specified	Steam-water	Correlation for frictional pressure gradient	60

Fig. 6.5 shows that present horizontal data covers lower portion of Lockhart and Martinelli plot, which is asymptotic in nature. From multiple regression analysis using Microsoft Excel -2007, the expression of two-phase multiplier in horizontal flow is obtained as,

$$\phi_W^2 = \frac{0.019}{X^3} + \frac{0.06}{X^2} - \frac{0.006}{X} + 1.397 \qquad (6.35)$$

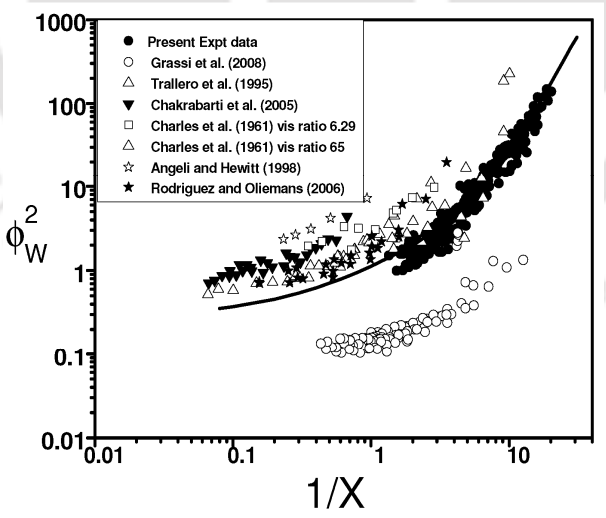

Fig. 6.5 Relationship between two-phase multiplier (Φ^2_W) with Lockhart-Martinelli parameter (X) in horizontal flow

A good regression coefficient value of 0.85 for the above expression is obtained from the regression statistics. The proposed correlation has been validated with present experimental data (100 data points) those are not used during the development of correlation as shown in Fig. 6.6a. The prediction shows a good accuracy with an average absolute error of 22% including all types of flow regimes. A ±22% error bars has been drawn in the figure based on this value. The error is less compared to other existing correlations as shown in Table 6.1.

Table 6.2 List of literatures used to prepare data bank

Authors	Pipe ID(m)	Pipe material	Viscosity ratio	Density ratio	Number of data points (*l-t* region)
Charles et al. (1961)	0.0264	Cellulose Acetate butyrate	6.29 65	1 1	12 19
Trallero et al. (1995)	0.0508	Acrylic	29.7	0.852	31
Angeli and Hewitt (1998)	0.0254	Stainless steel, Acrylic	1.6	0.801	5
Chakrabarti et al. (2005)	0.0254	PMMA	1.42	0.787	27
Rodriguez and Oliemans (2006)	0.0828	Steel	9.4	0.776	38
Grassi et al. (2008)	0.021	Polycarbonate	800	0.866	118
Present work	0.0254	PMMA	107	0.889	334
				Total	584

The proposed correlation has also been validated with literature data (those are used and not used in developing the correlation). Charles et al. (1961) data for the system having viscosity ratio 16.8 and density ratio 1.0 has been predicted. These data is in laminar-turbulent region, and is not used in developing the correlation. The prediction shows an average absolute error of 25% as shown in Fig. 6.6b and it is marked with an error bar of ±25%.

Similarly, data of Trallero et al. (1997) and Rodriguez and Oliemans (2006) (used in developing the correlation) have been predicted in Fig.6.6c and Fig.6.6d respectively. The system specification is as mentioned in Table 6.2.

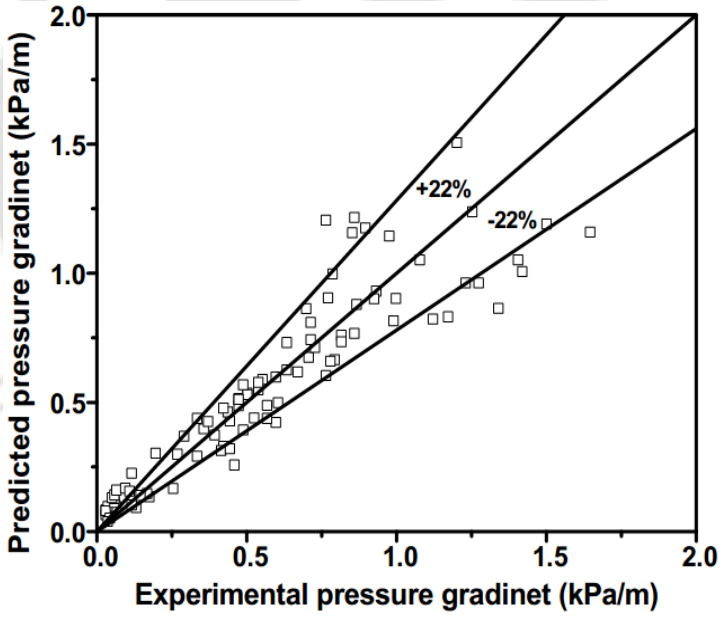

Fig. 6.6a Comparison between predicted and experimental pressure gradient in horizontal flow by Lockhart-Martinelli approach

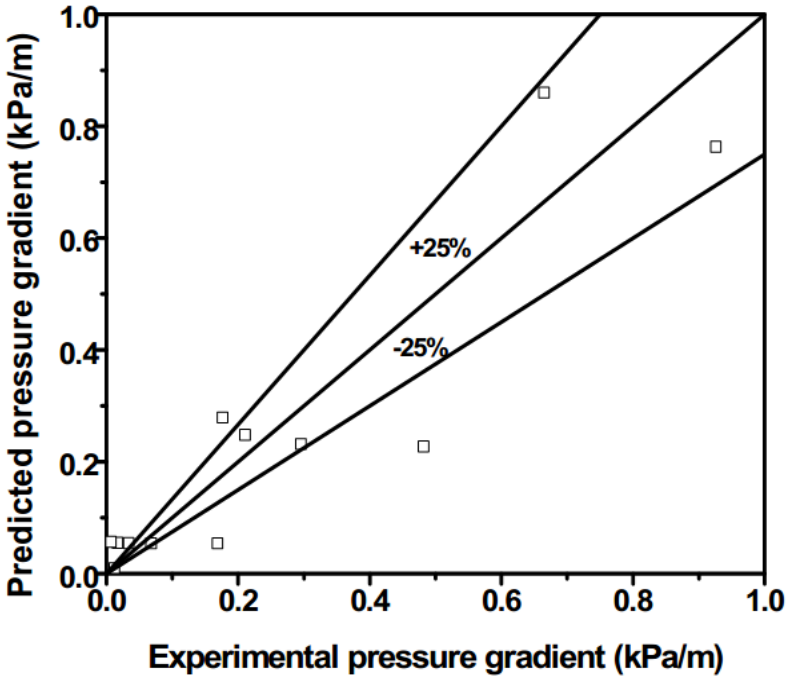

Fig. 6.6b Predicted pressure gradient data of Charles et al. (1961) by Lockhart-Martinelli approach

The prediction shows reasonable deviations of 25% and 29.1 % for Trallero et al. (1997) and Rodriguez and Oliemans (2006) respectively. The present correlation is developed based on large number of data bank, which includes wide range of viscosity, density, pipe diameter and pipe materials as mentioned in Table 6.2. Therefore, it has a wide applicability in predicting pressure drop characteristics especially for a two-fluid flow in pipeline.

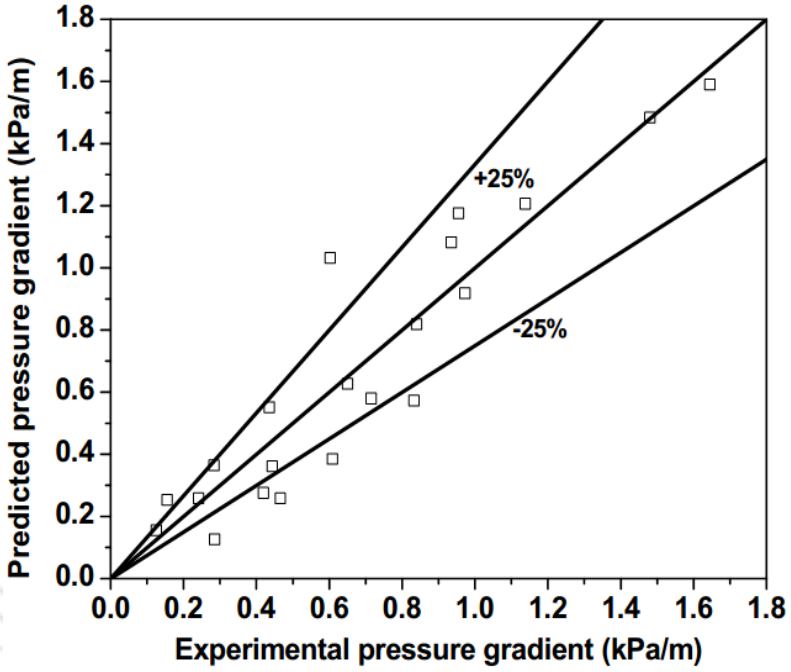

Fig. 6.6c Predicted pressure gradient data of Trallero et al. (1997) by Lockhart-Martinelli approach

6.3.2.2 Dimensional analysis

The development of a correlation based on the dimensional analysis method has been described now, since % deviation in correlation based approach (Section 6.3.2.1) considering all the flow patterns are quite high. The methodology of "Buckingham's Pi-Theorem" has followed to

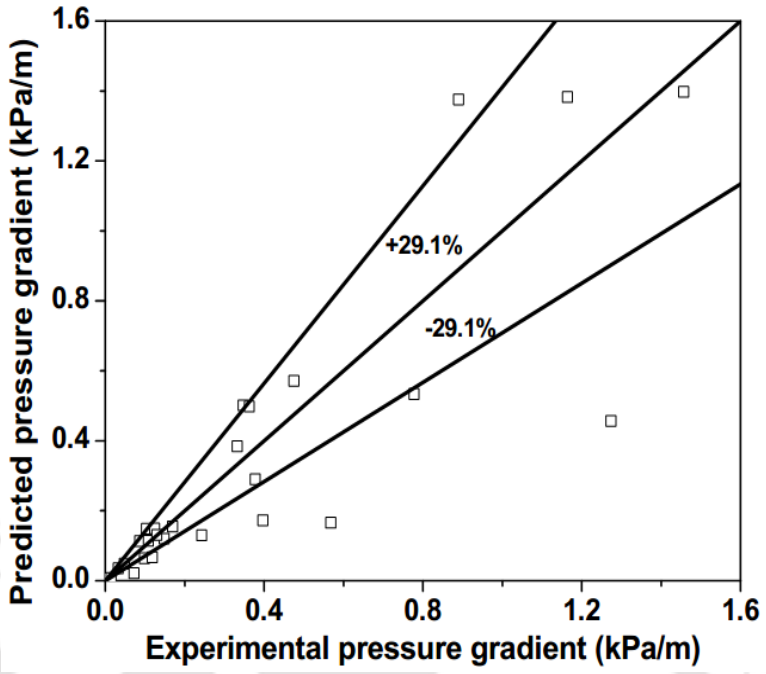

Fig. 6.6d Predicted pressure gradient data of Rodriguez and Oliemans (2006) by Lockhart-Martinelli approach

derive the dimensionless groups for the present system. Then, a generalize correlation among the dimensionless groups has been formulated by multiple regression analysis using the present experimental results.This analysis gives more accurate solution by reducing the number of separate variables in the problem to a smaller number of dimensional groups of variables. The benefit of dimensional analysis is that it provides correlations that are easy to apply and gives accurate prediction.

From the experimental study it has been observed that pressure gradient is a function of various dynamic properties of the system and the phenomena is described by following functional relation:

$$f\left(\frac{\Delta P}{L}, U_{SO}, U_{SW}, D, \rho_O, \rho_W, \mu_W, \mu_O, \sigma\right) = 0 \tag{6.36}$$

Here, roughness is not taken into account because of smooth pipe (Acrylic, PMMA) used in the present experimental work. The details of the dimensionless analysis are not described here. The combined form of relevant dimensionless groups is as follows,

$$\frac{\Delta P}{L}\left(\frac{D}{U_{SO}^2 \rho_O}\right) = \lambda \left(\frac{U_{SW}}{U_{SO}}\right)^{\alpha} \left(\frac{\mu_O}{\mu_W}\right)^{\beta} \left(\frac{\mu_O}{D U_{SO} \rho_O}\right)^{\gamma} \left(\frac{\mu_W}{D U_{SW} \rho_W}\right)^{\delta} \left(\frac{\sigma}{U_{SW} \mu_W}\right)^{\kappa} \tag{6.37}$$

Where, $\lambda, \alpha, \beta, \gamma, \delta$ and κ are constants. These constant are evaluated from multiple regression analysis in Microsoft Excel using the present experimental data. From this analysis we have estimated α and β as zero and the Eq. (6.37) becomes,

$$\frac{\Delta P}{L} = 3.25 \left(\frac{\mu_O}{D U_{SO} \rho_O}\right)^{1.15} \left(\frac{\mu_W}{D U_{SW} \rho_W}\right)^{-0.19} \left(\frac{\sigma}{U_{SW} \mu_W}\right)^{0.001} \left(\frac{D}{U_{SO}^2 \rho_O}\right)^{-1} \tag{6.38}$$

$$\frac{\Delta P}{L} = 3.25 \, \mathrm{Re}_O^{-1.15} \, \mathrm{Re}_W^{0.19} \left(\frac{\sigma}{U_{SW} \mu_W}\right)^{0.001} \left(\frac{U_{SO}^2 \rho_O}{D}\right) \tag{6.39}$$

The regression coefficient and standard error of Eq. (6.39) are found to be 0.9 and 0.26 respectively. The correlation gives excellent prediction as shown in Fig.6.7. Proposed correlation using dimensionless analysis predicted experimental pressure gradient for all the flow pattern with an average absolute error of 17.9%, which is very less compared to all other correlations. Still, there is a scope for further improvement of the proposed correlation. The correlation does not account for the effect of change of mixture properties, especially effective mixture viscosity during the phase inversion. The accuracy of the correlation can be improved by accounting for the change in mixture viscosity across this

phenomenon. The effective mixture viscosity would drastically increase when oil changes to a continuous phase from its dispersed phase. However, the present correlation is applicable for simultaneous flow of oil and water through a smooth pipe having a Reynolds number ranging from 3.15 to 259.94 for oil, and 2500 to 26,667 for water and Eotvos number ($E_O = \Delta\rho g D^2 / \sigma$)~ 28.4.

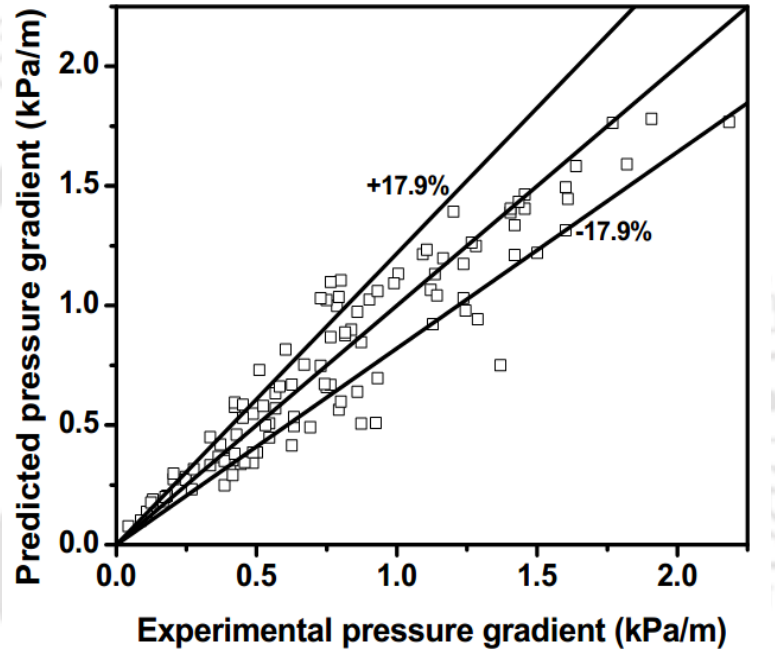

Fig. 6.7 Comparison between predicted and experimental pressure gradient in horizontal flow by dimensional analysis

In a recent publication, Al-Wahaibi (2012) proposed the following correlation to predict the frictional pressure gradient of liquid-liquid two-phase flow through horizontal pipeline.

$$\frac{dp}{dx} = 2.4\left(\frac{f_{cor}\rho_m U_m^2}{2D}\right)^{0.8} \tag{6.40}$$

$$\frac{1}{\sqrt{f_{cor}}} = -2\log\left(\frac{\varepsilon/D}{0.25} - \frac{4.518}{\mathrm{Re}_m}\log\left(\frac{6.9}{\mathrm{Re}_m} + \left(\frac{\varepsilon/D}{0.25}\right)^{1.11}\right)\right) \tag{6.41}$$

Where Re_m is mixture Reynolds number $\left(\rho_m D U_m/\mu_m\right)$ and ε is pipe roughness factor. The correlation is applicable for separated flow (stratified and dual continuous flow). In the present study, we have predicted our experimental data (pressure drop of wavy stratified and stratified mixed flow pattern) using the same correlation to check its applicability. The parity plot is shown in Fig. 6.8 with an average absolute error of 34% (error bar is drawn based on this value in figure), which is higher than the error obtained from the proposed correlation in the present study.

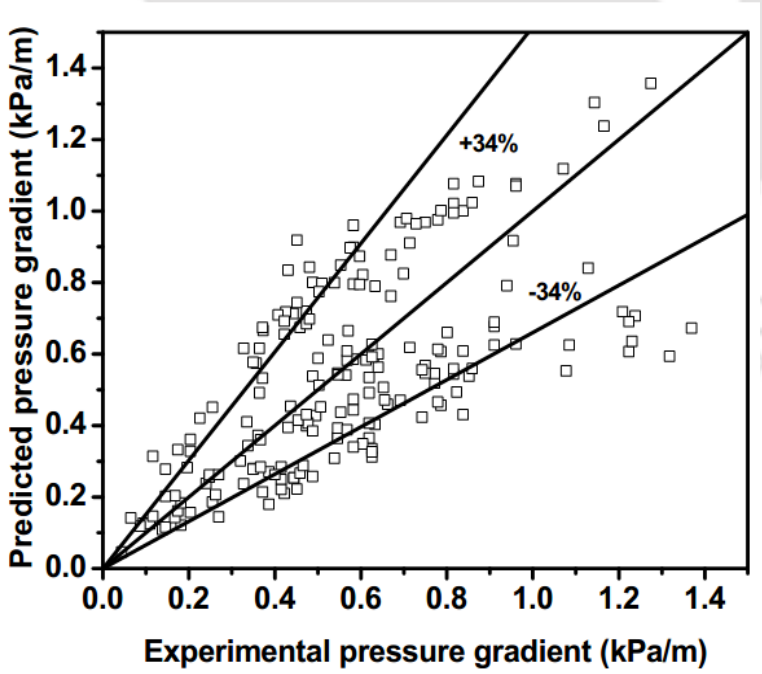

Fig. 6.8 Comparison between predicted and experimental pressure gradient using Al-Wahaibi (2012) correlation

6.3.2.3 Comparison with two-fluid model

Two-fluid model has been used to predict the pressure gradient of a separated flow pattern like stratified and annular flow. The governing equations for horizontal stratified flow are as follows

Water phase: $$-A_W\left(\frac{dp}{dz}\right)-\tau_W S_W \pm \tau_i S_i = \quad (6.42)$$

Oil phase : $$-A_O\left(\frac{dp}{dz}\right)-\tau_O S_O \pm \tau_i S_i = 0 \quad (6.43)$$

where, τ_W, τ_O and τ_i are water, oil and interfacial shear stresses respectively. S_O and S_W are the wall wetted perimeter of oil and water phases respectively, and S_i is the interfacial length. A_O and A_O are the cross sectional area occupying by oil and water respectively. All the stress (τ_W , τ_O and τ_i) have calculated using the equations given by Ullmann and Brauner (2006). The pressure gradient of wavy stratified flow pattern in the present work has been predicted and the parity plot is shown in Fig. 6.9. It shows that two fluid model has predicted the pressure gradient data with an average absolute error of 30.5%. An error bar of ±30.5% is drawn on the plot based on this value. The error is higher in comparison to that of 17.9% (from Eq. 6.39) and 22% (from Eq. 6.35) obtained from the present work.

Later on Zhang et al. (2012) proposed a correlation for interfacial shear to improve the accuracy of two-fluid model. This modified correlation has also been adopted in the present study to predict the pressure gradient of wavy stratified flow. The proposed expression for interfacial shear (Zhang et al. (2012)) is as follows.

$$\tau_i = \sqrt{\frac{f_W \Theta_W + f_O (1-\Theta_W)}{2}} \sqrt{\rho_m \left[\Theta_W \tau_W + (1-\Theta_W) \tau_O \right]} \times (U_O - U_W) \tag{6.44}$$

Where Θ_W is water wall wetted wall fraction defined as:

$$\Theta_W = \frac{S_W}{S_W + S_O} \tag{6.45}$$

The pressure gradient of wavy stratified flow of the present work has been predicted with an average absolute error of 28.6% as shown in Fig. 6.10. Although, it improves the accuracy of the two-fluid model, but further improvement is necessary to be applicable for the present system.

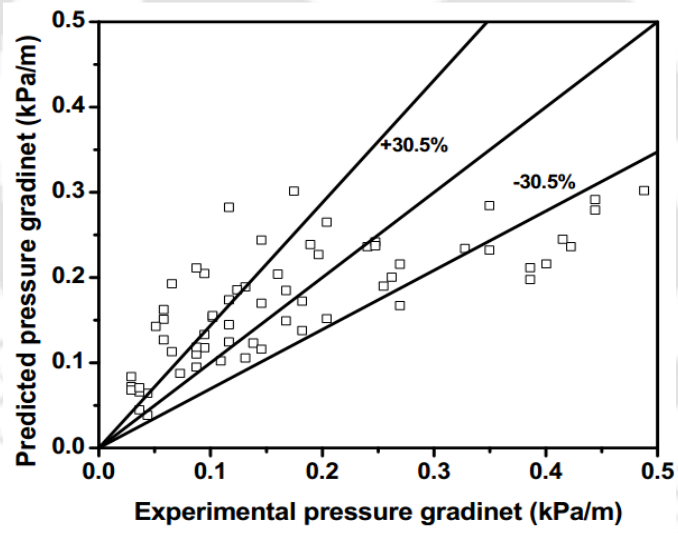

Fig. 6.9. Comparison between predicted and experimental pressure gradient using two-fluid model Ullmann and Brauner (2006).

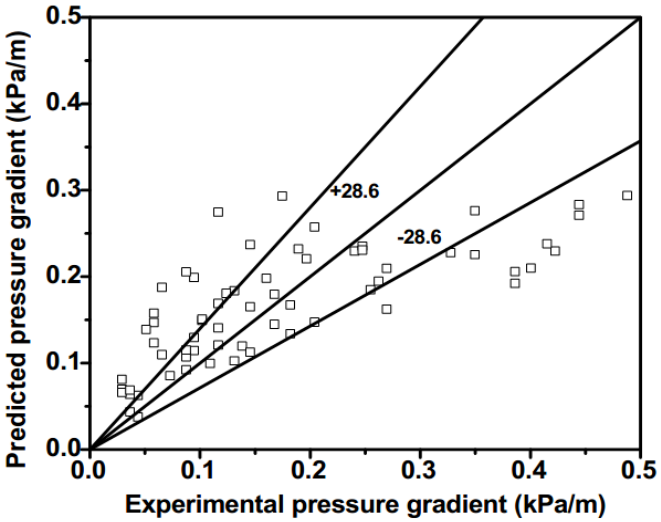

Fig. 6.10. Comparison between predicted and experimental pressure gradient using modified two-fluid model Zhang et al. (2012)

6.3.3 Development of correlation in inclined flow

Next an attempt has been made to develop two correlations for 5° upward inclined pipeline to predict pressure drop. First correlation has been developed by following the Lockhart-Martenelli approach and the other one by dimensional analysis as given in the above section.

6.3.3.1 Lockhart-Martinelli approach

The pressure drop of inclined pipeline is function of various inclinations, fluid properties and geometries. It is very difficult to develop a generalized correlation to predict pressure drop in inclined pipeline. So in this study modified the Lockkart-Martinelli correlation with the present experimental data of 5° upward inclined pipeline only and predicted the pressure gradient in inclined pipeline. For this purpose 80% of the experimental data has

been used for the development of the correlation and 20% of the data is used for validating the correlation. The present experimental data belongs to laminar oil and turbulent water region. As discussed in the Section 6.3.2.1 Martinelli parameter and two phase multiplier have been calculated and correlated using multiple regression analysis as shown in the Fig. 6.11. The correlation obtained from the regression analysis for 5° upward inclined flow is as follows

$$\phi_W^2 = \frac{0.282}{X^2} - \frac{1.033}{X} + 3.526 \qquad (6.46)$$

The regression coefficient of 0.942 has been obtained from the regression statistics. The proposed correlation has been validated with 80 data points of 5° upward inclined pipeline which are not used during the development of the correlation. The correlation has given good accuracy in prediction of pressure gradient in inclined pipeline as shown in Fig. 6.12 with very less error percentage that is 6.6% error.

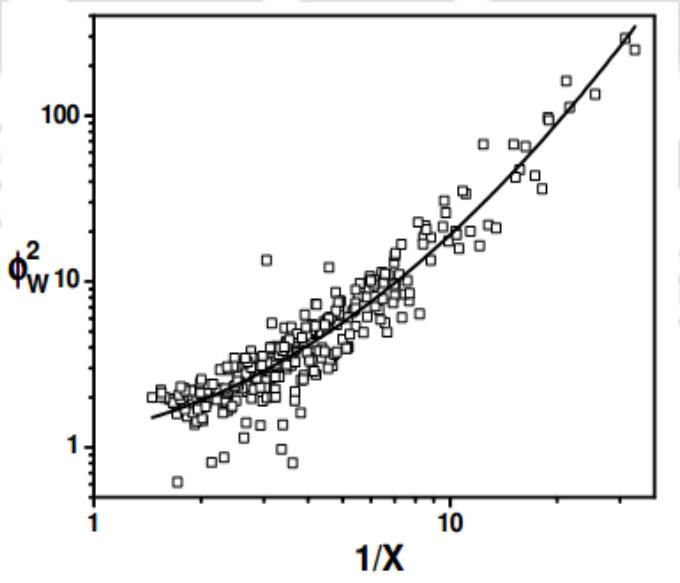

Fig. 6.11 Relationship between two-phase multiplier (Φ^2_W) with Lockhart-Martinelli parameter (X) in inclined flow

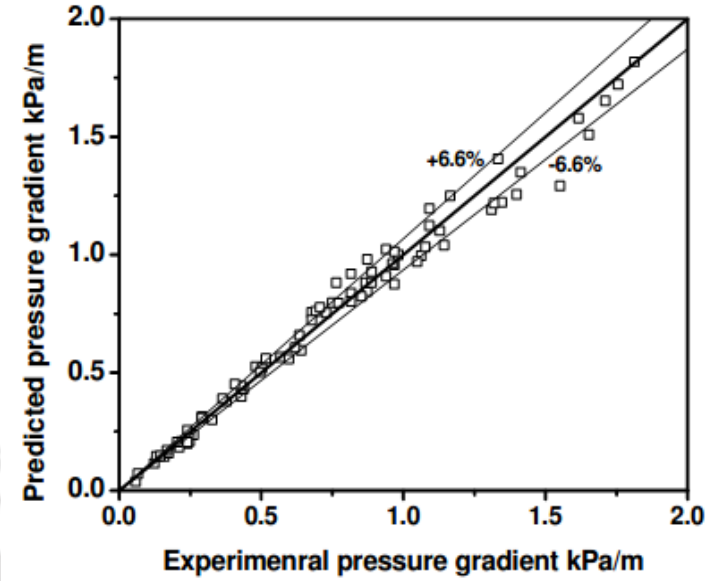

Fig. 6.12 Comparison between predicted and experimental pressure gradient in inclined flow by Lockhart-Martinelli approach

6.3.3.2 Dimensional analysis

Another correlation has been proposed based on dimensional analysis as discussed in Section 6.3.2.2. The correlation has been developed from 80% of 5° upward inclined experimental data and correlation is validated with 20% of the experimental data (Which are not used in the development of correlation). From the experiments it is noticed that inclination has also significantly effects the pressure drop. The parameters which effects the pressure drop of inclined flow is as follows

$$f\left(\frac{\Delta P}{L}, U_{SO}, U_{SW}, D, \rho_O, \rho_W, \mu_W, \mu_O, \sigma, \theta\right) = 0 \qquad (6.47)$$

All the dependent parameters except θ (because it is constant which is 5° upward) are grouped and solved using regression analysis, the proposed correlation for inclined flow is as follows

$$\frac{\Delta P}{L} = 0.339\,\mathrm{Re}_O^{-3.547}\,\mathrm{Re}_W^{-0.615}\left(\frac{U_{SO}^2\rho_O}{D}\right)\left(\frac{\sigma}{U_{SW}\mu_W}\right)^{0.002} \tag{6.48}$$

The proposed correlation has been used to predict the pressure drop data which is not used in the development of correlation. The proposed correlation has given very good accuracy in prediction as shown in Fig. 6.13. The error percentage is very less in inclined pipeline that is 4.9% this is due only one system data has been used for the development of correlation and prediction. The proposed correlation predicted the experimental results within error of ±4.9% which shows improvement than the modified Lockhart-Martinelli correlation.

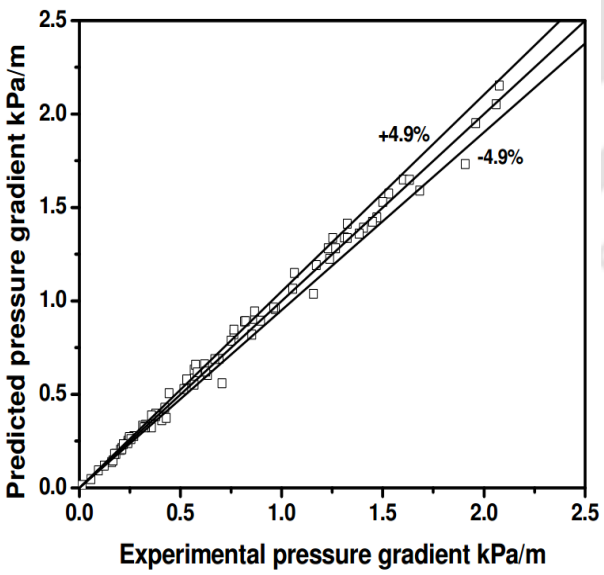

Fig. 6.13 Comparison between predicted and experimental pressure gradient in inclined flow by dimensional analysis

6.4 Entrainment model for pressure drop prediction of annular flow

The past literature (Chapter 2) shows that there is less number of theoretical studies available to predict pressure drop of liquid-liquid flow through horizontal and inclined pipes. Especially based on the flow pattern only two fluid model is available to predict pressure drop of annular flow pattern by neglecting entrainment at the interface. Here an attempt has been made to predict the pressure drop of annular flow by considering entrainment at the interface. For the calculation of entrainment at the oil-water interface the expression given by Al-Wahaibi and Angeli (2009) model has been used. This entrainment fraction is incorporated in the two fluid model for better prediction of pressure drop of annular flow. The proposed model has been validated with present experimental results as well as data available in the literature.

6.4.1 Model development for entrainment

A schematic of annular flow configuration has been shown Fig. 6.14, it indicates that some oil drops may present in the water (annular flow region) and vice versa. For such cases, knowledge of amount of entrainment is essential for accurate prediction of pressure drop.

Al-Wahaibi et al. (2007b) suggested that interfacial tension and gravity forces will be likely to stabilize the wavy disturbance on the oil-water interface caused by Kelvin-Helmholtz instability. If these wave disturbance (destabilizing forces) cannot be balanced by the interfacial and gravity forces (stabilizing forces) resulting waves become unstable. Therefore, these unstable waves will continue to grow until a drop detaches from the wave.

It happens when the surface tension force (which prevents deformation) is found lesser than that of the drag force acting on the wave crest

(Al-Wahaibi et al. (2007b)). At this condition wave, amplitude reaches its critical value and the critical wave amplitude of oil (a_o) and water (a_w) control the entrainment volume of one phase into another. Therefore, a force balance on the wave crests and troughs is needed for predicting the critical wave amplitude of oil (a_o) and water (a_w) at which drops tends to detach from one phase into the other. These critical values are essential in the development of a physical model for entrainment of oil into water (E_o) and entrainment of water into oil (E_w) during annular flow.

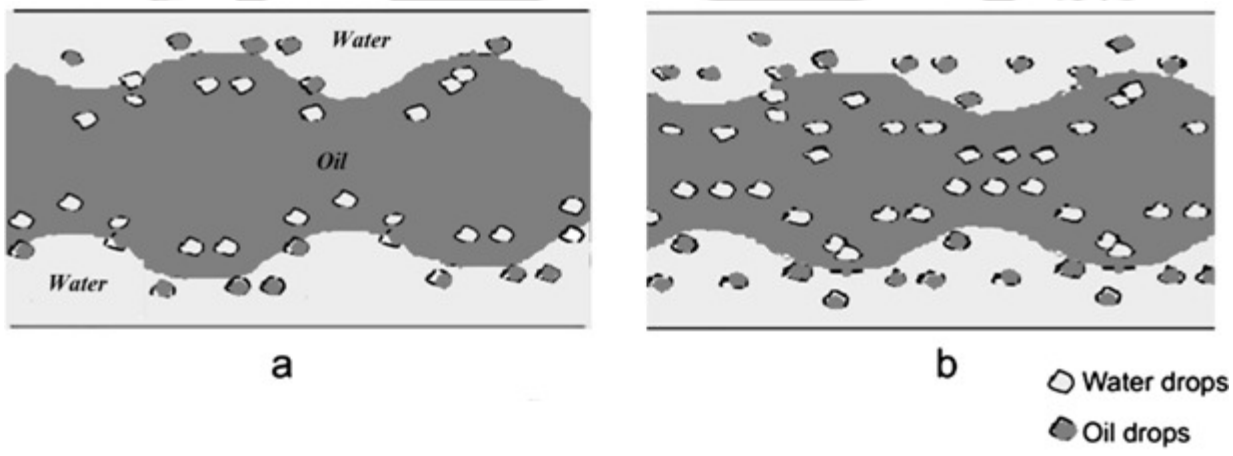

Fig. 6.14 Schematic of the annular flow pattern (a) low and (b) high velocities showing distribution of phases**.**

By doing a simple balance between the rate of drop entrainment (R_A) and the rate of drop deposition (R_D) one can predict the entrainment theoretically. The rate of deposition is directly proportional to the droplet concentration (C_D), which is found to be the accepted

practice in liquid–liquid flows (Al-Wahaibi and Angeli (2009)). At this condition, it can be written as

$$R_D = k_D C_D \tag{6.49}$$

Where (C_D) is the droplet concentration (kg/m^3) and (k_D) is the deposition rate constant (m/s) and at equilibrium,

$$R_A = R_D \tag{6.50}$$

Thus, the rate of entrainment and deposition of each phase should be found to predict the entrainment of oil into water (E_o) and entrainment of water into oil (E_w) during annular flow.

6.4.1.1 Rate of entrainment

The rate of entrainment (R_A) can be calculated from the volume of wave, since the drops are formed from the separated (detached) waves. The geometry of the wave is shown in Fig. 6.15 a-b. The figure shows a control volume during annular flow flowing through a horizontal pipe. It consists of number of waves ($N_{w,cv}$) in a controlled volume with an axial length (L_s). Assumption is that the waves are in symmetrical sinusoidal shape with wavelength (λ) and amplitude (a) along the whole axes. The entrainment fractions of oil and water (E_o and E_w) during annular flow can be calculated based on this controlled volume.

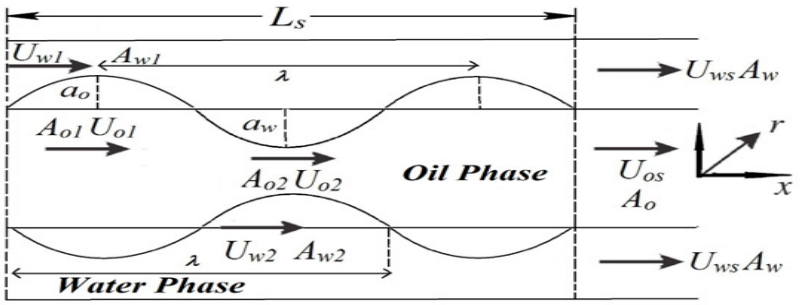

(a) Side view

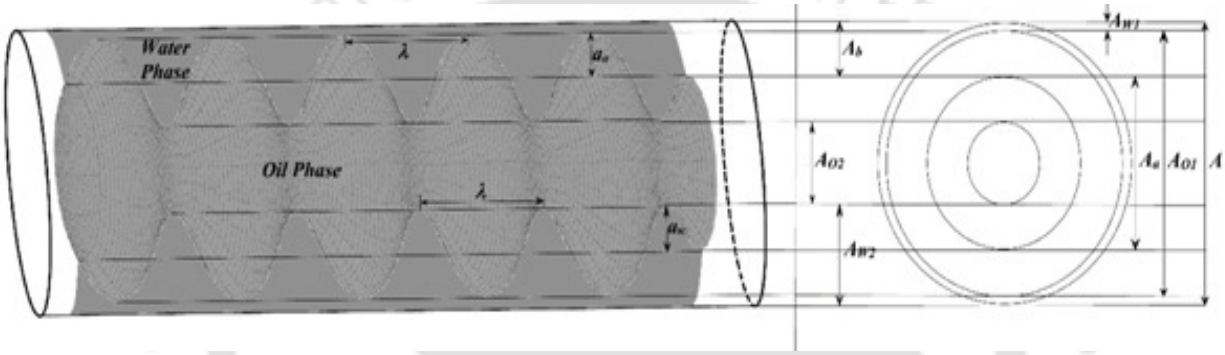

(b) Cross sectional view

Fig. 6.15 Control volume in the pipe that is used to calculate entrainment rate

Assume that each wave detached from wave crest or wave trough of the opposite phase will provide one drop, likewise neglect the effect of these entrained drops on the waves. The rate of entrainment for oil as well as for water is depending on the mass of entrained drops ($\boldsymbol{M_{ent} = V_{ent} \times \rho_{ent}}$), which are waves detached from opposite phases, per period of the entrainment phenomena ($\boldsymbol{\tau_{cv}}$) in the control volume and area of control volume ($\boldsymbol{A_{cv}}$). Therefore, the rate of entrainment for both the phases (oil or water) can be written as:

$$R_A = \frac{V_{ent}\rho_{ent}N_{w,cv}}{A_{cv}\tau_{cv}};\ \text{where}\ A_{cv} = L_s S_i\ \ \&\ \ N_{w,cv} = \frac{L_s}{\lambda} \tag{6.51}$$

where 'V_{ent}' is the entrained volume, which are detached from each wave crest or wave trough, 'ρ_{ent}' is the entrained phase density. To find the period of entrainment phenomena (τ_{cv}) in the control volume, it must calculated by dividing the wavelength with the difference between oil and water velocities at the oil waves for (R_{Ao}) and at the water waves for (R_{Aw}), from where entrained drops are formed.

$\tau_{cv} = \dfrac{\lambda}{|U_{wi} - U_{oi}|}$, Where '$i$' is '1' for E_o and '2' for E_w respectively.

$$R_{Ao} = \frac{V_{ent\_o}\rho_o |U_{w1} - U_{o1}|}{\pi D_a \lambda^2} \tag{6.52a}$$

$$R_{Aw} = \frac{V_{ent\_w}\rho_w |U_{w2} - U_{o2}|}{\pi D_a \lambda^2} \tag{6.52b}$$

In the above equations, 'U_{o1}' represents the velocity of oil below the oil wave whereas 'U_{w1}' is the velocity of water above the oil wave. Similarly, 'U_{w2}' represents the water velocity below the water wave and 'U_{o2}' the oil velocity above the water wave (as in Fig. 6.15a).

By using continuity equations, the velocities of the oil and water for above and below the respective waves are calculated as:

$$U_{ws}A_b = U_{w1}A_{w1} = U_{w2}A_{w2} \tag{6.53a}$$

$$U_{os}A_a = U_{o1}A_{o1} = U_{o2}A_{o2} \tag{6.53b}$$

In the above equation, to simplify the calculation part, superficial velocities ($\boldsymbol{U_{ws}}$ or $\boldsymbol{U_{os}}$) are taken for uninterrupted flat interface of annular flow (left side part of equations (6.53a, b)). Where '$\boldsymbol{A}$', '$\boldsymbol{U}$' represents respective areas and velocities.

6.4.1.2 Volume of the entrained wave

Fig. 6.16 is modified from the source Al-Wahaibi et al. (2007b). To predict the critical wave amplitude they developed the correlation as given below based on a force balance on deformed waves in the direction of flow (as in Fig. 6.16) by neglecting surface tension forces on a symmetrical wave.

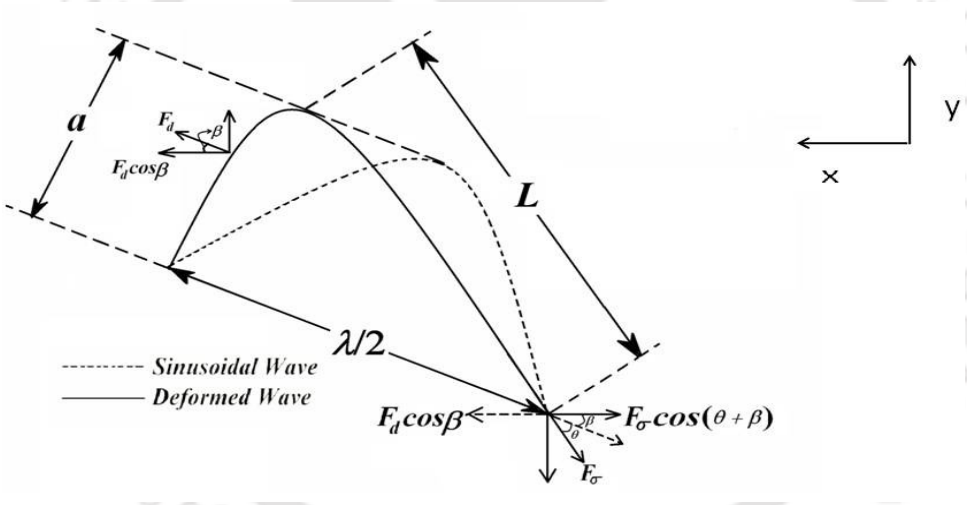

Fig. 6.16 Force balance on a deformed two-dimensional wave on the oil-water interface

$$C_d \cdot A_{wave}^{oil} \cdot \rho_w \cdot \frac{\left(U_{w1}-U_{o1}\right)^2}{2} \cdot \cos\beta = \sigma \cdot 2S_i \cdot \cos\left(\theta+\beta\right);\ \text{where}\ \ \cos\theta = \frac{\left(\lambda/2\right)}{\sqrt{a_o^2+\left(\lambda/2\right)^2}} \qquad (6.54a)$$

$$C_d \cdot A_{wave}^{water} \cdot \rho_o \cdot \frac{\left(U_{w2}-U_{o2}\right)^2}{2} \cdot \cos\beta = \sigma \cdot 2S_i \cdot \cos\left(\theta+\beta\right);\ \text{where}\ \ \cos\theta = \frac{\left(\lambda/2\right)}{\sqrt{a_w^2+\left(\lambda/2\right)^2}} \qquad (6.54b)$$

where 'C_d' is the drag coefficient, 'A_{wave}' is the area of the deformed wave as in Fig. 6.16,'σ' is the interfacial tension. Here the stabilizing forces are surface tension forces (F_σ) on the right, whereas destabilizing forces are drag forces (F_d) on the left, acting on the wave. Therefore, drops will appear when the drag force acting on the wave exceeds surface tension force acting on the wave interface. In addition, '$\cos\theta$' can be calculated as the shape of the deformed wave resembles a right angled triangle (Fig. 6.16).

In the above equations (6.54a, b) the unknown parameters are drag coefficient (C_d), wavelength (λ) and critical wave amplitude (a) for oil and water. To calculate the critical wave amplitude, experimental oil and water superficial velocities (U_{os} and U_{ws}) at the onset of entrainment, from where the first drops emerges at the interface are used. According to Al-Wahaibi et al. (2007b) these critical amplitudes (a) are higher than that of the ones found above the onset ones, where the critical amplitudes are calculated using new superficial velocities formed above the onset of entrainment. Therefore the difference in the volumes and the wave amplitudes at the onset of entrainment conditions to the volumes and the wave amplitudes at the new higher superficial velocities found above the onset of entrainment, will correspond to the volumes of drops formed from the detached waves. It is assumed that, at onset and above the onset of entrainment all wave amplitudes are taken as critical amplitudes for drop formation for calculating the volume of entrained fractions of each phase. Also waves having higher amplitudes will easily split into drops. Rodriguez and Bannwart (2008) studied Stability analysis for annular flow and suggested that, by incorporating theoretical minimum wavelength (D/2) into the transition model fits the best agreement with literature and their data. This means with that minimum wavelength (D/2) accepts the stability criteria for annular flow mostly. Therefore, in this model assumed the

wavelength of half pipe diameter for the calculation of the critical amplitudes. Which is also satisfied the selected literature data in this study.

The final modified equation of drag coefficient is taken from the Al-Wahaibi et al. (2007b)

$$C_d = 4.9\times10^{-8}\times \mathrm{Re}_{os}^{0.77}\times \mathrm{Re}_{ws}^{0.86}\times\frac{\mu_o}{\mu_w} \tag{6.55}$$

The area of the wave is calculated by

$$A_{wave}^{water} = \int_0^{\lambda/2} a_w \sin\left(\frac{2\pi x}{\lambda}\right)dx = \frac{a_w\lambda}{\pi} = \frac{\overline{a_w}D^2}{\pi}$$

Then the normalized area of oil and water waves can be given by dividing the above equation with 'D^2' as:

$$\Rightarrow \overline{A_{wave}^{water}} = \frac{\overline{a_w}}{\pi};\ \text{similarly}\ \overline{A_{wave}^{oil}} = \frac{\overline{a_o}}{\pi} \tag{6.56}$$

Difference between the velocities in the equations (6.54a, b) can also be calculated as:

$$\frac{(U_{w1}-U_{o1})^2}{2} = \frac{\left(\frac{U_{ws}A_b}{A_{w1}} - \frac{U_{os}A_a}{A_{o1}}\right)^2}{2} = \frac{\left(\frac{U_{ws}\overline{A_b}}{\overline{A_{w1}}} - \frac{U_{os}\overline{A_a}}{\overline{A_{o1}}}\right)^2}{2} = \frac{\left(U_{ws}\overline{A_b}\,\overline{A_{o1}} - U_{os}\overline{A_a}\,\overline{A_{w1}}\right)^2}{2\left(\overline{A_{o1}}\,\overline{A_{w1}}\right)^2};\ (6.57a)$$

where $A_{o1} = A_a + 2A_{wave}^{oil};\quad A_{w1} = A_b - 2A_{wave}^{oil}\quad \therefore\ \overline{A_{o1}} = \overline{A_a} + 2\overline{A_{wave}^{oil}};\quad \overline{A_{w1}} = \overline{A_b} - 2\overline{A_{wave}^{oil}}$

$$\frac{(U_{w2}-U_{o2})^2}{2} = \frac{\left(\frac{U_{ws}A_b}{A_{w2}} - \frac{U_{os}A_a}{A_{o2}}\right)^2}{2} = \frac{\left(\frac{U_{ws}\overline{A_b}}{\overline{A_{w2}}} - \frac{U_{os}\overline{A_a}}{\overline{A_{o2}}}\right)^2}{2} = \frac{\left(U_{ws}\overline{A_b}\,\overline{A_{o2}} - U_{os}\overline{A_a}\,\overline{A_{w2}}\right)^2}{2\left(\overline{A_{o2}}\,\overline{A_{w2}}\right)^2};\tag{6.57b}$$

where $A_{o2} = A_a - 2A_{wave}^{water};\quad A_{w2} = A_b + 2A_{wave}^{water}\quad \therefore\ \overline{A_{o2}} = \overline{A_a} - 2\overline{A_{wave}^{water}};\quad \overline{A_{w2}} = \overline{A_b} + 2\overline{A_{wave}^{water}}$

6.4.1.3 For horizontal flow

By incorporating Eq.6.55, 6.56 and 6.57a, b in 6.54a, b, got the 8th order equation in normalized amplitudes of oil and water respectively as given below:

$$a_1\overline{a_o}^{8}+a_2\overline{a_o}^{7}+a_3\overline{a_o}^{6}+a_4\overline{a_o}^{5}+a_5\overline{a_o}^{4}+a_6\overline{a_o}^{3}+a_7\overline{a_o}^{2}+a_8\overline{a_o}+a_9=0 \qquad (6.58)$$

$$b_1\overline{a_w}^{8}+b_2\overline{a_w}^{7}+b_3\overline{a_w}^{6}+b_4\overline{a_w}^{5}+b_5\overline{a_w}^{4}+b_6\overline{a_w}^{3}+b_7\overline{a_w}^{2}+b_8\overline{a_w}+b_9=0 \qquad (6.59)$$

Where:

$$a_1=4k_1^4-M_ok_4^4;\quad b_1=4k_1^4-M_wk_4^4;\quad a_2=16k_1^3k_2+4M_ok_3k_4^3;\quad -b_2=16k_1^3k_2+4M_wk_3k_4^3$$

$$a_3=k_1^4\left(\frac{\lambda}{D}\right)^2+24k_1^2k_2^2-6M_ok_3^2k_4^2+4M_ok_4^3k_5;\quad b_3=k_1^4\left(\frac{\lambda}{D}\right)^2+24k_1^2k_2^2-6M_wk_3^2k_4^2+4M_ok_4^3k_5$$

$$a_4=4k_1^3k_2\left(\frac{\lambda}{D}\right)^2+16k_1k_2^3+4M_ok_3^3k_4-12M_ok_3k_4^2k_5;$$

$$-b_4=4k_1^3k_2\left(\frac{\lambda}{D}\right)^2+16k_1k_2^3+4M_wk_3^3k_4-12M_wk_3k_4^2k_5$$

$$a_5=6k_1^2k_2^2\left(\frac{\lambda}{D}\right)^2+4k_2^4-M_ok_3^4+12M_ok_4k_3^2k_5-6M_ok_4^2k_5^2;$$

$$b_5=6k_1^2k_2^2\left(\frac{\lambda}{D}\right)^2+4k_2^4-M_wk_3^4+12M_wk_4k_3^2k_5-6M_wk_4^2k_5^2$$

$$a_6=4k_1k_2^3\left(\frac{\lambda}{D}\right)^2-4M_ok_3^3k_5+12M_ok_4k_5^2k_3;\quad -b_6=4k_1k_2^3\left(\frac{\lambda}{D}\right)^2-4M_wk_3^3k_5+12M_wk_4k_5^2k_3$$

$$a_7=k_2^4\left(\frac{\lambda}{D}\right)^2-6M_ok_3^2k_5^2+4M_ok_4k_5^3;\quad b_7=k_2^4\left(\frac{\lambda}{D}\right)^2-6M_wk_3^2k_5^2+4M_wk_4k_5^3$$

$$-a_8=4M_ok_3k_5^3;\quad b_8=4M_wk_3k_5^3;\quad a_9=-M_ok_5^4;\quad b_9=-M_wk_5^4$$

$$k_1=\left(\frac{\lambda}{D}\right)\left(\frac{8}{\pi^2}\right)\left(U_{os}\overline{D_a}^{2}+U_{ws}\left(1-\overline{D_a}^{2}\right)\right);\quad k_2=\left(1-\overline{D_a}^{2}\right)\overline{D_a}^{2}\left(U_{ws}-U_{os}\right)$$

$$k_3=\left(\frac{\lambda}{D}\right)\left(\frac{8}{\pi^2}\right)\left(1-2\overline{D_a}^{2}\right);\quad k_4=\left(\frac{\lambda}{D}\right)^2\left(\frac{8}{\pi^2}\right)^2;\quad k_5=\overline{D_a}^{2}\left(1-\overline{D_a}^{2}\right)$$

$$M_o=\left(\frac{4\pi^2\sigma\overline{D_a}}{C_d\rho_wD}\right)^2;\quad M_w=\left(\frac{4\pi^2\sigma\overline{D_a}}{C_d\rho_oD}\right)^2 \qquad (6.60a)$$

6.4.1.4 For Inclined flow

By incorporating equations Eq.6.55, 6.56 and 6.57a, b in 6.54a, b got the 10^{th} order equation in normalized amplitudes of oil and water respectively as given below:

$$a_1\overline{a_o}^{10}+a_2\overline{a_o}^{9}+a_3\overline{a_o}^{8}+a_4\overline{a_o}^{7}+a_5\overline{a_o}^{6}+a_6\overline{a_o}^{5}+a_7\overline{a_o}^{4}+a_8\overline{a_o}^{3}+a_9\overline{a_o}^{2}+a_{10}\overline{a_o}+a_{11}=0$$

$$b_1\overline{a_w}^{10}+b_2\overline{a_w}^{9}+b_3\overline{a_w}^{8}+b_4\overline{a_w}^{7}+b_5\overline{a_w}^{6}+b_6\overline{a_w}^{5}+b_7\overline{a_w}^{4}+b_8\overline{a_w}^{3}+b_9\overline{a_w}^{2}+b_{10}\overline{a_w}+b_{11}=0$$

where:

$$a_1=-4M_o\tan^2(\beta)k_4^4;\quad b_1=-4M_w\tan^2(\beta)k_4^4;$$

$$a_2=16M_o\tan^2(\beta)k_3k_4^3+4M_o\tan(\beta)k_4^4\left(\frac{L}{D}\right);$$

$$b_2=-16M_w\tan^2(\beta)k_3k_4^3+4M_w\tan(\beta)k_4^4\left(\frac{L}{D}\right);$$

$$a_3=-24M_o\tan^2(\beta)k_3^2k_4^2+16M_o\tan^2(\beta)k_4^3k_5-16M_o\tan(\beta)k_3k_4^3\left(\frac{\lambda}{D}\right)-M_ok_4^4\left(\frac{\lambda}{D}\right)^2;$$

$$b_3=-24M_w\tan^2(\beta)k_3^2k_4^2+16M_w\tan^2(\beta)k_4^3k_5+16M_w\tan(\beta)k_3k_4^3\left(\frac{\lambda}{D}\right)-M_wk_4^4\left(\frac{\lambda}{D}\right)^2;$$

$$a_4=16M_o\tan^2(\beta)k_3^3k_4-48M_o\tan^2(\beta)k_3k_4^2k_5+24M_o\tan(\beta)k_3^2k_4^2\left(\frac{\lambda}{D}\right)$$
$$-16M_o\tan(\beta)k_4^3k_5\left(\frac{\lambda}{D}\right)+4M_o\tan(\beta)k_3k_4^3\left(\frac{\lambda}{D}\right)^2;$$

$$b_4=-16M_o\tan^2(\beta)k_3^3k_4+48M_o\tan^2(\beta)k_3k_4^2k_5+24M_o\tan(\beta)k_3^2k_4^2\left(\frac{\lambda}{D}\right)$$
$$-16M_o\tan(\beta)k_4^3k_5\left(\frac{\lambda}{D}\right)-4M_o\tan(\beta)k_3k_4^3\left(\frac{\lambda}{D}\right)^2;$$

$$a_5=-4M_o\tan^2(\beta)k_3^4+48M_o\tan^2(\beta)k_4k_3^2k_5-24M_o\tan^2(\beta)k_4^2k_5^2-16M_o\tan(\beta)k_4k_3^3\left(\frac{\lambda}{D}\right)$$
$$+48M_o\tan(\beta)k_3k_4^2k_5\left(\frac{\lambda}{D}\right)+k_1^2\left(\frac{\lambda}{D}\right)^2+4k_1^4-6M_ok_3^2k_4^2\left(\frac{\lambda}{D}\right)^2+4M_ok_5k_4^3\left(\frac{\lambda}{D}\right)^2;$$

$$b_5 = -4M_w \tan^2(\beta) k_3^4 + 48M_w \tan^2(\beta) k_4 k_3^2 k_5 - 24M_w \tan^2(\beta) k_4^2 k_5^2 + 16M_w \tan(\beta) k_4 k_3^3 \left(\frac{\lambda}{D}\right)$$
$$- 48M_w \tan(\beta) k_3 k_4^2 k_5 \left(\frac{\lambda}{D}\right) + k_1^2 \left(\frac{\lambda}{D}\right)^2 + 4k_1^4 - 6M_w k_3^2 k_4^2 \left(\frac{\lambda}{D}\right)^2 + 4M_w k_5 k_4^3 \left(\frac{\lambda}{D}\right)^2;$$

$$a_6 = -16M_o \tan^2(\beta) k_3^3 k_5 + 48M_o \tan^2(\beta) k_4 k_5^2 k_3 + 4M_o \tan(\beta) k_3^4 \left(\frac{\lambda}{D}\right) - 48M_o \tan(\beta) k_4 k_5 k_3^2 \left(\frac{\lambda}{D}\right)$$
$$+ 24M_o \tan(\beta) k_4^2 k_5^2 \left(\frac{\lambda}{D}\right) + 4k_1^3 k_2 \left(\frac{\lambda}{D}\right)^2 + 16k_1^3 k_2 + 4M_o k_3^3 k_4 \left(\frac{\lambda}{D}\right)^2 - 12M_o k_3 k_5 k_4^2 \left(\frac{\lambda}{D}\right)^2;$$

$$b_6 = 16M_w \tan^2(\beta) k_3^3 k_5 - 48M_w \tan^2(\beta) k_4 k_5^2 k_3 + 4M_w \tan(\beta) k_3^4 \left(\frac{\lambda}{D}\right) - 48M_w \tan(\beta) k_4 k_5 k_3^2 \left(\frac{\lambda}{D}\right)$$
$$+ 24M_w \tan(\beta) k_4^2 k_5^2 \left(\frac{\lambda}{D}\right) - 4k_1^3 k_2 \left(\frac{\lambda}{D}\right)^2 - 16k_1^3 k_2 - 4M_w k_3^3 k_4 \left(\frac{\lambda}{D}\right)^2 + 12M_w k_3 k_5 k_4^2 \left(\frac{\lambda}{D}\right)^2;$$

$$a_7 = -24M_o \tan^2(\beta) k_3^2 k_5^2 + 16M_o \tan^2(\beta) k_4 k_5^3 + 16M_o \tan(\beta) k_3^3 k_5 \left(\frac{\lambda}{D}\right) - 48M_o \tan(\beta) k_4 k_3 k_5^2 \left(\frac{\lambda}{D}\right)$$
$$+ k_1^4 \left(\frac{\lambda}{D}\right)^2 + 6k_1^2 k_2^2 \left(\frac{\lambda}{D}\right)^2 + 24k_1^2 k_2^2 - M_o k_3^4 \left(\frac{\lambda}{D}\right)^2 + 12M_o k_4 k_5 k_3^2 \left(\frac{\lambda}{D}\right)^2 - 6M_o k_4^2 k_5^2 \left(\frac{\lambda}{D}\right)^2;$$

$$b_7 = -24M_w \tan^2(\beta) k_3^2 k_5^2 + 16M_w \tan^2(\beta) k_4 k_5^3 - 16M_w \tan(\beta) k_3^3 k_5 \left(\frac{\lambda}{D}\right) + 48M_w \tan(\beta) k_4 k_3 k_5^2 \left(\frac{\lambda}{D}\right)$$
$$+ k_1^4 \left(\frac{\lambda}{D}\right)^2 + 6k_1^2 k_2^2 \left(\frac{\lambda}{D}\right)^2 + 24k_1^2 k_2^2 - M_w k_3^4 \left(\frac{\lambda}{D}\right)^2 + 12M_w k_4 k_5 k_3^2 \left(\frac{\lambda}{D}\right)^2 - 6M_w k_4^2 k_5^2 \left(\frac{\lambda}{D}\right)^2;$$

$$a_8 = -16M_o \tan^2(\beta) k_3 k_5^3 + 24M_o \tan(\beta) k_3^2 k_5^2 \left(\frac{\lambda}{D}\right) - 16M_o \tan(\beta) k_5^3 k_4 \left(\frac{\lambda}{D}\right) + 4k_2 k_1^3 \left(\frac{\lambda}{D}\right)^2$$
$$+ 4k_1 k_2^3 \left(\frac{\lambda}{D}\right)^2 + 16k_1 k_2^3 - 4M_o k_3^3 k_5 \left(\frac{\lambda}{D}\right)^2 + 12M_o k_4 k_3 k_5^2 \left(\frac{\lambda}{D}\right)^2;$$

$$b_8 = 16M_w \tan^2(\beta) k_3 k_5^3 + 24M_w \tan(\beta) k_3^2 k_5^2 \left(\frac{\lambda}{D}\right) - 16M_w \tan(\beta) k_5^3 k_4 \left(\frac{\lambda}{D}\right) - 4k_2 k_1^3 \left(\frac{\lambda}{D}\right)^2$$
$$- 4k_1 k_2^3 \left(\frac{\lambda}{D}\right)^2 - 16k_1 k_2^3 + 4M_w k_3^3 k_5 \left(\frac{\lambda}{D}\right)^2 - 12M_w k_4 k_3 k_5^2 \left(\frac{\lambda}{D}\right)^2;$$

$$a_9 = -4M_o \tan^2(\beta) k_5^4 + 16M_o \tan(\beta) k_3 k_5^3 \left(\frac{\lambda}{D}\right) + 6k_2^2 k_1^2 \left(\frac{\lambda}{D}\right)^2 + k_2^4 \left(\frac{\lambda}{D}\right)^2 + 4k_2^4 - 6M_o k_3^2 k_5^2 \left(\frac{\lambda}{D}\right)^2 + 4M_o k_4 k_5^3 \left(\frac{\lambda}{D}\right)^2;$$

$$b_9 = -4M_w \tan^2(\beta) k_5^4 - 16M_w \tan(\beta) k_3 k_5^3 \left(\frac{\lambda}{D}\right) + 6k_2^2 k_1^2 \left(\frac{\lambda}{D}\right)^2 + k_2^4 \left(\frac{\lambda}{D}\right)^2 + 4k_2^4 - 6M_w k_3^2 k_5^2 \left(\frac{\lambda}{D}\right)^2 + 4M_w k_4 k_5^3 \left(\frac{\lambda}{D}\right)^2;$$

$$a_{10} = 4M_o \tan(\beta) k_5^4 \left(\frac{\lambda}{D}\right) + 4k_2^3 k_1 \left(\frac{\lambda}{D}\right)^2 - 4M_o k_3 k_5^3 \left(\frac{\lambda}{D}\right)^2;$$

$$b_{10} = 4M_w \tan(\beta) k_5^4 \left(\frac{\lambda}{D}\right) - 4k_2^3 k_1 \left(\frac{\lambda}{D}\right)^2 + 4M_w k_3 k_5^3 \left(\frac{\lambda}{D}\right)^2;$$

$$a_{11} = k_2^4 \left(\frac{\lambda}{D}\right)^2 - M_o k_5^4 \left(\frac{\lambda}{D}\right)^2; \quad b_{11} = k_2^4 \left(\frac{\lambda}{D}\right)^2 - M_w k_5^4 \left(\frac{\lambda}{D}\right)^2;$$

$$k_1 = \left(\frac{\lambda}{D}\right)\left(\frac{8}{\pi^2}\right)\left(U_{os}\overline{D_a}^2 + U_{ws}\left(1-\overline{D_a}^2\right)\right); \quad k_2 = \left(1-\overline{D_a}^2\right)\overline{D_a}^2\left(U_{ws}-U_{os}\right)$$

$$k_3 = \left(\frac{\lambda}{D}\right)\left(\frac{8}{\pi^2}\right)\left(1-2\overline{D_a}^2\right); \quad k_4 = \left(\frac{\lambda}{D}\right)^2\left(\frac{8}{\pi^2}\right)^2; \quad k_5 = \overline{D_a}^2\left(1-\overline{D_a}^2\right)$$

$$M_o = \left(\frac{4\pi^2\sigma\overline{D_a}}{C_d\rho_w D}\right)^2; \quad M_w = \left(\frac{4\pi^2\sigma\overline{D_a}}{C_d\rho_o D}\right)^2 \tag{6.60b}$$

Based on the above Eq.6.58-6.59 for both horizontal and inclined annular flows as discussed earlier the volume of entrained fraction can be calculated as the difference between the volumes of the waves at the onset of entrainment and above the onset of entrainment conditions (higher than the onset of entrainment superficial velocities).

$$V_{ent} = V_{wave}^{onset} - V_{wave}^{new\ condition} \tag{6.61}$$

The detailed calculation of entrainment volumes (V_{ent}^{oil} *and* V_{ent}^{water}) has been given in Eqs. A.20-A.22 of Appendix.

6.4.1.5 Rate of deposition

The deposition rate of oil and water drops can be formulated as:

$$R_{Do} = K_{Do} C_{Do};\ R_{Dw} = K_{Dw} C_{Dw} \tag{6.62}$$

Where deposition concentrations of oil and water can be given as:

$$C_{Do} = \left(\frac{(W_o)_b}{Q_b S} \right);\ C_{Dw} = \left(\frac{(W_w)_a}{Q_a S} \right)$$

where 'K_{Do}', 'K_{Dw}' are the deposition rate constants; 'C_{Do}', 'C_{Dw}' are the concentrations; '$(W_o)_b$', '$(W_w)_a$'are the mass flow rates of oil drops in the annular phase and water drops in core phase respectively. 'Q_a', 'Q_b' are the volumetric flow rate of the core layer and annular layer; 'S' is the slip factor measured by velocity ratio between the oil drops and the annular phase and also it is assumed there is no slip between the oil drops and the annular phase, therefore $S = 1$.

Now the ratio of mass flow rate to the volumetric flow rate can be written as:

$$\frac{(W_o)_b}{Q_b} = \frac{(M_o)_b}{V_b};\quad \frac{(W_w)_a}{Q_a} = \frac{(M_w)_a}{V_a} \tag{6.63}$$

There is no correlation in the literature for the deposition rate constant (K_{Do}) in horizontal or inclined liquid-liquid annular flow. So, in this present study the equation suggested by McCoy and Hanratty (1977) for vertical annular gas-liquid flows and frictional velocity (U^*) is taken from Al-Wahaibi and Angeli (2009).

$$K_{Do} = 0.17 \times U_o^*;\ \ K_{Dw} = 0.17 \times U_w^*;\ \ \text{where}\ \ U_w^* = \sqrt{\frac{\tau_b}{\rho_w}}\ \ \text{and}\ U_o^* = \sqrt{\frac{\tau_i}{\rho_o}} \tag{6.64}$$

6.4.1.6 Calculation for the entrained fractions

Entrainment of water drops into the core phase (E_w) and oil drops into the annular phase (E_o) can be calculated by considering average volumes of core and annular phases. The final expression of entrainment fractions of oil (E_o) and water (E_w) are formulated as:

$$E_o = (1-\alpha_b) = \left(\frac{V_o}{V_o+V_w}\right)_b = \frac{(V_o)_b}{V_b} = \left(\frac{M_o}{\rho_o}\right)_b \frac{1}{V_b} = \left(\frac{M_o}{V}\right)_b \frac{1}{(\rho_o)_b} = \left(\frac{W_o}{Q}\right)_b \frac{1}{(\rho_o)} = \frac{(W_o)_b}{Q_b \rho_o} \quad (6.65a)$$

$$E_w = (1-\alpha_a) = \left(\frac{V_w}{V_o+V_w}\right)_a = \frac{(V_w)_a}{V_a} = \left(\frac{M_w}{\rho_w}\right)_a \frac{1}{V_a} = \left(\frac{M_w}{V}\right)_a \frac{1}{(\rho_w)_a} = \left(\frac{W_w}{Q}\right)_a \frac{1}{(\rho_w)} = \frac{(W_w)_a}{Q_a \rho_w} \quad (6.65b)$$

where final equations of density for core and annular phases are expressed as:

$$\rho_a = \rho_o (1-E_w) + \rho_w E_w; \text{ similarly } \rho_b = \rho_w (1-E_o) + \rho_o E_o \quad (6.66)$$

The details analysis for the above expressions (Eqs. 6.65a – 66.66) are given in Appendix (Eqs. A.23-A.27).

Therefore at equilibrium, the rate of deposition (R_D) is equal to the rate of entrainment (R_A) and by substituting Eq.6.65 a, b into Eq.6.63 the following equations are found:

$$R_{Ao} = R_{Do} = K_{Do} \frac{(W_o)_b}{Q_b} = K_{Do} \cdot \rho_o \cdot E_o; \quad \because E_o = \frac{(W_o)_b}{Q_b \rho_o} \quad (6.67a)$$

$$R_{Aw} = R_{Dw} = K_{Dw} \frac{(W_w)_a}{Q_a} = K_{Dw} \cdot \rho_w \cdot E_w; \quad \because E_w = \frac{(W_w)_a}{Q_a \rho_w} \quad (6.67b)$$

By equating Eq.6.52 with Eq.6.67a, b it reduces finally into following correlations, which can predict the entrained fractions:

$$R_{Ao} = \frac{V_{ent}^{oil} \rho_o \left| U_{w1} - U_{o1} \right|}{\pi D_a \lambda^2} = K_{Do} \cdot \rho_o \cdot E_o \quad \therefore E_o = \frac{V_{ent}^{oil} \left| U_{w1} - U_{o1} \right|}{\pi K_{Do} \overline{D_a} D^3} \tag{6.68a}$$

$$R_{Aw} = \frac{V_{ent}^{water} \rho_w \left| U_{w2} - U_{o2} \right|}{\pi D_a \lambda^2} = K_{Dw} \cdot \rho_w \cdot E_w \quad \therefore E_w = \frac{V_{ent}^{water} \left| U_{w2} - U_{o2} \right|}{\pi K_{Dw} \overline{D_a} D^3} \tag{6.68b}$$

6.4.2 Model development for Pressure gradient

This model is derived based on the two-fluid model following the methodology discussed by Brauner (1991). Let us generally consider an annular flow arrangement of two immiscible fluids Oil (***o***) and Water (***w***), in an inclined pipe of inclination (***β***) with the horizontal, as showed in Fig. 6.17. Later this inclination is taken as zero, since we are considering only horizontal flow. The fundamental forms of the momentum equations for the core (***a***) and annular (***b***) regions by assuming fully developed flow are:

$$-A_a \left(\frac{dP}{dx} \right) \mp \tau_i S_i + \rho_a A_a g \sin \beta = 0; \quad \text{core region;} \tag{6.69}$$

$$-A_b \left(\frac{dP}{dx} \right) \pm \tau_i S_i - \tau_b S_b + \rho_b A_b g \sin \beta = 0; \quad \text{annular region;} \tag{6.70}$$

where the upper signs in Eq. 6.69 and 6.70 correspond to a downward flow of core region; 'A_a', 'A_b', 'ρ_a' and 'ρ_b' are the flow areas and equivalent densities of the core (***a***) and annular (***b***) regions respectively. Then by eliminating the pressure gradient $\left(\frac{dP}{dx}\right)$, from the Eq.6.69 and 6.70 yields:

$$-\frac{\tau_b S_b}{A_b} + \left(\rho_b - \rho_a \right) g \sin \beta \pm \tau_i S_i \left(\frac{1}{A_a} + \frac{1}{A_b} \right) = 0 \tag{6.71}$$

Then the wall shear stress 'τ_b' can be expressed as:

$$\tau_b = f_b\left(\frac{\rho_b U_b^2}{2}\right);\ \text{where}\ f_b = C_b \cdot \mathrm{Re}_b,\ \ \mathrm{Re}_b = \left(\frac{D_b U_b}{\upsilon_b}\right)^{-n_b}, D_b = \frac{4A_b}{S_b}, \tag{6.72}$$

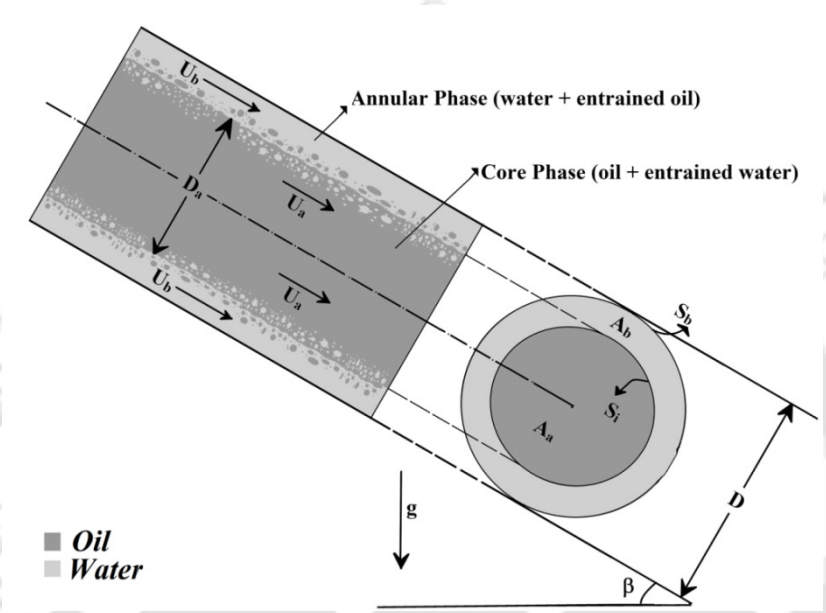

Fig. 6.17 Schematic description of two-phase annular flow.

where 'S_b' and 'f_b' are the perimeter and friction factor of the inner wall of the pipe, based on the annulus hydraulic diameter 'D_b' and the corresponding Reynolds number is given by 'Re_b' with proportionality friction constant 'C_b'. By considering, the common interactions between the two phases (as the interfacial shear and the relative velocities), the unknown parameters 'f_b' and 'D_b' can be calculated.

$$\tau_i = f_i\left(\frac{\rho_a (U_a - U_b)^2}{2}\right);\ \text{where}\ f_i = B \cdot C_a \cdot \mathrm{Re}_a;\ \ \mathrm{Re}_a = \left(\frac{D_a U_a}{\upsilon_a}\right)^{-n_a} \tag{6.73}$$

Here 'B' is the augmentation of the interfacial shear due to the interfacial waviness.

In Eq.6.72 and 6.73 the proportionality constants 'C_a', 'C_b' and flow regime parameters 'n_b', 'n_a' are chosen according to the flow regimes in core and annular phases. The flow regimes in annular flow are four types namely: (a) laminar-laminar (L-L), (b) laminar-turbulent (L-T), (c) turbulent-laminar (T-L) and (d) turbulent-turbulent (T-T) regimes. Therefore, these constants value are given based on the flow regimes as C = 16 and n = 1 for laminar flow; and C= 0.046 and n= 0.2 for turbulent flow conditions.

In the liquid-liquid systems the interface gives the impression of smooth long waves in almost all cases, and thus the 'B' can be ignored (B = 1). By assuming no slip between the core and annular phases in each region, the actual phase velocities ($\boldsymbol{U}$) can be calculated based on the volumetric flows ($\boldsymbol{Q}$) and entrainment fractions ($\boldsymbol{E}$).

Therefore, volumetric flow rates are given by:

$$Q_o = Q_a\alpha_a + Q_b\left(1-\alpha_b\right) = Q_a\left(1-E_w\right) + Q_bE_o \tag{6.74a}$$

$$Q_w = Q_b\alpha_b + Q_a\left(1-\alpha_a\right) = Q_b\left(1-E_o\right) + Q_aE_w \tag{6.74b}$$

The individual volumetric flow rates are given as:

$$Q_o = U_{os}A,\ Q_a = U_aA_a,\ Q_b = U_bA_b,\ Q_w = U_{ws}A,\ Q_a = U_aA_a,\ Q_b = U_bA_b \tag{6.75}$$

So actual phase velocities are required to get individual volume flow rates (Q_o, Q_w, $Q_a and\ Q_b$).The detailed calculation of phase velocities is shown in Appendix (Eqs. A.28-A.32).

The final expressions formed using above Eq.6.74a-Eq.6.75 yields:

$$\phi = \frac{U_{os}}{U_{ws}} \tag{6.76a}$$

$$\overline{U_a} = \frac{\overline{A}}{\overline{\overline{A_a}}}\left(\frac{E_o - \phi(1-E_o)}{\phi(E_o + E_w - 1)}\right); \text{ where } \frac{A/D^2}{A_a/D^2} = \frac{\overline{A}}{\overline{\overline{A_a}}} \tag{6.76b}$$

$$\text{and } \overline{U_b} = \frac{\overline{A}}{\overline{\overline{A_b}}}\left(\frac{\phi E_w - (1-E_w)}{(E_o + E_w - 1)}\right); \text{ where } \frac{A/D^2}{A_w/D^2} = \frac{\overline{A}}{\overline{\overline{A_w}}} \;\&\; \overline{U_b} = \frac{U_b}{U_{ws}} \tag{6.76c}$$

'U_{os}' and 'U_{ws}' are the superficial velocities; and the dimensional variables are defined by:

$$\begin{aligned}
&\overline{D_a} = \frac{D_a}{D};\ \overline{S_i} = \frac{S_i}{D} = \frac{\pi D_a}{D} = \pi\overline{D_a};\ \overline{S_b} = \frac{S_b}{D} = \frac{\pi D}{D} = \pi;\ \overline{\mathrm{A}} = \frac{A}{D^2} = \frac{\pi D^2}{4D^2} = \frac{\pi}{4};\\
&\overline{\mathrm{A}_a} = \frac{A_a}{D^2} = \frac{\pi D_a^2}{4D^2} = \frac{\pi}{4}\overline{D_a}^2;\ \overline{\mathrm{A}_b} = \frac{A_b}{D^2} = \frac{\pi\left(D^2 - D_a^2\right)}{4D^2} = \frac{\pi}{4}\left(1 - \overline{D_a}^2\right);\\
&\overline{D_b} = \frac{4\overline{A_b}}{\overline{S_b}} = \frac{4\frac{\pi}{4}\left(1-\overline{D_a}^2\right)}{\pi} = \left(1-\overline{D_a}^2\right)
\end{aligned} \tag{6.77}$$

Introducing these non-dimensional variables into Eq. 6.72 and Eq.6.73 gives:

$$\begin{aligned}
\tau_i &= C_a\left(\frac{\overline{D_a}\,\overline{U_a}\upsilon_o}{\upsilon_a}\right)^{-n_a}\left(\frac{DU_{os}}{\upsilon_o}\right)^{-n_a}\left(\frac{\rho_a\left(\overline{U_a}U_{os}\right)^2}{2}\right)\left(1-\frac{\overline{U_b}}{\overline{\overline{U_a}}}\frac{1}{\phi}\right)^2\\
\tau_b &= C_b\left(\frac{\overline{D_b}\,\overline{U_b}\upsilon_w}{\upsilon_b}\right)^{-n_b}\left(\frac{DU_{ws}}{\upsilon_w}\right)^{-n_b}\left(\frac{\rho_b\left(\overline{U_b}U_{ws}\right)^2}{2}\right)
\end{aligned} \tag{6.78}$$

By introducing these interfacial and wall stresses of Eq.6.78 in Eq.6.71 yields:

$$\begin{aligned}
&-\left[\left(\frac{C_b}{D}\right)\left(\frac{DU_{ws}}{\upsilon_w}\right)^{-n_b}\left(\frac{\rho_b U_{ws}^2}{2}\right)\right]\left[\frac{\overline{S_b}}{\overline{\overline{A_b}}}\overline{U_b}^2\left(\frac{\overline{D_b}\,\overline{U_b}\upsilon_w}{\upsilon_b}\right)^{-n_b}\right] + (\rho_b - \rho_a)\, g\sin\beta\\
&\pm\left[\left(\frac{C_a}{D}\right)\left(\frac{DU_{os}}{\upsilon_o}\right)^{-n_a}\left(\frac{\rho_a U_{os}^2}{2}\right)\right]\left[\overline{S_i}\,\overline{U_a}^2\left(\frac{\overline{D_a}\,\overline{U_a}\upsilon_o}{\upsilon_a}\right)^{-n_a}\right]\left(1-\frac{\overline{U_b}}{\overline{\overline{U_a}}}\frac{1}{\phi}\right)^2\left(\frac{1}{\overline{\overline{A_a}}}+\frac{1}{\overline{\overline{A_b}}}\right) = 0
\end{aligned}$$

Dividing this whole equation with $\left[\left(\frac{4C_a}{D}\right)\left(\frac{DU_{os}}{\upsilon_o}\right)^{-n_a}\left(\frac{\rho_o U_{os}^2}{2}\right)\right]$ yields the following equation

$$\pm\left[\left(\frac{\rho_a}{\rho_o}\right)\left(\frac{\overline{D_a}\,\overline{U_a}\upsilon_o}{\upsilon_a}\right)^{-n_a}\left(1-\frac{\overline{U_b}}{\overline{\overline{U_a}}}\frac{1}{\phi}\right)^2\overline{S_i}\,\overline{U_a}^2\left(\frac{1}{\overline{\overline{A_a}}}+\frac{1}{\overline{\overline{A_b}}}\right)\right]-\left[\chi^2\left(\frac{\rho_b}{\rho_w}\right)\left(\frac{\overline{D_b}\,\overline{U_b}\upsilon_w}{\upsilon_b}\right)^{-n_b}\frac{\overline{S_b}}{\overline{\overline{A_b}}}\overline{U_b}^2\right]+4Y=0 \quad (6.79)$$

Here 'χ^2' and 'Y' are the two-phase flow parameters defined as

$$\chi^2=\frac{\left[\left(\frac{4C_b}{D}\right)\left(\frac{DU_{ws}}{\upsilon_w}\right)^{-n_b}\left(\frac{\rho_w U_{ws}^2}{2}\right)\right]}{\left[\left(\frac{4C_a}{D}\right)\left(\frac{DU_{os}}{\upsilon_o}\right)^{-n_a}\left(\frac{\rho_o U_{os}^2}{2}\right)\right]} \text{ and } Y=\frac{(\rho_b-\rho_a)\,g\sin\beta}{\left[\left(\frac{4C_a}{D}\right)\left(\frac{DU_{os}}{\upsilon_o}\right)^{-n_a}\left(\frac{\rho_o U_{os}^2}{2}\right)\right]} \quad (6.80)$$

Since the non-dimensional velocities, '$\overline{U_a}$' and '$\overline{U_b}$' and the other parameters are all functions of the core diameter, '$\overline{D_a}$', of Eq.6.79 in general it is defined as

$$\overline{D_a}=f\left\{\chi^2,Y,\phi,n_a,n_b,E_o,E_w\right\} \quad (6.81)$$

By eliminating 'τ_i' from Eq.6.69, and Eq.6.70 two-phase pressure gradient becomes

$$\Rightarrow-\left(\frac{dP}{dx}\right)(A_b+A_a)-\tau_b S_b+(\rho_a A_a+\rho_b A_b)\,g\sin\beta=0$$

The expression of above pressure gradient equation can be written as in the following dimensionless forms (calculation procedure has been shown in Eqs. A. 33-35, Appendix),

$$\Phi_o=\frac{-\left(\frac{dP}{dx}\right)}{\left[\left(\frac{4C_a}{D}\right)\left(\frac{DU_{os}}{\upsilon_o}\right)^{-n_a}\left(\frac{\rho_o U_{os}^2}{2}\right)\right]}=\frac{1}{4}\chi^2\frac{\rho_b}{\rho_w}\frac{\overline{S_b}\,\overline{U_b}^2}{\left(\overline{A_a}+\overline{A_b}\right)}\left(\frac{\overline{D_b}\,\overline{U_b}\upsilon_w}{\upsilon_b}\right)^{-n_b}-\overline{\rho}Y \quad (6.82a)$$

$$\Phi_w = \frac{-\left(\frac{dP}{dx}\right)}{\left[\left(\frac{4C_b}{D}\right)\left(\frac{DU_{ws}}{\upsilon_w}\right)^{-n_b}\left(\frac{\rho_w U_{ws}^2}{2}\right)\right]} \times \frac{\left[\left(\frac{4C_a}{D}\right)\left(\frac{DU_{os}}{\upsilon_o}\right)^{-n_a}\left(\frac{\rho_o U_{os}^2}{2}\right)\right]}{\left[\left(\frac{4C_a}{D}\right)\left(\frac{DU_{os}}{\upsilon_o}\right)^{-n_a}\left(\frac{\rho_o U_{os}^2}{2}\right)\right]} = \frac{\Phi_o}{\chi^2} \qquad (6.82b)$$

Here $\overline{\rho} = \frac{\rho_a \overline{A_a} + \rho_b \overline{A_b}}{\left(\overline{A_a} + \overline{A_b}\right)\left(\rho_b - \rho_a\right)}$

Where '$\boldsymbol{\Phi_o}$' and '$\boldsymbol{\Phi_w}$' represents the references of the two-phase pressure gradient of the respective fluids which gives the pressure reduction associated with the transportation of oil in a core flow configuration and water in an annular flow configuration. The expressions of '$\boldsymbol{\chi^2}$' and '$\boldsymbol{Y}$' in Eq.6.80 are evolved from the normalization procedure, which includes not only superficial Reynolds numbers, but also unknown actual two-phase parameters. Thus, '$\boldsymbol{\Phi_o}$', '$\boldsymbol{\Phi_w}$', '$\boldsymbol{\chi^2}$' and '$\boldsymbol{Y}$' include mixed superficial and actual parameters. For the convenience, it is suggested to present the Eq.6.80, 6.82a, b in terms of the Lockhart-Martinelli parameter '$\boldsymbol{\chi_s^2}$', because it is fully based on the superficial variables. The final expression of Lockhart-Martinelli parameter '$\boldsymbol{\chi_s^2}$', can be expressed in the following form (the detailed calculation has been shown in Appendix Eq.A.36-40).

$$\chi_s^2 = \frac{\left(\frac{dP}{dx}\right)_{ws}}{\left(\frac{dP}{dx}\right)_{os}} = \chi^2 \frac{\left(\frac{C_{ws}}{C_b}\right)\mathrm{Re}_{ws}^{(n_b - n_{ws})}}{\left(\frac{C_{os}}{C_a}\right)\mathrm{Re}_{os}^{(n_a - n_{os})}} \qquad (6.83)$$

The constants '$\boldsymbol{n_{os}}$', '$\boldsymbol{n_{ws}}$', '$\boldsymbol{C_{os}}$' and '$\boldsymbol{C_{ws}}$' are evaluated from Reynolds numbers '$\mathbf{Re}_{os}$' and '$\mathbf{Re}_{ws}$', of oil and water respectively. These Reynolds numbers are calculated based on the superficial velocities of respective phases and may be different from the actual Reynolds

numbers '$\mathbf{Re}_a$' and '$\mathbf{Re}_b$' of Eq.6.72 and Eq.6.73. In some cases, like at adequately low flow rates, where the oil and water are in laminar flow regime (for both the actual and superficial Reynolds numbers, i.e. $n_a=n_{os}=1$ and $n_b=n_{ws}=1$) Eq.6.83 gives an equivalent condition: $\chi_s^2 = \chi^2$. Similarly, at higher flow rates, where the oil and water are in turbulent flow regime (for both the actual and superficial Reynolds numbers, i.e. $n_a=n_{os}=0.2$ and $n_b=n_{ws}= 0.2$) Eq.6.83 satisfies: $\chi_s^2 = \chi^2$. Other than these two flow regimes, two-phase flow parameter 'χ^2' may be different from the Lockhart-Martinelli parameter 'χ_s^2'.

6.4.3 Calculations procedure and analytical solutions

If all the values (such as superficial oil and water flow velocities 'U_{os}' and 'U_{ws}', tube inner diameter, interfacial tension and physical properties of oil and water) are available then we can incorporate in the Eq.6.79 in terms of $\overline{D_a}$. As given in Eq.6.81, if the entrainment fractions (E_o) and (E_w) are known from experimental procedures or from above mentioned entrainment model, a solution for $\overline{D_a}$ can be yielded which are summarized below in calculation part.

For the pipes with inclination and in the Laminar (oil)-Laminar (water) flow regime, Eq.6.80 and Eq.6.83 reduces to the following forms (substitution is shown in Eq.A.41- in Appendix).

$$\Rightarrow \chi_s^2 = \frac{\left[\left(\frac{4C_b}{D}\right)\left(\frac{DU_{ws}}{\upsilon_w}\right)^{-n_b}\left(\frac{\rho_w U_{ws}^2}{2}\right)\right]}{\left[\left(\frac{4C_a}{D}\right)\left(\frac{DU_{os}}{\upsilon_o}\right)^{-n_a}\left(\frac{\rho_o U_{os}^2}{2}\right)\right]} = \frac{1}{\phi}\left(\frac{\mu_w}{\mu_o}\right) \qquad (6.84a)$$

$$\therefore Y = \frac{(\rho_b - \rho_a)\, g \sin\beta}{\left[\left(\frac{4C_a}{D}\right)\left(\frac{DU_{os}}{\upsilon_o}\right)^{-n_a}\left(\frac{\rho_o U_{os}^2}{2}\right)\right]} = \frac{(\rho_b - \rho_a)\, gD^2 \sin\beta}{32\mu_o U_{os}} \qquad (6.84b)$$

and after incorporating equation Eq.6.77 in the Eq.6.76b and Eq.6.76c gives:

$$\overline{U_a} = \frac{\overline{A}}{\overline{A_a}}\overline{F} = \frac{\overline{F}}{\overline{D_a}^2};\ \text{where}\ \ \overline{F} = \left(\frac{E_o - \phi(1-E_o)}{\phi(E_o + E_w - 1)}\right)\ \text{and}\ \ \frac{\overline{A}}{\overline{A_a}} = \frac{1}{\overline{D_a}^2}$$

$$\overline{U_b} = \frac{\overline{A}}{\overline{A_b}}\overline{G} = \frac{\overline{G}}{\left(1-\overline{D_a^2}\right)};\ \text{where}\ \ \overline{G} = \left(\frac{\phi E_w - (1-E_w)}{(E_o + E_w - 1)}\right)\ \text{and}\ \ \frac{\overline{A}}{\overline{A_b}} = \frac{1}{\left(1-\overline{D_a}^2\right)}$$

Therefore by introducing non-dimensional parameters from Eq.6.77 into Eq.6.79 gives:
(The detailed calculations are provided in Appendix Eq.A.42)

$$\Rightarrow \pm\left[\left(1 - \frac{\overline{G}}{\overline{F}}\frac{\overline{D_a}^2}{\left(1-\overline{D_a}^2\right)}\frac{1}{\phi}\right)^2\left(\frac{\overline{F}}{\overline{D_a}^4}\right)\right] = \left[\frac{1}{\phi}\left(\frac{\mu_b}{\mu_a}\right)\frac{\overline{G}}{\left(1-\overline{D_a}^2\right)^2}\right] - Y\cdot\left(1-\overline{D_a}^2\right)\cdot\left(\frac{\mu_o}{\mu_a}\right)$$

$$\text{for '+'}\ \Rightarrow \left[\left(1 - \frac{\overline{G}}{\overline{F}}\frac{\overline{D_a}^2}{\left(1-\overline{D_a}^2\right)}\frac{1}{\phi}\right)^2\left(\frac{\overline{F}}{\overline{D_a}^4}\right)\right] = \left[\frac{1}{\phi}\left(\frac{\mu_b}{\mu_a}\right)\frac{\overline{G}}{\left(1-\overline{D_a}^2\right)^2}\right] - Y\cdot\left(1-\overline{D_a}^2\right)\cdot\left(\frac{\mu_o}{\mu_a}\right)$$

This equation can be further reduced to separate equation in terms of dimensionless core diameter. The calculation has been given in Appendix Eq.A.43-A.44. The final expression is as shown:

$$\Rightarrow \overline{D_a}^{10}(b_1c_1) - 3\overline{D_a}^8(b_1c_1) + 3\overline{D_a}^6(b_1c_1) - \overline{D_a}^4\left(b_1c_1 - b_1 + \left(\phi^2 + \left(\overline{G}/\overline{F}\right)^2 + 2\left(\overline{G}/\overline{F}\right)\right)\right) + 2\overline{D_a}^2\left(\phi^2 + \left(\overline{G}/\overline{F}\right)\right) - \phi^2 = 0;$$

$$\Rightarrow x^5(b_1c_1) - 3x^4(b_1c_1) + 3x^3(b_1c_1) - x^2\left(b_1c_1 - b_1 + \left(\phi^2 + \left(\overline{G}/\overline{F}\right)^2 + 2\left(\overline{G}/\overline{F}\right)\right)\right) + 2x\left(\phi^2 + \left(\overline{G}/\overline{F}\right)\right) - \phi^2 = 0;$$

Here $\overline{D_a} = \sqrt{x}\ \ \forall(x > 0)$

Where 'x' is the positive real root of the above equation.

$$\text{for '}-\text{'} \Rightarrow \left[\left(1-\frac{\overline{G}}{\overline{F}}\frac{\overline{D_a}^2}{\left(1-\overline{D_a}^2\right)}\frac{1}{\phi}\right)^2\left(\frac{\overline{F}}{\overline{D_a}^4}\right)\right]=-\left[\frac{1}{\phi}\left(\frac{\mu_b}{\mu_a}\right)\frac{\overline{G}}{\left(1-\overline{D_a}^2\right)^2}\right]+Y\cdot\left(1-\overline{D_a}^2\right)\cdot\left(\frac{\mu_o}{\mu_a}\right)$$

Above equation yields: $a^2+b\cdot c=0$ which gives:

$$\Rightarrow\overline{D_a}^{10}\left(b_1c_1\right)-3\overline{D_a}^8\left(b_1c_1\right)+3\overline{D_a}^6\left(b_1c_1\right)+\overline{D_a}^4\left(b_1-b_1c_1+\left(\phi^2+\left(\overline{G}/\overline{F}\right)^2+2\left(\overline{G}/\overline{F}\right)\right)\right)-2\overline{D_a}^2\left(\phi^2+\left(\overline{G}/\overline{F}\right)\right)+\phi^2=0;$$

$$\Rightarrow y^5\left(b_1c_1\right)-3y^4\left(b_1c_1\right)+3y^3\left(b_1c_1\right)+y^2\left(b_1-b_1c_1+\left(\phi^2+\left(\overline{G}/\overline{F}\right)^2+2\left(\overline{G}/\overline{F}\right)\right)\right)-2y\left(\phi^2+\left(\overline{G}/\overline{F}\right)\right)+\phi^2=0;$$

Here $\overline{D_a}=\sqrt{y}\ \ \forall\left(y>0\right)$; where '$y$' is the positive real root of the above equation.

Therefore, for horizontal flow'c_1' becomes zero as 'β' is zero:

So, for horizontal flow: $a=\sqrt{b\cdot c}=\sqrt{b_1\overline{D_a}^4}=\overline{D_a}^2\sqrt{b_1}$

$$\therefore\left[\phi\left(1-\overline{D_a}^2\right)-\overline{D_a}^2\left(\overline{G}/\overline{F}\right)\right]=\overline{D_a}^2\sqrt{b_1}\Rightarrow\overline{D_a}^2\left(\sqrt{b_1}+\left(\overline{G}/\overline{F}\right)+\phi\right)=\phi;$$

$$\Rightarrow\left(\left(\phi\left(\frac{\mu_b}{\mu_a}\right)\left(\overline{G}/\overline{F}\right)\right)^{1/2}+\left(\overline{G}/\overline{F}\right)+\phi\right)\overline{D_a}^2=\phi;\quad\therefore\overline{D_a}=\left(\frac{\phi}{\left(\left(\phi\left(\frac{\mu_b}{\mu_a}\right)\left(\overline{G}/\overline{F}\right)\right)^{1/2}+\left(\overline{G}/\overline{F}\right)+\phi\right)}\right)^{1/2}\qquad(6.85)$$

For special case of perfect annular flow, Eq.6.85 becomes:

$$\overline{D_a}=\left(\frac{\phi}{\left(\sqrt{\phi k_l}+1+\phi\right)}\right)^{1/2}\ \text{where}\ k_l=\left(\frac{\mu_b}{\mu_o}\right)\because\mu_a=\mu_o;\mu_b=\mu_w\ \text{at}\ E_o=E_w=0\qquad(6.86)$$

$$\Rightarrow\left(1-\overline{D_a}^2\right)=\left(1-\frac{\phi}{\left(\left(\phi\left(\frac{\mu_b}{\mu_a}\right)\left(\frac{\overline{G}}{\overline{F}}\right)\right)^{1/2}+\left(\frac{\overline{G}}{\overline{F}}\right)+\phi\right)}\right)\therefore\frac{1}{\left(1-\overline{D_a}^2\right)}=\frac{\left(\left(\phi\left(\frac{\mu_b}{\mu_a}\right)\left(\frac{\overline{G}}{\overline{F}}\right)\right)^{1/2}+\left(\frac{\overline{G}}{\overline{F}}\right)+\phi\right)}{\left(\left(\phi\left(\frac{\mu_b}{\mu_a}\right)\left(\frac{\overline{G}}{\overline{F}}\right)\right)^{1/2}+\left(\frac{\overline{G}}{\overline{F}}\right)\right)}$$

Eq.6.82a gives the following form by incorporating non-dimensional parameters of Eq.6.77.

$$\Phi_o=\frac{1}{4}\frac{1}{\phi}\left(\frac{\mu_w}{\mu_o}\right)\frac{\rho_b}{\rho_w}\frac{\pi\overline{U_b}^2}{\left(\overline{A_a}+\overline{A_b}\right)}\left(\frac{\upsilon_b}{\overline{D_b}\,\overline{U_b}\,\upsilon_w}\right)-\overline{\rho}Y=\frac{1}{4}\frac{1}{\phi}\left(\frac{\mu_b}{\mu_o}\right)\frac{\pi\overline{U_b}}{\pi/4}\left(\frac{1}{\left(1-\overline{D_a}^2\right)}\right)-\overline{\rho}Y;$$

$$\Rightarrow\Phi_o=\frac{1}{\phi}\left(\frac{\mu_b}{\mu_o}\right)\frac{\overline{G}}{\left(1-\overline{D_a}^2\right)^2}-\overline{\rho}Y=\frac{1}{\phi}\left(\frac{\mu_b}{\mu_o}\right)\overline{G}\left(\frac{\left(\left(\phi\left(\frac{\mu_b}{\mu_a}\right)\left(\frac{\overline{G}}{\overline{F}}\right)\right)^{1/2}+\left(\frac{\overline{G}}{\overline{F}}\right)+\phi\right)}{\left(\left(\phi\left(\frac{\mu_b}{\mu_a}\right)\left(\frac{\overline{G}}{\overline{F}}\right)\right)^{1/2}+\left(\frac{\overline{G}}{\overline{F}}\right)\right)}\right)^2-\overline{\rho}Y \quad (6.87)$$

Where $\overline{\rho}=\frac{\rho_a\overline{A_a}+\rho_b\overline{A_b}}{\left(\overline{A_a}+\overline{A_b}\right)\left(\rho_b-\rho_a\right)}=\frac{\rho_a\overline{D_a}^2+\rho_b\left(1-\overline{D_a}^2\right)}{\left(\rho_b-\rho_a\right)}$

For special case of pure annular horizontal flow, Eq.6.87 becomes:

$$\Phi_o=\frac{1}{\phi}k_l\left(\frac{\left(\sqrt{\phi k_l}+1+\phi\right)}{\left(\sqrt{\phi k_l}+1\right)}\right)^2;\ \text{where}\ k_l=\left(\frac{\mu_b}{\mu_o}\right)\because\mu_a=\mu_o;\mu_b=\mu_w\ \text{at}\ E_o=E_w=0 \quad (6.88)$$

From the equation Eq.6.82a, dimensionless pressure gradient can be calculated as:

$$\Phi_o=\frac{-\left(\frac{dP}{dx}\right)}{\left[\left(\frac{4C_a}{D}\right)\left(\frac{DU_{os}}{\upsilon_o}\right)^{-n_a}\left(\frac{\rho_o U_{os}^2}{2}\right)\right]}\Rightarrow-\left(\frac{dP}{dx}\right)=\Phi_o\left(\frac{4^2\times16}{D}\right)\left(\frac{1}{\mathrm{Re}_{os}}\right)^{n_a/1}\left(\frac{\rho_o U_{os}^2}{2}\right)$$

$$\Rightarrow -\left(\frac{dP}{dx}\right)=\Phi_o\left(\frac{32\rho_o U_{os}^2}{D\,\mathrm{Re}_{os}}\right)$$

While for mixed flow regimes consider Laminar (oil) - Turbulent (water), Eq.6.80, 6.83 reduces to (substitution has been shown in Appendix Eq.A.46-A.48)

$$\chi_s^2=\frac{\left[\left(\frac{4C_b}{D}\right)\left(\frac{DU_{ws}}{\upsilon_w}\right)^{-n_b}\left(\frac{\rho_w U_{ws}^2}{2}\right)\right]}{\left[\left(\frac{4C_a}{D}\right)\left(\frac{DU_{os}}{\upsilon_o}\right)^{-n_a}\left(\frac{\rho_o U_{os}^2}{2}\right)\right]}$$

$$\Rightarrow \chi_s^2=\frac{0.046}{16}\left[\frac{\mu_w}{\mu_o}\cdot\frac{1}{\phi}\cdot \mathrm{Re}_{ws}^{0.8}\right]=k_{l1}\frac{1}{\phi};\ \text{ where } k_{l1}=\frac{0.046}{16}\left[\frac{\mu_w}{\mu_o}\cdot \mathrm{Re}_{ws}^{0.8}\right] \qquad (6.89a)$$

$$\Rightarrow \chi_s^2=\frac{0.046}{16}\left[\left(\frac{\mu_w}{\mu_o}\right)^{0.2}\cdot\left(\frac{\rho_w}{\rho_o}\right)^{0.8}\cdot\frac{1}{\phi^{1.8}}\cdot \mathrm{Re}_{os}^{0.8}\right]=k_{l2}\frac{1}{\phi^{1.8}};\ \text{where } k_{l2}=\frac{0.046}{16}\left[\left(\frac{\mu_w}{\mu_o}\right)^{0.2}\cdot\left(\frac{\rho_w}{\rho_o}\right)^{0.8}\cdot \mathrm{Re}_{os}^{0.8}\right] \qquad (6.89b)$$

Therefore by introducing non-dimensional parameters from Eq.6.77 into Eq.6.79 results

$$\Rightarrow \pm\left[\left(\frac{\rho_a}{\rho_o}\right)\left(\frac{\upsilon_a}{\overline{D}_a\overline{U}_a\upsilon_o}\right)\left(1-\frac{\overline{G}}{\overline{F}}\frac{\overline{D}_a^{\,2}}{\left(1-\overline{D}_a^{\,2}\right)}\frac{1}{\phi}\right)^2\overline{S}_i\overline{U}_a^{\,2}\left(\frac{1}{\overline{A}_a}+\frac{1}{\overline{A}_b}\right)\right]=\left[\chi^2\left(\frac{\rho_b}{\rho_w}\right)\left(\frac{\upsilon_b}{\overline{D}_b\overline{U}_b\upsilon_w}\right)^{0.2}\frac{\overline{S}_b}{\overline{A}_b}\overline{U}_b^{\,2}\right]-4Y$$

By simplifying the above equation (the detail calculation is shown in Appendix, Eqs. 49-50),

$$\Rightarrow \pm\left(\phi\left(1-\overline{D}_a^{\,2}\right)-\overline{D}_a^{\,2}\left(\overline{G}/\overline{F}\right)\right)^2=\left[\overline{D}_a^{\,4}\cdot\chi_s^2\cdot\phi^2\left(\frac{\mu_o}{\mu_a}\right)\left(\frac{\rho_b}{\rho_w}\right)\left(\frac{\upsilon_b}{\upsilon_w}\right)^{0.2}\frac{\overline{G}^{1.8}}{\overline{F}}\right]-Y\cdot\left(1-\overline{D}_a^{\,2}\right)^3\cdot\phi^2\cdot\left(\frac{\overline{D}_a^{\,4}}{\overline{F}}\right)\left(\frac{\mu_o}{\mu_a}\right)$$

$$\text{for '+'}\Rightarrow a^2=\left[\overline{D}_a^{\,4}\cdot\chi_s^2\cdot\phi^2\left(\frac{\mu_o}{\mu_a}\right)\left(\frac{\rho_b}{\rho_w}\right)\left(\frac{\upsilon_b}{\upsilon_w}\right)^{0.2}\frac{\overline{G}^{1.8}}{\overline{F}}\right]\left(1+Y\cdot\left(\overline{D}_a^{\,2}-1\right)^3\left(\frac{\rho_w}{\rho_b}\right)\left(\frac{\upsilon_w}{\upsilon_b}\right)^{0.2}\frac{\chi_s^{-2}}{\overline{G}^{1.8}}\right)=m\cdot n$$

After simplification the above equation results the following expression (The detailed calculation has been given in Eqs.A. 51-52)

$$\Rightarrow \overline{D_a}^{10}(m_1n_1)-3\overline{D_a}^{8}(m_1n_1)+3\overline{D_a}^{6}(m_1n_1)-\overline{D_a}^{4}\left(m_1n_1-m_1+\left(\phi^2+\left(\overline{G}/\overline{F}\right)^2+2\left(\overline{G}/\overline{F}\right)\right)\right)+2\overline{D_a}^{2}\left(\phi^2+\left(\overline{G}/\overline{F}\right)\right)-\phi^2=0;$$

$$\Rightarrow z_1^{5}(m_1n_1)-3z_1^{4}(m_1n_1)+3z_1^{3}(m_1n_1)+z_1^{2}\left(m_1-m_1n_1+\left(\phi^2+\left(\overline{G}/\overline{F}\right)^2+2\left(\overline{G}/\overline{F}\right)\right)\right)-2z_1\left(\phi^2+\left(\overline{G}/\overline{F}\right)\right)+\phi^2=0;$$

Here $\overline{D_a}=\sqrt{z_1}\ \ \forall(z_1>0)$; where '$z_1$' is the root of the above equation; where for a horizontal flow 'n_1' becomes zero as 'β' is zero.

So, for horizontal flow: $a=\sqrt{m\cdot n}=\sqrt{m_1\overline{D_a}^{4}}=\overline{D_a}^{2}\sqrt{m_1}$

$$\Rightarrow\left(\phi\left(1-\overline{D_a}^{2}\right)-\overline{D_a}^{2}\left(\overline{G}/\overline{F}\right)\right)=\overline{D_a}^{2}\sqrt{m_1}\Rightarrow\overline{D_a}^{2}\left(\sqrt{m_1}+\left(\overline{G}/\overline{F}\right)+\phi\right)=\phi;$$

$$\therefore\overline{D_a}=\left(\frac{\phi}{\left(\chi_s\phi\left(\left(\frac{\mu_o}{\mu_a}\right)\left(\frac{\rho_b}{\rho_w}\right)\left(\frac{\upsilon_b}{\upsilon_w}\right)^{0.2}\frac{\overline{G}^{1.8}}{\overline{F}}\right)^{0.5}+\left(\overline{G}/\overline{F}\right)+\phi\right)}\right)^{1/2}\quad\text{where }\chi_s\phi=\left(\phi^{0.1}k_{l2}^{0.5}\right)or\left(\sqrt{\phi k_{l1}}\right)\tag{6.90}$$

For special case of pure annular horizontal flow, Eq.6.90 becomes:

$$\overline{D_a}=\left(\frac{\phi}{\chi_s\phi+1+\phi}\right)^{1/2}\quad\because\mu_a=\mu_o;\mu_b=\mu_w;\rho_a=\rho_o;\rho_b=\rho_w\text{ at }E_o=E_w=0\tag{6.91}$$

Therefore by introducing non-dimensional parameters from Eq.6.77 into Eq.6.82a:

(calculation has been shown in Eqs.A.53 – 54 in Appendix)

$$\Rightarrow \Phi_o = \chi_s^2 \frac{\rho_b}{\rho_w}\left(\frac{\upsilon_b}{\upsilon_w}\right)^{0.2} \frac{\overline{G}^{1.8}}{\left(1-\overline{D_a}^2\right)^2} - \left(\frac{\left(\rho_a \overline{D_a}^2 + \rho_b\left(1-\overline{D_a}^2\right)\right) gD\sin\beta\left(\frac{D}{\mu_o}\right)^{0.2}}{32\rho_o^{0.8}U_{os}^{1.8}}\right) \tag{6.92}$$

For special case of pure annular horizontal flow, Eq.6.92 becomes:

$$\Phi_o = \frac{\chi_s^2}{\left(1-\overline{D_a}^2\right)^2} \because \mu_a = \mu_o; \mu_b = \mu_w; \rho_a = \rho_o; \rho_b = \rho_w \text{ at } E_o = E_w = 0$$

$$\Rightarrow \Phi_o = \chi_s^2\left(\frac{\chi_s\phi + 1 + \phi}{\chi_s\phi + 1}\right)^2 \text{ where } \chi_s^2 = \frac{k_{l1}}{\phi} or \frac{k_{l2}}{\phi^{1.8}} \;\&\; \chi_s\phi = \left(\phi^{0.1}k_{l2}^{0.5}\right) or \left(\sqrt{\phi k_{l1}}\right): \tag{6.93}$$

Here dimensionless core diameter ($\overline{D_a}$) equations are not representing as simple equations. Besides the coefficients of ($\overline{D_a}$) is having different magnitudes in varying powers of 10. Which may leads to miscalculation of ($\overline{D_a}$). So we proposed a simple semi empirical equation which includes the gravity function as a one dimensional equation into horizontal equations (6.85, 6.90). This empirical equation is developed based on present experimental data and (Grassi et al., 2008), which is given as:

For negative inclination:

$$\Rightarrow \overline{D_a} = \left(\frac{\phi}{\left(\left(\phi\left(\frac{\mu_b}{\mu_a}\right)\left(\overline{G}/\overline{F}\right)\right)^{1/2} + \left(\overline{G}/\overline{F}\right) + \phi\right)}\right)^{1/2} - \left(0.313(Y) + 0.016\right) \tag{6.85a}$$

For positive inclination:

$$\Rightarrow \overline{D_a} = \left(\frac{\phi}{\left(\left(\phi \left(\frac{\mu_b}{\mu_a} \right) \left(\overline{G} / \overline{F} \right) \right)^{1/2} + \left(\overline{G} / \overline{F} \right) + \phi \right)} \right)^{1/2} - \left(11.70 \left(Y \right) + 0.025 \right) \qquad (6.90a)$$

The normalized forms of equations Eq.6.72, Eq.6.73 can be calculated as given below in cases (1, 2):

Case 1: Laminar (oil)-Laminar (water)

For laminar (oil)–laminar (water) flow regime above normalized equations becomes:

$$\tau_i = \frac{8 \cdot \mu_a \cdot U_{os} \cdot \overline{F}}{D \cdot \overline{D_a}^3} \left(\frac{\phi \left(1 - \overline{D_a}^2 \right) - \overline{D_a}^2 \left(\overline{G} / \overline{F} \right)}{\phi \left(1 - \overline{D_a}^2 \right)} \right)^2 \qquad (6.94)$$

$$\tau_b = \left(\frac{8 \cdot \mu_b \cdot U_{ws} \cdot \overline{G}}{D \cdot \left(1 - \overline{D_a}^2 \right)^2} \right) \qquad (6.95)$$

Case 2 Laminar (oil)-Turbulent (water)

For laminar (oil)-turbulent (water) flow regime, interfacial tension 'τ_i' will be same as in Eq.6.94 but wall shear stress 'τ_b' becomes:

$$\tau_b = \left(\frac{0.023 \cdot \upsilon_b^{0.2} \cdot \rho_b \cdot U_{ws}^{1.8} \cdot \overline{G}^{1.8}}{D^{0.2} \cdot \left(1 - \overline{D_a}^2 \right)^2} \right) \qquad (6.96)$$

6.4.3.1 Optimal conditions

For achieving a maximum pressure reduction, one must explore the correlation $\frac{\partial \Phi}{\partial \phi_o} = 0$; which yields the optimum input velocity ratio (ϕ_m) i.e. at this ratio the maximum pressure

reduction can be obtained. Thus, for L-L and L-T flows, utilizing **'Φ_o',** optimum input velocity ratio (**ϕ_m**) becomes (details are shown in Appendix Eq.A.55-A.57):

$$\therefore \phi_m = \frac{1}{\left(\sqrt{k_l}+1\right)^2}; \frac{1}{\left(\sqrt{k_l}-1\right)^2}; \frac{\left(k_l+\sqrt{k_l\left(k_l-4\right)}-2\right)}{2}; \frac{\left(k_l-\sqrt{k_l\left(k_l-4\right)}-2\right)}{2} \qquad (6.97a)$$

where $k_l = k_l$ (of Eq.6.68) for $\mathrm{L(o)\&L(w)}$

There is no simple analytical expression of (**ϕ_m**) for the Laminar (oil)- Turbulent (water) case.

Then, the minimum power requirement for a given oil input is obtained by solving for '**Φ_m**' satisfying (as mentioned by Brauner (1991)),

$$\Phi_o^{'} = \left(\frac{\phi+1}{\phi}\right)\Phi_o \quad \therefore \frac{\partial \Phi_o^{'}}{\partial \phi} = 0 = \left(\frac{d\Phi_o^{'}}{d\phi}\right)_{\text{at constant } k_l}$$

Incorporating all the parameters in above equation and after simplification the final expression becomes as follows (details of calculation is shown in Appendix, Eqs.A.58-59).

$$\therefore \Phi_m = \frac{\left(k_l+\sqrt{k_l\left(k_l-4\right)}-2\right)}{2}; \frac{\left(k_l-\sqrt{k_l\left(k_l-4\right)}-2\right)}{2}; \frac{z_1^2}{k_l} \quad \text{where } 'z_1' \text{ are the roots of } \mathrm{f}\{z\}=0 \qquad (6.97b)$$

$$\text{where } \mathrm{f}\{z\} = z^4 + z^3\left(\frac{3k_l}{k_l-1}\right) + z^2\left(\frac{k_l+2k_l^2}{k_l-1}\right) + z\left(\frac{4k_l^2}{k_l-1}\right) + \left(\frac{2k_l^2}{k_l-1}\right)$$

where $k_l = k_l$ (of Eq.6.68) for $\mathrm{L(o)\&L(w)}$

6.4.4 Solution methodology

The equations are solved with the help of **MATLAB** (2012a). A brief flow chart of the algorithm is mentioned in Fig. 6.18 details of algorithm areas follow.

1. For a given set of input data (viscosities, densities, and superficial velocities of both the phases, interfacial tension, and inner diameter of the pipe/tube), first calculate the superficial Reynolds number for the oil and water ($\mathbf{Re}_{os}$ and $\mathbf{Re}_{ws}$), dimensionless superficial velocity ratio ($\boldsymbol{\varphi}$), and drag coefficient ($\boldsymbol{C_d}$) as given in Eq.6.83, Eq.6.86a and Eq.6.55 respectively. These are independent of entrainment fractions ($\boldsymbol{E_o}$ and $\boldsymbol{E_w}$) and the core diameter ($\boldsymbol{D_a}$).
2. Initially started with the conditions of no entrainment and evaluated the program with dimensionless core diameter ($\overline{\boldsymbol{D_a}}$) in the range of (0 to 1) to calculate the new entrainment fractions ($\boldsymbol{E_o}$, $\boldsymbol{E_w}$) by using Eq.6.69 and 6.70.
3. Then, calculated the dimensionless critical amplitudes ($\overline{\boldsymbol{a_o}}$,$\overline{\boldsymbol{a_w}}$) of individual waves from the Eq.6.58 and 6.59 (which are further deformed into drops of volumes ($\boldsymbol{V_{ent}^{oil}}$, $\boldsymbol{V_{ent}^{water}}$) in the Eq.6.91. Here, in 11th order Eq.6.58 and 6.59, excluded roots which are having imaginary and negative values and took the positive real values only. If no positive root is formed, proceed for next iteration of dimensionless core diameter ($\overline{\boldsymbol{D_a}}$).
4. Based on the flow regimes (i.e. *L(o)-L(w)* or *L(o)-T(w)*), volume of entrainment fractions ($\boldsymbol{V_{ent}^{oil}}$,$\boldsymbol{V_{ent}^{water}}$) are used for calculating new entrainment fractions (E_o, E_w). Since, there are no experimental data for calculating the wave volume at new condition (explained in section Volume of entrained wave); assumed its value as zero. By using these (E_o, E_w) new dimensionless core diameter ($\overline{\boldsymbol{D_a}}$) and two phase pressure gradient $\left(\frac{\boldsymbol{dP}}{\boldsymbol{dx}}\right)$ are calculated as in Eq.6.85, Eq.6.90 and Eq.6.82a respectively.

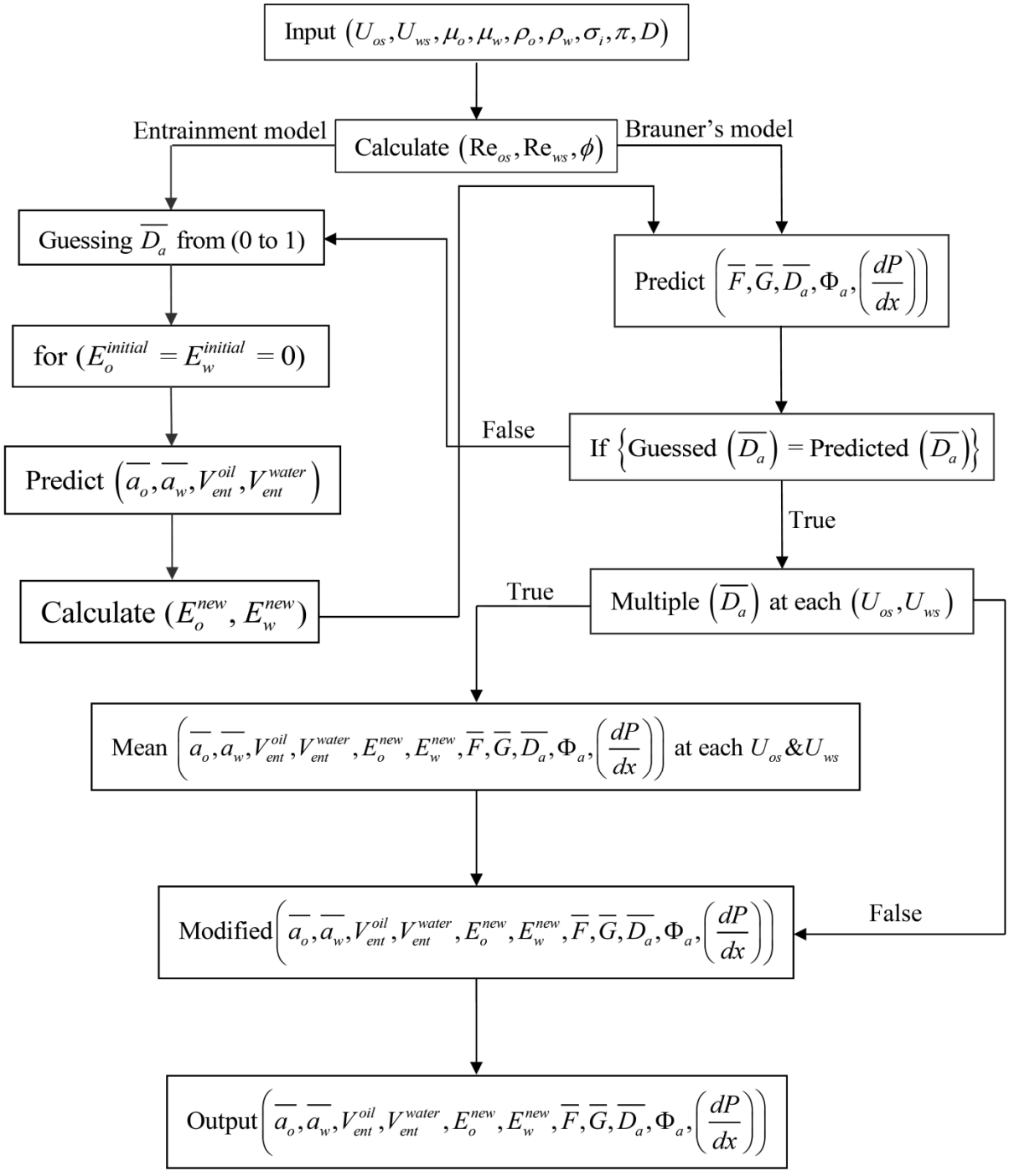

Fig. 6.18 Flow chart of the model to solve in MATLAB

6.4.4.1 Prediction of annular pressure gradient in horizontal and inclined pipeline

The pressure gradients obtained in the horizontal and inclined pipeline as discussed in Section 6.2 have been predicted using the developed model with and without entrainment and the parity plots has been given in Fig. 6.19a, b and Fig. 6.20a, b respectively.

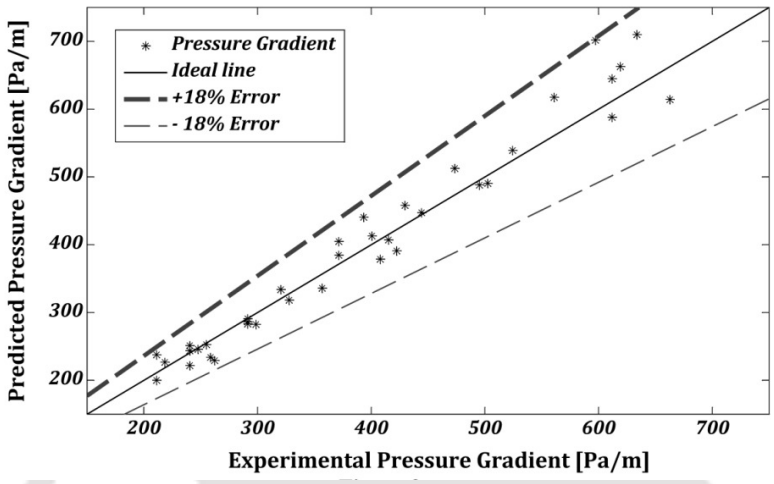

Fig. 6.19a Comparison of predicted and experimental pressure gradient without entrainment (i.e. $E_o = E_w = 0$) in horizontal flow

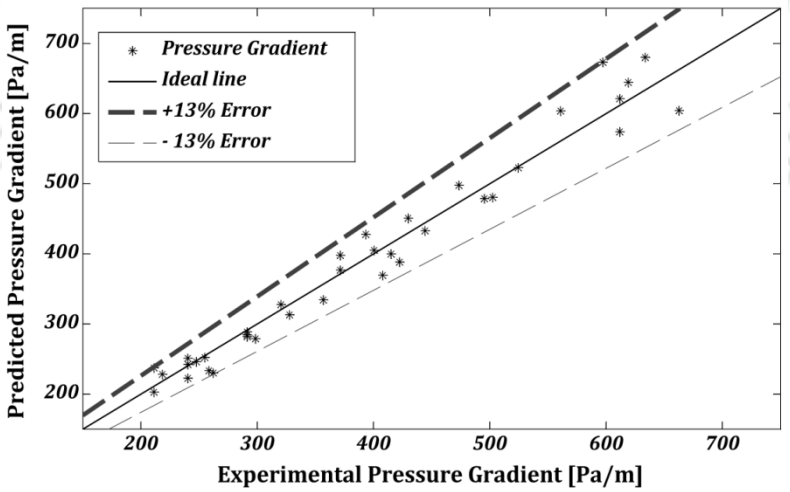

Fig. 6.19b Comparison of predicted and experimental pressure gradient with entrainment in horizontal flow

The predicted pressure gradient in horizontal pipeline without entrainment has been compared with experimental pressure gradient as shown in Fig. 6.19a. The figure shows that the predicted result gives a percentage error deviation of ±18%. To improve the accuracy in prediction the same data are predicted again considering the entrainment fraction. Now, it gives a good accuracy with a percentage error deviation of ±13% only, as shown in Fig. 6.19b. The above results proves that a significant improvement is obtained from the proposed model by considering the entrainment fractions of oil and water (i.e. $\boldsymbol{E_o}$ and $\boldsymbol{E_w}$) using the Eq.6.62 and 6.63.

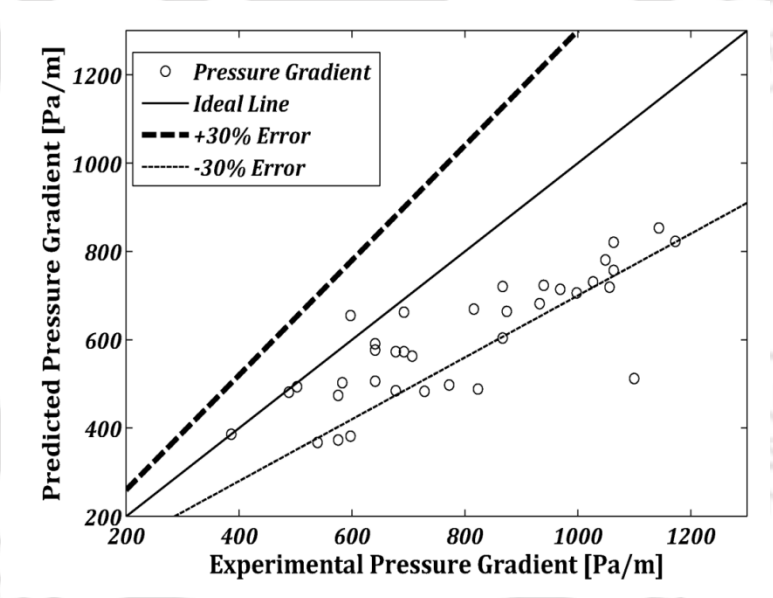

Fig. 6.20a Comparison of predicted and experimental pressure gradient without entrainment (i.e. $E_o = E_w = 0$) in inclined flow

The annular flow pressure gradient data has been predicted using the developed model without and with entrainment fraction. The comparison of experimental and predicted results have been given in Fig. 6.20a and b respectively. Fig. 6.20a shows that the model has predicted the experimental results within the 30% error. After incorporation of

entrainment fraction the percentage prediction has been increase and all the predicted results are within 20% error as given in Fig. 6.20b. The model gives notable improvement in prediction after incorporation of entrainment fraction.

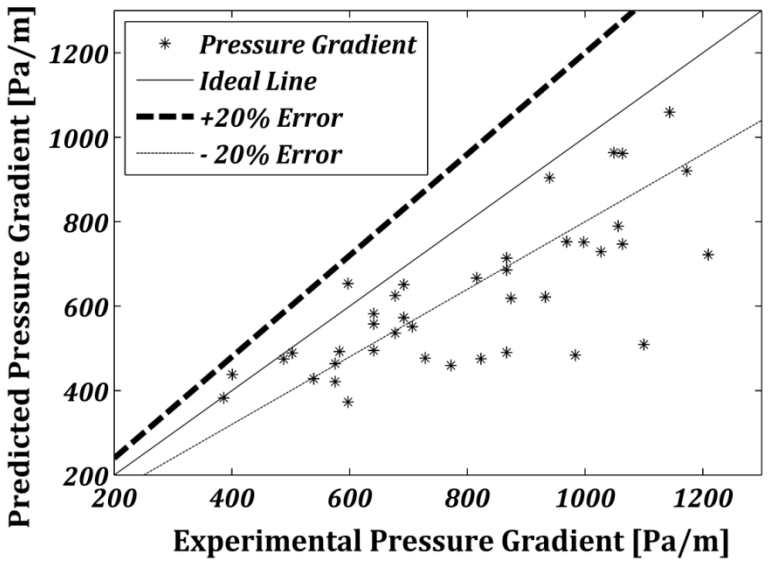

Fig. 6.20b Comparison of predicted and experimental pressure gradient with entrainment in inclined flow

6.4.4.2 Validation of the model

Validation of the model for horizontal pipeline flow

The proposed model has been validated with available horizontal literature data. For this purpose the Grassi et al. (2008) and Oliemans, 1986) data have been selected. Grassi et al. (2008) conducted experiments with viscous oil having the viscosity ratio of 800 and density ratio of 0.886 in 0.021 m ID horizontal pipeline. The predicted results of pressure gradient data of Grassi et al. (2008) without and with entrainment fraction have been shown in Fig. 6.21a-b respectively. The Fig.6.21b shows that the entrainment fraction

improves the accuracy in prediction of pressure gradient with a small deviation of only ±15% while the Fig. 6.21a. shows a deviation of ±20%.

Next the proposed model has been used to predict the pressure gradient data Oliemans (1986) data. He measured the pressure gradient for a horizontal annular flow in a 2 inch inner-diameter of Perspex pipe. A very high viscous oil (viscosity of 3 Pa s and density of 975 kg /m^3) and water (viscosity = 1 mPa.s and density = 995kg/m^3) with interfacial tension of 0.044 N/m were considered as test fluids. The percentage deviation in predicted results using present model are plotted in Fig. 6.19a-b. The results without entrainments give a large deviation with 32% (Fig. 6.19a). The entrainment value reduces this deviation as shown in Fig. 6.19b of value 28% from the ideal line. Where, ideal line is defined as zero percentage deviation of predicted result from the experimental data.

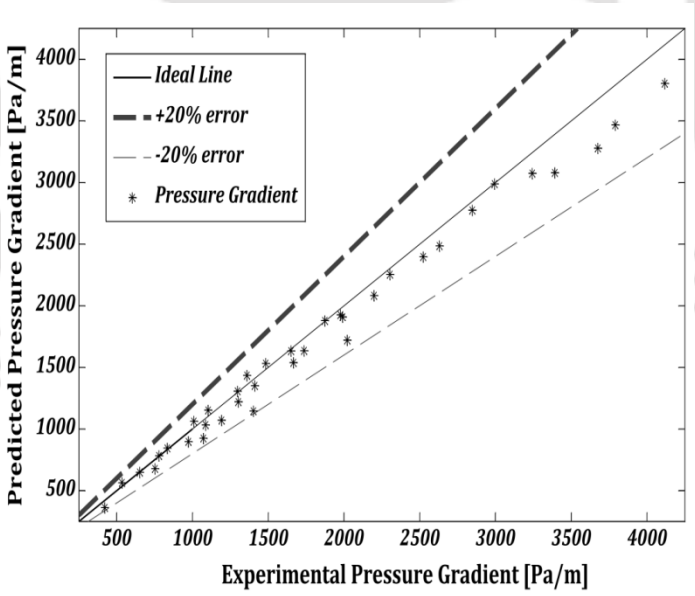

Fig. 6.21a Comparison of predicted and experimental pressure gradient of Grassi el al. (2008) for horizontal flow without entrainment.

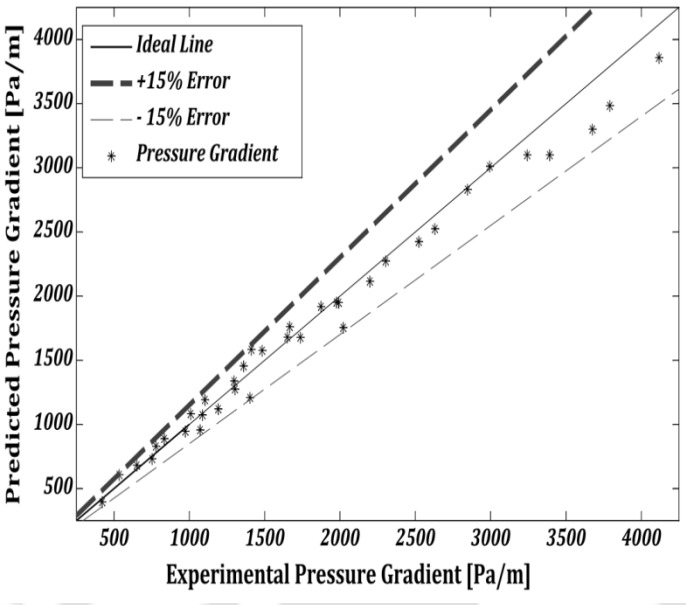

Fig. 6.21b Comparison of predicted and experimental pressure gradient of Grassi el al. (2008) for horizontal flow with entrainment.

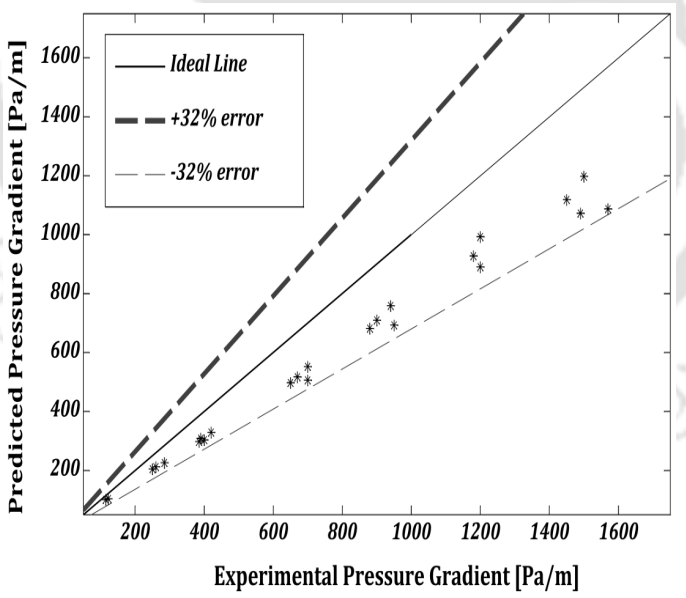

Fig. 6.22a Comparison of predicted and experimental pressure gradient of Oliemans (1986) for horizontal flow without entrainment.

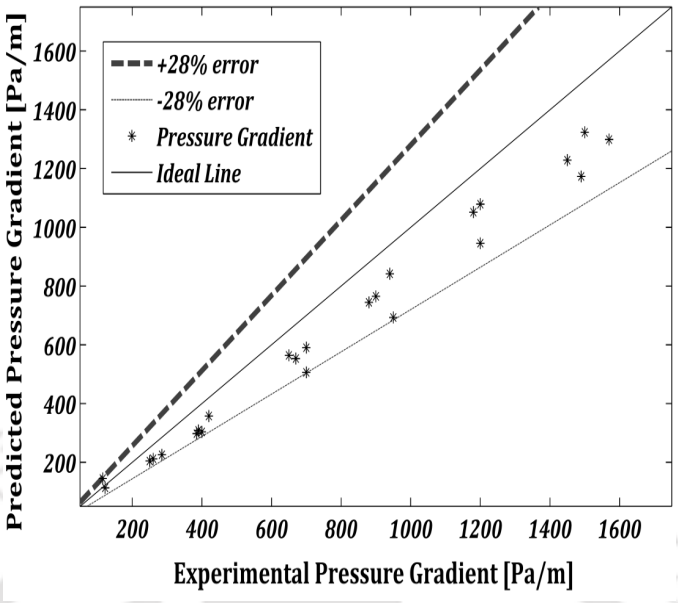

Fig. 6.22b Comparison of predicted and experimental pressure gradient of Oliemans (1986) for horizontal flow with entrainment.

Validation of the model for inclined pipeline flow

The model has also been validated for inclined pipeline flow by predicting the annular flow experimental data of Grassi et al. (2008) for system of inclinations +15°, +10° and –10° and the predicted results of pressure gradient are shown in Fig. 6.23-6.25a-b respectively. Fig. 6.23a, 6.24a, and 6.25a shows the comparison between the experimental data of (Grassi et al., (2008)) and the predicted pressure gradient using the model based on without entrainment condition, while, Fig. 6.23b, 6.24b, and 6.25b shows the comparison plot with incorporation of entrainment fraction. In Fig. 6.23a there are only 50% of the data points are showing ±30% agreement. While Fig. 6.23b shows the very good agreement of ±20% for almost all the data points for the inclination of +15°. In Fig.6.24a and 6.25a shows the agreement of ±30% and ±30% for all the data points respectively. Which is further

improved in Fig. 6.24b and 6.25b showing the good agreement with the predicted data points of ±20%and ±20% respectively. As the results clearly shows that the model is showing significant improvement in higher inclinations also.

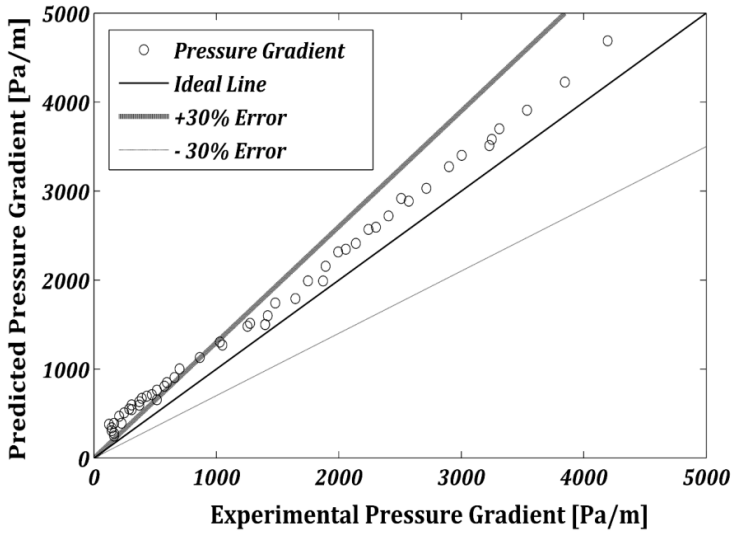

Fig. 6.23a Comparison of predicted and experimental pressure gradient of Grassi el al. (2008) for +15°inclined flow without entrainment.

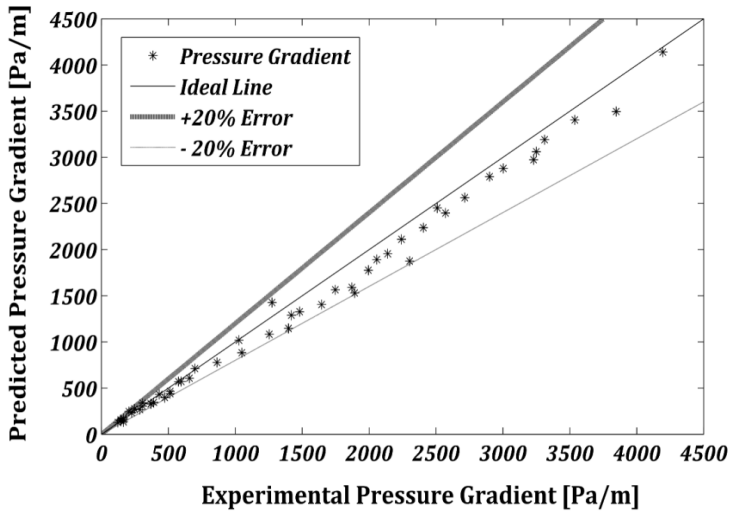

Fig. 6.23b Comparison of predicted and experimental pressure gradient of Grassi el al. (2008) for +15°inclined flow with entrainment.

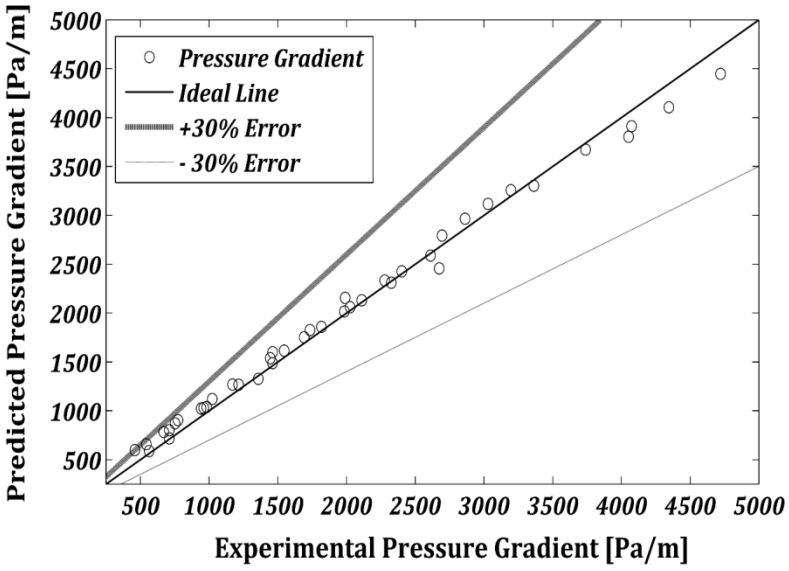

Fig. 6.24a Comparison of predicted and experimental pressure gradient of Grassi et al. (2008) for +10°inclined flow without entrainment.

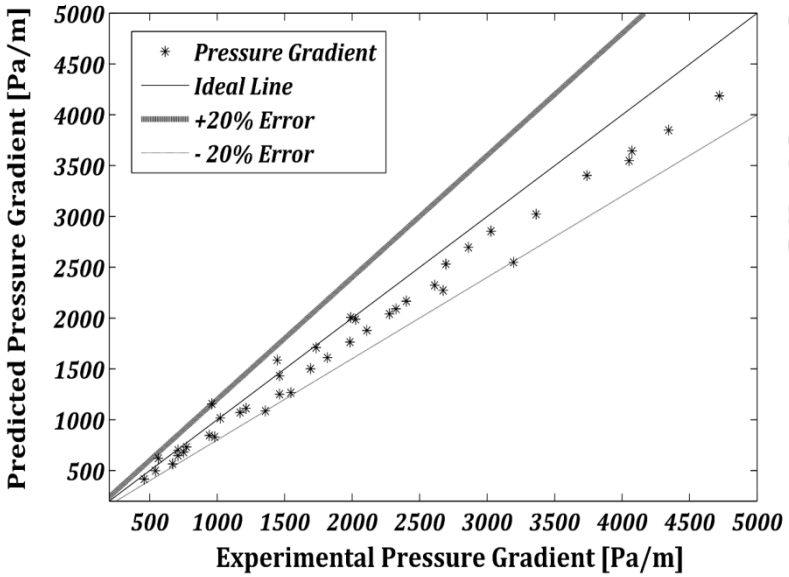

Fig. 6.24b Comparison of predicted and experimental pressure gradient of Grassi et al. (2008) for +10°inclined flow with entrainment.

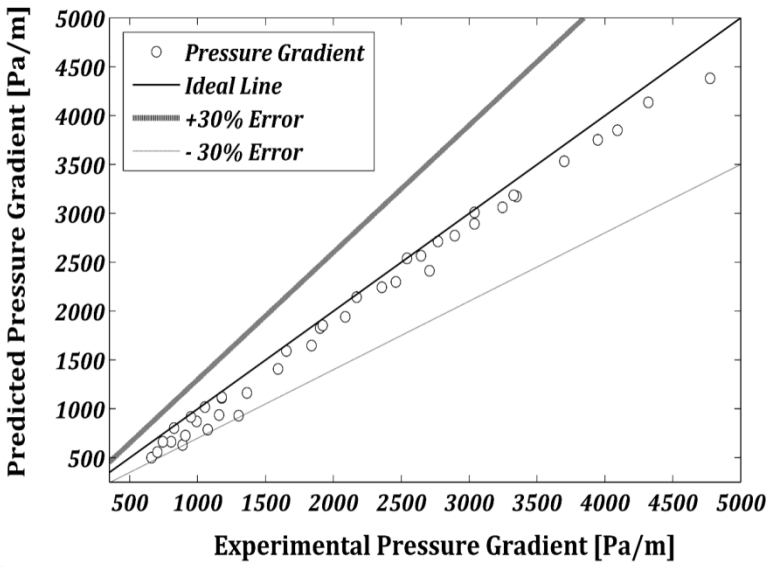

Fig. 6.25a Comparison of predicted and experimental pressure gradient of Grassi et al. (2008) for -10°inclined flow without entrainment.

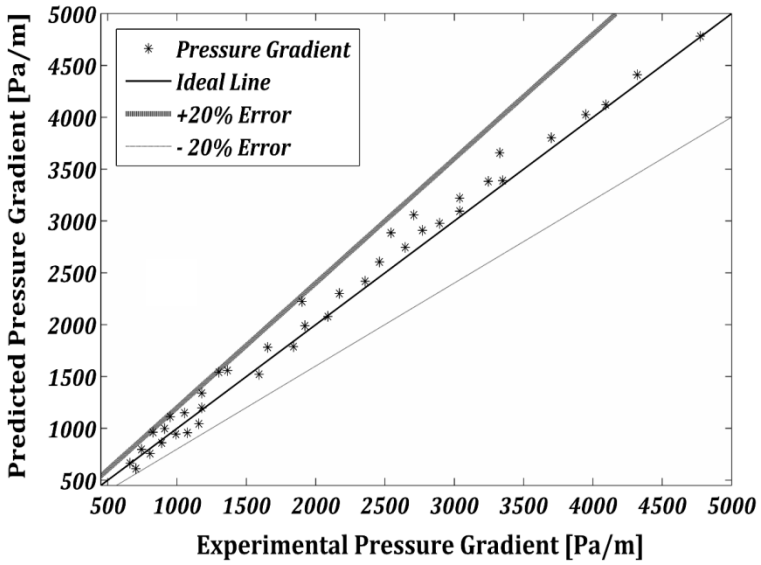

Fig. 6.25b Comparison of predicted and experimental pressure gradient of Grassi et al. (2008) for -10°inclined flow with entrainment.

6.5 Holdup prediction

The measured holdup in both horizontal and inclined pipeline has been predicted by the existing models in the literature. For this three models have been adopted such as Homogeneous flow model, Arney et al. (1993) model and Olimens (1986).

6.5.1 Homogeneous flow model

Homogeneous flow theory provides the simplest technique for the analyzing two-phase (or multi phase) flows. Suitable average properties are determined and mixture is treated as a pseudo fluid that obeys the usual equations of single phase flow. In the present study the holdup of plug, slug, dispersion of oil in water and dispersion of water in oil flow pattern have been predicted using homogeneous flow model in both the pipelines. The pressure drop has been calculated from the equation given below

$$\left(dP/dz\right) = 2f_m \frac{\rho_m U_m^2}{D} - \rho_m g \sin\theta \qquad (6.98)$$

Where the mixture velocity $U_m = U_O + U_W$ (6.99)

Mixture density $\rho_m = H_W \rho_W + (1-H_W)\rho_O$ (6.100)

Here H_W is given as $H_W = \frac{Q_W}{Q_W + Q_O}$ (6.101)

Q_W and Q_O are volumetric flow rates of water and oil

The friction factor in Eq. (6.98) is obtained as

$$f_m = \frac{16}{Re_m} \text{ for } Re_m < 2100 \qquad (6.102a)$$

$$= \frac{0.079}{Re_m^{0.25}} \text{ for } 2100 < \text{Re}_m < 2 \times 10^4 \quad (6.102b)$$

$$\text{Where } \boldsymbol{Re_m} = \frac{\rho_m U_m D}{\mu_m} \quad (6.103)$$

The mixture viscosity μ_m is calculated from Mc Adams formula given by

$$\frac{\boldsymbol{1}}{\mu_m} = \frac{\boldsymbol{x}}{\mu_O} + \frac{\boldsymbol{1\text{-}x}}{\mu_W} \quad (6.104)$$

Where x is the mass fraction of oil and μ_O, μ_W are viscosities of oil and water respectively.

The calculated values of holdup and pressure gradient of horizontal (Fig. 6.26 and Fig. 6.27) and inclined flow (Fig. 6.28 and Fig. 6.29) have been validated with experimental results. Fig. 6.26 shows that homogeneous flow model predicted holdup of plug, slug and dispersed flows in horizontal pipeline with good prediction (error %±20). The predicted results of pressure gradient are given in Fig. 6.27 which shows an average absolute error ±35%. The pressure drop of slug flow has been deviated much, plug and dispersed flows are in line with experimental results. The predicted holdup and pressure drop of inclined pipeline has been shown in Fig. 6.28 and Fig. 6.29 respectively. From the figures it is observed that the model has been predicted holdup (Fig. 6.28) of 5° upward inclined with good accuracy of ±20. The predicted pressure gradients are compared with experimental values and observed that all the data lies within the error ±25%.

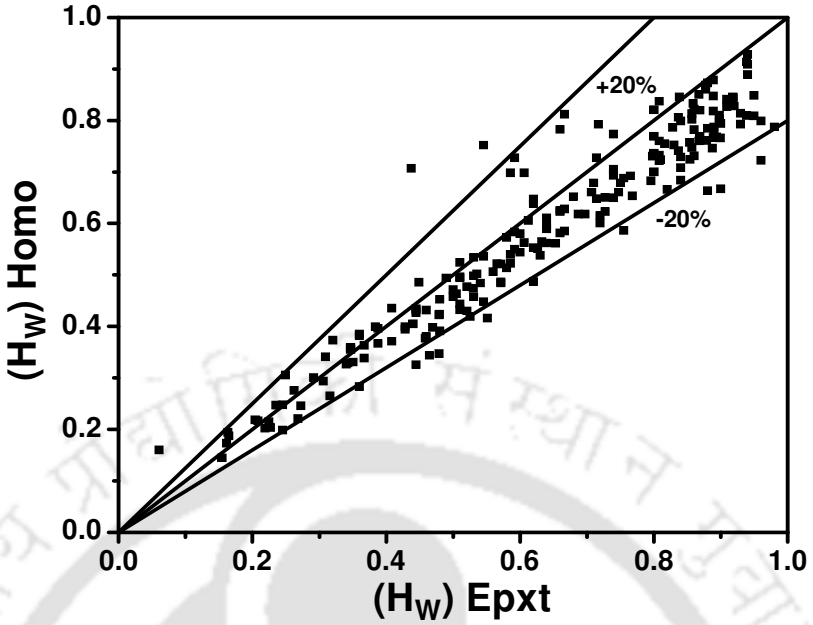

Fig. 6.26 Comparison of measured and predicted holdup in horizontal flow by homogeneous flow model

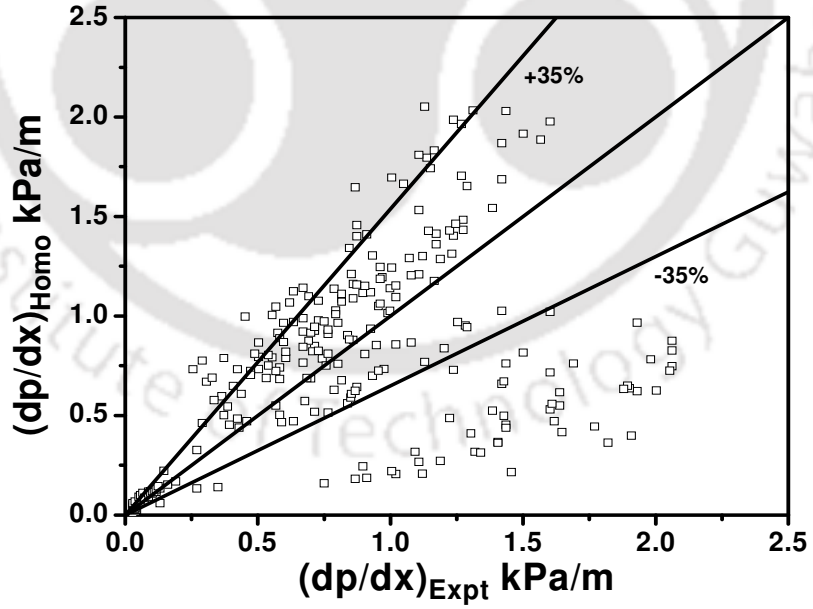

Fig. 6.27 Comparison of measured and predicted pressure gradient in horizontal flow by homogeneous flow model

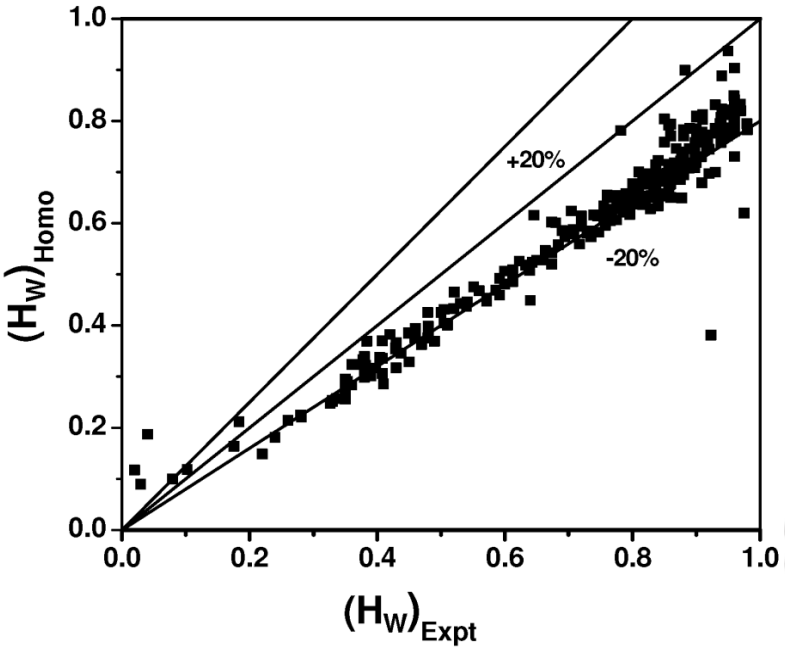

Fig. 6.28 Comparison of measured and predicted holdup in inclined flow by homogeneous flow model

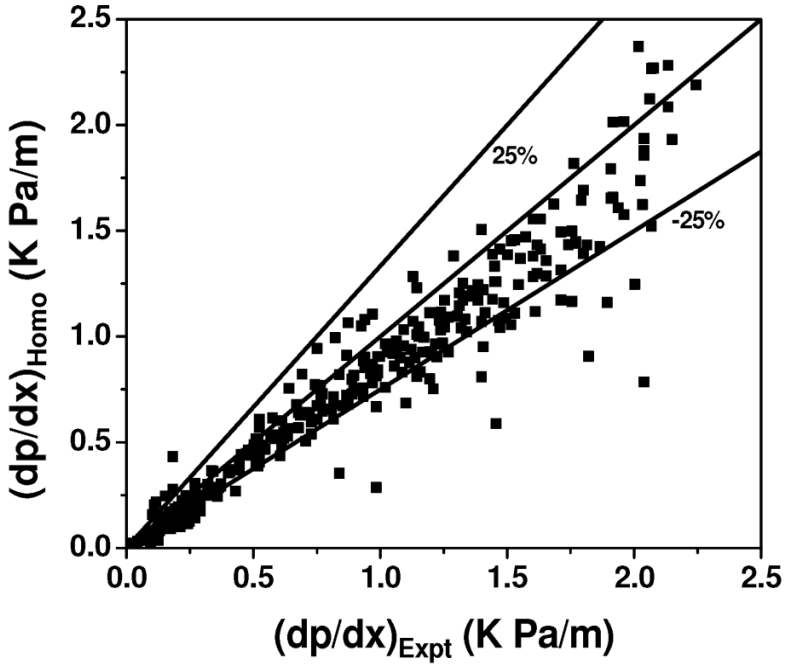

Fig. 6.29 Comparison of measured and predicted pressure gradient in inclined flow by homogeneous flow model

6.5.2 Arney et al. (1993) model

The experimental pressure gradient values of annular and wavy stratified flow in both the pipelines have been predicted by using Arney et al. (1993) model, which is developed by considering turbulence at the interface. The friction factor suggested by the model is as follows $\lambda_W = \frac{0.316}{Re_{Arney}^{0.25}}$ (6.105)

The modified Reynolds number Re_{Arney} is defined as

$$Re_{Arney} = \frac{\rho_c D u_m}{\mu_m}\left[1+\eta^4\left(\frac{\mu_W}{\mu_O}-1\right)\right] \quad (6.106)$$

Where u_m is the mixture superficial velocity ($u_m = u_W + u_O$) and ρ_c is the average mixture density defined as

$$\rho_c = \left(1-\eta^2\right)\rho_W + \eta^2\rho_O \quad (6.107)$$

$$\eta = \sqrt{1-H_W} \quad (6.108)$$

To calculate average density holdup data is required in the same work Arney et al. (1993) proposed a correlation to calculate determine water holdup H_W is provided

$$H_W = C_W\left[1+0.35\left(1-C_W\right)\right] \quad (6.109)$$

Where C_W is input water cut calculated as $C_W = \left(U_{SW}/U_{SW}+U_{SO}\right)$ (6.110)

Where the pressure gradient is computed as

$$\left(dP/dz\right)_{Arney} = \frac{\lambda_{Arney}\rho_c u_m^2}{2D} \qquad (6.111)$$

For each comparison the H_W value has been calculated from the correlation given in Eq. (6.109).

Holdup and pressure drop of horizontal pipeline have been predicted using the above mentioned model and the results are given in Fig. 6.30 and Fig. 6.31 respectively.

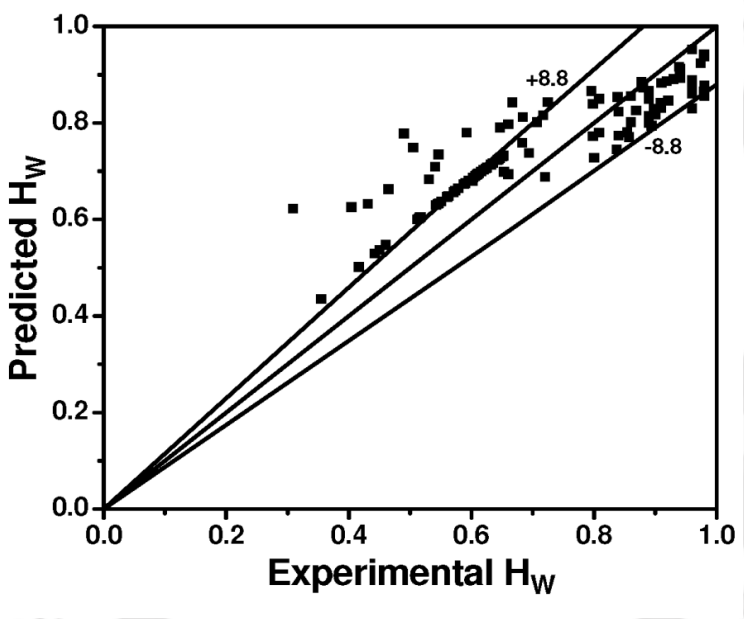

Fig. 6.30 Comparison of measured and predicted holdup in horizontal flow by Arney et al. (1993) model

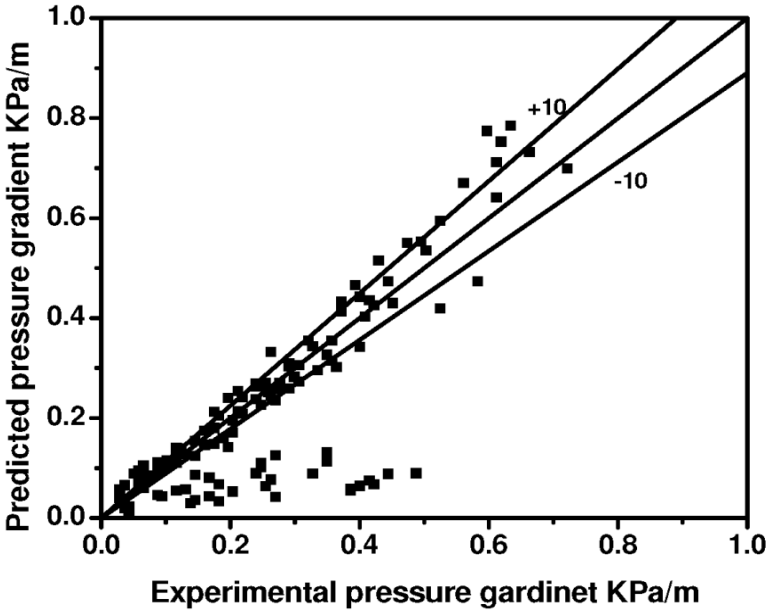

Fig. 6.31 Comparison of measured and predicted pressure gradient in horizontal flow by Arney et al. (1993) flow model

Arney et al. (1993) model has been predicted the holdup of annular and stratified wavy flow pattern with very good accuracy in prediction. All the predicted results are within the average absolute error of ±8.8%. The model has also predicted the pressure gradient data with an average absolute error of ±10%.

The holdup and pressure drop of 5° upward inclined pipeline has also been predicted using Arney et al. (1993) model and the predicted results are shown in Fig. 6.32 and Fig. 6.33 respectively. The predicted holdup of annular and wavy stratified flow is in line with the experimental results with very less error of ±10%. The predicted pressure gradient data are in good agreement with the experimental results within the error of ±20%. Arney et al. (1993) model has been proposed only for annular flow but in this study an attempt has

been made to predict pressure gradient of both annular and wavy stratified flow and observed good prediction with less error in both the systems.

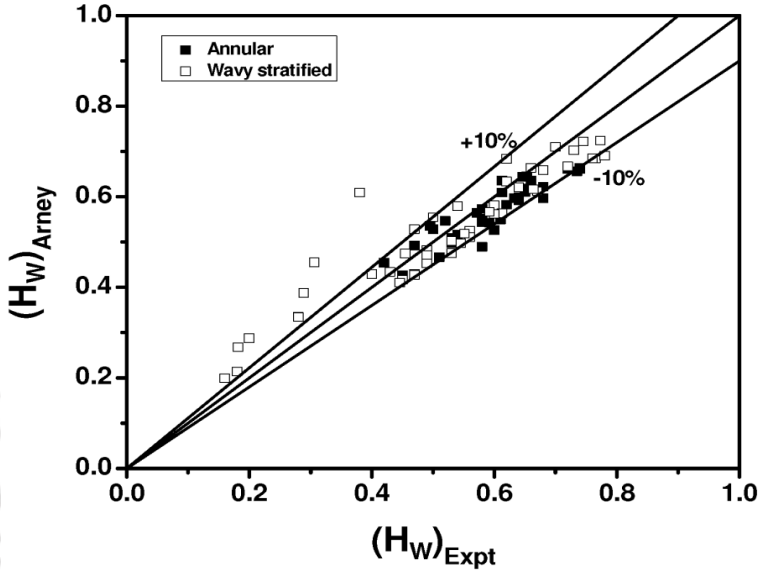

Fig. 6.32 Comparison of measured and predicted holdup in inclined by Arney et al. (1993) model

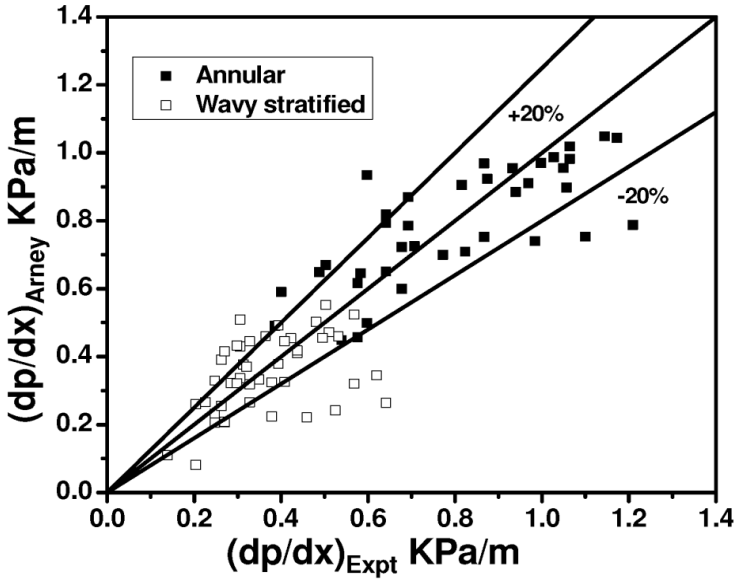

Fig. 6.33 Comparison of measured and predicted pressure gradient in inclined flow by Arney et al. (1993) flow model

6.5.3 Oliemans (1986) model

The correlation proposed by Oliemans (1986) to predict water hold up is used here to predict hold up of all the flow patterns which is as follows

$$H_W = C_W\left[1+0.2\left(1-C_W\right)^5\right] \tag{6.112}$$

The holdup data calculated from the above equation for all the flow patterns has been used in the homogeneous flow model (Eq.6.98, 6.100, 6.102a, 6.102b) to calculate pressure drop of both horizontal and inclined flow. The predicted results of holdup and pressure gradient of horizontal flow are depleted in Fig. 6.34 and Fig. 6.35 respectively. Fig. 6.34 shows that all the predicted results are matched well with experimental results within the average error of ±21.2%.

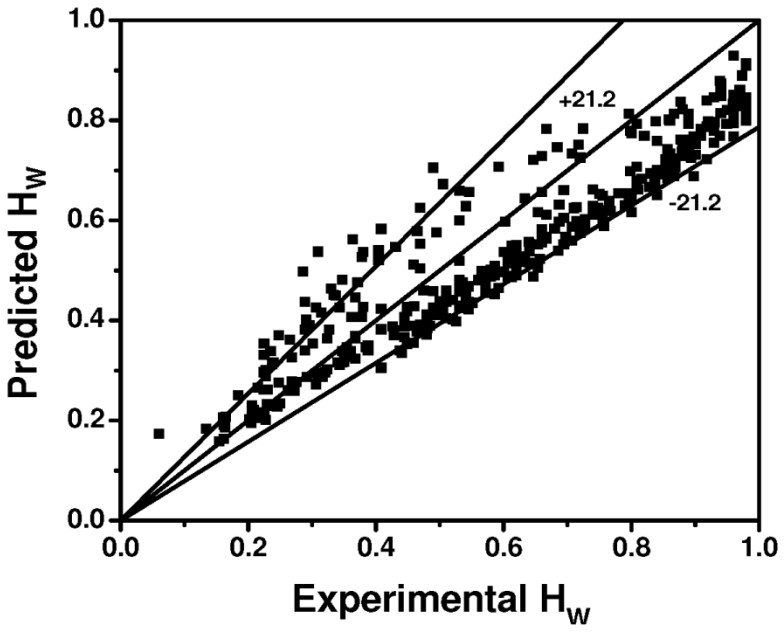

Fig. 6.34 Comparison of measured and predicted holdup in horizontal flow by Olinemans (1986) model

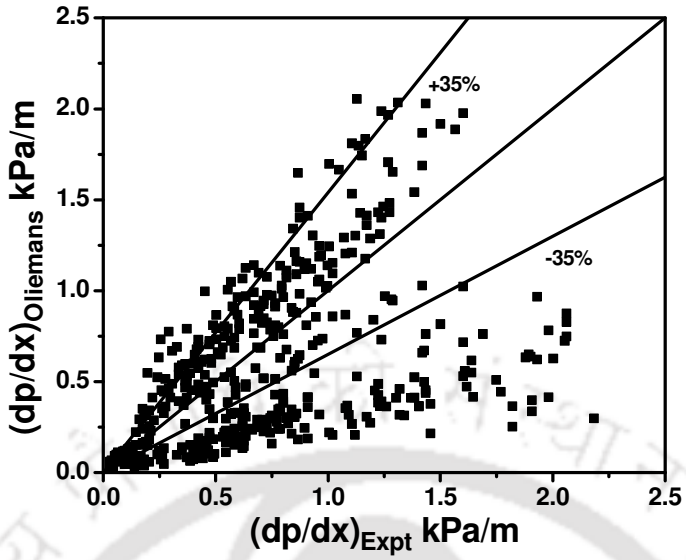

Fig. 6.35 Comparison of measured and predicted pressure gradient in horizontal flow by Oliemans (1986) flow model

The measured holdup values have been use in homogeneous flow model to predict pressure drop of all the flow patterns as shown in Fig. 6.35. It shows the model has given absolute average error of ±35%. Stratified mixed flow pattern pressure drop has been varied much with the experimental values this may be due to homogeneous flow is meant only for single phase flows.

The predicted holdup and pressure drop of 5° upward inclined pipeline using the above model has been given in Fig. 6.36 and Fig. 6.37 respectively. Oliemans (1986) model has been predicted the holdup of all the flow patterns with good accuracy in prediction. All the predicted results are within ±25% error. The predicted pressure gradient of inclined pipeline is in good agreement with the experimental results with the error of ±22% for all the flow patterns. Incorporation of Oliemans (1986) holdup into homogeneous flow model has shown improvement in prediction.

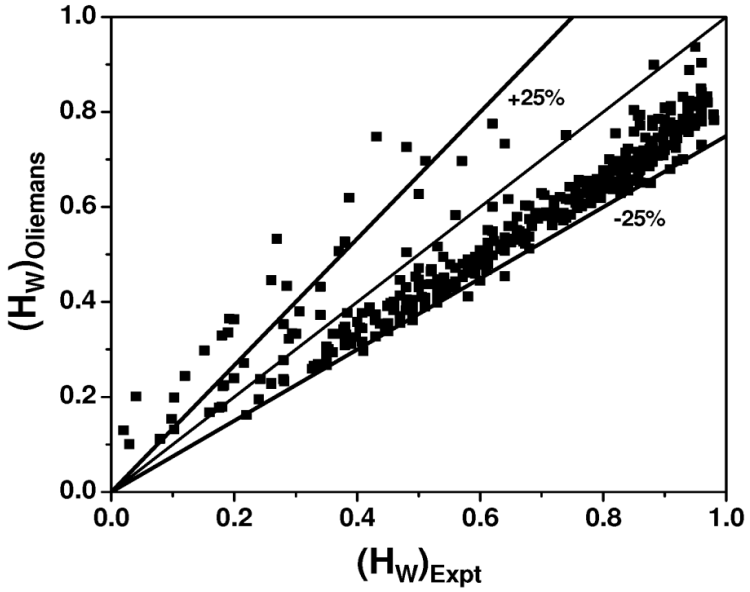

Fig. 6.36 Comparison of measured and predicted holdup in inclined flow by Olinemans (1986) model

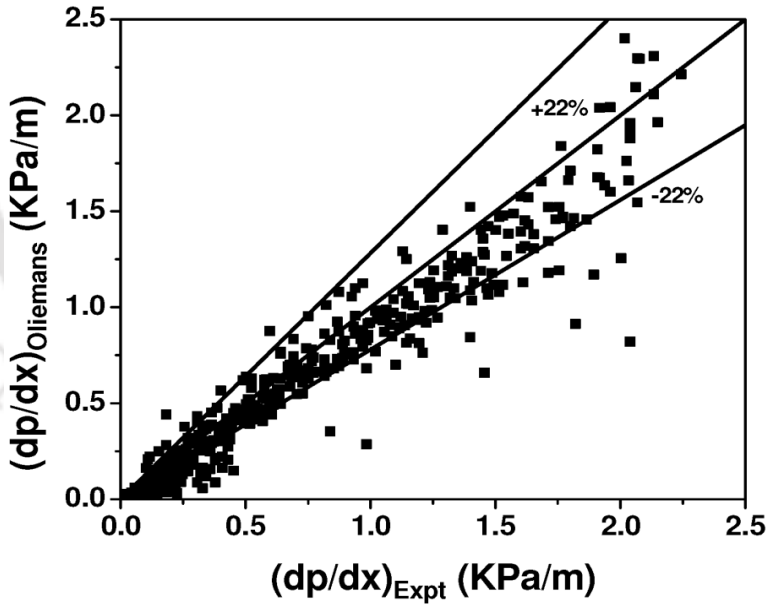

Fig. 6.37 Comparison of measured and predicted pressure gradient in inclined flow by Oliemans (1986) flow model

6.6 Conclusions

The holdup and pressure drop of horizontal and 5° upward inclined pipeline have been measured experimentally. The measure pressure drop in horizontal pipeline has been predicted using correlations available in the literature. The existing correlations give poor prediction for liquid-liquid flow. Then two correlations are developed to predict pressure drop for liquid-liquid horizontal and $+5^{\circ}$ inclined flow by following Lockhart-Martinelli approach and dimensionless analysis. Modified Lockhart-Martinelli correlation has been predicted the horizontal pressure gradient within the error of 22% where as correlation obtained from dimensional analysis gives better prediction (17.9%). In inclined pipeline dimensional analysis has given good prediction of 4.9% than modified Lockhart-Martinelli correlation (6.6%). A model has been developed to predict pressure drop of annular flow by incorporating entrainment of either phases for horizontal and inclined pipeline flow. The developed model has shown notable improvement in prediction of pressure drop in both the cases. The prediction accuracy in horizontal and inclined flow has been increased to 5% and 10% respectively. This entrainment model is validated with the present experimental results and other literature data. Holdup of horizontal and inclined pipes is predicted by the existing models with good precision.

Chapter 7

Numerical simulation of flow patterns in inclined pipeline

7.1 Introduction

Past literature (Chapter 2) shows that analytical, theoretical and numerical methods (CFD simulations) are used to predict flow patterns and its transition boundaries. In present work (Chapter 5), PNN technique gives the better prediction than the analytical models but it cannot explain the physics of the flow phenomena. Due to this reason numerical simulation technique has been adopted further to predict the flow patterns. The literature shows that there are few works on the prediction of flow patterns in horizontal pipeline by CFD. It is also noted that CFD simulation of flow patterns of inclined two-phase flow is not available in literature (Chapter 2). So, the flow patterns of viscous oil-water flow through inclined pipeline have been numerically simulated using ANSYS FLUENT^{TM} 6.2. For this Volume of Fluid (VOF) method has been employed to predict various flow patterns by assuming unsteady flow, immiscible liquid pair (viscous oil and water), constant liquid properties, and co-axial flow. Five flow patterns (plug flow, slug flow, wavy stratified flow, stratified mixed flow and annular flow) have been predicted using CFD simulation in upward inclined pipe line. The simulation results have been validated with experimental results. The results give good proximity with the experimental data (Chapter 4).

Numerical analysis

CFD is a study where governing equations are solved numerically by some iterative approach and the parameter values obtained at the end of the computational process are taken as final results, provided they satisfy a desired tolerance criterion. All the details regarding the selection of models and solution methodology are clearly given in Fluent manual (2006). The same is summarized here to get an idea regarding the analysis.

7.2 Finite Volume Method

There are many approaches available when particular CFD simulations are carried out. There are three main methods mainly used in simulations such as Finite Difference Method (FDM), Finite Element Method (FEM) and Finite Volume Method (FVM). Among these three methods Finite volume method has been selected in the present study. This is a numerical method which works based on the integral conservation laws. It is used for solving partial differential equations that calculates the values of the conserved variables averaged across the volume. The integral conservation law is enforced for small control volumes defined by the computational mesh. One advantage of FVM over FDMs is that it does not require a structured mesh (although a structured mesh can also be used). Furthermore, FVM is preferable to other methods as a result of the fact that boundary conditions can be applied non-invasively. This is true because the values of the conserved variables are located within the volume element, and not at nodes or surfaces. FVMs are especially powerful on coarse, non-uniform grids and in calculations where the mesh moves to track interfaces or shocks.

FVMs are extensively used in fluid mechanics and many other engineering areas governed by conservative systems that can be written in integral control volume form. The primary advantages of these methods are numerical robustness, applicability on very general unstructured meshes, and the intrinsic local conservation properties of the resulting schemes. To use FVM concrete choice of control volumes, type of approximation inside them and numerical methods for evaluation of integrals and fluxes are required to be chosen carefully in advance. This method (Based on the control volume formulation of analytical fluid dynamics) involves simple steps as described briefly.

i. In FVM, computational domain is first tessellated into a collection of non-overlapping control volumes that completely cover the domain i.e. to divide the domain into a number of control volumes where the variable of interest is located at the centroid of the control volume. The control volumes are divided in to two categories: cell-centered and vertex-centered control volume. In the cell-centered finite volume method shown, the triangles themselves serve as control volumes with solution unknowns (degrees of freedom) stored on a per triangle basis. In the vertex centered finite volume method, control volumes are formed as a geometric dual to the triangle complex and solution unknowns stored on a per triangulation vertex basis.

ii. Integrates the differential form of the governing equations (very similar to the control volume approach) over each control volume.

iii. Interpolation profiles are then assumed in order to describe the variation of the concerned variable between cell centroids. The resulting equation is called the

discretized or discretization equation. In this manner, the discretization equation expresses the conservation principle for the variable inside the control volume.

The most compelling feature of the FVM is that the resulting solution satisfies the conservation of quantities such as mass, momentum, energy, and species. This is exactly satisfied for any control volume as well as for the whole computational domain and for any number of control volumes. Even a coarse grid solution exhibits exact integral balances. Since FVMs are conservative they automatically satisfy the jump conditions and hence give physically correct weak solutions.

7.3 Volume of Fluid (VOF) Method

In the present study Volume of fluid (VOF) technique has been selected which is control volume based technique with suitable discretization schemes for each equation. The VOF model can model two or more immiscible fluids by solving a single set of momentum equations and tracking the volume fraction of each of the fluids throughout the domain. Typical applications include the prediction of jet breakup, the motion of large bubbles in a liquid, the motion of liquid after a dam break, and the steady or transient tracking of any liquid-gas interface. There are some limitations of VOF model such as

i. VOF must used with the pressure-based solver. The VOF model is not available with either of the density-based solvers.
ii. All control volumes must be filled with either a single fluid phase or a combination of phases, it does not allow for void regions where no fluid of any type is present.
iii. The second-order implicit time-stepping formulation cannot be used with the VOF explicit scheme.

In the present study VOF method has been employed as this method proves to be beneficial for the computation in terms of accounting for the interfacial interactions very effectively.

7.3.1 Governing equations

Modeling of multiphase flow needs special attention due to the presence of number of phases, time, space variant interfaces, multiple scales and large number of interacting phenomena. Considering the hydrodynamics of liquid-liquid flow VOF technique for two-phase flow modeling available in FLUENT has been selected for this case. VOF method solves a single set of momentum equations for both the phases. The details of the governing equations can be obtained from the FLUENT users guide.

Continuity:

$$\frac{\partial(\rho)}{\partial t}+\nabla.(\rho U)=\sum_{q}S_{q} \tag{7.1}$$

Where, ρ, U, t, S and q are density, velocity, time and mass source of q^{th} phase respectively. In the present case the source term, S is zero.

Momentum:

A single momentum equation sis solved throughout the domain and the resulting velocity field is shared among the phases. It can be written as

$$\frac{\partial(\rho U)}{\partial t}+\nabla.(\rho U.U)=-\nabla P+\nabla.\left[\mu\left(\nabla U+\nabla U^{T}\right)\right]+(\rho g)+F \tag{7.2}$$

Where P, g, F, μ are pressure in the flow field, acceleration due to gravity, body force acting on the system and viscosity of the flowing fluid, respectively.

7.3.2 Secondary phase tracking

The VOF method calculates the volume fraction of each liquid in each cell throughout the domain. In each control volume, the fraction of all the phases sum up to unity. In this method all variables and physical properties are shared by each fluid. Since volume fraction of each phase is known at each location the physical properties of phases are represented by volume averaged values. The presence of either of phases or mixture of them can be traced depending upon these properties and the volume fraction values. In another way, if the volume fraction of q^{th} in the cell is denoted as α_q, then the probable situations are

- $\alpha_q = 0$: the cell does not contain any fluid q.
- $\alpha_q = 1$: the cell is occupied solely by fluid q.
- $0 < \alpha_q < 1$: the cell contains the interface

Based on the local volume fraction in each cell the appropriate variables and properties are calculated in each control volume within the computational domain. The density and viscosity used in Eq. 7.1 and 7.2 are estimated as

$$\rho = \sum_{1}^{p} \rho_q \alpha_q \tag{7.3}$$

$$\mu = \sum_{1}^{p} \mu_q \alpha_q \tag{7.4}$$

A separate continuity equation for α_q is considered as follows

$$\frac{\partial \alpha_q}{\partial t} + \left(U_q . \nabla\right) = S_{\alpha q} \tag{7.5}$$

For each cell the following relation is also valid

$$\Sigma_1^p \alpha_q = 1 \tag{7.6}$$

Here p is the number of phases, in case of two-phase flow $p = 2$.

7.3.3 Interface treatment

VOF model makes use of a piecewise-linear approach to construct interface between two fluids. It assumes that the interface between the two fluids has linear slop within each cell. Based on the information about the volume fraction and it derivatives in the cell it calculates the position of linear interface relative to the center of each partially filled cell is calculated as a first step of interface reconstruction. After that the advection amount of fluid though each face is calculated using the computed linear interface representation, and information on the normal and tangential velocity distribution on the face. By balancing the fluxes in the previous step the volume fraction of each cell is attained.

7.3.4 Surface tension and wall adhesion

The VOF model accounts the surface tension along the interface between the phases. The surface tension model uses the continuum surface force (CSF) model (Brackbill (1992)). In this model surface tension effect is added in the momentum equation with the pressure drop, where the pressure drop is calculated from the surface tension coefficient σ' and the surface curvature (through radii R_1 and R_2) by the Young Laplace equation as follows:

$$\Delta P = \sigma\left(\frac{1}{R_1} + \frac{1}{R_2}\right) \tag{7.7}$$

ΔP is the pressure drop of two fluids on either side of the interface.

7.4 Numerical Simulation

The flow domain has been constructed and meshed in GAMBIT^{TM} and the solver chosen is ANSYS FLUENT^{TM}. The geometry consists of a +5° upward inclined pipeline with internal diameter of 0.025 m and material of construction used for the pipe is Perspex. The dimensions of the geometry have been shown in Fig. 7.1. Oil and water were introduced into the pipe through a T- junction at the entry section where water and oil enter into the pipe from the horizontal and vertical directions, respectively. The geometry of the system can be assumed to consist of four sections-water inlet, oil inlet, outlet of the pipe and the test section. An immiscible pair of liquids is chosen with coaxial flow assumed. An unsteady state solver has been employed for the computation purpose. Further, the simulations are run in 2-Dimensional geometry.

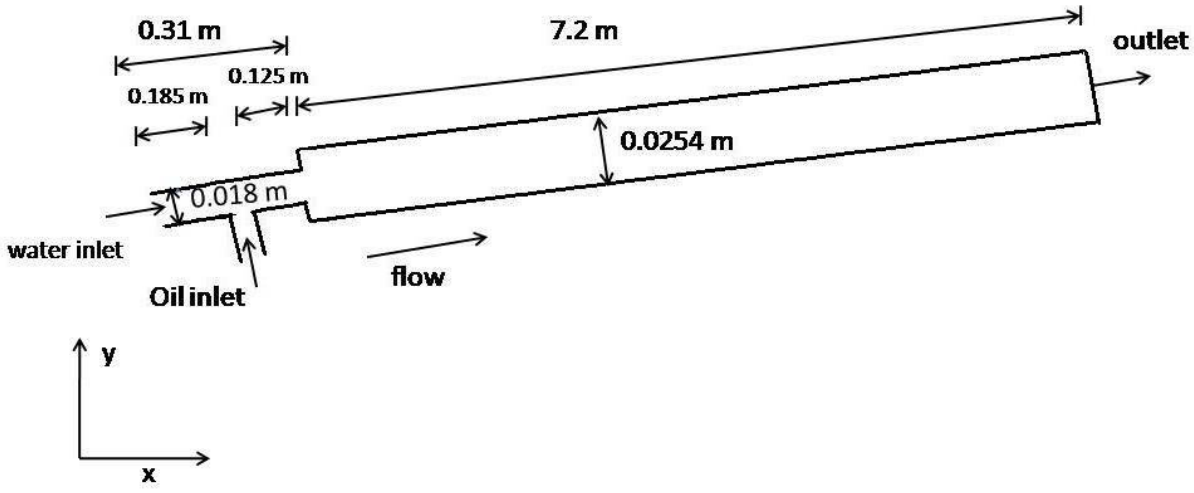

Fig. 7.1 Schematic of flow domain and dimensions

7.4.1 Meshing of the model

The meshing of the 2D geometry has been done using GAMBIT software. Fig. 7.2 shows the meshed geometry of the pipe line. Quadrilateral meshing scheme has been selected to account the surface tension effect more precisely. In order to capture the hydrodynamics at the interface the numbers of girds are higher at the interface than the film area.

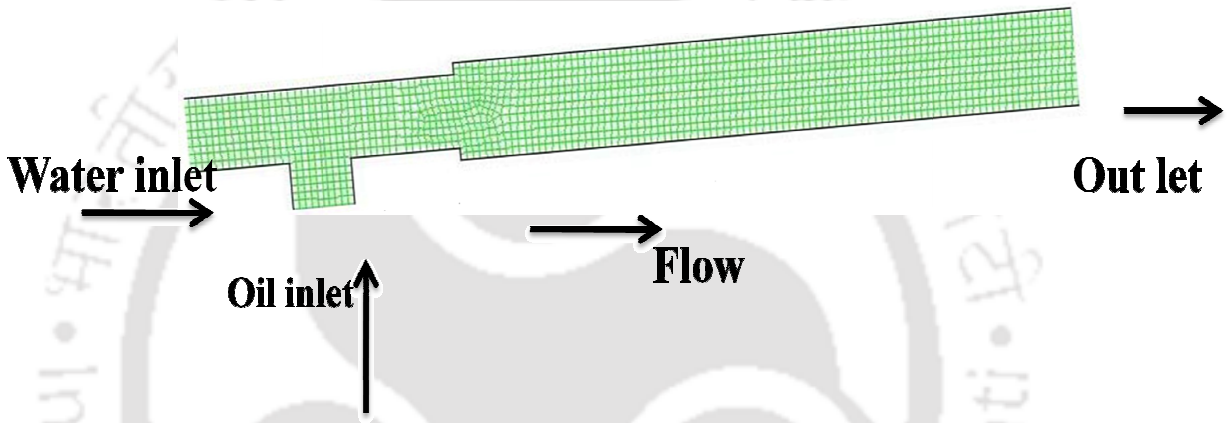

Fig. 7.2 Meshed form of flow domain

7.4.2 Initial and boundary conditions

❖ **Initial condition**

In all the cases the flow has been initialized by filling the pipe with water from the water inlet at a particular superficial velocity and then oil has been introduced into the pipe.

❖ **Inlet boundary conditions**

The oil velocity is specified at the oil inlet and water velocity at water inlet in the entry section. Thus considering the uniform velocity distribution the velocity conditions are:

- At x=0, y=0;

  $U_x = U_{water}$ and $U_y = 0$

- At x = 0.185 m and y = –0.08 m,

  $U_y = U_{oil}$ and $U_x = 0$

❖ **Wall boundary conditions**

A stationary no slip, no penetration boundary condition is imposed on the pipe wall. In addition the contact angle has been provided during the simulation is 8.45° to account the wall wetting behavior of the fluids with pipe wall.

❖ **Outlet boundary conditions**

At the outlet of the pipe pressure outlet condition has been selected and the diffusion flux for the variables are set at zero.

7.4.3 Discretization methods

Two-phase flow is dynamic in nature due to this variation of flow phenomena both in time and space has been considered in the simulations. A transient simulation has been conducted with a time step of 0.001 s. continuity equation has been discretized by PRESTO algorithm (Patankar (1980)) while the momentum equations are discretized by first order upwind method. For pressure velocity coupling PISO (Issa (1986)) algorithm has been used.

7.4.4 Solution Methodology

Both the phases are introduced at their respective inlets and the transient simulation has been started. The superficial velocities of both oil and water are corresponding to the given

experimental conditions have been set as inlet conditions. Then all the above mentioned equations are solved in Fluent by VOF method. The equations are first converted into algebraic forms which are then solved numerically. Unsteady state and pressure based solver are employed in this case. The time step used in the following computations is 0.001s. The equations are integrated over the control volume and the parameters (pressure and velocity) are conserved by solving the momentum and continuity equations using the PISO pressure-velocity coupling scheme. The continuity equations have been discretized using PRESTO algorithm while the momentum equations make use of a first order upwind discretization scheme. For the interface, VOF uses the Geometric Reconstruct interpolation scheme. After few time steps, the flow of both the phases has been identified to track the formation of flow patterns.

7.5 Simulation Results

7.5.1 Grid independent study

A grid independent study has been conducted with three computational grids of 12,853, 46955, 61, 109 cells to select the optimum grid size for the computational simulations. Simulations are conducted for one case study in all the mesh elements mentioned above at U_{SW} = 0.06 m/s; U_{SO} = 0.14 m/s (wavy stratified flow pattern). The volume fraction contours of simulated results for all the mesh elements have been shown in Fig. 7.3a, b and c respectively. The red colored portion in all the figures represents oil phase and blue portion is water. As shown in Fig. 7.3a the mesh with 12,853 cells is poor in predicting the wavy stratified flow pattern so extra number of cells is tested at the same flow conditions. Fortunately, systems with 46,955 and 61,109 cells have been given the same

volume fraction of oil and water at this flow conditions. Therefore based on the volume fraction contour results 46,955 cells have been selected as optimum number of cells simulation. The mesh consists of 2707 and 44248 quadrilateral mesh elements on the entry section and the pipe line respectively has been selected for the present study.

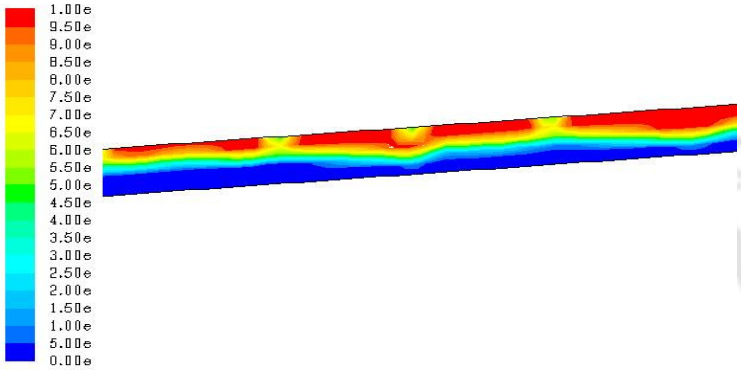

a) 12,853Mesh elements

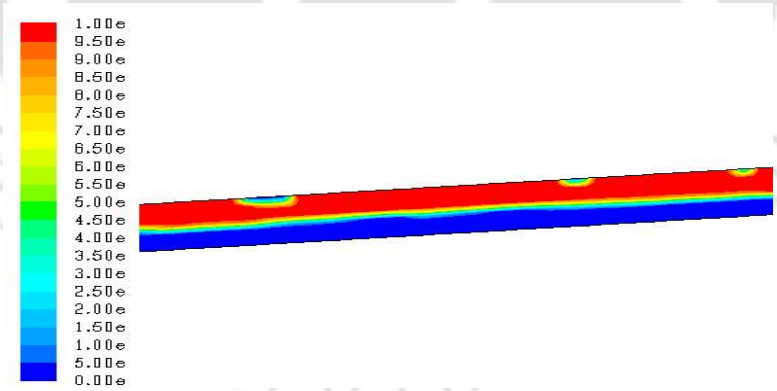

b) 46,955 Mesh elements

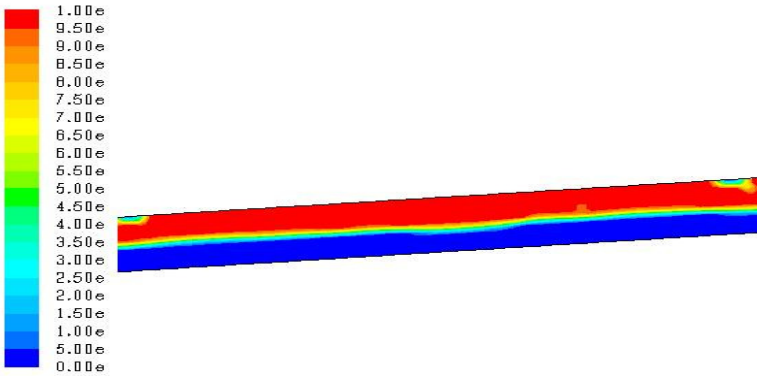

c) 61,109 Mesh elements

Fig. 7.3 Volume fraction contours of oil and water at U_{SW} = 0.06 m/s; U_{SO} = 0.14 m/s

7.5.2 Prediction of flow patterns

Simulations have been performed by taking various data points in the flow pattern map of inclined pipe line given in Chapter 6, for five different flow patterns namely plug, slug, wavy stratified, stratified mixed and annular flow. The simulated results for all the five flow patterns are discussed below.

a. Prediction of plug flow

Simulations have been performed to identify plug flow regime in the range of superficial velocities traced from the flow pattern map (Chapter 4, Fig. 4.4). The results obtained from the CFD simulation and experimental results have been compared here for a pair of superficial velocities of both the fluids. In all the figures volume fraction contours have been shown for the better understanding of the interfacial morphology of oil and water. Fig. 7.4a and Fig. 7.4b shows the comparison of predicted flow patterns with experimental observations at same flow conditions, which show good agreement with experimental

results. At lower phase superficial velocities the length of liquid bride between the two consecutive plugs is long, as the velocity increase the length of the liquid bridge decreases and number of oil plugs increases. The size of the oil plugs generally increases with rise in oil velocity such divergence has also been accounted by VOF model, which can be known from the Fig. 7.4a and Fig. 7.4b.

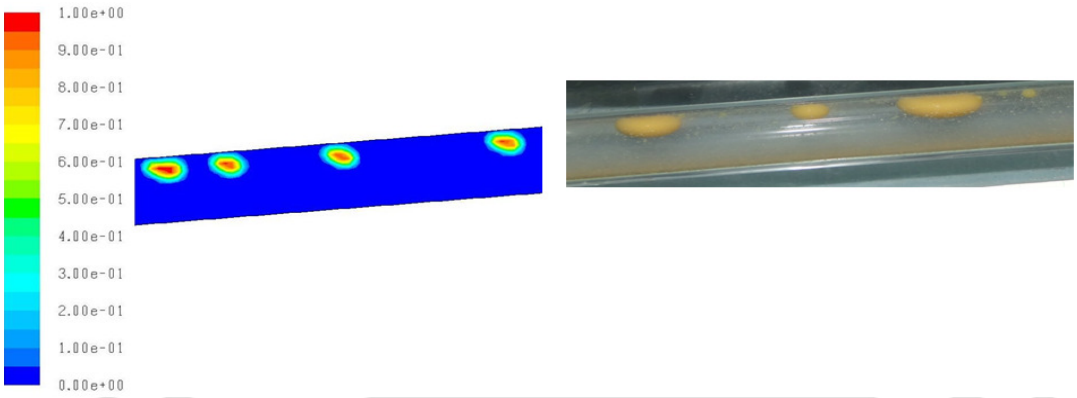

a) U_{SO} =0.025 m/s and U_{SW} = 0.27 m/s

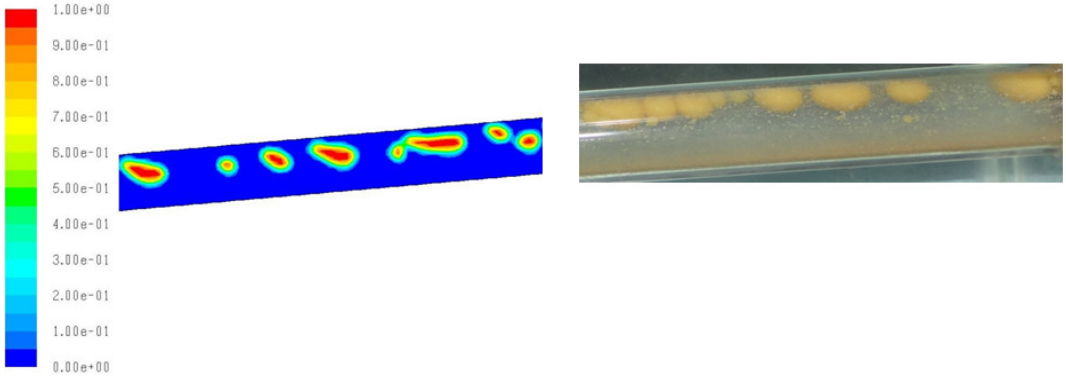

b) U_{SO} = 0.1 m/s and U_{SW} = 0.373 m/s

Fig.7.4 Comparison of plug flow results: simulated and experimental

b. Prediction of slug flow

Simulations have been carried out in the whole range of slug flow identified in the experimental study and the results of two cases are given here. Fig. 7.5a and Fig. 7.5b gives the simulated result and photograph slug flow pattern at U_{SO}= 0 .046 m/s, U_{SW} = 0.17 m/s and U_{SO}= 0.1 m/s U_{SW} = 0.237m/s. The simulated results are in line with the experimental results of the slug flow pattern. From the figures (Fig. 7.5a and Fig. 7.5b) it is observed that the length of the oil slug has been increased with enhancement in oil velocity. In the present simulation this effect is clearly predicted.

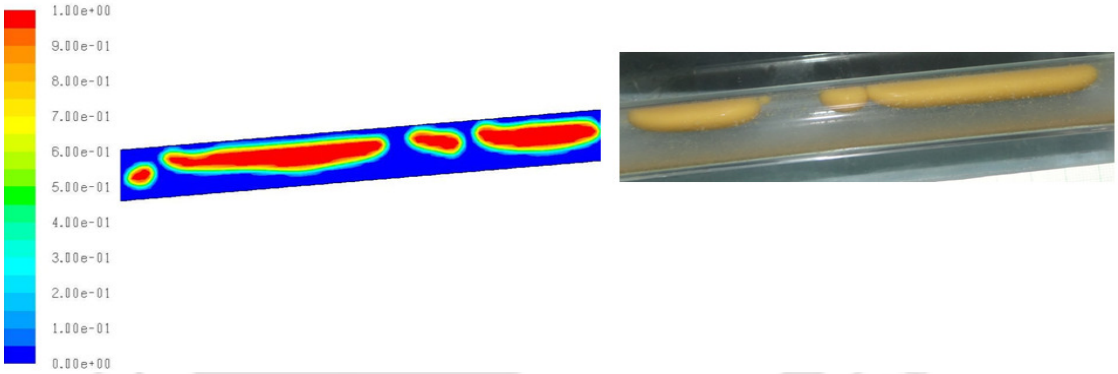

a) U_{SO}= 0 .046 m/s and U_{SW} = 0.17 m/s

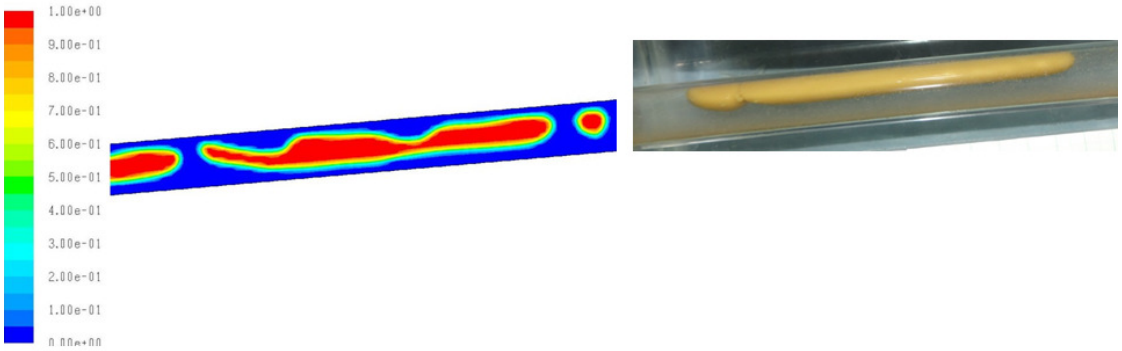

b) U_{SO}= 0.1 m/s and U_{SW} = 0.237m/s

Fig. 7.5 Comparison of slug flow results: simulated and experimental

c. Prediction of wavy stratified flow

Wavy stratified flow pattern has been predicted from the simulations conducted in the range of superficial velocities of the flow pattern noticed from the experiment (Chapter 4) and here presenting two case studies (U_{SO} = 0 .13 m/s, U_{SW} = 0.1 m/s and U_{SO} = 0.1 m/s U_{SW} = 0.17 m/s) for the comparison. The simulated results at these buoyancy conditions have been validated with the experimental results (images of interfacial morphology) at the same flow conditions as shown in Fig. 7.6a and b. The result shows that VOF methodology successfully predicted the wavy stratified flow pattern with clear interface with waviness. The amplitude of the waves at the interface increases with enhancement in mixture velocity which is manifestly reflected from the simulated results. This describes that VOF method is capable of predicting this sensitive nature of wave behavior at the interface.

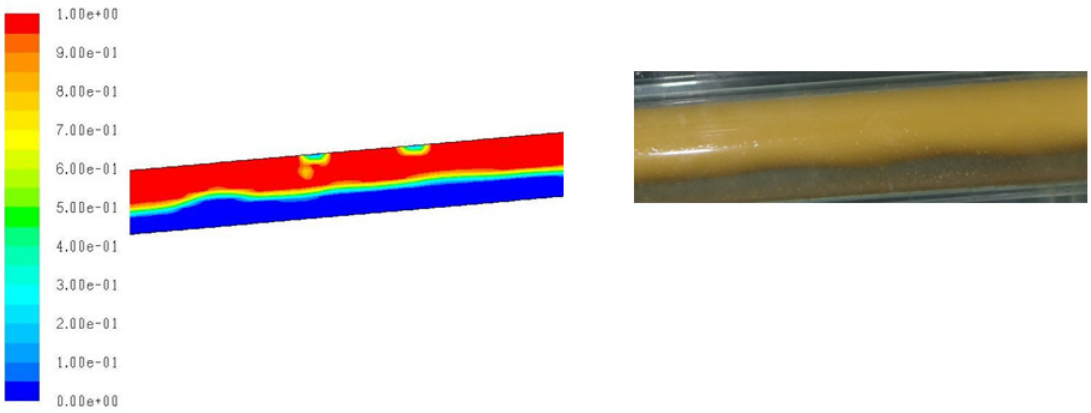

a) U_{SO} = 0 .13 m/s and U_{SW} = 0.1 m/s

b) U_{SO} = 0.1 m/s and U_{SW} = 0.17 m/s

Fig. 7.6 Comparison of wavy stratified flow results: simulated and experimental

d. Prediction of stratified mixed flow

Stratified mixed flow pattern recognized in the experimental range (U_{SW} = 0.067-0.44m/s to U_{SO}= 0.15-0.63 m/s) as given in Chapter 4 has been simulated to predict this flow pattern. The simulated results have been compared with the experimental photographs at same flow conditions in Fig. 7.7a and b. The morphology acquired in both the cases is similar to the experimental results. The stratified mixed flow regime has been predicted very well with stratification of phases and oil drops at the interface by VOF method. Fig.

7.7b reveals that with increase in mixture superficial velocity the number of oil droplets at the interface has been enhanced. This is also properly encountered by VOF technique in predicting stratified mixed flow patter.

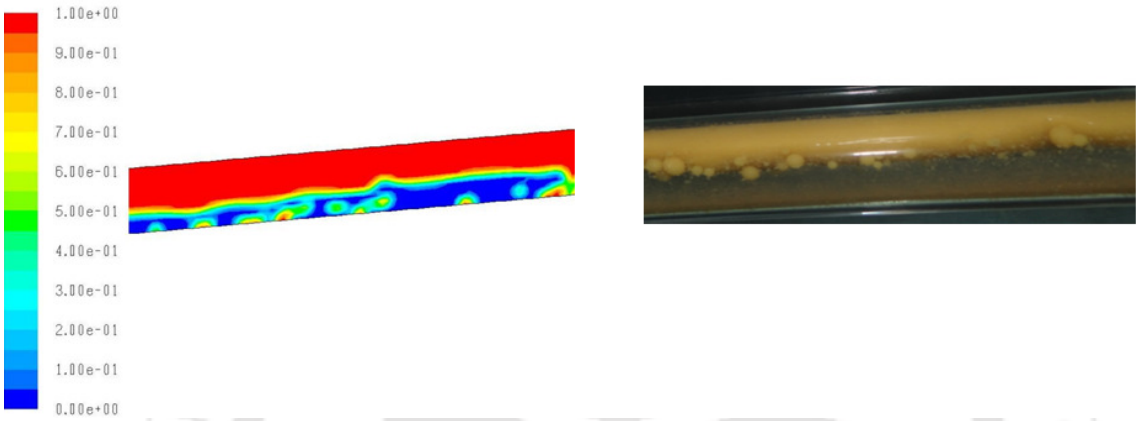

a) U_{SO} =0.37 m/s and U_{SW} = 0.23 m/s

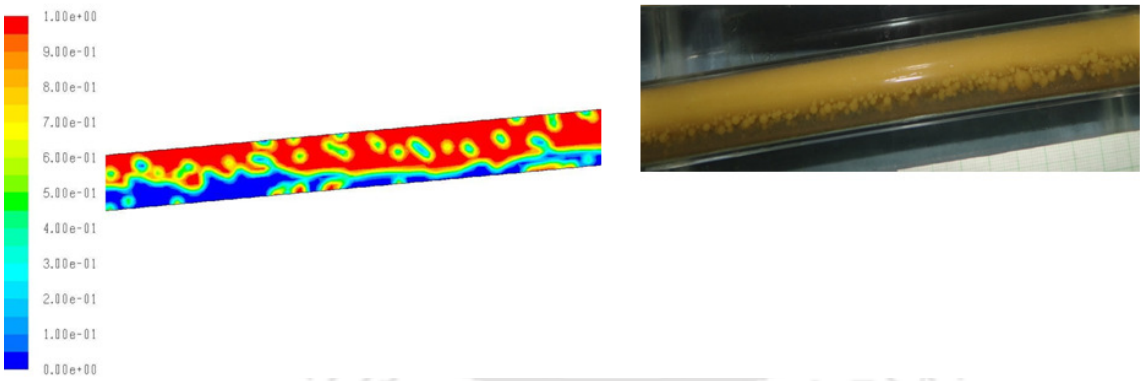

b) U_{SO} =0.468 m/s and U_{SW} = 0.17 m/s

Fig. 7.7 Comparison of stratified mixed flow results: simulated and experimental

e. Prediction of annular flow

Annular flow pattern has been occupied a small region in the experimental flow pattern map as shown in Fig. 4.4. Simulations have been carried out to predict annular flow pattern and the results are depleted in Fig. 7.8a and b for pair of mixture velocities. Comparison of

both experimental and simulation results at same flow conditions shows good prediction of annular flow pattern with VOF technique. Simulations have been carried out at various combinations of superficial velocities to get the entire region of annular flow.

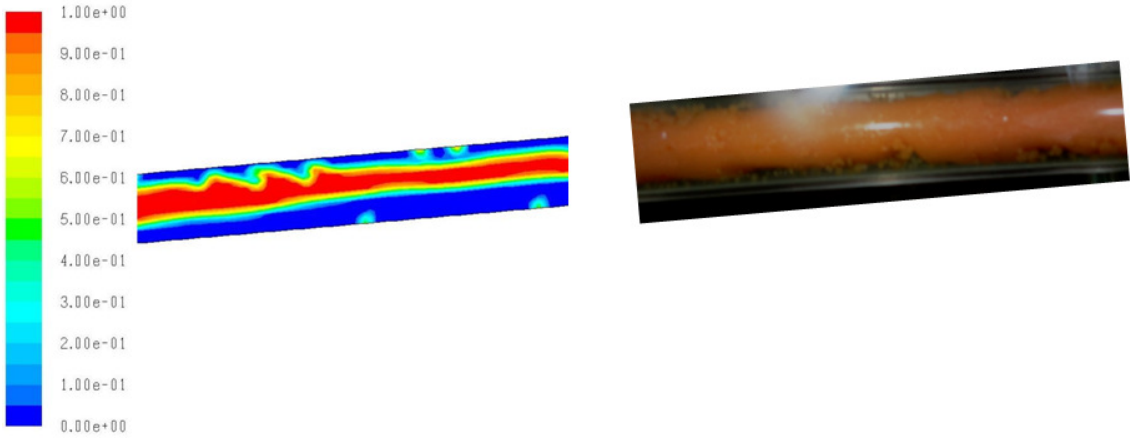

a) U_{SO} =0.535 m/s and U_{SW} = 0.41 m/s

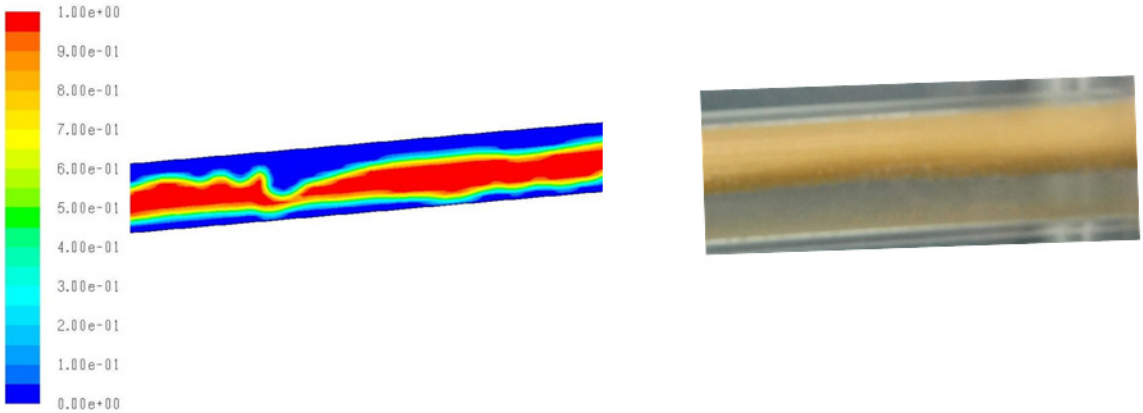

b) U_{SO} =0.531 m/s and U_{SW} = 0.611 m/s

Fig. 7.8 Comparison of annular flow results: simulated and experimental

7.6 Validation of simulated results with experiment

The simulated results are compared with experimental results reported in Chapter 6 in order to validate the simulation. For this the simulated data points are superimposed on the experimental flow pattern map of inclined pipeline (Fig. 4.4) and the comparison plot is shown in Fig. 7.9. The flow pattern map has been represented in terms U_{SO} and U_{SW}. In the figure the curves represents the transition boundaries of flow patterns identified in the experiment study of inclined pipeline and scattered data points denotes the simulated results. All the simulated results are showing the good prediction of interfacial morphologies.

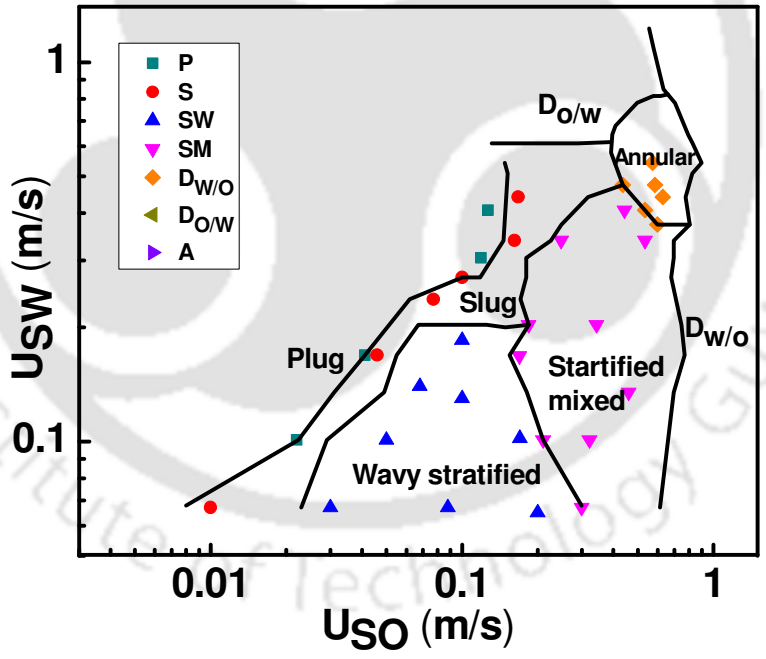

Fig. 7.9 Comparison of simulated flow pattern map with the experimental transition boundaries

7.7 Conclusions

Computational fluid dynamic study has been conducted to predict flow patterns of viscous oil-water flow through 5° upward inclined pipe line. Simulations have been conducted in 46,955 cell mesh which is selected on the basis of grid independence study. Simulations are performed using VOF methodology for plug, slug and separated flows (wavy stratified, stratified mixed and annular flow). All above mentioned flow patterns have been successfully predicted using CFD package in Fluent 6.2. The simulated results have been validated with the experimental results. Validation shows good prediction accuracy of all the above mentioned flow patterns. The present results reveal the inherent ability of VOF to predict almost entire flow pattern map with excellent accuracy except two dispersed regions.

Chapter 8

Conclusion and Recommendations

The present study investigates the hydrodynamics of viscous oil-water flow through horizontal and 5° upward inclined pipeline. Seven different flow patterns have been identified by visual and photographic technique in both the systems. All the flow patterns observed in both the system are represented in flow pattern map. Inclined flow pattern map has been compared with horizontal flow pattern map to know the effect of inclination on flow patterns. Horizontal flow pattern map has been compared with literature data (Raj et al. (2005)) with same pipe diameter to study the effect of viscosity on flow patterns.

The flow pattern transitions of both the cases have been predicted by analytical models. Analytical models gave poor prediction in few cases (transition of slug to annular, slug to wavy stratified, dispersion of oil in water at higher velocities, etc). So Artificial Neural Network technique has been adopted to predict the flow patterns observed in both horizontal and inclined pipeline. Probabilistic neural network has been selected for this purpose. The network has been constructed with the data collected from present experimental and past literature work. The completely trained PNN has been used to predict the flow patterns of horizontal and inclined flow. It gives the good accuracy in both the cases. PNN has been predicted all the flow patterns in horizontal and inclined pipeline within error of 5% and 10% respectively. The developed network has also been validated by predicting the flow pattern maps available in the literature. The predicted transition

boundaries of both the methods (analytical and PNN) have also been compared. The comparison shows that PNN gives higher accuracy for both the flows.

Experiments have been performed to measure the pressure drop and holdup of oil-water mixture in the horizontal and 5° upward inclined pipeline. The measured pressure drop and holdup has been represented as function of phase superficial velocities to know the effect of superficial velocities on holdup and pressure drop for both the cases. Measured pressure drop in horizontal pipeline has been predicted using the correlations available for gas-liquid flow in literature as there is no generalized correlation available for liquid-liquid flows. A new form of Lockhart-Martenille correlation has been developed for the liquid-liquid system and a new correlation has also been proposed based on dimensional analysis in both the cases. Experimental pressure gradient has been predicted using the correlations proposed in the present study and observed a good success. Next an attempt has been made to develop a model to predict pressure gradient of annular flow pattern considering entrainment of one phase into other in horizontal and inclined pipeline. The model has been developed based on the two fluid model (Brauner (1991) and entrainment model (Al-Wahaibi and Angeli (2009)). The proposed model has been validated with literature data for different systems. The developed model shows good improvement in prediction after incorporation of entrainment fraction. The measured holdup in the both the systems has been predicted using Homogeneous flow model, Arney et al. (1993) and Oliemans (1986) model. The predicted results are in good agreement with the experimental results.

Computational fluid dynamics technique has been applied to predict flow patterns observed in the 5° upward inclined pipeline. Simulations are performed using VOF methodology for plug, slug and separated flows (wavy stratified, stratified mixed and

annular flow). CFD simulation predicts above mentioned flow patterns successfully. The present results reveal the inherent ability of VOF to predict almost entire flow pattern map with excellent accuracy except two dispersed regions. The simulated results are validated with the experimental results to show the applicability of CFD technique in flow pattern prediction.

8.1 Conclusions

The salient features of present work are-

i. Seven different flow patterns namely plug, slug, wavy stratified, stratified mixed, annular, dispersion of oil in water and dispersion of water in oil flow pattern have been identified in both horizontal and 5° upward inclined pipeline. The observed flow patterns are represented in the form of flow pattern map and compared them for better understanding the impact of inclination on hydrodynamics of liquid-liquid two-phase flow.

ii. The plug, slug and stratified mixed flow patterns appear at lower velocities in inclined pipeline than horizontal pipe. The total annular flow region is shifted at higher mixture velocities in inclined pipe and it exists in a wider range of superficial velocities than horizontal flow. Low inclination has no significant effect on transition boundaries of dispersed flow patterns ($D_{O/W}$ and $D_{W/O}$).

iii. Higher viscosity favors annular flow pattern, which is identified in the present study and it is not reported in Raj et al. (2005). Dispersed flows starts at lower velocities in present study than that of Raj et al. (2005).

iv. The flow pattern transitions of both the pipelines have been predicted by analytical models. It gives the good prediction for transition boundary of dispersion of water in oil and wavy stratified to stratified mixed flow pattern and shows poor prediction for rest of the transition boundaries in both the flow (inclined and horizontal).

v. Probabilistic Neural Network (PNN) technique has been applied for the prediction of flow patterns in horizontal and inclined pipes. It has been predicted all the flow patterns in horizontal pipeline within error of 5% and 10% in the inclined pipeline. PNN has been validated with other literature data with good accuracy. This technique gives better prediction than analytical models.

vi. Holdup and pressure drop are measured in horizontal and inclined pipes. Two correlations are developed to predict pressure drop for horizontal and $+5^{\circ}$ inclined flow by following Lockhart-Martinelli approach and dimensionless analysis.

vii. A model has been developed to predict pressure drop of annular flow by incorporating entrainment of either phases for both the pipeline flows. This entrainment model is validated with the present experimental results and other literature data.

viii. Holdup of horizontal and inclined pipes is predicted by the existing models with good precision.

ix. Plug, slug, wavy stratified, stratified mixed and annular of $+5^{\circ}$ inclined flow are simulated using VOF method and validated with experimental observations.

8.2 Recommendations of future work

Based on the information obtained from the hydrodynamics of liquid-liquid flow in pipe lines, the following investigations are recommended for future study.

i. The work can be extended for different inclinations using same liquid pair to investigate the effect of inclination on hydrodynamics. Attempt can be initiated applying CFD analysis.

ii. Experiments using different pipe materials are proposed to understand the effect of wetability on flow patterns.

iii. Liquid-liquid flow needs to be investigated in various pipe networks like road crossing, U-bends.

iv. Experimental studies are recommended to measure the entrainment fraction.

v. Development of a generalized pressure drop correlation for all the inclination is recommended.

vi. Numerical simulation of dispersed flow patterns and pressure drop in different pipe networks are suggested.

References

Abduvayt, P., Manabe, R., Watanabe, T., Arihara, N., "Analysis of oil/water-flow tests in horizontal, hilly terrain and vertical pipes," *SPE Prod. Oper.,* pp.123-133, (2006).

Alkaya, B., "Oil-water flow patterns and pressure gradients in slightly inclined pipes," *M.S. Thesis,* University of Tulsa, Tulsa, Oklahoma (2000).

Al-Wahaibi T, Smith M, Angeli P., "Transition between stratified and non-stratified horizontal oil-water flows: part II (mechanism of drop formation)," *Chem. Eng. Sci.,* **62**, 2929-2940 (2007b).

Al-Wahaibi, T. and Angeli P., "Transition between stratified and non-stratified horizontal oil-water flows: part I (stability analysis)," *Chem. Eng. Sci.,* **62**, 2915-2928 (2007a).

Al-Wahaibi, T. and Angeli, P., "Experimental study on interfacial waves in stratified horizontal oil-water flow," *Int. J. Multiphase Flow,* **37**, 930-940 (2011).

Al-Wahaibi, T. and Angeli, P., "Onset of entrainment and degree of dispersion in dual continuous horizontal oil-water flows," *Exp. Ther. Fluid Sci.,* **33**, 774-781(2009b).

Al-Wahaibi, T. and Angeli, P., "Predictive model of the entrained fraction in horizontal oil-water flows" Chem. Eng. Sci. **64**, 2817-2825 (2009a).

Al-Wahaibi, T., "Pressure gradient correlation for oil-water separated flow in horizontal pipes," *Exp. Ther. Fluid Sci.,* **42**, 196-203 (2012).

Al-Wahaibi, T., Yusuf, N., Al-Wahaibi, Y., Al-Ajmi, A., "Experimental study on the transition between stratified and non-stratified horizontal oil-water flow," *Int. J. Multiphase flow,* **38**, 126-135 (2012).

Al-Yaari M., Al-Sarkhi, A., Abu-Sharkh, B., "Effect of drag reducing polymers on water holdup in an oil–water horizontal flow," *Int. J. Multiphase flow,* **44**, 29-33 (2012).

Al-Yaari, M. A. and Abu-Sharkh, B. F., "CFD prediction of stratified oil-water flow in a horizontal pipe," *Asian Trans. Eng.,* **1**, 68-75 (2010).

Al-Yaari, M. A. and Abu-Sharkh, B. F., "Effect of drag reducing polymers on water holdup in an oil-water horizontal flow," *Int. J. Multiphase flow,* **44**, 29-33 (2012).

Andreini, P. A., Greeff, P., Galbiati, L., Kuklwetter,A., Sutgia,G., **"**Oil-water flow in small diameter tubes" *International Symposium on Liquid-Liquid Two-Phase Flow And Transport Phenomena*, pp. 3-7, Antalya,Turkey (1997).

Angeli, P. and Hewitt, G. F., "Flow Structure in Horizontal Oil -Water Flow," *Int. J. Multiphase flow,* **26**, 1117-1140 (2000).

Angeli, P. and Hewitt, G.F., "Pressure Gradient in Horizontal Liquid-Liquid Flows," *Int. J. Multiphase flow,* **24**, 1183-1203 (1998).

Angeli, P., Lovick, S. Lum, Y.L., "Investigations on the Three-Layer Pattern During L-L Flows," *40th European Two-Phase Flow Group Meeting,* Stockholm (2002).

Angeli, P.A., "Liquid–liquid dispersed flows in horizontal pipes" Ph.D. thesis, Imperial College, University of London (1996).

Arirachakaran, S., Oglesby, K.D., Malinowsky, M.S., Shoham, O., Brill, J.P., "An analysis of oil/water flow phenomena in horizontal pipes" *In SPE Production Operating Symposium*, pp. 155-167. Oklahoma (1989).

Arney, M., Bai, R.,Guevara, E., Joseph, D.D., Liu, K., "Friction factor and holdup studies for lubricated pipelining: I. Experiments and correlations," *Int. J. Multiphase Flow,* **19**, 1061-1076 (1993).

Atmaca S., "Characterization of oil-water flow in horizontal and slightly inclined pipes" *M.S. Thesis*. University of Tulsa, Tulsa, Oklahoma (2007).

Balakhrisna,T., Ghosh, S., Das, G., Das, P.K., "Oil-water flows through sudden contraction and expansion in a horizontal pipe-Phase distribution and pressure drop," *Int. J. Multiphase flow,* **36**, 13-24 (2010).

Bandel, J., "Druckverlust und Warmeugang beiderverdamp fungsi edender kaltemittel im durch-stromten waage rechtenrohr," PhD thesis, University of Karlsruhe (1973).

Bankoff, S.G., 1960. "A variable density single-fluid model two-phase flow with particular reference to steam-water," *J. Heat trans.,* **11**, 265-272.

Bannawart, A. C., Rodriguez, O, M. H., Carvalho, C. H. M. de, Wang, I. S., Vara, R. M. O., "Flow patterns in heavy crude oil-water flow," *ASME*, **126**, 184-189 (2004).

Bannwart, A.C., "A simple model for pressure gradient in horizontal core," *J. Braz. Soc. Mec.Sci.,* **21**, 233-244 (1999).

Bannwart, A.C., "Modeling Aspects of Oil-Water Core-Annular Flows," *J. Pet. Sci. Eng.,* **32**, 127-143 (2001).

Bannwart, A.C., "Wave speed and volumetric fraction in core annular flow," *Int. J. Multiphase flow,* **24**, 961-974 (1998).

Barnea, D., Sohahm, O., Taitel, Y., Dukler, A.E., "Gas-liquid flow in inclined tubes: flow pattern transition for upward flow," *Chem. Eng. Sci.,* **40**, 131-136 (1985).

Baroczy, C. J., "A systematic correlation for two-phase pressure drop," *Chem. Eng. Prog. Symp.Ser.,* **62**, 232-249 (1965).

Basheer, I. A. and Hajmeer, M., "Artificial neural networks: fundamentals, computing, design and application," *J. Microbial. Methods,* **43**, 3-31 (2000).

Beratta, A., Ferrari, P., Galbiati, L., Andreini, P.A., "Horizontal oil-water flow in small diameter tubes pressure drop," *Int. Commun. Heat Mass Trans.,* **24**, 231-239 (1997b).

Beretta, A., Ferrari, P., Galbiati, L., Andreini, P.A., "Horizontal oil-water flow in small diameter tubes flow pattern," *Int. Commun. Heat Mass Trans.,* **24**, 223-229 (1997a).

Brackbill, J.U., Kothe, D.B., Zemach, C., "A continuum method for modeling surface tension," J. *Comput. Phys.,* **100**, 335 -354 (1992).

Brauner, N. and Maron, M.D., "Flow pattern transitions in two-phase liquid-liquid flow in horizontal tubes," *Int. J. Multiphase flow,* **18**, 123-140 (1992).

Brauner, N. and Maron, M.D., "The role of interfacial shear modeling in predicting the stability of stratified two-phase flow," *Chem. Eng. Sci.,* **8**, 2867-2879 (1993).

Brauner, N., "The prediction of flow dispersed boundaries in liquid-liquid and gas-liquid systems," *Int. J. Multiphase flow,* **27**, 885-910 (2001).

Brauner, N., "Two Phase Liquid-Liquid Annular Flow," *Int. J. Multiphase flow,* **17**, 59-76 (1991).

Brauner, N., Maron, D. M., Rovinsky, J., "A two fluid model for stratified flows with curved interfaces," *Int. J. Multiphase flow,* **24**, 975-1004 (1998).

Brown, R.A.S. and Govier, G.W., "High-speed photography in the study of two-phase flow," *Can. J. Chem. Eng.,* **39**, 159-164 (1961).

Castro, M.S. De, Pereira, C.C., Santos J.N.D., Rodriguez, O.M.H., "Geometrical and kinematic properties of interfacial waves in stratified oil-water flow in inclined pipe," *Exp. Ther. Fluid Sci.,* **37**, 171-178 (2012).

Chakrabarti, D. P., Das, G., Das, P. K., "Identification of stratified liquid-liquid flow through horizontal pipes by a non-intrusive optical probe," *Chem. Eng. Sci.,* **62**, 1861-1876 (2007).

Chakrabarti, D. P., Piligrim, A, Sastry, M. K. S., Das, G., "Identification of liquid-liquid flow pattern in a horizontal pipe using artificial neural networks," *Chem. Eng. Commun.,* **198**, 273-285 (2011).

Chakrabarti, D.P., Das, G., and Ray, S., "Pressure drop in liquid-liquid two phase horizontal flow: experiment and prediction," *Chem. Eng. Technol.,* **28**, 1003-1009 (2005).

Chakrabarti, D.P., Das, G., Das, P.K., "The transition from water continuous to oil continuous flow pattern," *AIChE J.,* **52**, 3668-3678 (2006).

Charles, M. E., Govier, G. W., Hodgson, G. W., "The horizontal flow of equal density oil-water mixtures," *Can. J. Chem. Eng.,* **39**, 27**-** 36 (1961).

Charles, M.E. and Redberger, R.J., "The reduction of pressure gradients in oil pipelines by the addition of water: numerical analysis of stratified flow," *Can. J. Chem. Eng.,* **40**, 70-75 (1962).

Chawla, J. M., "Warmeubergang and druckfall in waagerechten rohren bei der stromung von verdampfenden kaltemitteln" . *Chapter Lg1-Lg2*, **523**. VDI-Forschungsh (1967).

Chisholm, D., "A Lockhart-Martinelli basis for the correlation for two-phase flow," *Int. J. Heat Mass Trans.,* **10**, 1767–1778 (1967).

Chisholm, D., "Pressure gradient due to friction during the flow of evaporating two phase mixtures in smooth tubes and channels," *Int. J. Heat Mass Trans.,* **16**, 347-358 (1973).

Cicchitti, A., Lombardi, C., Silvestri, M., Soldaini, G., Zavattarelli, R., "Two-phase cooling experiments pressure drop, heat transfer and burnout measurements," *Energia Nucleare*, **7**, 407-425 (1960).

Clark, A. F. and Shapiro, A., *U.S. Patent No. 2*, **533**,878(1949).

Clark, K.A., *Private communication* (1948).

Cox, A.L., "A study of horizontal and downhill two-phase oil-water flow," *M.S. thesis*, The University of Texas (1985).

Dallman, J.C., Laurinat, J.E., Hanratty, T.J., "Entrainment for horizontal annular gas-liquid flow," *Int. J. Multiphase Flow,* **10**, 677-690 (1984).

Dallman, J.C., Laurinat, J.E., Hanratty, T.J., "Entrainment for horizontal annular gas-liquid flow," *Int. J. Multiphase Flow,* **10**,677-690 (1984).

De, B., Mandal, T.K., Das, G., "Experimental studies on phase inversion in a small diameter horizontal pipe," Chem. Eng. Res. Des., **88**, 819-826 (2010a).

De, B., Mandal, T.K., Das, G., "The rivulet flow pattern during oil-water horizontal flow through a 12 mm pipe," *Exp. Ther. Fluid Sci.,* **34**, 625-632 (2010b).

Demori, M., Ferrari, V., Strazza, D., "A sensor system for oil fraction estimation in a two phase oil-water flow," *Proc. Chemistry,* **1**, 1247-1250 (2009).

Ding, Z.X., Ullah, K., Huang, Y., "A comparison of predictive oil/water holdup models for production log interpretation in vertical and deviated wellbores" *In Proceedings SPWLA 35th Annual Logging Symposium*, pp. 1-12, Tulsa, OK, USA (1994).

Du, M., Jin, N.D., Gao, Z.K., Wang, Z.Y., Zhai, L.S., "Flow pattern and water holdup measurements of vertical upward oil-water two-phase flow in small diameter pipes," *Int. J. Multiphase Flow,* **41**, 91-105 (2012).

El-Sebakhy, E. A., "Flow regimes identification and liquid-holdup prediction in horizontal multiphase flow based on neuro-fuzzy inference systems," *Math. Comp. Sim.,* **80**, 1854-1866 (2010).

Fairuzov, Y.V., Arenas-Medina P., Verdejo- Fierro J., Gonzalez-Islas R., "Flow pattern transitions in horizontal pipelines carrying oil-water mixtures: Full-scale experiments," *J. Ene. Res. Tech.,* **122**, 169-176 (2000).

Flores, J.G., "Oil-water flow in vertical and deviated wells," *Ph.D. Dissertation*, The University of Tulsa, Tulsa, Oklahoma (1997).

Fluent 6.3 User's Guide, *Fluent Inc.,* Lebanon, USA (2006).

Friedel, L., "Pressure drop during gas/vapor-liquid flow in pipes," *Int. Chem. Eng.,* **20**, 352-367 (1980).

Fujji, T., Ohta, J., Nakazawa, T., Morimoto,O., "The behavior of an immiscible equal density liquid-liquid two-phase flow in horizontal tube," *JSME, J. Series B,* **37**, 22-29 (1994).

Gada, V.H. and Sharma, A., "Analytical and level-set method based numerical study on oil-water smooth/wavy stratified-flow in an inclined plane-channel," *Int. J. Multiphase Flow,* **38**, 99-117 (2012).

Gat S., "Two-phase liquid-liquid concurrent flow in inclined tubes," *M.Sc. Thesis,* Faculty of Engineering, Tel-Aviv University (2002).

Ghosh, S., Das, G., Das, P.K., "Simulation of core annular down flow through CFD a comprehensive study," *Chem. Eng. Prog.,* **49**, 1222-1228 (2010).

Govier, G.W., Sullivan, G.A., Wood, R.K., "The upward vertical flow of oil-water mixtures," *Can. J. Chem. Eng.,* **9**, 67-75 (1961).

Grassi, B., Strazza, D., Poesio,P., "Experimental validation of theoretical models in two-phase high-viscosity ratio liquid-liquid flows in horizontal and slightly inclined pipes," *Int. J. Multiphase Flow,* **34**, 950-965 (2008).

Guzhov, A., Grishin, A.D., Medredev, V.F., Medredeva, O.P., "Emulsion formation during the flow of two liquids in a pipe," *Neft Khoz 8,* pp. 58-61, Russia (1973).

Hadziabdic, M., Oliemans, R.V. A., "Parametric study of a model for determining the liquid flow-rates from the pressure drop and water hold-up in oil-water flows," *Int. J. Multiphase Flow,* **33**, 1365-1394 (2007).

Hajmeer, M. and Basheer, I., "A probabilistic neural network approach for modeling and classification of bacterial growth/no-growth data," *J. Microbiol. Methods* **51**, 217-226 (2002).

Halman, J.P., *Experimental methods for engineers*. McGraw-Hill, New York, (1989).

Hamad, F.A., Imberton, F., Brunn, H.H., "An Optical Probe for measurement in liquid-liquid two-phase flow," *Meas. Sci. Technol.,* **8,** 1122-1132 (1997).

Hamad, F.A., Pierscionek, B.K., Brunn, H.H., "A dual optical probe for volume fraction, drop velocity and drop size measurements in liquid-liquid two-phase flow," *Meas. Science Techn.,* **11**, 1307-1318 (2000).

Hapanowicz, J. and Troniewski, L., "Two-phase flow of liquid-liquid mixture in the range of the water droplet pattern," *Chem. Eng. Proc.,* **41**, 165-172 (2002).

Hapanowicz, J., "Slip between the phases in two-phase water-oil flow in a horizontal pipe," *Int. J. Multiphase Flow,* **34**, 559-566 (2008).

Hapanowicz, J., Troniewski, L., Witczak S., "Flow patterns of water-oil mixture flowing in horizontal pipes" *International symposium on liquid-liquid two- phase flow and transport phenomena*, Antalya, Turkey (1997).

Hasan, A.R. and Kabir, C.S., "A new model for two-phase oil/water flow; production log interpretation and tubular calculations," *SPE*, 193-199 (1990).

Hasan, A.R. and Kabir, C.S., "A simplified model for oil/water flow in vertical and deviated wellbores," *SPE In Proceedings and Facilities*, **141**, 56-62 (1999).

Hewitt, G. and Hall-Taylor, N., "Annular two-phase flow," *Pergamon Press*. New York (1970).

Hill, A.D. and Oolman, T., "Production logging tool behavior in two-phase inclined flow," *J. Pet. Tech.,* **34**, 2432-2440 (1982).

Ishii, M. and Grolmes, M., "Inception criteria for droplet entrainment in two-phase concurrent film flow," *AIChE J.,* **21**, 308-317 (1975).

Issa R. I., "Solution of the implicitly discretized fluid flow equations by operator splitting," *J. Comp. Phys.,* **62**, 40-65 (1986).

Jana A. K., Mandal, T.K., Chakrabarti, D.P., Das, G., Das, P.K., "An optical probe for liquid-liquid two-phase flows," *Meas. Sci. Technol.,* **18**, 1563-1575 (2007).

Jana, A.K., Das, G., Das, P.K., "Flow regime identification of two-phase liquid-liquid up flow through vertical pipe," *Chem. Eng. Sci.,* **61**, 1500-1515 (2006).

Jana, A.K., Das, G., Das, P.K., "The hydrodynamics of liquid-liquid up flow through a venture meter," *Int. J. Multiphase Flow,* **34**, 1119-1129 (2008).

Joseph, D. D., Renardy, M., Renardy, Y., "Instability of the flow of two immiscible liquids with different viscosities in a pipe," *J Fluid Mech,***141**, 309-317 (1984).

Julia, E. J., Basar, O., Jae-Jun, J., Takashi, H., Mamoru, I., "Flow regime development analysis in adiabatic upward two-phase flow in a vertical annulus," *Int. J. Heat and Fluid Flow,* **32**, 164-75 (2011).

Kaushik, V. V. R., Ghosh, S., Das, G., Das, P. K., "CFD simulation of core annular flow through sudden contraction and expansion," *J. Pet. Sci. Eng.,* **86-87**,153-164 (2012).

Kumara, W.A.S., Halvorsen, B.M., Melaaen, M.C., "Particle image velocimetry for characterizing the flow structure of oil-water flow in horizontal and slightly inclined pipes," *Chem. Eng. Sci.,* **65**, 4332-4349 (2010a).

Kumara, W.A.S., Halvorsen, B.M., Melaaen, M.C., "Single-beam gamma densitometry measurements of oil-water flow in horizontal and slightly inclined pipes," *Int. J. Multiphase Flow,* **36**, 467-480 (2010b).

Kurban, A.P.A., "Stratified liquid-liquid flow," *Ph.D. Dissertation*, Imperial College, London, U.K (1997).

Liu, J. P., Niu, Y. M., Chen, J. P., Ch en, Z. J., Feng, X. "Experimentation and correlation of R744 two-phase flow through short tubes," *Exp. Ther. Fluid Sci.,* **28**, 565-573 (2004).

Lockhart, R.W. and Martinelli, R.C., "Proposed correlation of data for isothermal two-phase two-component in pipes," *Chem. Eng. Prog.,* **45**, 39-48 (1949).

Lopez de, B. M. and Beus, A. A, S., "Experiments for entrainment rate of droplets in the annular regime," *Int. J. Multiphase Flow,* **27**, 685-699 (2001).

Lovick, J. and Angeli, P., "Experimental studies on the dual continuous flow pattern in oil-water flows," *Int. J. Multiphase Flow,* **30**, 139-157 (2004).

Lum, J.Y., Lovick, J., Angeli, P., "Low Inclination Oil-water Flows," *Can. J. Chem. Eng.,* **82**, 303-315 (2004).

Lum, J.Y.L., Al-Wahaibi, T., Angeli, P., "Upward and downward inclination oil-water flows," *Int. J. Multiphase Flow,* **32**, 413-435 (2006).

Malhotra, A., "Study of two phase and three phase flows in large diameter horizontal pipes," *M.S. thesis*, Ohio University, Athens, Ohio (1995).

Malinowsky, M. S. “An experimental study oil-water and air-oil-water flowing mixtures in horizontal pipes,” *M.S. Thesis,* The University of Tulsa (1975).

Mandal, T. K., Chakrabarti, D. P, Das, G., “Oil water flow through different diameter pipes similarities and differences,” *Chem. Eng. Res. Des.,* **85**, 1123- 1128 (2007).

Mandal, T. K., Das, G., Das, P. K., “An appraisal of liquid-liquid slug flow in different pipe orientations,” *Int. J. Multiphase Flow,* **36**, 661-671(2010).

Mao, K. Z., Tan, K. C., Ser, W., “Probabilistic neural-network determination for pattern classification” *IEEE Tran. Neural Network*, **1**, 1009-1016 (2000).

McCoy, D.D. and Hanratty, T.J., “Rate of deposition of droplets in annular two-phase flow,” *Int. J. Multiphase Flow,* **3**, 319-331 (1977).

Morgan, R.G., Markides, C.N., Hale, C.P., Hewitt, G.F., “Horizontal liquid-liquid flow characteristics at low superficial velocities using laser-induced fluorescence,” *Int. J. Multiphase Flow,* **43**, 101-117 (2012).

Morgan, R.G., Markides, C.N., Zadrazil, I., Hewitt, G.F., “Characteristics of horizontal liquid-liquid flows in a circular pipe using simultaneous high-speed laser-induced fluorescence and particle velocimetry,” *Int. J. Multiphase Flow,* **49**, 99-118 (2013).

Mukherjee, H.K., Brill, J.P., Beggs, H.D., “Experimental study of oil-water flow in inclined pipes” *Transactions of the ASME*, **103**, 56-66 (198).

Mukhopadhyay, H., “An experimental study of two-phase oil-water flow in inclined pipes,” *M.S. Thesis,* University of Tulsa (1977).

Muller Steinhagen, H. and Heck, H., “A simple friction pressure drop correlation for two phase flow in pipes,” *Chem. Eng. Prog.,* **20**, 291-308 (1986).

Nadler, M. and Mewes, D., "Flow induced emulsification in the flow of two immiscible liquids in horizontal pipes," *Int. J. Multiphase Flow,* **23**, 55-68 (1997).

Oddie, G., Shi, H., Durlofsky, L.J., Aziz, K., Pfeffer, B., Holmes, J. A., "Experimental study of two and three phase flows in large diameter inclined pipes," *Int. J. Multiphase Flow,* **29**, 527-558 (2003).

Oglesby, K.D., "An experimental study on the effects of oil viscosity, mixture velocity, and water fraction on horizontal oil**-**water flow," *M.S. Thesis*, The University of Tulsa (1979).

Oliemans, R.V.A., **"**The lubricating-film model for core-annular flow," *Ph.D Thesis,*The Delft University Press (1986).

Oliemans, R.V.A., Ooms G., Wu, H.L., Duijvestijn, A., "Core-annular oil/water flow: the turbulent-lubricating-film model and measurement in a 5 cm pipe loop," *Int. J. Multiphase Flow,* **13**, 23-31 (1987).

Ooms, G., Pourquie, M.J.B.M., Poesio, P., "Numerical study of eccentric core-annular flow," *Int. J. Multiphase Flow,* **42**, 74-79 (2012).

Ooms, G., Segal, A., Van Der Wees, A.J., "A theoretical model for core-annular flow of a very viscous oil core and a water annulus through a horizontal pipe," *Int. J. Multiphase Flow,* **10**,41-60 (1984).

Pan, L. and Hanratty, T.J., "Correlation of entrainment for annular flow in vertical pipes" *Int. J. Multiphase Flow,* **28**, 363-384 (2002a).

Pan, L. and Hanratty, T.J., "Correlation of entrainment for annular flow in horizontal pipes," *Int. J. Multiphase Flow,* **28**, 385-408 (2002b).

Panagou, E.Z., Kodogiannis, V., Nychas, G.J.E., "Modeling fungal growth radial basis neural networks: The case of the ascomycetous fungus Monascusruber van Tieghem*," Int. J. Food Microbiol,* **117**, 276-286 (2007).

Patankar, S.V., "*Numerical heat transfer and fluid flow,"* Taylor and Francis Hemisphere, Washington, D.C (1980).

Poesio, P., "Experimental determination of pressure drop and statistical properties of oil-water intermittent flow through horizontal pipe," *Exp. Ther. Fluid Sci.,***32**, 1523-1529 (2008).

Poesio, P., Strazza, D., Sotgia, G., "Very-viscous-oil/water/air flow through horizontal pipes: pressure drop measurement and prediction," *Chem. Eng. Sci.,* **64**, 1136-1142 (2009).

Quiben, J.M., "Experimental and analytical study of two-phase pressure drops during evaporation in horizontal tubes," *Ph.D. Thesis*, University Pierre et Marie Curie, Paris, France (2005).

Raj, T. S., Chakrabarti, D. P., Das, G., "Liquid-liquid stratified flow through horizontal conduits," *Chem. Eng. Technol.,* **28**, 899-907 (2005).

Rodriguez, O.M.H. and Bannwart, A.C., "Experimental study on interfacial waves in vertical core flow," *J. Pet. Sci. Eng.,* **54**,140-148 (2006).

Rodriguez, O.M.H. and Bannwart, A.C., "Stability analysis of core-annular flow and neutral stability of wave number," *AIChE J.,* **54**, 20-31 (2008).

Rodriguez, O.M.H. and Oliemans, R.V. A., "Experimental study on oil-water flow in horizontal and slightly inclined pipes," *Int. J. Multiphase Flow,* **32**, 323-343 (2006).

Rodriguez, O.M.H., Bannwart, A.C., Carvalho, C.H.M. De., "Pressure loss in core-annular flow: Modeling, experimental investigation and full-scale experiments," J. Pet. Sci. Eng., **65**, 67-75 (2009).

Russell, T. W. F. and Charles, M. E., "The effect of the less viscous liquid in the laminar flow of two immiscible liquids," *Can. J. Chem. Eng.,* **37**, 18-24 (1959).

Russell, T. W. F., Hodgson, G. W., Govier, G. W., "Horizontal pipeline flow of mixtures of oil and water," *Can. J. Chem. Eng.,* **37**, 11-17 (1959).

Saisoran, S. and Wongwises, S., "An inspection of viscosity model for homogeneous two-phase flow pressure drop prediction in a horizontal circular micro-channel" *Int. Commun. Heat Mass Trans.,* **35**, 833- 838 (2008).

Scot, P.M. and Knudsen, J.G., "Two-phase liquid-liquid flow in pipes," *AIChE Symposium Series,* **68**, 38-44 (1972).

Scott, G. M., "A study of two-phase liquid-liquid flow at variable inclinations," *M.S. Thesis*, The University of Texas (1985).

Sharma A., Al-Sarkhi, A., Sarica, C., Zhang, H.Q., "Modeling of oil-water flow using energy minimization concept," *Int. J. Multiphase Flow,* **37**, 326-335 (2011).

Sharma, H., Das, G., Samanta, A. N., "ANN-Based prediction of two-phase gas-liquid flow patterns in a circular conduit," *AIChE J.,* **52***,* 3018-3028 (2006).

Simmons, M.J.H. and Azzopardi, B.J., "Drop size distributions in dispersed liquid-liquid pipe flow," *Int. J. Multiphase Flow,* **27**, 843-859 (2001).

Soleimani, A., "Phase distribution and associated phenomena in oil-water flows in horizontal tubes," *Ph.D. Dissertation*, Imperial College, University of London (1999).

Sotgia, G., Tartarini, P., Stalio, E., "Experimental analysis of flow regimes and pressure drop reduction in oil-water mixtures," *Int. J. Multiphase Flow,* **34**, 1161-1174 (2008).

Spect, D. F., "Probabilistic neural networks" *Neural Networks*, **3**,109-118 (1990).

Stalpelberg, H.H. and Mewes, D., "The flow of two immiscible liquids and air in horizontal gas-liquid pipe," *Winter Annual Meeting of the ASME*, pp. 89-96 (1990).

Strazza, D., Grassi, B., Demori, M., Ferrari, V., Poesio P., "Core-annular flow in horizontal and slightly inclined pipes: Existence, pressure drops, and hold-up," *Chem. Eng. Sci.,* **66**, 2853-2863 (2011).

Sun, L. and Mishima, K., "Evaluation analysis of prediction methods for two-phase flow pressure drop in mini-channels," *Int. J. Multiphase Flow,* **35**, 47-54 (2009).

Taitel, Y. and Dukler, A.E., "A theoretical approach to the Lockhart-Martinelli correlation for stratified flow," *Int. J. Multiphase Flow,* **2**, 591-595 (1976).

Trallero, J. L., Sarica, C., Brill, J. P., **"**A study of oil/water flow patterns in pipes," *SPE Productions & Facilities 36609*, 165-172 (1997).

Trallero, J.L., "Oil-water flow patterns in horizontal pipes," *Ph.D. Dissertation. Thesis,* University of Tulsa, Tulsa, Oklahoma (1995).

Ullmann, A. and Brauner, N., "Closure relations for two-fluid models for two-phase stratified smooth and stratified wavy flows," *Int. J. Multiphase Flow,* **32**, 82-105 (2006).

Ullmann, A., Zamir, M., Gat, S., Brauner, N., "Multi-holdups in co-current stratified flow in inclined tubes," *Int. J. Multiphase Flow,* **29**, 1565-1581 (2003b).

Ullmann, A., Zamir, M., Gat, S., Brauner, N., "Stratified laminar countercurrent flow of two liquid phases in inclined tubes," *Int. J. Multiphase Flow,* **29**, 1583-1604 (2003a).

Valle, A. and Kvandal, H., "Pressure drop and dispersion characteristics of separated oil-water flow," *In Proceedings 1st International Symposium On Two-Phase Flow Modeling Experimentation*, pp. 583-591Rome, Italy (1995).

Valle, A. and Utvik, O.H., "Pressure drop, flow pattern and slip for two phase crude oil/water flow: experiments and model predictions," *International symposium on liquid-liquid two-phase flow and transport phenomena*, Antalya, Turkey (1997).

Vedapuri, D., Bessette, D., Jepson W.P., "A segregated flow model to predict water layer thickness in oil-water flows in horizontal and slightly inclined pipelines," *In Proceedings Multiphase'97*, pp.75-105, Cannes, France (1997)

Vedapuri. D., "Studies on oil-water flow in inclined pipelines," *M.S. Thesis*, The faculty of Russ College of engineering and technology, Ohio University (1999).

Vigneaux, P., Chenois, P., Hulin, J.P., "Liquid-liquid flows in an inclined pipe," *AIChE J.,* **34**, 781-789 (1988).

Walvekar, R.G., Thomas S.Y. Choong, T.S.Y., Hussain, S.A., Khalid, M., Chuah, T.G., "Numerical study of dispersed oil-water turbulent flow in horizontal pipe," *J. Pet. Sci. Eng.,* **65**,123-128 (2009).

Wang, W., Gong, J., Angeli, P., "Investigation on heavy crude-water two phase flow and related flow characteristics," *Int. J. Multiphase Flow,* **37**, 1156-1164 (2011).

Wegmann, A. and Von Rohr P.R., "Two phase liquid-liquid flows in pipes of small diameters," *Int. J. Multiphase Flow,* **32**, 1017-1028 (2006).

Weisman, J. and Kang, S.Y., "Flow pattern transitions in vertical and upward inclined lines," *Int. J. Multiphase flow,* **7**, 271-291 (1981).

Xu, J., Li, D., Guo, J., Wu, Y., "Investigations of phase inversion and frictional pressure gradients in upward and downward oil-water flow in vertical pipes," *Int. J. Multiphase Flow,* **36**, 930-939 (2010).

Xu, M., Xiong, R.H., Li, Y.F., Yang, J.M., Luo, X., Yu, Y.B., Zhao, T.Z., "Pattern transition and holdup behavior of horizontal oil-water pipe flow," *ICMF*, pp.1-6 (2010).

Xu, W., Xu, L., Cao, Z., Chen, J., Liu, X., Hu, J., "Normalized least-square method for water hold-up measurement in stratified oil-water flow," *Flow Meas. Instru.,* **27**, 71-80 (2012).

Xu, X.-X., "Study on oil-water two-phase flow in horizontal pipelines," *J.Pet. Sci. Eng.,* **59**, 43-58 (2007).

Yipping, L., Hua, Z., Shuhua, W., Jing, W., "Prediction of Pressure Gradient and Holdup in Small Eotvos Number Liquid-Liquid Segregated Flow," *Chin. J. Chem. Eng.,* **16**, 184-191(2008).

Yusuf, N., Al-Wahaibi ,Y., Al-Wahaibi, T., Al-Ajmi, A., Olawale, A. S, Mohammed, I. A., "Effect of oil viscosity on the flow structure and pressure gradient in horizontal oil-water flow," *Chem. Eng. Res. Des.,* **90**, 1019-1030 (2011).

Zavareh, F., Hill, A.D., Podio, A.L., "Flow regimes in vertical and inclined oil/water flow in pipes," *Paper SPE 18215, Presented at the 63rd Annual Technical Conference and Exhibition*, Houston, Texas (1988).

Zhang, H.Q., Vuong, D.H. and Sarica, C., "Modeling high-viscosity oil/water concurrent flow in horizontal and vertical pipes," *SPE Journal*, pp. 243-250 (2012).

Zong, Y.B., Jin, N.D., Wang, Z.Y., Gao, Z.K., Wang, C., "Nonlinear dynamic analysis of large diameter inclined oil-water two phase flow pattern," *Int. J. Multiphase Flow,* **36**, 166-183 (2010).

Appendix

1. Uncertainty and repeatability of the experimental results

The repeatability of the experimental results and the uncertainty associated with them are discussed in this section.

The error in a measurement is usually defined as the deference between its true value and experimental value. In general three types of errors are encountered during conducting an experiment.

a) Human error

b) Systematic error

c) Random error

Human error arises when experimenter make a mistake like misreading of an instrument, setup experiments incorrectly or mistake in a calculation. So it is not a source of experimental error. It is basically experimenter's error and 100% recoverable.

On the other hand, systematic error is an inherent error of the experimental setup. This causes the results to be skewed in the same direction every time. For example, a rotameter reads 0.2 LMP when no fluid is flowing through it. It can be solved by calibrating the rotameter.

Finally, random error arises because no measurement can be made with infinite precision. This error will cause a series of measurements to be sometimes too large and sometimes too small. An example of random error can arises when making timing with a stopwatch to note traveling time of fluids between two points. It is not a human error because finite

reaction time of a person is not a mistake; it is part of limitation of the experimental process. It can be reduced by averaging the several measurements.

A.1 Error estimation on oil flow rate measurement

Here oil flow rate is measured by measuring the time required to fill 4 cm height of the tank (calibrated), by this measurement as the total amount of water present in the mixture is know. By subtracting the water flow rate from the mixture flow rate, flow rate of oil can be known. In this type of measurement error can be estimated by reproducibility of experiment and also by the uncertainty analysis.

Reproducibility of oil flow rate measurement

Four readings have been taken for each oil flow rate and average value is taken as volumetric flow rate which is used to calculate oil superficial velocity in the pipe. The reading shows a reproducibility of each reading with an average error of ±0.5%. One sample calculation for oil flow rate of 1.46402×10^{-4} m^3/s is shown below.

Let us consider measuring the oil flow rate at water flow rate of 10LPM (1.6667×10^{-4} m^3/s). Volume of 4 cm height of the graduated tank (pre-calibrated) is 12.313 liters (fixed). The time counted for four repeated readings are 39.25, 39.38, 39.27 and 39.42 respectively. Calculation of oil volumetric flow rates are shown in the following Table A.1.

Table. A.1 Error calculation for volumetric flow rate

S.No	Time of measurement (sec)	Total volume (T_V)	Water volume (from water rotameter) liters	Obtained oil volume liters	Measured oil volumetric flow rate (m^3/s)	Average oil volumetric flow rate(m^3/s)	% error from average value
1	39.25	12.313	6.5416	5.7713	1.4704×10^{-4}	1.464×10^{-4}	-0.433
2	39.38	12.313	6.633	5.749	1.46×10^{-4}		0.272

3	39.42	12.313	6.545	5.768	1.4688×10^{-4}	-0.326

Uncertainty analysis for oil flow rate measurement

The term uncertainty is used to quantify the error. Let the result 'R' is to be calculated from a set of independent variables i.e. R= R (X_1, X_2, X_3,…. X_N). If δX_i is an uncertainty in X_i then the impact of uncertainty in a single measurement on the calculated result is

$$\partial R_{Xi} = \left(\frac{\partial R}{\partial X_i}\right)\delta X_i \tag{A.1}$$

$\frac{\partial R}{\partial X_i}$ is the sensitivity for result R with respect to X_i. When all independent variables appear into the results R then the individual variables are combined by square root methods as

$$\delta R = \left[\left(\frac{\partial R}{\partial X_1}\delta X_1\right)^2 + \left(\frac{\partial R}{\partial X_2}\delta X_2\right)^2 + \left(\frac{\partial R}{\partial X_3}\delta X_3\right)^2 + \ldots.. + \left(\frac{\partial R}{\partial X_N}\delta X_N\right)^2\right]^{1/2} \tag{A.2}$$

Oil flow rate (Q_O) is measured by taking the time (least count of stop watch is 0.01 sec) required to fill 4 cm height of the tank, least count of the tank is 1 mm.

Oil flow rate is given as:

$$Q_O = Q_T - Q_W \tag{A.3}$$

Q_T is total volumetric flow rate and Q_W is volumetric flow rate of water.

The overall uncertainty associated in carrying out this measurement can be evaluated as

$$\delta Q_O = \left[\left(\frac{\partial Q_o}{\partial Q_T}\delta Q_T\right)^2 + \left(\frac{\partial Q_o}{\partial Q_W}\delta Q_W\right)^2\right]^{1/2} \tag{A.4}$$

$$\delta Q_O = \left[\left(1\times\delta Q_T\right)^2 + \left(-1\times\delta Q_W\right)^2\right]^{1/2} \tag{A.5}$$

A sample calculation of uncertainty is discussed here. The collection time of $Q_T = 2.373 \times 10^{-4}$ m^3/s is 51.59 s at a combined flow rate of $Q_W = 1.667 \times 10^{-4}$ m^3/s and $Q_O = 7.06238 \times 10^{-5}$ m^3/s for water and oil respectively. δQ_T and δQ_W are 5×10^{-3} and 0.334×10^{-5} respectively for the present system. Incorporating all the data in Eq. A.5, it becomes

$$\delta Q_O = [(1 \times 5\times 10^{-3})^2 + (-1 \times 0.334 \times 10^{-5})^2]^{1/2} \quad \text{(A.6)}$$

This yields an uncertainty of 6.1×10^{-4}.

The inaccuracy in the measurement is very less and acceptable.

Error in measurement of height is only due to time measurement which is 1%.

A.2 Uncertainty analysis for pressure drop measurement

Pressure drop is calculated from the following equation

$$\Delta P = \Delta \rho g h \quad \text{(A.7)}$$

Where $\Delta\rho$ is the density difference of the manometer fluids, g is gravitational force and h is height difference in the two limbs of manometer.

$$\Delta P = f(h) \quad \text{(A.8)}$$

The overall uncertainty associated in measurement of pressure drop is written as

$$\partial P = \left(\frac{\partial P}{\partial h}\right)\delta h \quad \text{(A.9)}$$

$$\partial P = \Delta \rho g \delta h = 0.59\times 0.098\times 1 = 0.058 \quad \text{(A.10)}$$

Finally this yields an uncertainty of 0.058.

Error estimation of C_W

Here the water cut C_W has been calculated from the following expression

$$C_W = U_{SW} / U_{SW} + U_{SO} \quad \text{(A.11)}$$

Where U_{SW} and U_{SO} are superficial velocities of water and oil phase respectively which are calculated from the volumetric flow rate of both the fluids. The error estimation of C_W has been given in table below. The oil and water flow rates has been taken from the table mentioned above.

Table. A.2 Error estimation of C_W

S.No	Water volumetric flow rate (m^3/s)	Oil volumetric flow rate(m^3/s)	Average oil volumetric flow rate (m^3/s)	C_W	Average C_W	% error
1	1.6667×10^{-4}	1.4704×10^{-4}	1.464×10^{-4}	0.531	0.532	0.204
2	1.6667×10^{-4}	1.46×10^{-4}		0.533		-0.127
3	1.6667×10^{-4}	1.4688×10^{-4}		0.532		0.15

From the above table it shows that the maximum and minimum error in prediction are +0.20 and -0.13% respectively.

Uncertainty analysis in calculation of C_W

$$C_w = f(V_W, V_O) \quad \text{(A.12)}$$

$$\partial C_w = \left[\left(\frac{\partial C_w}{\partial V_w} \delta V_w \right)^2 + \left(\frac{\partial C_w}{\partial V_o} \delta V_o \right)^2 \right]^{1/2} \quad \text{(A.13)}$$

$$\partial C_W = \left[\left(\frac{(V_W + V_O)(1) - V_W}{(V_W + V_O)^2} \delta V_W \right)^2 + \left(\frac{(V_W + V_O)(0) - V_W(1)}{(V_W + V_O)^2} \delta V_O \right)^2 \right]^{1/2} \quad \text{(A.14)}$$

Sample calculation at $V_W = 0.1$ m/s and $V_O = 0.1$ m/s has been carried out. δV_W is taken measurement error from Rotameter and δV_O is taken from the uncertainty of oil velocity.

$$\partial C_W = \left[\left[\frac{0.1 \times 0.334 \times 10^{-5}}{0.2^2} \right]^2 + \left[\frac{-0.1 \times 6.1 \times 10^{-4}}{0.2^2} \right]^2 \right]^{1/2} \quad \text{(A.15)}$$

This yields an uncertainty of 1.52×10^{-3}.

A.3 Uncertainty analysis in calculation of holdup

The water holdup has been estimated by collecting the entrapped holdup in a measuring cylinder. The measuring cylinder has a least count of 1 ml.

The holdup is defined as,

$$H_W = \frac{\nu_W}{\nu_W + \nu_O} \quad \text{(A.16)}$$

Here H_W is water holdup

v_W is volume of water

v_O is volume of oil

The overall uncertainty associated in carrying out this measurement can be evaluated as

$$\delta H_W = \left[\left(\frac{\partial H_W}{\partial \nu_W} \delta \nu_W \right)^2 + \left(\frac{\partial H_W}{\partial \nu_O} \delta \nu_O \right)^2 \right]^{1/2} \quad \text{(A.17)}$$

$$= \left[\left(\frac{V_O}{\nu^2} \delta \nu_W \right)^2 + \left(-\frac{V_W}{\nu^2} \delta \nu_O \right)^2 \right]^{1/2} \quad \text{(A.18)}$$

Where v is total volume of mixture i.e $v = v_W + v_O$

A sample calculation for $H_W = 0.53$ is given below

$$\delta H_W = [(230/490^2 \times 1)^2 + (-260/490^2 \times 1)^2]^{0.5} \quad \text{(A.19)}$$

This yields an uncertainty of 1%.

The inaccuracies in the measurements induce an uncertainty of 1%.

2. Calibration of oil flow rate:

Oil flow rate obtained from this method is calibrated with help of a pre-calibrated Micro Motion Corolis mass flow meter (Make: Emerson Process Management, Sensor Model: R100S128NQBZEZZZZ, Transmitter Model:1700R11ABFEZZZ) when it was available at the latter stage of the experiments. The calibration plot is plotted in Fig. A4.1, which shows a goo correlation coefficient ($R^2 = 0.99$).

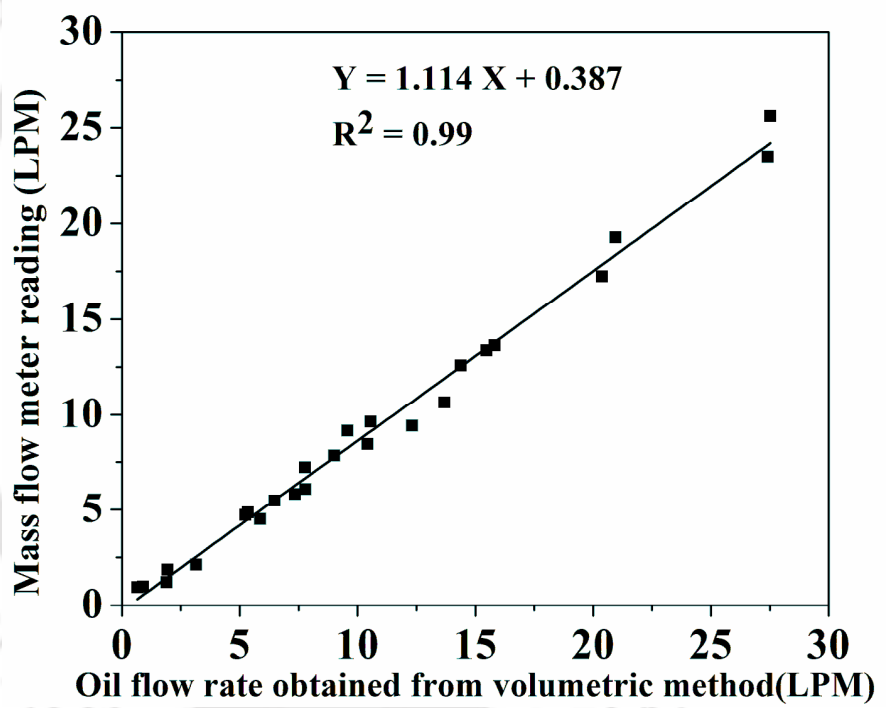

Fig. A4.1: Calibration plot of oil flow rate

3. AAPE, mean and standard deviation of correlations and different models

Table A.3 Correlations used for the prediction of pressure drop

Correlation	AAPE	Mean	Standard deviation
Lockhart and Martinelli (1949)	1398	-1398	658.37
Cicchitti (1960)	60	60	22.7
Chawla (1965)	750	-750	213
Chisholm (1967)	1164	-1164	499
Chisholm (1973)	3078	-3078	1254
Friedel (1980)	300	-300	168.5
Muller Steinhagan–Heck (1986)	60	-16.93	74.2

Table A.4 Lockhart-Martinelli Approach

Author	AAPE	Mean	Standard deviation
Charles et al. (1961)	25.5	4.64	33.5
Trallero et al. (1997)	25	-0.389	32.73
Rodriguez and Oliemans (2006)	29.1	6.76	38.68
Present work (Horizontal)	22	-15.07	50.19

Table A.5 Dimensional Analysis for Horizontal

Author	AAPE	Mean	Standard deviation
Present work (Horizontal)	17.89	-1.48	22.67

Table A.6 Liquid-liquid two-phase flow correlations

Correlation	**AAPE**	**Mean**	**Standard deviation**
Two-fluid model Ullmann and Brauner (2006).	30.05	-31.8	66.5
Al-Wahaibi (2012) correlation	34	-3.21	41.8
Modified two-fluid model Zhang et al. (2012)	28.6	50.8	48.2

Table A.7 Pressure drop correlations in inclined flow

Correlation	**AAPE**	**Mean**	**Standard deviation**
Lockhart-Martinelli Approach	6.6	0.98	8.53
Dimensional Analysis	4.9	-0.73	6.88

Table A.8 Entrainment model

Author	**AAPE**	**Mean**	**Standard deviation**
Oliemans, (1986) (0°)	28	-7.3636	10.30
Grassi et al. (2008) (+15°)	20	-18.65	8.52
Grassi et al. (2008) (+10°)	20	-7.86	7.87
Grassi et al. (2008) (-10°)	20	8.48	33.74
Present work (0°)	13	8.87	11.19
Present work (+5°)	20	-4.34	11.25

Table A.9 Models used for holdup prediction

Model	AAPE	Mean	Standard deviation
Horizontal			
Homogeneous flow model	20	5.79	15.8
Oliemans (1986) flow model	21.2	4.525	21.74
Arney et al. (1993) model	8.8	-9.6	16.91
Inclined flow			
Homogeneous flow model	20	13.21	41.5
Oliemans (1986) flow model	25	7.86	42.77
Arney et al. (1993) model	10	-0.217	14.5

4. Calculations for entrainment model

a) The volume of sinusoidal waves can be calculated as

$$V_{wave} = S_i \int_0^{\lambda/2} a \sin\left(\frac{2\pi x}{\lambda}\right) dx = \frac{\cancel{\pi} D_a a_i \lambda}{\cancel{\pi}} = \bar{a} \cdot \overline{D_a} \cdot D^3 \tag{A.20}$$

This expression is incorporated in the Eq. (6.54) results:

$$V_{ent} = D^3 \left[\left(\bar{a} \cdot \overline{D_a} \right)_{onset} - \left(\bar{a} \cdot \overline{D_a} \right)_{newcondition} \right] \tag{A.21}$$

Therefore individual entrainment volumes can be given as:

$$V_{ent}^{oil} = D^3 \left[\left(\overline{a_o} \cdot \overline{D_a} \right)_{onset} - \left(\overline{a_o} \cdot \overline{D_a} \right)_{newcondition} \right]; \quad V_{ent}^{water} = D^3 \left[\left(\overline{a_w} \cdot \overline{D_a} \right)_{onset} - \left(\overline{a_w} \cdot \overline{D_a} \right)_{newcondition} \right] \tag{A.22}$$

b) Calculation for entrained fractions

Average volume concentrations of core and annular can be given as:

$$\alpha_a = \left(\frac{V_o}{V_o + V_w}\right)_a ; \quad \alpha_b = \left(\frac{V_w}{V_o + V_w}\right)_b \tag{A.23}$$

Total volume of oil and water can be given by:

$$V_o = (V_o)_a + (V_o)_b ; \; V_w = (V_w)_a + (V_w)_b \tag{A.24}$$

Thus, for a pure core phase (a) and a pure annular phase (b): $\alpha_a = \alpha_b = 1$ and suffixes 'a' and 'b' can be replaced with 'o' and 'w' respectively, since entrainments are $E_o = E_w = 0$.

Therefore mass and volume of core phase (a) and annular phase (b) are formulated as:

$$M_a = (M_w + M_o)_a ; \; V_a = (V_w + V_o)_a ; \; M_b = (M_w + M_o)_b ; \; V_b = (V_w + V_o)_b \tag{A.25}$$

The density of oil and water can be defined as:

$$\frac{(M_o)_a}{(V_o)_a} = \left(\frac{M_o}{V_o}\right)_a = \frac{(M_o)_b}{(V_o)_b} = \left(\frac{M_o}{V_o}\right)_b = \frac{M_o}{V_o} = \rho_o ; \; \frac{(M_w)_a}{(V_w)_a} = \left(\frac{M_w}{V_w}\right)_a = \frac{(M_w)_b}{(V_w)_b} = \left(\frac{M_w}{V_w}\right)_b = \frac{M_w}{V_w} = \rho_w \tag{A.26}$$

Based on the above equations density of core phase can be calculated as:

$$\frac{M_a}{V_a} = \left(\frac{M_o + M_w}{V_o + V_w}\right)_a = \left(\frac{M_o}{V_o + V_w}\right)_a + \left(\frac{M_w}{V_o + V_w}\right)_a = \rho_a ;$$

$$\therefore \; \rho_a = \left(\frac{M_o}{V_o} \times \frac{V_o}{V_o + V_w}\right)_a + \left(\frac{M_w}{V_w} \times \frac{V_w}{V_o + V_w}\right)_a = \left(\rho_o \times (1 - E_w)\right) + \left(\rho_w \times E_w\right) \tag{A.27}$$

c) Calculation of actual phase velocities

By replacing volumetric flow rates of Eq.6.75 in Eq.6.74 a, b resulted:

$$A=\frac{U_b A_b}{U_{os}}(1-\alpha_b)+\left(\frac{U_a}{U_{os}}\right)A_a\alpha_a=\frac{U_b A_b}{U_{os}}E_o+\left(\frac{U_a}{U_{os}}\right)A_a(1-E_w) \tag{A.28}$$

$$A\left(\frac{U_{ws}}{U_{os}}\right)=\frac{U_b A_b}{U_{os}}\alpha_b+\left(\frac{U_a}{U_{os}}\right)A_a(1-\alpha_a)=\frac{U_b A_b}{U_{os}}(1-E_o)+\left(\frac{U_a}{U_{os}}\right)A_a E_w \tag{A.29}$$

From the Eq.A.28

$$U_b A_b=\frac{U_{os}}{E_o}\left(A-\overline{U_a}A_a(1-E_w)\right);\ \text{where}\ \ \overline{U_a}=\frac{U_a}{U_{os}} \tag{A.30}$$

and by incorporating this in Eq.A.29 gives:

$$A\left(\frac{U_{ws}}{U_{os}}\right)=\frac{(1-E_o)}{E_o}\left(A-\overline{U_a}A_a(1-E_w)\right)+\overline{U_a}A_a E_w=A\frac{(1-E_o)}{E_o}+\overline{U_a}A_a\frac{(E_o+E_w-1)}{E_o} \tag{A.31}$$

$$\Rightarrow A\left(\frac{1}{\phi}-\frac{(1-E_o)}{E_o}\right)\frac{E_o}{(E_o+E_w-1)}=\overline{U_a}A_a \tag{A.32}$$

d) Calculation of dimensionless pressure gradient

$$\pm\tau_i S_i=A_b\left(\frac{dP}{dx}\right)+\tau_b S_b-\rho_b A_b g\sin\beta;\quad -A_a\left(\frac{dP}{dx}\right)+\rho_a A_a g\sin\beta=\pm\tau_i S_i \tag{A.33}$$

By eliminating 'τ_i' from Eqs.6.69 and 6.6.70 (in the Chapter 6) gives

$$\Rightarrow -\left(\frac{dP}{dx}\right)(A_b+A_a)-\tau_b S_b+(\rho_a A_a+\rho_b A_b)g\sin\beta=0 \tag{A.34}$$

Divide the above equation with $\left[\left(\frac{4C_a}{D}\right)\left(\frac{DU_{os}}{\upsilon_o}\right)^{-n_a}\left(\frac{\rho_o U_{os}^2}{2}\right)\right]\left[D^2\left(\overline{A_c}+\overline{A_w}\right)\right]$;

replacing $\frac{-\left(\frac{dP}{dx}\right)}{\left[\left(\frac{4C_a}{D}\right)\left(\frac{DU_{os}}{\upsilon_o}\right)^{-n_a}\left(\frac{\rho_o U_{os}^2}{2}\right)\right]}$ and $\frac{\rho_a\overline{A_a}+\rho_b\overline{A_b}}{\left(\overline{A_a}+\overline{A_b}\right)(\rho_b-\rho_a)}$ with 'Φ_o' & '$\overline{\rho}$'

(A.35)

e) Lockhart -Martinelli Parameter calculation

$$\chi_s^2=\frac{\left(\frac{dP}{dx}\right)_{ws}}{\left(\frac{dP}{dx}\right)_{os}};$$

where $\left(\frac{dP}{dx}\right)_{os}=\frac{4}{D}f_{os}\left(\frac{\rho_o U_{os}^2}{2}\right)$; with $f_{os}=C_{os}\left(\frac{DU_{os}}{\upsilon_o}\right)^{-n_{os}}$

(A.36)

$$\left(\frac{dP}{dx}\right)_{ws}=\frac{4}{D}f_{ws}\left(\frac{\rho_w U_{ws}^2}{2}\right);\ \text{with}\ f_{ws}=C_{ws}\left(\frac{DU_{ws}}{\upsilon_w}\right)^{-n_{ws}}$$

(A.37)

which can be further evaluated in terms of two phase pressure gradient as:

$$\left(\frac{dP}{dx}\right)_{os}=\frac{4}{D}C_{os}\left(\frac{DU_{os}}{\upsilon_o}\right)^{-n_{os}}\left(\frac{\rho_o U_{os}^2}{2}\right)=\left(\frac{4C_{os}}{D}\times\frac{C_a}{C_a}\right)\left[\left(\frac{DU_{os}}{\upsilon_o}\right)^{-n_{os}}\frac{\left(\frac{DU_{os}}{\upsilon_o}\right)^{-n_a}}{\left(\frac{DU_{os}}{\upsilon_o}\right)^{-n_a}}\right]\left(\frac{\rho_o U_{os}^2}{2}\right)$$

(A.38)

$$\Rightarrow\left(\frac{dP}{dx}\right)_{os}=\left[\left(\frac{4C_a}{D}\right)\left(\frac{DU_{os}}{\upsilon_o}\right)^{-n_a}\left(\frac{\rho_o U_{os}^2}{2}\right)\right]\left(\frac{C_{os}}{C_a}\right)\left(\frac{DU_{os}}{\upsilon_o}\right)^{-(n_{os}-n_a)}$$

$$=\left[\left(\frac{C_{os}}{C_a}\right)\left(\frac{DU_{os}}{\upsilon_o}\right)^{-(n_{os}-n_a)}\right]\left(\frac{\left(\frac{dP}{dx}\right)_{TP}}{\Phi_o}\right)$$

(A.39)

Similarly: $$\left(\frac{dP}{dx}\right)_{ws} = \left[\left(\frac{C_{ws}}{C_b}\right)\left(\frac{DU_{ws}}{\upsilon_w}\right)^{-(n_{ws}-n_b)}\right]\left(\frac{\left(\frac{dP}{dx}\right)_{TP}}{\Phi_w}\right) \quad \text{(A.40)}$$

f) Calculations procedure and analytical solution

$$\chi_s^2 = \chi^2 \frac{\left(\frac{C_{ws}}{C_b}\right)\mathrm{Re}_{ws}^{(n_b-n_{ws})}}{\left(\frac{C_{os}}{C_a}\right)\mathrm{Re}_{os}^{(n_a-n_{os})}} = \frac{\left[\left(\frac{4C_b}{D}\right)\left(\frac{DU_{ws}}{\upsilon_w}\right)^{-n_b}\left(\frac{\rho_w U_{ws}^2}{2}\right)\right]}{\left[\left(\frac{4C_a}{D}\right)\left(\frac{DU_{os}}{\upsilon_o}\right)^{-n_a}\left(\frac{\rho_o U_{os}^2}{2}\right)\right]} \quad \text{(A.41)}$$

$$\pm\left[\left(\frac{\rho_a}{\rho_o}\right)\left(\frac{\upsilon_a}{\overline{D}_a \overline{U}_a \upsilon_o}\right)\left(1-\frac{\overline{G}}{\overline{F}}\frac{\overline{D}_a^{\,2}}{\left(1-\overline{D}_a^{\,2}\right)}\frac{1}{\phi}\right)^2 \overline{S}_i \overline{U}_a^{\,2}\left(\frac{1}{\overline{A}_a}+\frac{1}{\overline{A}_b}\right)\right] = \left[\chi^2\left(\frac{\rho_b}{\rho_w}\right)\left(\frac{\upsilon_b}{\overline{D}_b \overline{U}_b \upsilon_w}\right)\frac{\overline{S}_b}{\overline{A}_b}\overline{U}_b^{\,2}\right] - 4Y$$

$$\Rightarrow \pm\left[\left(\frac{\rho_a}{\rho_o}\right)\left(\frac{\upsilon_a}{\overline{D}_a \upsilon_o}\right)\left(1-\frac{\overline{G}}{\overline{F}}\frac{\overline{D}_a^{\,2}}{\left(1-\overline{D}_a^{\,2}\right)}\frac{1}{\phi}\right)^2 \pi \overline{D}_a \overline{U}_a\left(\frac{4}{\pi}\frac{1}{\overline{D}_a^{\,2}}\frac{1}{\left(1-\overline{D}_a^{\,2}\right)}\right)\right]$$

$$= \left[\chi^2\left(\frac{\rho_b}{\rho_w}\right)\left(\frac{\upsilon_b}{\left(1-\overline{D}_a^{\,2}\right)\upsilon_w}\right)\frac{\pi}{\frac{\pi}{4}\left(1-\overline{D}_a^{\,2}\right)}\overline{U}_b\right] - 4Y \quad \text{(A.42)}$$

g) In terms of dimensionless core diameter

$$\text{for '+'} \Rightarrow \left[\left(1-\frac{\overline{G}}{\overline{F}}\frac{\overline{D}_a^{\,2}}{\left(1-\overline{D}_a^{\,2}\right)}\frac{1}{\phi}\right)^2\left(\frac{\overline{F}}{\overline{D}_a^{\,4}}\right)\right] = \left[\frac{1}{\phi}\left(\frac{\mu_b}{\mu_a}\right)\frac{\overline{G}}{\left(1-\overline{D}_a^{\,2}\right)^2}\right] - Y\cdot\left(1-\overline{D}_a^{\,2}\right)\cdot\left(\frac{\mu_o}{\mu_a}\right)$$

Multiplying above equation with $\left(1-\overline{D_a}^2\right)^2\cdot\phi^2\cdot\left(\frac{\overline{D_a}^4}{\overline{\overline{F}}}\right)$ gives:

$$\Rightarrow\left[\phi\left(1-\overline{D_a}^2\right)-\overline{D_a}^2\left(\overline{G}/\overline{F}\right)\right]^2=\left[\left(\phi\left(\frac{\mu_b}{\mu_a}\right)\left(\overline{G}/\overline{F}\right)\right)\overline{D_a}^4\right]-Y\cdot\left(1-\overline{D_a}^2\right)^3\cdot\phi^2\cdot\left(\frac{\mu_o}{\mu_a}\right)\cdot\left(\frac{\overline{D_a}^4}{\overline{\overline{F}}}\right) \quad \text{(A.43)}$$

$$\Rightarrow\left[\phi\left(1-\overline{D_a}^2\right)-\overline{D_a}^2\left(\overline{G}/\overline{F}\right)\right]^2=\left[\left(\phi\left(\frac{\mu_b}{\mu_a}\right)\left(\overline{G}/\overline{F}\right)\right)\overline{D_a}^4\right]\left(1-Y\cdot\left(1-\overline{D_a}^2\right)^3\cdot\left(\frac{\mu_o}{\mu_b}\right)\cdot\left(\frac{\phi}{\overline{\overline{G}}}\right)\right)\Rightarrow a^2=b\cdot c;$$

$$\Rightarrow a^2=\left[\phi\left(1-\overline{D_a}^2\right)-\overline{D_a}^2\left(\overline{G}/\overline{F}\right)\right]^2=\left[\phi^2\left(1-\overline{D_a}^2\right)^2+\overline{D_a}^4\left(\overline{G}/\overline{F}\right)^2-2\overline{D_a}^2\left(\overline{G}/\overline{F}\right)\left(1-\overline{D_a}^2\right)\right];$$

$$\Rightarrow a^2=\left[\phi^2\left(1+\overline{D_a}^4-2\overline{D_a}^2\right)+\overline{D_a}^4\left(\overline{G}/\overline{F}\right)^2-2\overline{D_a}^2\left(\overline{G}/\overline{F}\right)+2\overline{D_a}^4\left(\overline{G}/\overline{F}\right)\right];$$

$$\Rightarrow a^2=\left[\overline{D_a}^4\left(\phi^2+\left(\overline{G}/\overline{F}\right)^2+2\left(\overline{G}/\overline{F}\right)\right)-2\overline{D_a}^2\left(\phi^2+\left(\overline{G}/\overline{F}\right)\right)+\phi^2\right];$$

$$\Rightarrow c=\left(1-Y\cdot\left(1-\overline{D_a}^2\right)^3\cdot\left(\frac{\mu_o}{\mu_b}\right)\cdot\left(\frac{\phi}{\overline{\overline{G}}}\right)\right);$$

$$\Rightarrow b\cdot c=\left[b_1\overline{D_a}^4\right]\left(1+c_1\cdot\left(\overline{D_a}^2-1\right)^3\right);\ \text{where}\ b_1=\left(\phi\left(\frac{\mu_b}{\mu_a}\right)\left(\overline{G}/\overline{F}\right)\right);\ c_1=Y\cdot\left(\frac{\mu_o}{\mu_b}\right)\cdot\left(\frac{\phi}{\overline{\overline{G}}}\right);$$

$$\Rightarrow b\cdot c=\left[b_1\overline{D_a}^4\right]\left(1+c_1\cdot\left(\overline{D_a}^2-1\right)^3\right)=b_1\overline{D_a}^4+b_1\overline{D_a}^4c_1\left(\overline{D_a}^6-3\overline{D_a}^4+3\overline{D_a}^2-1\right);$$

$$\Rightarrow b\cdot c=\overline{D_a}^{10}\left(b_1c_1\right)-3\overline{D_a}^8\left(b_1c_1\right)+3\overline{D_a}^6\left(b_1c_1\right)-\overline{D_a}^4\left(b_1c_1-b_1\right);\quad\therefore a^2-b\cdot c=0\ \text{gives:} \quad \text{(A.44)}$$

$$\Rightarrow\overline{D_a}^{10}\left(b_1c_1\right)-3\overline{D_a}^8\left(b_1c_1\right)+3\overline{D_a}^6\left(b_1c_1\right)+\overline{D_a}^4\left(b_1-b_1c_1+\left(\phi^2+\left(\overline{G}/\overline{F}\right)^2+2\left(\overline{G}/\overline{F}\right)\right)\right)-2\overline{D_a}^2\left(\phi^2+\left(\overline{G}/\overline{F}\right)\right)+\phi^2=0; \quad \text{(A.45)}$$

h) Dimensionless form of Lockhart-Martinelli parameter 'χ_s^2'

$$\chi_s^2=\chi^2\frac{\left(\frac{C_{ws}}{C_b}\right)\mathrm{Re}_{ws}^{\left(n_b-n_{ws}\right)}}{\left(\frac{C_{os}}{C_a}\right)\mathrm{Re}_{os}^{\left(n_a-n_{os}\right)}}=\frac{\left[\left(\frac{4C_b}{D}\right)\left(\frac{DU_{ws}}{\upsilon_w}\right)^{-n_b}\left(\frac{\rho_wU_{ws}^2}{2}\right)\right]}{\left[\left(\frac{4C_a}{D}\right)\left(\frac{DU_{os}}{\upsilon_o}\right)^{-n_a}\left(\frac{\rho_oU_{os}^2}{2}\right)\right]} \quad \text{(A.46)}$$

$$\Rightarrow \chi_s^2 = \frac{\left[\left(\frac{\cancel{4}C_b}{\cancel{D}}\right)\left(\frac{DU_{ws}}{\upsilon_w}\right)^{-\cancel{n}_b^{0.2}}\left(\frac{\rho_w U_{ws}^2}{2}\right)\right]}{\left[\left(\frac{\cancel{4}C_a}{\cancel{D}}\right)\left(\frac{DU_{os}}{\upsilon_o}\right)^{-\cancel{n}_a^{1}}\left(\frac{\rho_o U_{os}^2}{2}\right)\right]} \times \frac{\mathrm{Re}_{os}^{0.2}}{\mathrm{Re}_{os}^{0.2}} = \left(\frac{C_b}{C_a}\right)\mathrm{Re}_{os}^{1-0.2}\left(\frac{\rho_w U_{ws}^2}{\rho_o U_{os}^2}\right)\left(\mathrm{Re}_{os}\times\mathrm{Re}_{ws}\right)^{0.2}$$

$$\Rightarrow \chi_s^2 = \frac{0.046}{16}\left[\frac{\mu_w}{\mu_o}\cdot\frac{1}{\phi}\cdot\mathrm{Re}_{ws}^{0.8}\right] = k_{l1}\frac{1}{\phi};\quad \text{where } k_{l1} = \frac{0.046}{16}\left[\frac{\mu_w}{\mu_o}\cdot\mathrm{Re}_{ws}^{0.8}\right] \tag{A.47}$$

$$\Rightarrow \chi_s^2 = \frac{\left[\left(\frac{\cancel{4}C_b}{\cancel{D}}\right)\left(\frac{DU_{ws}}{\upsilon_w}\right)^{-\cancel{n}_b^{0.2}}\left(\frac{\rho_w U^2_{ws}}{2}\right)\right]}{\left[\left(\frac{\cancel{4}C_a}{\cancel{D}}\right)\left(\frac{DU_{os}}{\upsilon_o}\right)^{-\cancel{n}_a^{1}}\left(\frac{\rho_o U^2_{os}}{2}\right)\right]} \times \frac{\mathrm{Re}_{os}^{0.2}}{\mathrm{Re}_{os}^{0.2}} = \left(\frac{C_b}{C_a}\right)\mathrm{Re}_{os}^{1-0.2}\left(\frac{\rho_w U_{ws}^2}{\rho_o U_{os}^2}\right)\left(\mathrm{Re}_{os}\times\mathrm{Re}_{ws}\right)^{0.2}$$

$$\Rightarrow \chi_s^2 = \frac{0.046}{16}\left[\left(\frac{\mu_w}{\mu_o}\right)^{0.2}\cdot\left(\frac{\rho_w}{\rho_o}\right)^{0.8}\cdot\frac{1}{\phi^{1.8}}\cdot\mathrm{Re}_{os}^{0.8}\right] = k_{l2}\frac{1}{\phi^{1.8}};\ \text{where } k_{l2} = \frac{0.046}{16}\left[\left(\frac{\mu_w}{\mu_o}\right)^{0.2}\cdot\left(\frac{\rho_w}{\rho_o}\right)^{0.8}\cdot\mathrm{Re}_{os}^{0.8}\right] \tag{A.48}$$

Therefore by introducing non-dimensional parameters from Eq.6.77 into Eq.6.79

$$\Rightarrow \pm\left[\left(\frac{\rho_a}{\rho_o}\right)\left(\frac{\upsilon_a}{\overline{D}_a\overline{U}_a\upsilon_o}\right)\left(1-\frac{\overline{G}}{\overline{F}}\frac{\overline{D}_a^2}{\left(1-\overline{D}_a^2\right)}\frac{1}{\phi}\right)^2\overline{S_i}\overline{U_a}^{\cancel{2}}\left(\frac{1}{\overline{A}_a}+\frac{1}{\overline{A}_b}\right)\right] = \left[\chi^2\left(\frac{\rho_b}{\rho_w}\right)\left(\frac{\upsilon_b}{\overline{D}_b\overline{U}_b\upsilon_w}\right)^{0.2}\frac{\overline{S}_b}{\overline{A}_b}\overline{U}_b^2\right] - 4Y$$

$$\Rightarrow \pm\left[\left(\frac{\rho_a}{\rho_o}\right)\left(\frac{\upsilon_a}{\cancel{\overline{D}_a}\upsilon_o}\right)\left(1-\frac{\overline{G}}{\overline{F}}\frac{\overline{D}_a^2}{\left(1-\overline{D}_a^2\right)}\frac{1}{\phi}\right)^2\cancel{\pi}\,\cancel{\overline{D}_a}\overline{U}_a\left(\frac{4}{\cancel{\pi}}\frac{1}{\overline{D}_a^2}\frac{1}{\left(1-\overline{D}_a^2\right)}\right)\right]$$

$$= \left[\chi^2\left(\frac{\rho_b}{\rho_w}\right)\left(\frac{\upsilon_b}{\left(1-\overline{D}_a^2\right)\upsilon_w}\right)^{0.2}\frac{\cancel{\pi}}{\frac{\cancel{\pi}}{4}\left(1-\overline{D}_a^2\right)}\overline{U}_b^{1.8}\right] - 4Y \tag{A.49}$$

Multiplying above equation with $\left(1-\overline{D_a}^2\right)^3\cdot\phi^2\cdot\left(\frac{\overline{D_a}^4}{\overline{F}}\right)\cdot\left(\frac{\mu_o}{\mu_a}\right)$ gives:

$$\Rightarrow\pm\left[\left(\frac{\mu_a}{\mu_o}\right)\left(1-\frac{\overline{G}}{\overline{F}}\frac{\overline{D_a}^2}{\left(1-\overline{D_a}^2\right)}\frac{1}{\phi}\right)^2\left(\frac{A}{\overline{D_a}^4}\frac{\overline{F}}{\left(1-\overline{D_a}^2\right)}\right)\left(1-\overline{D_a}^2\right)^{\frac{2}{3}}\cdot\phi^2\cdot\left(\frac{\overline{D_a}^4}{\overline{F}}\right)\left(\frac{\mu_a}{\mu_a}\right)\right]$$

$$=\left[\chi_s^2\left(\frac{\rho_b}{\rho_w}\right)\left(\frac{\upsilon_b}{\upsilon_w}\right)^{0.2}\frac{A}{\left(1-\overline{D_a}^2\right)^{0.2}}\frac{\overline{G}^{1.8}}{\left(1-\overline{D_a}^2\right)^{2.8}}\left(1-\overline{D_a}^2\right)^3\cdot\phi^2\cdot\left(\frac{\overline{D_a}^4}{\overline{F}}\right)\left(\frac{\mu_o}{\mu_a}\right)\right]-AY\cdot\left(1-\overline{D_a}^2\right)^3\cdot\phi^2\cdot\left(\frac{\overline{D_a}^4}{\overline{F}}\right)\left(\frac{\mu_o}{\mu_a}\right)$$

$$\Rightarrow\pm\left[\left(\frac{\phi\left(1-\overline{D_a}^2\right)-\overline{D_a}^2\left(\overline{G}/\overline{F}\right)}{\phi\left(1-\overline{D_a}^2\right)}\right)^2\cdot\left(1-\overline{D_a}^2\right)^2\cdot\phi^2\right]$$

$$=\left[\overline{D_a}^4\cdot\chi_s^2\cdot\phi^2\left(\frac{\mu_o}{\mu_a}\right)\left(\frac{\rho_b}{\rho_w}\right)\left(\frac{\upsilon_b}{\upsilon_w}\right)^{0.2}\frac{\overline{G}^{1.8}}{\overline{F}}\right]-Y\cdot\left(1-\overline{D_a}^2\right)^3\cdot\phi^2\cdot\left(\frac{\overline{D_a}^4}{\overline{F}}\right)\left(\frac{\mu_o}{\mu_a}\right)$$

$$\Rightarrow\pm\left(\phi\left(1-\overline{D_a}^2\right)-\overline{D_a}^2\left(\overline{G}/\overline{F}\right)\right)^2=\left[\overline{D_a}^4\cdot\chi_s^2\cdot\phi^2\left(\frac{\mu_o}{\mu_a}\right)\left(\frac{\rho_b}{\rho_w}\right)\left(\frac{\upsilon_b}{\upsilon_w}\right)^{0.2}\frac{\overline{G}^{1.8}}{\overline{F}}\right]-Y\cdot\left(1-\overline{D_a}^2\right)^3\cdot\phi^2\cdot\left(\frac{\overline{D_a}^4}{\overline{F}}\right)\left(\frac{\mu_o}{\mu_a}\right)$$

(A.50)

$$\text{for '+'}\Rightarrow a^2=\left[\overline{D_a}^4\cdot\chi_s^2\cdot\phi^2\left(\frac{\mu_o}{\mu_a}\right)\left(\frac{\rho_b}{\rho_w}\right)\left(\frac{\upsilon_b}{\upsilon_w}\right)^{0.2}\frac{\overline{G}^{1.8}}{\overline{F}}\right]\left(1+Y\cdot\left(\overline{D_a}^2-1\right)^3\left(\frac{\rho_w}{\rho_b}\right)\left(\frac{\upsilon_w}{\upsilon_b}\right)^{0.2}\frac{\chi_s^{-2}}{\overline{G}^{1.8}}\right)=m\cdot n$$

$$\Rightarrow a^2=\left[\overline{D_a}^4\left(\phi^2+\left(\overline{G}/\overline{F}\right)^2+2\left(\overline{G}/\overline{F}\right)\right)-2\overline{D_a}^2\left(\phi^2+\left(\overline{G}/\overline{F}\right)\right)+\phi^2\right];$$

(A.51)

$$\Rightarrow n=\left(1+Y\cdot\left(\overline{D_a}^{2}-1\right)^{3}\cdot\left(\frac{\rho_w}{\rho_b}\right)\left(\frac{\upsilon_w}{\upsilon_b}\right)^{0.2}\frac{\chi_s^{-2}}{\overline{G}^{1.8}}\right);$$

$$\Rightarrow m\cdot n=\left[m_1\overline{D_a}^{4}\right]\left(1+n_1\cdot\left(\overline{D_a}^{2}-1\right)^{3}\right);$$

where $m_1=\chi_s^2\cdot\phi^2\left(\frac{\mu_o}{\mu_a}\right)\left(\frac{\rho_b}{\rho_w}\right)\left(\frac{\upsilon_b}{\upsilon_w}\right)^{0.2}\frac{\overline{G}^{1.8}}{\overline{F}};n_1=Y\cdot\left(\frac{\rho_w}{\rho_b}\right)\left(\frac{\upsilon_w}{\upsilon_b}\right)^{0.2}\frac{\chi_s^{-2}}{\overline{G}^{1.8}};$

$$\Rightarrow m\cdot n=\left[m_1\overline{D_a}^{4}\right]\left(1+n_1\cdot\left(\overline{D_a}^{2}-1\right)^{3}\right)=m_1\overline{D_a}^{4}+m_1\overline{D_a}^{4}n_1\left(\overline{D_a}^{6}-3\overline{D_a}^{4}+3\overline{D_a}^{2}-1\right);$$

$$\Rightarrow m\cdot n=\overline{D_a}^{10}\left(m_1n_1\right)-3\overline{D_a}^{8}\left(m_1n_1\right)+3\overline{D_a}^{6}\left(m_1n_1\right)-\overline{D_a}^{4}\left(m_1n_1-m_1\right);\quad\therefore a^2-m\cdot n=0\text{ gives:}\tag{A.52}$$

$$\Rightarrow\overline{D_a}^{10}\left(m_1n_1\right)-3\overline{D_a}^{8}\left(m_1n_1\right)+3\overline{D_a}^{6}\left(m_1n_1\right)-\overline{D_a}^{4}\left(m_1n_1-m_1+\left(\phi^2+\left(\overline{G}/\overline{F}\right)^2+2\left(\overline{G}/\overline{F}\right)\right)\right)+2\overline{D_a}^{2}\left(\phi^2+\left(\overline{G}/\overline{F}\right)\right)-\phi^2=0;$$

For special case of pure annular horizontal flow, Eq.6.90 becomes:

$$\overline{D_a}=\left(\frac{\phi}{\chi_s\phi+1+\phi}\right)^{1/2}\quad\because\mu_a=\mu_o;\mu_b=\mu_w;\rho_a=\rho_o;\rho_b=\rho_w\text{ at }E_o=E_w=0$$

$$\Rightarrow 1-\overline{D_a}^{2}=\left(\frac{\chi_s\phi+1}{\chi_s\phi+1+\phi}\right)\quad\therefore\frac{1}{\left(1-\overline{D_a}^{2}\right)^{2}}=\left(\frac{\chi_s\phi+1+\phi}{\chi_s\phi+1}\right)^{2}\tag{A.53}$$

Therefore by introducing non-dimensional parameters from Eq.6.77 into Eq.6.82a:

$$\Phi_o=\frac{1}{4}\chi_s^2\frac{\rho_b}{\rho_w}\frac{\pi\overline{U_b}^{1.8}}{\left(\overline{A_a}+\overline{A_b}\right)}\left(\frac{\upsilon_b}{\overline{D_b}\,\overline{U_b}\,\upsilon_w}\right)^{0.2}-\overline{\rho}Y=\frac{1}{4}\chi_s^2\frac{\rho_b}{\rho_w}\left(\frac{\upsilon_b}{\upsilon_w}\right)^{0.2}\frac{\pi\overline{U_b}^{1.8}}{4}\left(\frac{1}{\left(1-\overline{D_a}^{2}\right)^{0.2}}\right)-\overline{\rho}Y$$

$$\Rightarrow\Phi_o=\chi_s^2\frac{\rho_b}{\rho_w}\left(\frac{\upsilon_b}{\upsilon_w}\right)^{0.2}\frac{\overline{G}^{1.8}}{\left(1-\overline{D_a}^{2}\right)^{2}}-\left(\frac{\rho_a\overline{D_a}^{2}+\rho_b\left(1-\overline{D_a}^{2}\right)}{(\rho_b-\rho_a)}\cdot\frac{(\rho_b-\rho_a)gD\sin\beta\left(\frac{D}{\mu_o}\right)^{0.2}}{32\rho_o^{0.8}U_{os}^{1.8}}\right)\tag{A.54}$$

i) Optimal conditions

$$\Phi_o=\frac{1}{\phi}k_l\left(\frac{\left(\sqrt{\phi k_l}+1+\phi\right)}{\left(\sqrt{\phi k_l}+1\right)}\right)^{2}\quad\therefore\frac{\partial\Phi_o}{\partial\phi}=0=\left(\frac{d\Phi_o}{d\phi}\right)_{\text{at constant }k_l}\tag{A.55}$$

$$\Rightarrow \frac{d\Phi_o}{d\phi} = \frac{2k_l}{\phi}\left(\sqrt{\frac{k_l}{4\phi}}+1\right)\left(\frac{\left(\sqrt{\phi k_l}+1+\phi\right)}{\left(\sqrt{\phi k_l}+1\right)^2}\right) - \frac{k_l}{\phi^2}\left(\frac{\left(\sqrt{\phi k_l}+1+\phi\right)}{\left(\sqrt{\phi k_l}+1\right)}\right)^2 - \left(\frac{k_l}{\phi}\right)^{1.5}\frac{\left(\sqrt{\phi k_l}+1+\phi\right)^2}{\left(\sqrt{\phi k_l}+1\right)^3} = 0 \quad \text{(A.56)}$$

$$\therefore \phi_m = \frac{1}{\left(\sqrt{k_l}+1\right)^2}; \frac{1}{\left(\sqrt{k_l}-1\right)^2}; \frac{\left(k_l+\sqrt{k_l(k_l-4)}-2\right)}{2}; \frac{\left(k_l-\sqrt{k_l(k_l-4)}-2\right)}{2} \quad \text{(A.57)}$$

j) Calculation of optimum input velocity ratio ($\emptyset_m$)

$$\frac{d\Phi_o'}{d\phi} = \frac{k_l}{\phi^2}\left(\frac{\left(\sqrt{\phi k_l}+1+\phi\right)}{\left(\sqrt{\phi k_l}+1\right)}\right)^2 + \frac{2k_l(\phi+1)}{\phi^2}\left(\sqrt{\frac{k_l}{4\phi}}+1\right)\left(\frac{\left(\sqrt{\phi k_l}+1+\phi\right)}{\left(\sqrt{\phi k_l}+1\right)^2}\right)$$
$$-\frac{2k_l(\phi+1)}{\phi^3}\left(\frac{\left(\sqrt{\phi k_l}+1+\phi\right)}{\left(\sqrt{\phi k_l}+1\right)}\right)^2 - \left(\frac{k_l^{1.5}}{\phi^{2.5}}\right)\frac{(\phi+1)\left(\sqrt{\phi k_l}+1+\phi\right)^2}{\left(\sqrt{\phi k_l}+1\right)^3} = 0 \quad \text{(A.58)}$$

$$\therefore \Phi_m = \frac{\left(k_l+\sqrt{k_l(k_l-4)}-2\right)}{2}; \frac{\left(k_l-\sqrt{k_l(k_l-4)}-2\right)}{2}; \frac{z_1^2}{k_l} \quad \text{where } 'z_1' \text{ are the roots of } f\{z\}=0$$

$$\text{where } f\{z\} = z^4 + z^3\left(\frac{3k_l}{k_l-1}\right) + z^2\left(\frac{k_l+2k_l^2}{k_l-1}\right) + z\left(\frac{4k_l^2}{k_l-1}\right) + \left(\frac{2k_l^2}{k_l-1}\right) \quad \text{(A.59)}$$

Outcome of the dissertation

List of Publications

International Journals

1. **Anjali Dasari,** Anand B. Desamala, Ashok K. Dasmahapatra and Tapas K. Mandal "Experimental studies and PNN prediction on flow pattern of viscous oil-water flow through circular horizontal pipe" Industrial Engineering and Chemistry Research. 52(29), 2013, 7975-7985.
2. Anand Babu Desamala, **Anjali Dasari**, Vinayak Vijayan, Bharath Kumar Goshika, Tapas Kumar Mandal, Ashok DasMahapatra."CFD Simulation and validation of flow pattern transition boundaries during moderately viscous oil water two phase flow through horizontal pipe flow" World Academy of Science and Technology, 73, 2013, 1150-1155.

3. **Anjali Dasari**, Anand B. Desamala, Ujjal K Gosh, Ashok K. Dasmahapatra and Tapas K. Mandal "Pressure gradient studies in liquid-liquid horizontal flow: Experimental and correlation based prediction" Journal of Fluids Engineering. Journal of Fluids Engineering. 136(7), 2014, 071302-071317.

4. **Anjali Dasari**, Bharath Kumar Goshika, Ravi Thej Pilla, Tapas Kumar Mandal. "CFD simulation and validation of interfacial morphology of viscous oil-water flow through upward inclined pipe". International Journal of Current Engineering and Technology. 2, 2014 , 453-460.

5. **Anjali Dasari**, Bharath Kumar Goshika, Tapas Kumar Mandal. "Viscous oil-water flow through inclined pipe: Experimental and prediction of flow patterns". Chemical Engineering Research and Design. (**Under review**).

6. Anand B. Desamala, Vinayak Vijayan, **Anjali Dasari**, Ashok K. Dasmahapatra and Tapas K. Mandal. "CFD simulation of flow pattern transition during viscous oil-water flow through a horizontal pipeline". (**To be communicated**)

Conferences

1. **Anjali Dasari**, Anand B. Desamala, Ashok K. Dasmahapatra and Tapas K. Mandal "Flow pattern of viscous oil-water flow: Prediction by Probabilistic Neural Network (PNN) and validation with experimental data" in **CHEMCON 2011**, Dec 27-30, 2011 in Bangalore.

2. **Anjali Dasari,** Bharath Kumar Goshika, Tapas Kumar Mandal ."Experimental study of flow regimes of moderately viscous oil-water flow through inclined pipe" Presented in **International conference on fluid engineering 2012,** Noida.

3. **Anjali Dasari**, Anand B. Desamala, Ashok K. Dasmahapatra and Tapas K. Mandal "Correlation based pressure drop prediction of viscous oil-water two-phase flow through horizontal pipeline." Presented in **CHEMCON 2012**, NIT Jalandar.

4. **Anjali Dasari**, Bharath Kumar Goshika, Tapas Kumar Mandal. "**CFD** simulation of wavy stratified flow pattern through upward inclined pipe" Presented in **Reflux 1.0, 2013,** IIT Guwahati.